TITLE: THE STRUCTURE AND LATTICE DYNAMICS

           OF SPINEL

A thesis submitted for the degree of

DOCTOR OF PHILOSOPHY

at the University of Aston in Birmingham

by

PAUL THOMPSON B.Sc.(Hons.)

Physics Department

March, 1977

To My Mother and Father

<div align="center">CONTENTS</div>

CONTENTS (contd)

CONTENTS (contd)

Knowledge is not happiness, and science

but an exchange òf ignorance for that

which is another kind of ignorance

                              Byron

ABSTRACT.

The low energy phonon dispersion system in Spinel, $MgA\ell_2O_4$, has been investigated by neutron inelastic scattering using time of flight spectrometry and the observed data used to refine the twelve adjustable parameters of a theoretical model constructed on the rigid ion harmonic approximation of Kellermann. It is demonstrated that the same approximation may be used to give a good description of the dynamical behaviour of Magnetite, Fe_3O_4, previously studied by Samuelsen and Steinsvoll. Comparison of the ten repulsive parameters which describe the ion overlap interactions and the effective ionic charges shows that the former are very similar in the two cases and correspond to non-central forces. The good electrical conductivity in Magnetite, arising from electron hopping, is apparently accommodated within the rigid ion model primarily through modification of the effective ionic charges.

The elastic constants in spinels have contributions from both internal and external strains and expressions have been derived in terms of the model parameters for the latter. These have been used together with a numerical evaluation of the internal contributions to provide theoretical estimates of the elastic constants of both Spinel and Magnetite, which are in fair agreement with the experimental values.

From examination of the eigenvectors of the model at phonon wavevector $q \approx 0$, two infra-red active modes of vibration have been identified. However the derived frequencies are in poor agreement with those observed and this is believed to be a consequence of assuming the ions to be unpolarisable.

Conventionally the crystal structure of cubic spinel compounds is referred to the space group Fd3m, but there is a considerable body of experimental evidence inconsistent with this description. A more general, unified and consistent description is provided by the lower symmetry space group F$\bar{4}$3m. Therefore a very careful analysis based on single crystal X-ray and neutron diffraction studies of MgAℓ_2O$_4$ has been carried out and is also presented. Very precise atom positions have been derived from the analysis and it is concluded that the symmetry of magnesium aluminate is more correctly described by the space group F$\bar{4}$3m.

CHAPTER 1

INTRODUCTION

1.1) General

It is an implicit assumption underlying the whole of science that any experimental observation concerning a given phenomenon is consistent with the remaining experimental facts. It then follows that any proposed interpretation must be consistent with all the related facts and that if any one of them lies outside this description then that theory must be deemed to have failed.

The study of solid state physics is no exception to this general principle. It has been clearly established in particular, that the spacial arrangement of the atoms in a crystalline solid, especially their local and overall symmetry, is closely correlated with the physical behaviour that may be exhibited. Crystals with structures which include a centre of symmetry, for example, cannot exhibit piezoelectricity (Wooster, 1949). Similarly, though a crystal may be ionic, if its structure is centro-symmetrical then there can be no net ionic dipole moment even if we allow the possibility of vibrational motion, i.e. ferroelectricity is impossible.

A beautiful illustration of these ideas may be found amongst the perovskite structures of which $BaTiO_3$ is an excellent example. Above a temperature of about 393°K, this crystal has the centro-symmetrical cubic structure shown in figure 1.1a and in this form behaves as a classic dielectric material. As the temperature is lowered through the Curie point, however, the Ba^{2+} and Ti^{4+} ions become displaced in the same sense to produce a spontaneous dipole moment. Simultaneously, the same displacements destroy the cubic symmetry so that the appearance of the ferroelectric property, arising from the presence of the permanent dipoles, is associated with the formation of the non-

Oxygen 2− Ion

Barium 2+ Ion

Titanium 4+ Ion
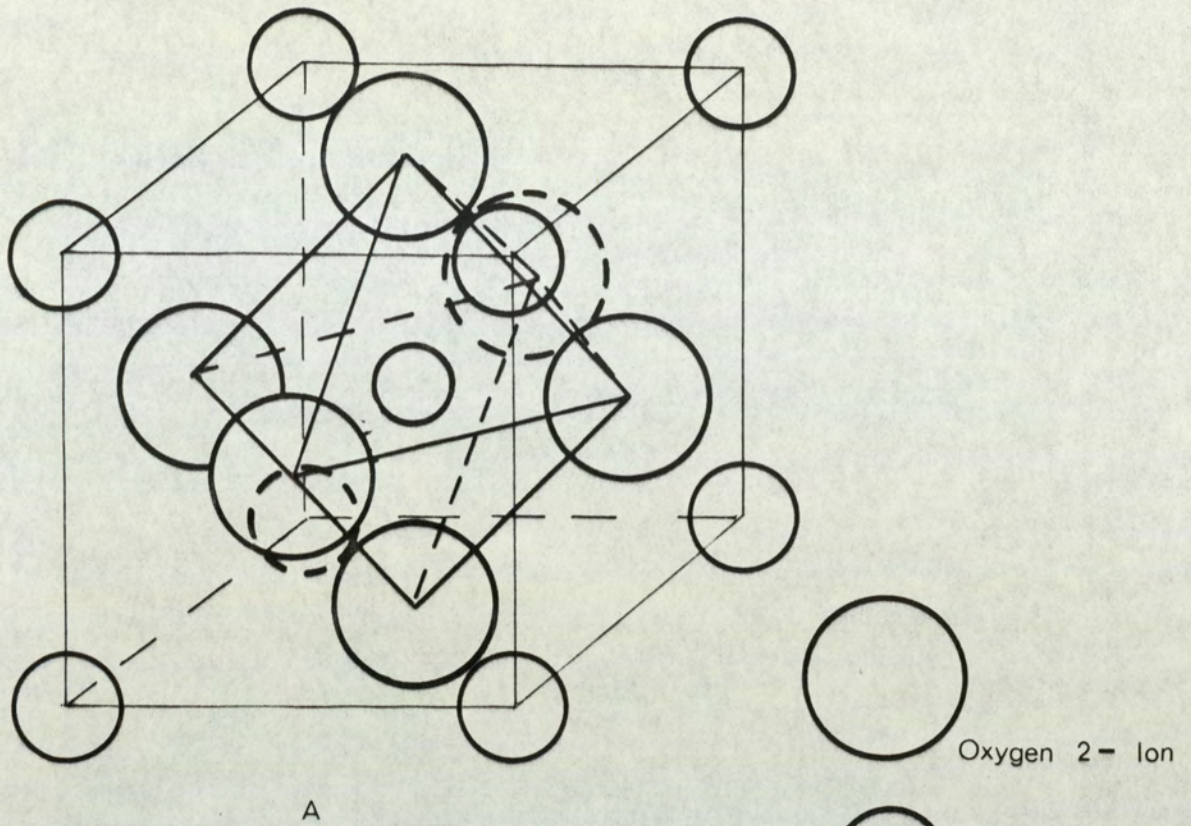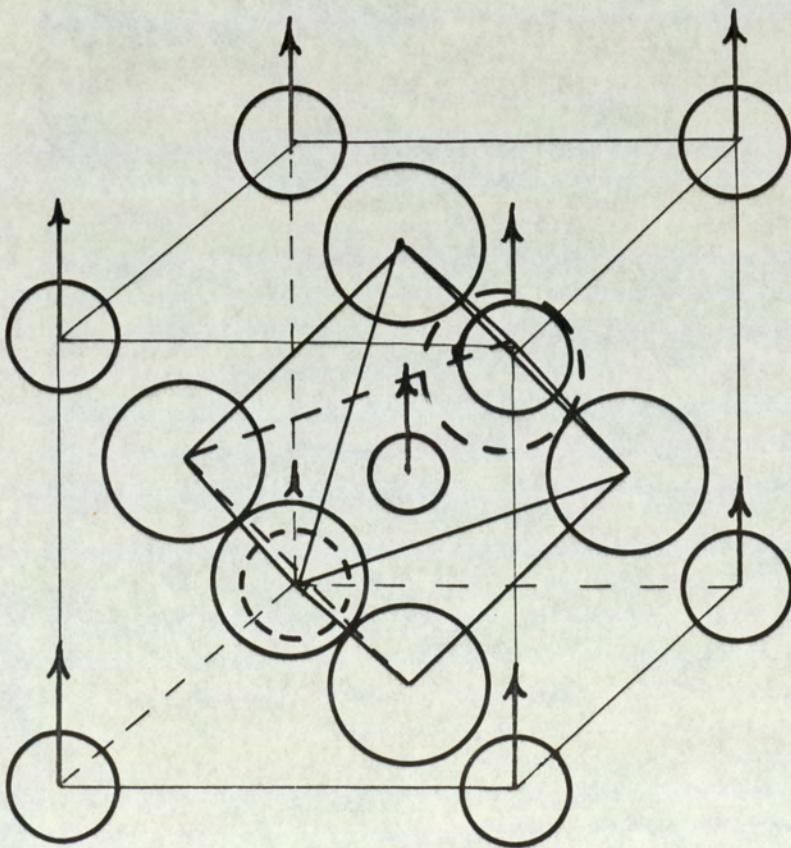
Figure 1.1 The Structure of Barium Titanate

centrosymmetrical tetragonal phase shown in figure 1.1b (Shirane, Danner and Pepinsky,1957).

Structural deformations are extremely common among the perovskites (see for example the $PbZrO_3-PbTiO_3$ system Sawaguchi, 1953) . In one case, a structural instability gives rise to antiferroelectricity. Here the dipole moments are arranged in opposite senses, and cancel leaving no net dipole moment per unit volume. This property is notoriously difficult to recognize, but is characterised in some cases by the high dielectric constants observed experimentally at low frequencies.

In reality the physical situation is more complicated than we have so far described,for atoms in solids do not remain stationary but vibrate in a localized region of space centred on their mean positions. The vibrations take place against the forces within the solid, and such forces must clearly have attractive and repulsive components which cancel at certain points to provide positions of stable equilibrium. These forces may be short range, like those in covalent crystals where electron sharing is responsible for the crystal cohesion, or long range like the Coulomb interaction found in ionic crystals, such as the alkali halides. Any scientific des- cription which attempts to explain the vibrational behaviour of the atoms in crystalline solids must therefore come to terms with this complexity.

The most convenient mathematical way of describing vibrational behaviour is to assume that all the atoms in a solid interact through forces which obey Hooke's law. This leads to the harmonic approximation in which the atoms vibrate in parabolic potential wells. The crystal as a whole may then be regarded as a system of independent sinusoidal waves called normal modes of vibration. If further the concept of quantisation is built into

the model so that each normal mode carries an energy $(n+\frac{1}{2})\hbar\omega$ (a phonon), then a description of the solid can be obtained which explains some of the salient features of its physical behaviour. Properties like specific heat capacity, phonon dispersion, elasticity, infra-red absorption spectra and the scattering of light by the Raman effect, for example, may all be immediately encompassed by this type of model. There are, however, certain properties which go beyond the scope of such a simple description. The pressure and temperature dependence of the elastic constants, thermal expansion and thermal conductivity depend on interactions between the phonons and to include these aspects of the behaviour of real solids, the model must be extended to include terms representing anharmonicity.

More recently it appears that there is an important connection between structural transitions and instabilities in certain normal modes of vibration, following a proposition by Cochran (1960) that the phonomenon of ferroelectricity in $BaTiO_3$ type compounds is directly associated with anomalous behaviour of a certain transverse optic vibration. This is best illustrated through the Lyddane-Sachs-Teller relationship (Lyddane et al.1941) which has been generalized by Cochran (1959a) to include structures containing several atoms per unit cell as

$$\frac{\varepsilon_o}{\varepsilon_\infty} = \prod_i \frac{\omega_{Li}^2}{\omega_{Ti}^2}$$

where ω_{Ti} and ω_{Li} are the normal mode angular frequencies of the ith transverse optic (TO) and longitudinal optic (LO) long wavelength vibrations. The temperature dependence of ε_o in $BaTiO_3$ is then explained by a decrease in the frequency of one particular TO vibration, a process which is known as "softening". Since 1960 experimental evidence on a number of compounds, using neutron

inelastic scattering, has confirmed this basic concept and it is now
thought that "soft modes" are the driving mechanism for many
structural transitions - see Shirane (1974) for an up to date
review.

1.2) The Spinel Compounds.

Compounds having a chemical formula of the kind AB_2X_4,
frequently crystallise with a structure related to that of the
mineral Magnesium Aluminate ($MgAl_2O_4$) known as Spinel. Usually
ionic in character, they are classified according to the anion
X^{2-} as oxide, sulphide, selenide and telluride spinels. In such
compounds charge neutrality is maintained through the cations A and
B which are most frequently 2+ and 3+ ions respectively, but other
configurations such as $Mg^{2+}_2 Ge^{4+} O_4^{2-}$ or $Na^+_2 W^{6+} O^{2-}_4$ are possible.
Evidently a large variety of metal ions may be substituted for A
and B and it is therefore perhaps not surprising that the spinels
are among the most extensive series of related chemical compounds
known. Indeed, more than two hundred different spinels have been
prepared and it is this chemical diversity, when combined with the
special character of the crystal structure (to be described) which
is responsible for the wide range of physical behaviour exhibited by
this remarkable family of compounds.

Important magnetic properties of practical importance
arise in spinels whenever transition ions like Fe^{3+}, Ni^{2+} or Co^{2+}
are present. For example, the spinel ferrites being simultaneously
both ferrimagnetic and electrically insulating are widely exploited
in the modern telecommunications industry, as their low eddy current
and hystersis losses make them useful materials for high frequency
applications. Other materials exploited in this way include
Magnetite which has been used as a coating for magnetic recording

tapes and certain manganese ferrites which are useful as magnetic switches and memory cores.

Among more recent applications is the use of single crystal Magnesium Aluminate as substrate material for the epitaxial growth of thin films of silicon and related semi-conductors (Manasevit and Forbes 1966). The same material is also used as the basis for an ultrasonic delay line at microwave fre-quencies.

A general review of the industrial applications of the spinel group of compounds has been given by Grimes (1975). For a comprehensive appraisal of the properties of the magnetic spinels see Smit (1971).

1.3) The Spinel Structure.

1.3.1) Space Group Fd3m.

According to the conventional description, the Spinel structure is based upon a nearly close packed cubic arrangement of the anions in which the metal ions occupy certain interstitial positions. The essential features of the unit cell, containing 8 molecular units shown in figure 1.2, were first described by Nishikawa (1915) and by W.H.Bragg (1915) who studied both $MgAl_2O_4$ and Fe_3O_4.

Two types of interstices arise, and in the arrangement described as the Normal structure, $^1/_8$ of the 64 possible tetrahedral positions (A-sites) are occupied by the divalent cations while $\frac{1}{2}$ of the 32 possible octahedral interstices (B-sites) contain trivalent ions. The local site symmetries and overall symmetry then correspond to the crystallographic space group Fd3m, the details of which are given in table 1.1. The cations are in special positions, and the structure is centrosymmetrical about
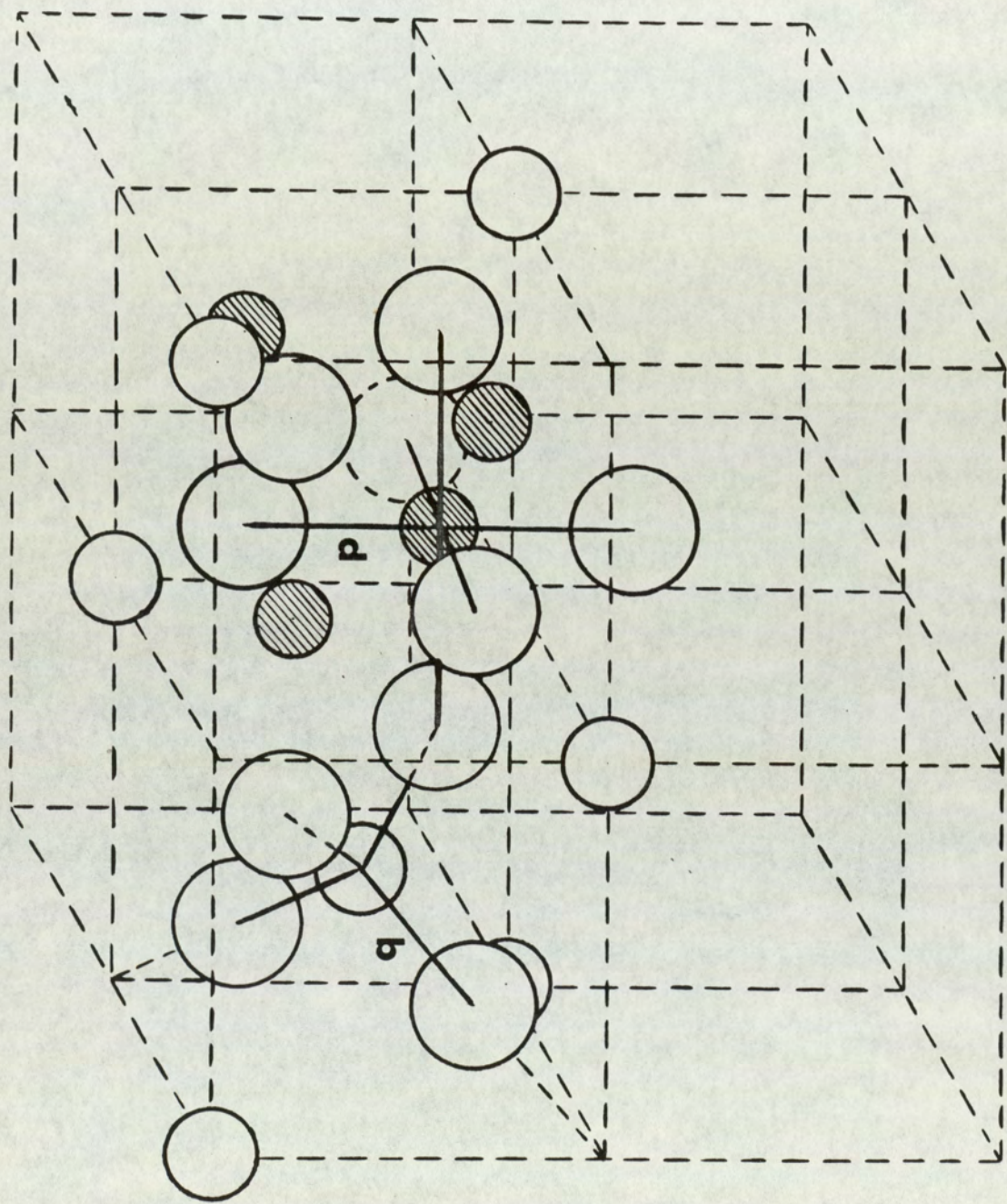
FIGURE 1.2 Spinel Structure (after Gorter, 1954)

the B-site. Since it is often useful to choose the latter as
origin of coordinates the atom positions for this case are also
given in Table 1.1. In either case, the anion positions are
specified in terms of a positional parameter, the u-parameter,
which, for an ideal spinel where the oxygen sublattice is perfectly
packed, and a conventional choice of origin, has a value of $^3/_8$.

In practice u is often larger, and for u > $^3/_8$ the anions
move in <111> directions outwards from the nearest tetrahedral site.
This movement destroys the perfect octahedral geometry surrounding
the B-sites and results in a distortion from cubic point symmetry
m3m, to the lower trigonal point symmetry $\overline{3}$m. Movement of the
anions in this sense also creates three different anion-anion se-
parations and for certain combinations of the lattice parameter (a)
and internal parameter (u) one of these bonds can be under severe
compression, so that there is a considerable overlap of the electronic
orbitals of these two anions. This has important consequences for
the structure and lattice dynamics of the spinel compounds which we
discuss in more detail in chapters 2 and 5.

In the description so far the cation distribution has been
assumed to be that corresponding to the Normal Spinel structure,
but other distributions of the cations over the A and B-sites are
possible of which one combination is known as the Inverse structure
(Barth and Posnjak, 1932; Wyckoff, 1951). In this case, half the
trivalent cations occupy the tetrahedral interstices while the
divalent cations together with the remaining trivalent cations share
those with octahedral surroundings. It is also possible for the
cation arrangement to be intermediate between these two situations
and the structure is then said to be partially inverted. Sometimes,
indeed, ordering of the various cations over the interstitial sites
can take place and this leads to other structures with quite different

Table 1.1

Space Group Fd3m : No.227

+ f.c.c translations $(0,0,0; 0,\frac{1}{2},\frac{1}{2}; \frac{1}{2},0,\frac{1}{2}; \frac{1}{2},\frac{1}{2},0;)$

(i) Origin at $\bar{4}$3m

No.of positions	point symmetry	Fractional Coordinates
8	$\bar{4}$3m	$0,0,0;$ $\frac{1}{4},\frac{1}{4},\frac{1}{4};$
16	$\bar{3}$m	$\frac{5}{8},\frac{5}{8},\frac{5}{8};$ $\frac{5}{8},\frac{7}{8},\frac{7}{8};$
		$\frac{7}{8},\frac{5}{8},\frac{7}{8};$ $\frac{7}{8},\frac{7}{8},\frac{5}{8};$
32	3m	$u,u,u;$ $\frac{1}{4}-u,\frac{1}{4}-u,\frac{1}{4}-u;$
		$u,\bar{u},\bar{u};$ $\frac{1}{4}-u,\frac{1}{4}+u,\frac{1}{4}+u;$
		$\bar{u},u,\bar{u};$ $\frac{1}{4}+u,\frac{1}{4}-u,\frac{1}{4}+u;$
		$\bar{u},\bar{u},u;$ $\frac{1}{4}+u,\frac{1}{4}+u,\frac{1}{4}-u;$

(ii) Origin at centre $\bar{3}$m

No.of positions	point symmetry	Fractional Coordinates
8	$\bar{4}$3m	$\frac{3}{8},\frac{3}{8},\frac{3}{8};$ $\bar{\frac{3}{8}},\bar{\frac{3}{8}},\bar{\frac{3}{8}};$
16	$\bar{3}$m	$0,0,0;$ $0,\frac{1}{4},\frac{1}{4};$ $\frac{1}{4},0,\frac{1}{4};$ $\frac{1}{4},\frac{1}{4},0;$
32	3m	$x,x,x;$ $x,\frac{1}{4}-x,\frac{1}{4}-x;$
		$\bar{x},\bar{x},\bar{x};$ $\bar{x},x-\frac{1}{4},x-\frac{1}{4};$
		$\frac{1}{4}-x,x,\frac{1}{4}-x;$ $\frac{1}{4}-x,\frac{1}{4}-x,x;$
		$x-\frac{1}{4},\bar{x},x-\frac{1}{4};$ $x-\frac{1}{4},x-\frac{1}{4},\bar{x};$

overall symmetries, see for example Cheary (1971).

According to this description then, any given cubic spinel structure may be characterized completely, within the space group Fd3m, by the three parameters, a,u and i the inversion, where the extent of the latter is believed to be a function of the Madelung energy, cationic size relative to interstitial site radius and the electronic configurations of the cations involved (Miller, 1959). The last factor mentioned here is connected with the crystal field effects which always arise when transition ions with non-spherical electronic ground states are present. According to McClure (1957) such ions are stabilized to an extent which depends upon the symmetry of their local environment, some environments being particularly favourable. In the case of the Spinel structure his calculations show that this effect gives rise to an octahedral site preference (see table 1.2) which for some ions, notably Cr^{3+}, is the dominant factor determining the cation distribution . Thus chromites, A Cr_2X_4, are invariably predicted to be Normal and this is in agreement with experimental observation.

Among other compounds, such as the ferrites, on the other hand, the balance between the different energy terms can be quite delicate so that the cation distribution in these cases can often be influenced by methods of preparation. $CoFe_2O_4$, for example, adopts the inverse structure when carefully annealed but is only partially inverted when quenched from the sintering temperature.

As will be discussed later, different arrangements of the cations over the two kinds of interstitial site leads to important changes in the Madelung energy and this in turn is be-lieved to account for the correlation between inversion and anion position parameter u. According to Gorter (1954), for example, Normal and Inverse compounds typically adopt structures with u = .387 and u = .380 respectively.

Table 1.2: Crystal field data for transition metal ions
(after McClure see text)

Number of electrons	Ion	Free Ion Russell-Saunders ground state	Stabilization (k cal)/mole energy Oct-site	Tet-site	Oct-site preference energy kcal/mole
1	Ti^{3+}	^2D	23.1	15.4	7.7
2	V^{3+}	^3F	30.7	28.7	2.0
3	V^{2+}	^4F	40.2	8.7	31.5
	Cr^{3+}	^4F	60.0	13.3	46.7
4	Cr^{2+}	^5D	24.0	7.0	17.0
	Mn^{3+}	^5D	35.9	10.6	25.3
5	Mn^{2+}	^6S	0	0	0
	Fe^{3+}	^6S	0	0	0
6	Fe^{2+}	^5D	11.4	7.5	3.9
	Co^{3+}	^5D	45	26	19
7	Co^{2+}	^4F	17.1	15.0	2.1
8	Ni^{2+}	^3F	29.3	6.5	22.8
9	Cu^{2+}	^2D	22.2	6.6	15.6
10	Zn^{2+}	^1S	0	0	0

1.3.2 Space Group F$\bar{4}$3m

As emphasized in section 1.1 the physical properties of solids are closely correlated with the spacial configuration of the atoms in their structures and the spinel compounds would normally be expected to conform with this general principle. Detailed consideration of the properties of a number of members of the spinel family have shown, however, that this is not the case (see sections 1.4, 1.5 and 1.6) and it was therefore proposed by Grimes (1971) that the symmetry of many of this class of compounds is more correctly described by the lower symmetry space group F$\bar{4}$3m, the details of which are given in table 1.3.

This alternative structure is acentric, for the 32 anions of the original unit cell now divide into two groups whose position coordinates are separately determined by parameters x_2 and x_3 respectively. The A-site cations, though retaining surroundings with tetrahedral symmetry and remaining at the same fixed positions as before, thus become crystallographically distinguishable. In addition, the B-site cations are no longer restricted to occupying the geometric centres of the oxygen octahedra but are allowed to move in a [111] direction, their displacements being controlled by a further positional parameter x_1. This latter displacement together with the division of the anions produces a different trigonal distortion at the B-sites so that the original inversion symmetry is removed.

The "ideal spinel" corresponds to $x_2 = {}^3/8$; $x_3 = {}^7/8$, $x_4 = {}^5/8$ and now when the anions are displaced from the perfectly packed configuration they again move in <111> directions but in the two groups to different extents. The combined effect of this together with that produced by x_1 is indicated by the arrows in figure 1.3. Finally, if parameters x_1, x_2 and x_3 are constrained

Table 1.3

Space group F$\overline{4}$3m : No. 216

+ f.c.c. translations $[0,0,0; \; 0,\tfrac{1}{2},\tfrac{1}{2}; \; \tfrac{1}{2},0,\tfrac{1}{2}; \; \tfrac{1}{2},\tfrac{1}{2},0]$

No.of positions	point symmetry	Fractional coordinates
4	$\overline{4}$3m	$0,0,0$
4	$\overline{4}$3m	$\tfrac{1}{4},\tfrac{1}{4},\tfrac{1}{4}$
16	3m	$x_1,x_1,x_1; \; \overline{x}_1,\overline{x}_1,x_1; \; \overline{x}_1,x_1,\overline{x}_1; \; x_1,\overline{x}_1,\overline{x}_1;$
16	3m	$x_2,x_2,x_2; \; \overline{x}_2,\overline{x}_2,x_2; \; \overline{x}_2,x_2,\overline{x}_2; \; x_2,\overline{x}_2,\overline{x}_2;$
16	3m	$x_3,x_3,x_3; \; \overline{x}_3,\overline{x}_3,x_3; \; \overline{x}_3,x_3,\overline{x}_3; \; x_3,\overline{x}_3,\overline{x}_3;$

B^{3+}

X^{2-}
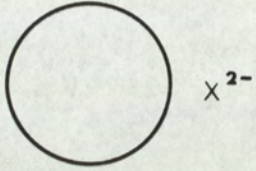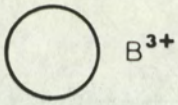
δ– parameters describe atom shifts from the
perfect configuration (see section 2.5)
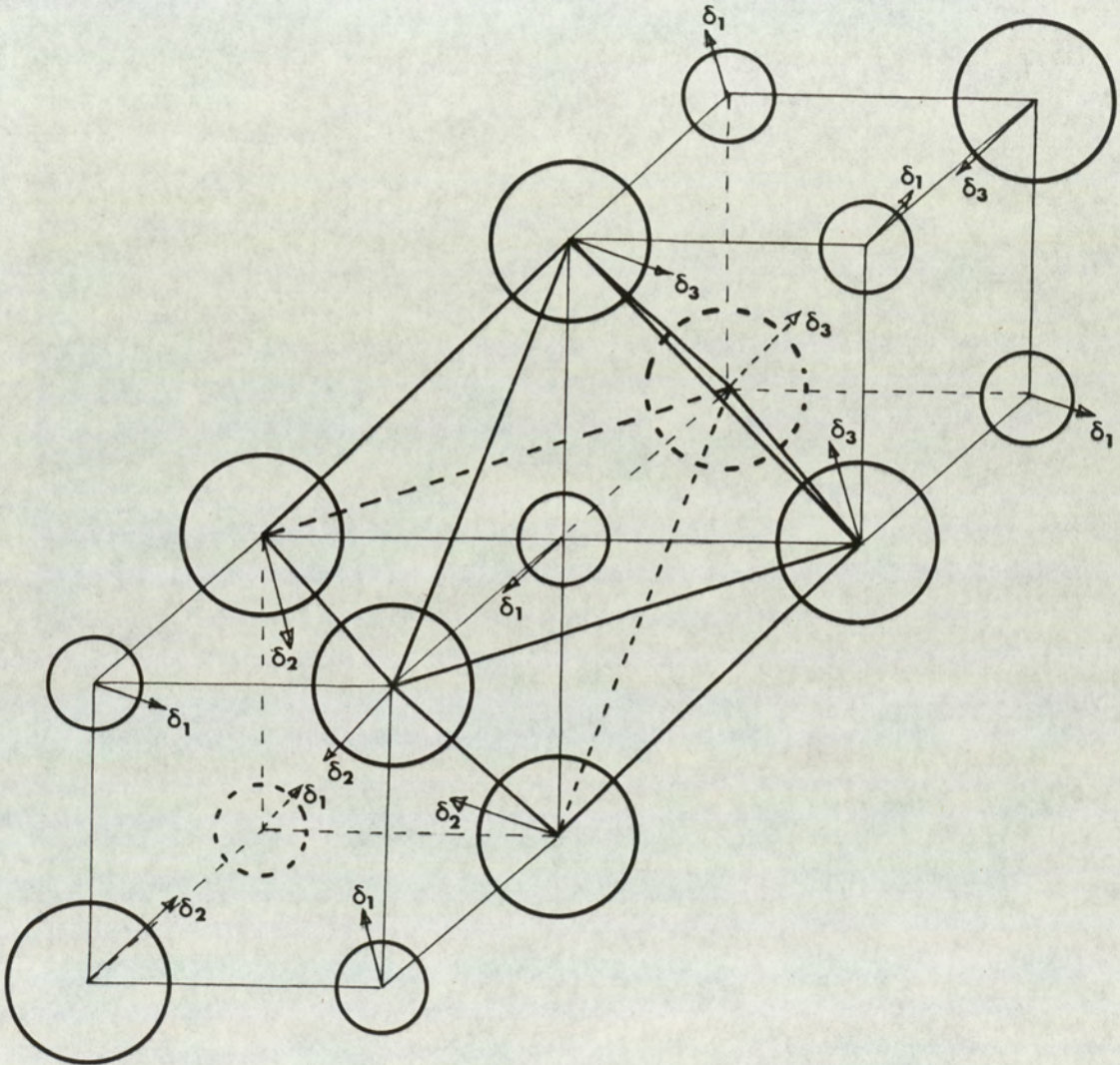
FIGURE 1.3   Octahedral site   under F$\bar{4}$3m Symmetry

so that $x_1 = {}^5/8$ and $x_3 = \frac{1}{4}-x_2$, then the symmetry once more corresponds to $Fd3m$.

1.4) Physical evidence in favour of $F\bar{4}3m$ symmetry.

1.4.1) Indirect evidence.

Crystallographic phase transitions are extremely common among the spinel compounds, the transformation usually involving a change from cubic to tetragonal symmetry with decreasing temperature. According to Dunitz and Orgel (1957) and Goodenough (1963) this may be understood as a manifestation of the Jahn-Teller effect, as the compounds concerned invariably contain transition ions like Cu^{2+}, Fe^{2+} or Mn^{3+} in which the electronic ground states are orbitally degenerate. In such spinels, it is believed that local structure distortions develop above the transition temperature in the cubic phase and that these increase in orientational coherence as the temperature decreases until their influence is eventually sufficient to induce an overall structural change (see for example Finch, Sinha and Sinha, 1958). The physical evidence supporting this description of the cubic phase includes the observation of Debye-Waller factor enhancement in x-ray diffraction (Cervinka, 1965), Mössbauer spectra (Tanaka, Tokoro and Aiyama, 1966) and complexities in the infra-red absorption spectra (Brabers, 1969). The latter are particularly significant as the additional absorption bands can be shown to correspond with those from a tetragonal spinel (e.g. Mn_3O_4) by examination of the spectra across a compositional range like $Mn_xFe_{3-x}O_4$.

In contrast to compounds of this kind, a cubic spinel series such as $Mg[Cr_x Al_{2-x}]O_4$ would be expected to be physically well behaved. The Cr^{3+} ion has the most marked octahedral site preference of any in the first transition series (table 1.2) and an

electronic ground state in octahedral surroundings with no orbital degeneracy, when Hund's rules are obeyed, i.e. no Jahn-Teller effect is expected. Nevertheless, X-ray diffraction studies by Grimes and Hilleard (1970) showed that increasing x in this series was accompanied by substantial increase in Debye-Waller factor in exactly analogous manner to the earlier observations of Cervinka on the Jahn-Teller series $Mn_x Fe_{3-x} O_4$. The conclusion was drawn that structural distortions must also exist in the chromite series and, moreover, that they must increase in severity with increase in chromium content.

Very similar conclusions were reached by Lou and Ballentyne (1968) from a study of the optical fluorescent spectra from a series of synthetic single crystals of the $Mg[Cr_x Al_{2-x}]O_4$ spinel group, an important feature of these spectra being, that above a chromium concentration of 2wt% a new selection rule is observed which identifies the symmetry of the octahedral site occupied by Cr^{3+} ions as 3m. The significance of the latter lies in the fact that it is incompatible with the crystallographic space group to which the spinel structure is normally referred but consistent with the X-ray diffraction observations, for if the local trigonal distortions had been of conventional $\bar{3}m$ symmetry an increase in severity would have been brought about through an increase in the oxygen position parameter u. According to Grimes and Hilleard, however, no change in this parameter was detectable within experimental error.

Experimental investigations of the electron spin resonance spectrum of the Cr^{3+} ion in natural Spinel (Stahl-Brada and Low, 1959) confirms local trigonal symmetry around the Cr^{3+} ion with a [111] direction as an axis of symmetry. However, as was emphasized by Henning and van den Boom (1973) electron spin resonance

does not clearly distinguish between trigonal point symmetries 3m and $\bar{3}$m, and the only indication of the former symmetry is that the splitting of the Cr^{3+} ion energy levels deduced for zero magnetic field indicates a stronger trigonal field than one would expect on the basis of the space group Fd3m. The latter assumes, of course, that the Cr^{3+} ion itself does not modify the B site provided by its host material, magnesium aluminate.

In experiments such as these in which magnesium aluminate is lightly doped with chromium, the local structural distortions might be expected to be dispersed among the octahedral sites according to the distribution of the Cr^{3+} ions, but it is possible, however, to envisage local 3m distortions which are organised in a regular periodic manner throughout the whole crystal (see figure 1.4). In the latter case, it is difficult to escape the conclusion that the distortion of the octahedral sites is something inherent in the Spinel structure which corresponds to a change of space group symmetry to $F\bar{4}3m$.

According to this view a change in physical behaviour through a spinel series can be understood as arising from a change in the degree of structural asymetry rather than as a change in the proportion of distorted to undistorted material and thus the change of space group was used by Grimes and Collett (1971a) to account for changes in the complexity of the infra-red absorption spectrum through the series $Mg[Cr_xA\ell_{2-x}]O_4$. Their observations, similar to those of Brabers (1969) on the Jahn-Teller series $Mn_xFe_{3-x}O_4$, were made on some polycrystalline samples previously investigated by X-ray diffraction (Grimes and Hilleard, 1970) and showed an increase in the number of absorption peaks from four in $MgAl_2O_4$ up to nine in $MgCr_2O_4$. Now it should be emphasized that the reproducibility of infra-red spectra from polycrystalline samples

[110]

[101]

[011]
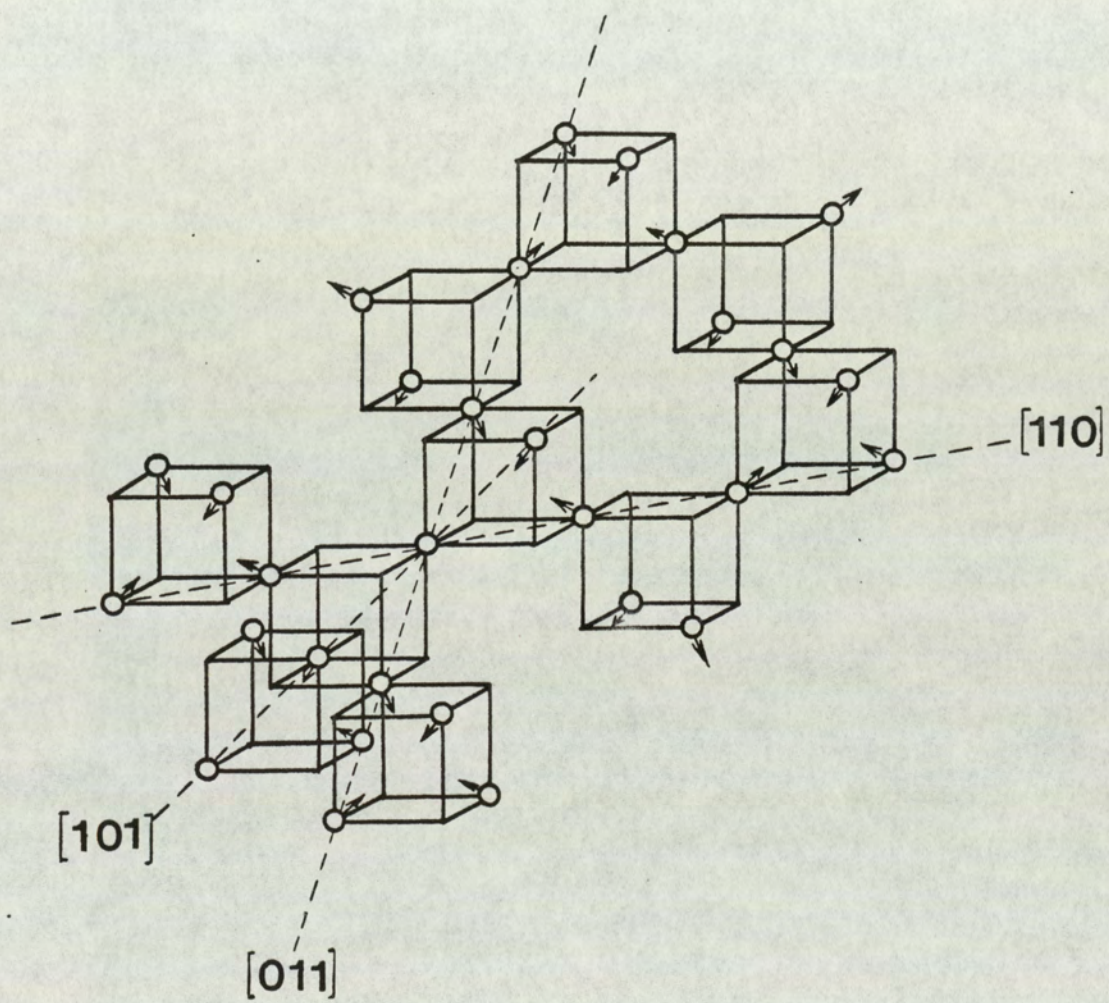
FIGURE 1.4   Octahedral ion sublattice

is not very good, for the number of peaks appearing and their shapes are influenced to some extent by particle size and methods of preparation [see for example in the case of the spinel compounds, De Angelis, 1969]. Nevertheless, it must be significant that similarly complex, though not identical spectra, have been reported for $MgCr_2O_4$, by several different observers (Hafner 1961; White and De Angelis, 1967; Tarte and Preudhomme, 1971) and that in no circumstances has a simple spectrum been observed from this compound.

In contrast to the observations of Grimes and Collett, it is interesting to note that studies of the infra-red spectra from the spinel series $Zn_xMg_{1-x}Cr_2O_4$ carried out by Tarte and Preudhomme (1963) reveal a decrease in complexity with increasing zinc content. Assuming that this indicates a reduction in the severity of the trigonal distortions, as Grimes (1971) points out, an almost distortion free $ZnCr_2O_4$ could then be expected and significantly, earlier examination of this compound by X-ray diffraction had yielded a Debye-Waller factor of $0.36A^2$ (Raccah, Bauchard and Wold, 1966) which is only one third of that observed with $MgCr_2O_4$.

Recapitulating then, the physical evidence from a number of different sources strongly supports the case for believing that structural distortions exist in the spinel series $Mg[Cr_xAl_{2-x}]O_4$. Moreover, it is evident that a unified and consistent explanation of all the related experimental facts is provided by referring the crystal structure to the space group $F\bar{4}3m$.

Now the possibility that the chromites are alone among the closely related spinel compounds in possessing a crystal structure of $F\bar{4}3m$ symmetry must be considered to be very unlikely and it was therefore suggested by Grimes (1971,1972a) that the

spinel structure might more generally be referred to $F\bar{4}3m$. It had been known for many years, for example, that some of the spinel ferrites have dielectric constants which can rise by several orders of magnitude, typically 10^2 to 10^4, at low frequencies (see for instance the observations of Polder (1960) on certain Mn-Zn and Ni-Zn ferrites) and it would seem natural to explain these observations in terms of permanent dipoles similar to those found in $BaTiO_3$. However, as Fairweather, Roberts and Welch (1952) realised, ferroelectricity is excluded by the centrosymmetric space group Fd3m to which the crystal structure had conventionally been referred and consequently the interpretation of low-frequency dielectric behaviour has presented considerable theoretical difficulties. In some cases, because measurements were made on polycrystalline specimens, it has been possible to explain the experimental observations in terms of a phenomenological model (Koops, 1951) where the dielectric is considered to be composed of good conducting crystallites separated by poor conducting intersurface layers. On the other hand, the resistivity and dielectric behaviour reported by van Uitert (1956) for certain Ni-Mn ferrites and by Peters and Standley (1958) for Mg-Mn ferrite appear to be quite different. The latter authors in particular were clearly seeking a crystallographic explanation as they state that (for $Mg_{0.1} Mn_{0.9} Fe_2O_4$) ... "The temperature and frequency dependence of the dielectric constant is very similar to that found when true dielectric relaxation is occurring ... and an explanation of the results ... in terms of the relaxation of permanent dipoles within the ferrite is envisaged. An order of magnitude calculation suggests that the high dielectric constant at low frequencies found at 200°C may be explained by the presence of permanent dipole moments of the order of 0.5 debye, indicating an effective charge separation of the order of $0.1\overset{o}{A}$."

These observations are clearly of considerable import-
ance in the context of the proposed change of space group for
spinel, for the order of magnitude of the ionic displacements en-
visaged by Grimes as responsible for the change of symmetry,
accounts precisely for the magnitude of the dipole moment estimated
by Peters and Standley.   Moreover, as emphasized by Grimes (1973a),
the symmetry of the ionic movements in $F\bar{4}3m$, shown in figure 1.4
is consistent with the absence of ferroelectricity noted by Fair-
weather et al. for the dipole moments, which are created are
arranged in opposite senses so that the property should be anti-
ferroelectricity.

1.4.2) <u>Direct evidence.</u>

In principle, it is possible to distinguish between the
two space groups proposed for spinel by conventional crystallo-
graphic methods, for reflexions of the type {hk0} with
$h+k = 4n \pm 2$ are systematically extinguished by the diamond glide
planes of the space group Fd3m, whereas they are allowed under
$F\bar{4}3m$ symmetry. Such "forbidden" reflexions have only been de-
finitely reported, however, following the observations of electron
diffraction patterns from single crystals. For example, the 200
and 420 reflexions have been observed with single crystals of
$MgAl_2O_4$ and $MgFe_2O_4$ by Hwang, Heuer, and Mitchell (1973) while
200, 420, 600 were reported for single crystal $MnFe_2O_4$ grown
epitaxially by van den Berg, Lodder and Mensinga (1976). The latter,
incidentally, provided a very nice confirmation of the inter-
pretation of the dielectric behaviour, of the polycrystalline
material of similar composition, proposed by Peters and Standley
(see section 1.4.1).

The electron diffraction technique has been criticised
as inappropriate when used in this way because the unusually

short wavelength at high voltages leads to severe multiple diffraction effects and therefore ambiguous interpretation. However, elegant experimental procedures have been adopted in the case of spinel to totally eliminate the multiple diffraction process as a source of intensity for the forbidden reflexions. The trick as Hwang et al. realised is to choose a specimen with [00$\bar{1}$] orientation for then only reflexions of the type h,k = 2n can occur in the zero layer of reciprocal space and, providing suitably thick crystals are chosen, it is impossible to obtain reflexions of the type h+k = 4n $\pm$ 2 by double diffraction. The possibility that the forbidden reflexions arise from higher order wavelength contamination may also be excluded as the voltage in an electron microscope is stabilised to an exceptional degree (1 part in 10^7), i.e. the electron wavelength is extremely well defined.

Unfortunately the electron diffraction technique does not lend itself readily to structural analysis, but from comparing ratios of intensities Heuer and Mitchell (1975) have estimated the extent of the off-centring of the $A\ell^{3+}$ ion to be just less than 0.01$\overset{o}{A}$.

These results, of course, do not exclude the possibility that the reflexions may be thermally excited. It is well known, for example, that if the cohesive forces have a considerable anharmonic component then reflexions can be produced which ordinarily would be accidental absences of the space group (see for example, the classic case of the 222 reflexions of diamond [Dawson and Willis, 1967] and silicon [Keating, Nunes, Batterman and Hastings, 1971].

In the case of neutron and X-ray diffraction on single crystals of Spinel, finite intensity is observed at the positions corresponding to the forbidden reflexions, but it proves difficult to eliminate multiple diffraction effects particularly at wave-

lengths which are suitable for revealing structural detail (see for example section 2.2.4. The effect is more serious in neutron diffraction than with X-rays, the dispersion spread for the latter being at least two orders of magnitude smaller than the former, i.e. $\delta\lambda/\lambda$ (neutrons) $\sim$ 1% whereas $\delta\lambda/\lambda$ (X-rays) $\sim$ 0.01% because of the sharpness of the characteristic lines. Thus careful experiments are required to eliminate multiple scattering of neutrons as a source of intensity for these reflexions. Such experiments have been performed on magnesium aluminate (Samuelsen and Steinsvoll 1975) and Magnetite (Samuelsen, 1974). In both cases attention was centred on the 0.0.2 reflexion but the results showed negligible intensity. This does not exclude the space group $F\bar{4}3m$, however, since it is possible to envisage suitable atom shifts, to both sets of oxygen ions and the octahedrally coordinated cation, which would in any case make the intensity for the 0.0.2 reflexion vanishingly small (see Heuer and Mitchell 1975).

Perhaps the most remarkable direct evidence for $F\bar{4}3m$ symmetry is provided by a recent structure analysis of the normal 2-4 spinel γ - $Ni_2Si\,O_4$ where the presence of a residual electron density in the final Fourier difference synthesis was revealed (Marumo, Isobe, Saito, Yagi and Akimoto, 1974). In this case, intensities were collected using $MoK\alpha$ X-radiation and 212 independent reflexions were used in a least squares refinement based on the space group $Fd3m$ to achieve an overall reliability index R = 1.7% with individual anisotropic temperature factors. The final Fourier difference synthesis showed eight quite prominent peaks $0.46\overset{o}{A}$ from the Ni ion in the 8 [111] directions. The height of these peaks was on average about $2e\overset{o}{A}{}^{-3}$ and the authors attributed their existence to the charge density asymmetry around the Ni^{2+} ion. However, a simpler interpretation based on the space group $F\bar{4}3m$ now seems more likely.

1.5) Distortion mechanism.

As explained in section 1.4.1, the Cr^{3+} ion in an octahedral environment would not be expected to be subject to the Jahn-Teller effect when in its normal electronic ground state. Confirmation of the latter may be obtained from measurements of magnetic susceptibility and in the case of $MgCr_2O_4$ in which it is believed that the structural distortions are exceptionally marked, such measurements have shown that the Cr^{3+} ion is indeed in its normal "high spin" state (Lotgering, 1962). The Jahn-Teller mechanism for producing structure distortions is then eliminated in this case and by analogy with the behaviour of small impurity ions in alkali halides it was therefore suggested by Grimes (1971) that the Cr^{3+} ion displacements might be produced through the local electrostatic potential conditions at the B sites.

These ideas were supported particularly by the case of $ZnFe_2O_4$ where the calculations of Hudson and Whitfield (1967) and experimental studies of ^{57}Fe Mössbauer spectrum by Evans, Hafner and Weber (1972) showed that the potential at the centre of an octahedral site is a maximum and thus by symmetry that there must be, in fact, two positions of minimum energy lying either side along a [111] axis through the site (Grimes 1974b). A large cation in such a situation (see figure 1.5) would be held at the centre of symmetry through the repulsive interactions with neighbouring anions but smaller cations such as Fe^{3+} or Cr^{3+} might be able to move nearer to positions of minimum energy and would thus become displaced off-centre (Grimes 1971; 1972a).

Detailed confirmation of the mechanism clearly can only come through careful refinement of the structure parameters of a series of spinel compounds, ideally at several different temperatures. Nevertheless, a rough indication that the above description is along

Δ = Barrier height
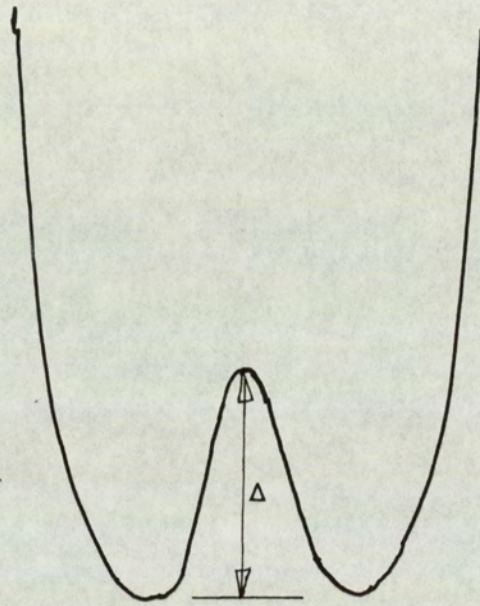
FIGURE 1.5   Potential energy distribution   along   a   [111] axis

through   an   octahedral   site

the right lines has been obtained by Grimes (1972a) from a simple
analysis of the presently available Debye-Waller factor data
from X-ray diffractions studies of zinc and cadmium spinels. For
these compounds it was assumed that a Debye Waller factor more
representative of the vibrational character of each structure could
be estimated from the monatomic relation,

$$B = \frac{6h^2 T}{\bar{km}\theta^2} \left[\phi \left(\frac{\theta}{T} \right) + \frac{\theta}{4T} \right]$$

(see International Tables, volume 2) providing $\bar{m}$ was interpreted
as mean atomic weight and θ estimated from the four most prominant
infra-red absorption bands. The excess Debye-Waller factor for each
zinc or cadmium compound could then be derived by comparison with
the corresponding X-ray diffraction data and as figure 1.6 shows
there is then quite a good correlation with the radius corresponding to the
octahedral nearest neighbour distance.

It should be noted finally, that such a mechanism also
accounts quite naturally for the difference between the infra-red
absorption spectra of magnesium and zinc chromite without invoking
special properties for the Cr^{3+} ion. On the new view, the increase
in anion "u" parameter following the introduction of the Zn^{2+} ion
onto the tetrahedral site, together with the smaller lattice constant
of $ZnCr_2O_4$ must lead to a smaller volume being available to the Cr^{3+}
ion and therefore to a closer approximation to Fd3m symmetry. A
similar argument would apply to the $A\ell^{3+}$ ion in $MgA\ell_2O_4$ for
although this ion is smaller than the Cr^{3+} ion a considerable re-
duction in the lattice parameter occurs with decreasing x in the
series $Mg[Cr_x A\ell_{2-x}]O_4$.
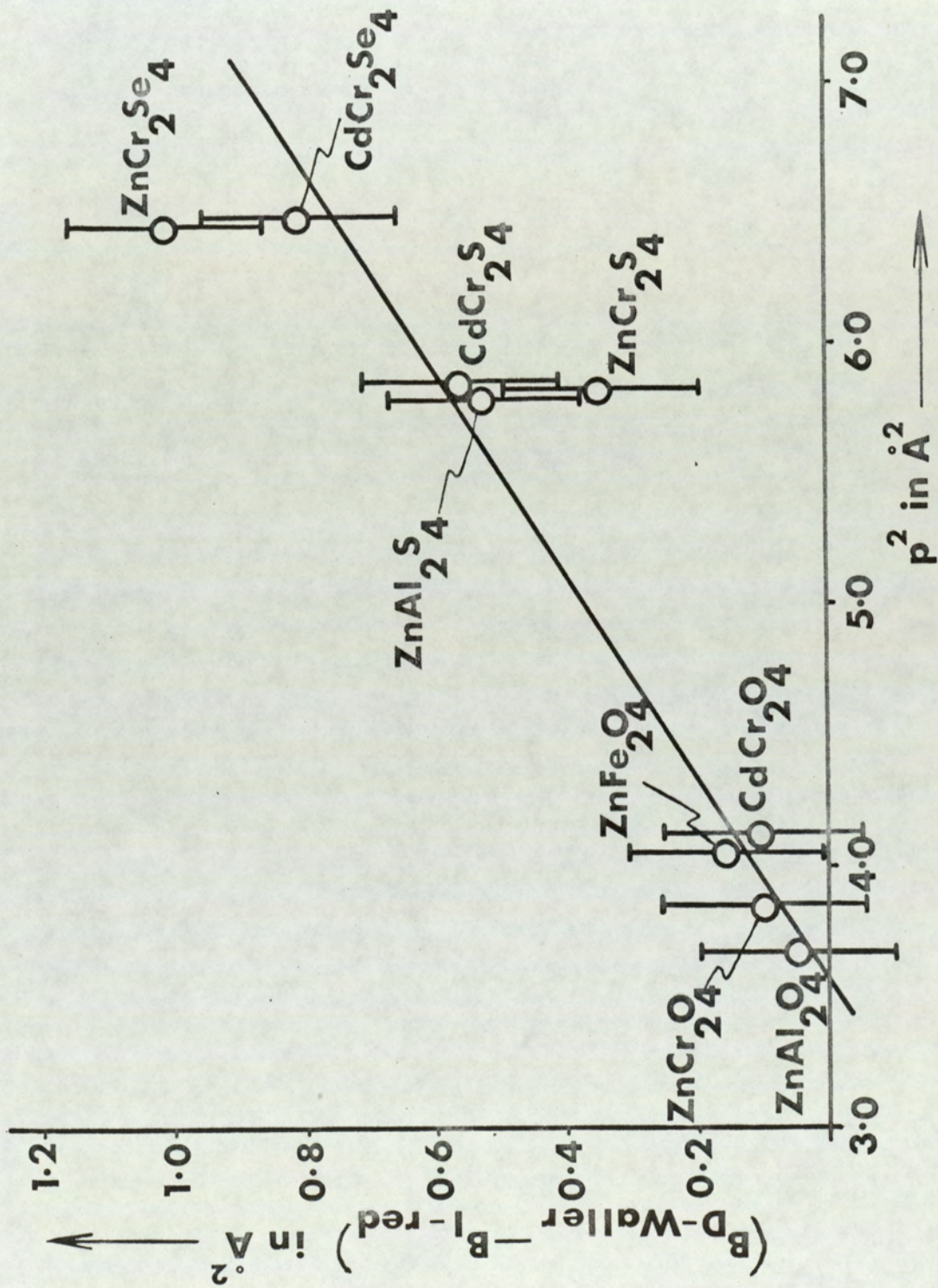
FIGURE 1.6 Excess Debye–Waller factor against octahedral site radius squared

1.6) Dynamic properties.

1.6.1) Ultrasonic measurements.

Ultrasonic measurements of the velocities of sound and therefore of the elastic constants have been made on a number of spinels and this has provided further insight into the nature of the phase transitions occurring in these compounds. In $NiCr_2O_4$ for example, a Jahn-Teller system, there is a remarkable relaxation of the $T_1 [110]$ mode as the temperature decreases towards 310°K below which this material becomes tetragonal (Kino,Lüthi and Mullen,1973).

The possibility of such relaxations was first emphasized by Born (1940) who pointed out that for cubic crystals the elastic constants must satisfy the conditions

$$C_{11} + 2C_{12} > 0$$

$$C_{11} - C_{12} > 0$$

$$C_{44} > 0$$

for mechanical stability. Any structural defect may lead to an elastic relaxation corresponding to one of these conditions and the symmetry of the defect may then be inferred from the selection rule observed (Heller and Nowick, 1965). Thus in the Jahn-Teller spinels which generally transform to tetragonal symmetry, at sufficiently low temperatures, it is the mode corresponding to $(C_{11}-C_{12})$ which relaxes.

Other spinel compounds, however, behave quite differently. Ultrasonic investigations on $ZnCr_2O_4$, for example, (Kino and Lüthi, 1971) show a softening of the shear mode elastic constant C_{44} in the neighbourhood of 40°K, which is consistent with the presence of a defect with trigonal symmetry and therefore with the off centr ing of the Cr^{3+} ion along a [111] direction. Similar observations have been made on $NiFe_2O_4$ (Gibbons, 1957) and on Magnetite, Fe_3O_4 (Moran and Lüthi, 1969).

The latter material is particularly interesting, for Magnetite actually undergoes a phase transition at 119°C in which the lower temperature phase was, at one time, believed to be of orthorhombic symmetry (Bickford, 1953; Hamilton 1958). More recent evidence, however, (Vieland, 1975; Iizumi and Shirane, 1975) has confirmed the initial interpretation of Rooksby and Willis (1953) who concluded that the low temperature form of Magnetite has trigonal symmetry.

1.6.2) Infra-red absorption spectra.

In the absence of any complete and adequate description of the lattice dynamics for compounds with the spinel structure the interpretation of the infra-red spectra since 1955 has been based on a theory proposed by Waldron (1955). In this model the two molecules in the rhombohedral primitive unit cell are divided into three groups namely, two AO_4 tetrahedra comprised of four oxygen ions each with an A cation at the centre and one B_4 tetrahedron the latter being composed of the four octahedral cations. The vibrations of each of these groups are then classified according to the species of the point group Td or $\bar{4}3m$ which is also supposed to be appropriate for the vibrations of the crystal as a whole. Waldron was thus led to the conclusion that there should be four infra-red active modes of vibration.

Since Waldron's paper, extensive experimental investigations have confirmed the presence of four primary infra-red active absorption peaks (see White and De Angelis (1967) for a useful review). These are, however, often accompanied by a number of weaker peaks or shoulders (Hafner 1961). In a few cases, as explained in section 1.4.1, it has been possible to relate these extra peaks to the presence of structural distortions associated with the B-site but mostly their origin has remained unexplained.

Few attempts have been made to account for the infra-red spectrum in terms of the vibrations of the crystal lattice as a whole, a fact attributable, no doubt, to the almost complete absence of any detailed phonon spectra on these compounds, which in turn is probably due to the difficulty of obtaining suitably large single crystals of spinel oxides on which neutron inelastic scattering measurements can be performed. Indeed, Magnetite is the only spinel compound so far where some detail of the low energy phonon dispersion system has been uncovered (Samuelsen and Steinsvoll, 1974). The inertia to set up dynamical models to describe the vibrations of these compounds has therefore been considerable. Without experimental data on the acoustic and low energy optic modes of vibration it is virtually impossible to obtain reliable information even from the simpler dynamical models, such as the rigid ion model of Kellermann (1940), for in the case of spinel even this model contains twelve adjustable parameters (see Chapter 5).

The first attempts to account for the infra red spectrum of Spinel in this conventional manner were made by Striefler and Barsh (1972). No phonon measurements existed on this compound at that time and this, coupled with the fact that forty two modes of vibration are expected in Spinel, makes the interpretation of the infra-red spectrum rather formidable. Nevertheless, Striefler and Barsh attempted to fit the observed infra-red and Raman spectra at zero wavevector using the rigid ion model. Their results are in poor agreement with the observed peaks except where the model was constrained to fit. This is perhaps not surprising for earlier results of other workers on simpler ionic compounds have shown that the rigid ion model can be in error as much as 50% for optical modes.

Prior to this work, a quite different interpretation had been proposed by Grimes (1974b) in which both prominent and

minor features of the infra-red spectrum were accounted for on a two-phonon mechanism. According to this view the absorption peaks correspond to critical points on the surface of the Brillouin zone rather than to the zone centre Γ.

In the case of a two-phonon process, wave vector conservation requires that $q_1 \pm q_2 \approx 0$ and energy conservation that $\hbar\omega_1 + \hbar\omega_2 = \hbar\omega$ where ω_1, ω_2 and ω are the angular frequencies of the two phonons and the incident photon respectively. Grimes noted that if the phonons concerned were acoustic then the energies at the Brillouin zone boundary as calculated from the known elastic constants (and assuming negligible dispersion !) were approximately half the energies of the infra-red bands and that a correspondence between the two could be obtained along the lines indicated in table 1.4.

In this connection it should be noted that overtones, i.e. two phonon processes involving phonons from the same branch, are not permitted when the space group is centrosymmetrical (e.g. Fd3m) but could occur if the space group were $F\bar{4}3m$. For example, two-phonon overtone states are forbidden for diamond (Fd3m symmetry) but permitted within the selection rules for zinc blende ($F\bar{4}3m$ symmetry) [Johnson, 1965]. Thus, the correct interpretation of the infra-red absorption spectrum from Spinel is intimately tied up with the problem of correct space group assignment.

1.6.3) Measurements of heat capacity.

The contribution from the lattice to the specific heat of a crystalline solid depends on the phonon density of states and providing this is known, for example from measurements of the phonon dispersion curves, it is then possible to evaluate the heat capacity. It is also well known that discontinuities in the density of states

Table 1.4: Correlation of infra-red and phonon energies
(after Grimes, 1972a)

Infra-red spectrum	Acoustic phonon spectrum			Twice phonon energy	
Grimes and Collett	Branch	Critical point	Energy		
(eV)			(eV)	(eV)	
.089*	L(111)	L	.047	2L	.094
.089	L(001)	X	.045	2L	.090
.065	T1(110)	X	.030	2T1	.060
.038	T(111)	L	.023	2T	.046

* minor feature in i-r spectrum

function, known as van Hove singularities (van Hove, 1953) corres-
pond to critical points on the phonon dispersion curves and that
the frequencies of the latter can be identified in the infra-red
absorption spectrum when this arises from two-phonon processes (see
for example, Johnson and Loudon, 1964).

In the case of $MgA\ell_2O_4$, the primary infra-red absorption
bands arise from two-phonon processes according to Grimes (see
section 1.6.2) and he therefore proposed a simulated density of
states leading to an expression for the heat capacity of the form

$$C_v = 2E\left(\frac{\theta_1}{T}\right) + 2D\left(\frac{\theta_2}{T}\right) + 2E\left(\frac{\theta_3}{T}\right) + D\left(\frac{\theta_4}{T}\right)$$

where $\theta_n = h\nu_n/k$ were determined from the four frequencies ν_n
of the infra-red absorption spectrum. This theoretical heat capacity
is compared with the experimental data of King (1955) in figure 1.7
which also shows the equivalent density of phonon states. The fit
to the experimental heat capacity is truly remarkable but great
caution should be observed in drawing conclusions from this, as the
heat capacity is fairly insensitive to the density of states function.
Nevertheless, it must be significant that this same formula has also
proved adequate for the estimation of the lattice contribution to the
heat capacity in several ferrites (Grimes 1974a). The case of zinc
ferrite is particularly interesting as this compound appears to exhibit
a Schottky anomaly which has been interpreted by Grimes (1974b) to
provide an estimate of the height of the potential barrier at the
centre of the octahedral sites. In $ZnFe_2O_4$ the barrier height works
out at $14.8 \pm .5 * 10^{-3}$ eV so that when the thermal energy is of this
order the Fe^{3+} ions are presumably able to hop between the two
equivalent minima.

Simulated density of phonon states
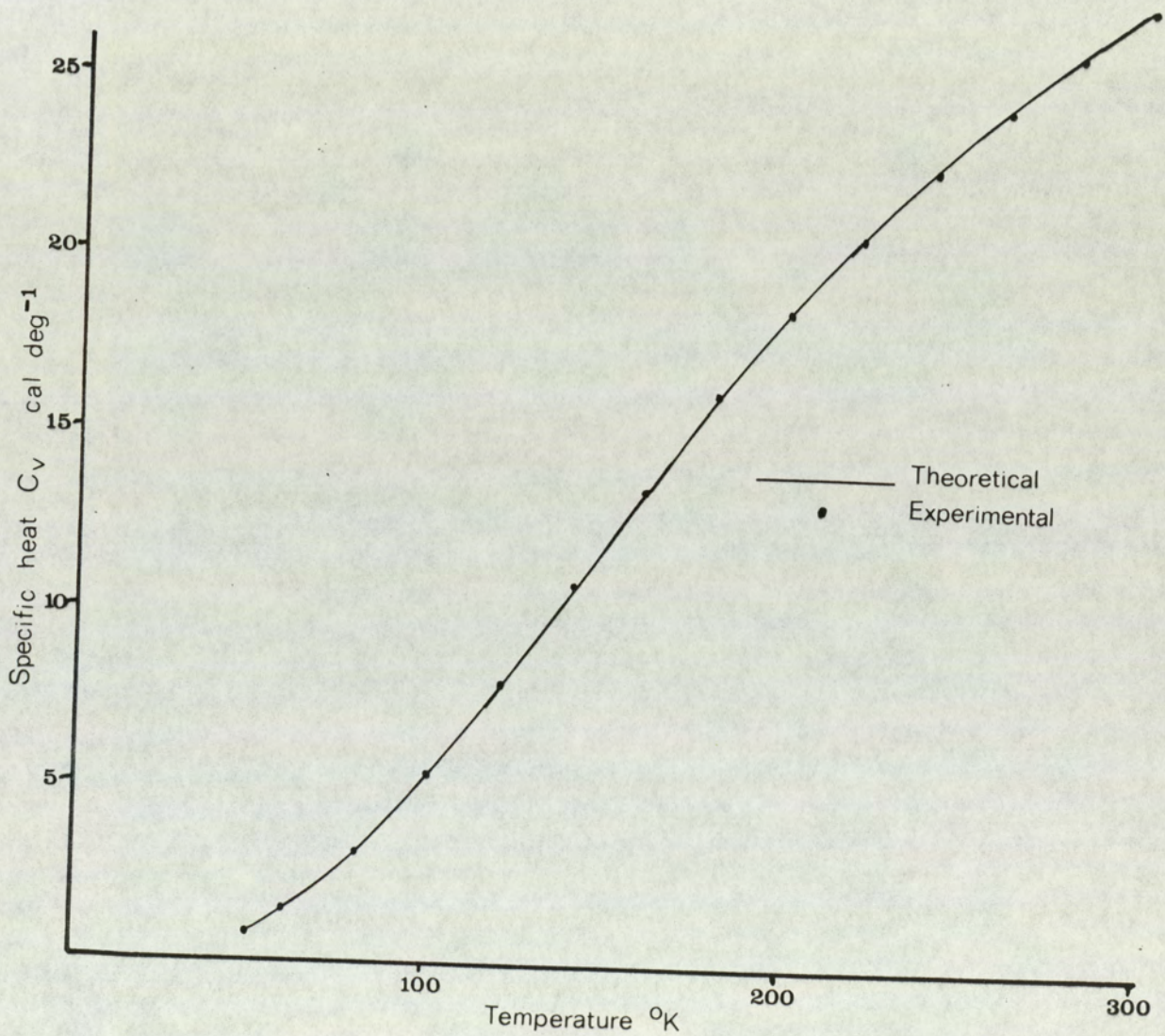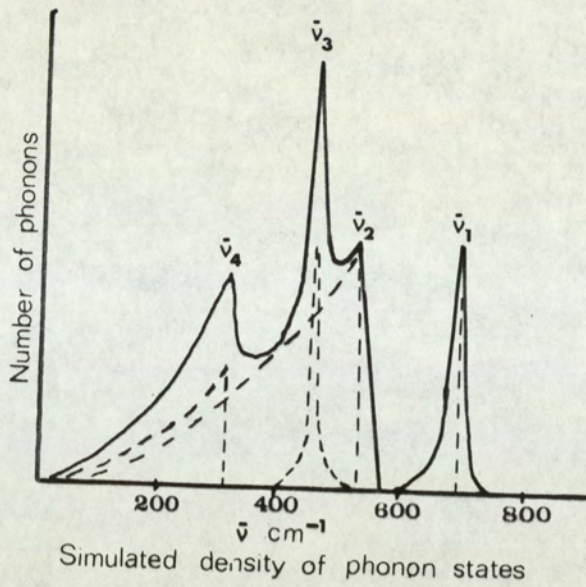
Figure 1·7 Specific heat of $MgAl_2O_4$

1.7) <u>Scope of the present work.</u>

In spite of considerable technological and scientific interest in the spinel group of compounds and extensive investigation of a wide range of their properties it is surprising to discover that their physical behaviour is really rather poorly understood. In many cases the problems are intimately connected with the lattice dynamics of the spinel structure on which very little information has been derived to date. Present knowledge as described in sections 1.6.1 and 1.6.2, is limited to a few measurements of the velocities of sound and to the observation of the infra-red absorption spectra - the latter obtained chiefly from samples of polycrystalline material. Inelastic neutron scattering studies have been made on only one material to any extent - Magnetite, Fe_3O_4 (Watanabe and Brockhouse 1962; Samuelsen and Steinsvoll, 1974 - the latter appearing after the commencement of the present work) and even here, results have been limited to an investigation of the acoustic and low lying optical modes.

In the work to be described the major objective has been to carry out an investigation of the acoustic phonon dispersion system in Magnesium Aluminate by inelastic neutron scattering and to construct a theoretical model of the dynamical behaviour of the same material along the lines of the rigid ion Kellermann theory for sodium chloride. The experimental results from both Fe_3O_4 and $MgA\ell_2O_4$ have been correlated with the aid of the adjustable parameters of this model and an initial indication of the disposition of the complete dispersion system of phonon branches has been obtained in each case. The corresponding eigenvectors have been used to identify those branches expected to be infra-red active.

Finally in view of the very extensive indirect physical evidence favouring a crystal structure with $F\bar{4}3m$ symmetry for the

spinel group of compounds and the direct evidence for this symmetry in the case of $MgAl_2O_4$ in particular (Hwang, Heuer and Mitchell, 1973; Heuer and Mitchell, 1975), it seemed worth attempting a more complete structure analysis based on single crystal diffraction data such as might provide the detailed information on atom positions so lacking at the present time. This investigation was based on measurements obtained through conventional X-ray and neutron diffractometry and is described in Chapter 2.

CHAPTER 2

REFINEMENT OF THE STRUCTURE PARAMETERS FOR SPINEL.

2.1) Introduction.

Because Bragg reflexions of the type {hko} with $(h+k) = 4n \pm 2$ are systematically extinguished by the diamond glide planes in Fd3m but permitted in $F\bar{4}3m$, the problem of deciding to which space group Spinel properly belongs is apparently quite straightforward. However, when the atomic displacements responsible for the difference of symmetry are very small and when more than one kind of atom can contribute to the "forbidden" reflexions so that the intensity of some of the latter are in any case vanishingly small, the problem assumes quite a different order of difficulty. In addition, because of the very high symmetry of both Fd3m and $F\bar{4}3m$ space groups, it turns out that multiple diffraction effects are unusually important and this further complicates the problem of detecting the decisive "forbidden" reflexions (see 2.2.4 below).

This last difficulty had not been realised at the outset of the present study. It was thought, indeed, that the ideal technique for the study of the small structural distortions believed to exist in $MgA\ell_2O_4$, following the work of Hwang, Heuer and Mitchell, would be neutron diffraction. It was known, for example, that the overall fit to structural data was often superior in neutron diffraction than in X-ray diffraction (see for instance Coppens, 1968). Moreover, following the early work by Bacon (1952) it was known that neutrons could distinguish Magnesium and Aluminium atoms, while the difference between the X-ray scattering factors of these two elements was thought to be too small to distinguish experimentally. Thus, neutron diffraction would provide an estimate of the extent of the inversion in $MgA\ell_2O_4$ which would otherwise have remained an unknown quantity.

The initial experiments in neutron diffraction with some 3mm cube samples of $MgA\ell_2O_4$ (cut from larger melt grown single

crystals obtained from R.R.E. Malvern) revealed two practical
difficulties of totally unexpected magnitude namely multiple
diffraction and extinction. Investigations of the former showed
immediately that although it might be possible to detect one or two
"forbidden" reflexions given access to neutrons of much longer wave-
length (the first experiments used $\lambda = 1.181\overset{o}{A}$) it would not be
possible to make such measurements at any wavelength adequate for
revealing the suspected structural detail corresponding to $F\bar{4}3m$
symmetry. A structure parameter refinement based on neutron
diffraction data would therefore have to rely on careful intensity
measurements of reflexions whose presence could be unambiguously
recognised i.e. on the conventional spinel reflexions alone.

Extinction effects, similarly, were so severe that some
correction for this aberration was clearly essential. In the
initial experiments, for example, dramatic intensity variations
were observed among the Bragg reflexions which are symmetry
related i.e. equivalent. Since it was hoped eventually to exploit
the existence of a large number of equivalents in Spinel a spherical
crystal sample would have been advantageous but at that time this
was thought too difficult to produce because of the hardness of
the material (Spinel has a hardness of 8 on Mohs' scale).

The greatest difficulty in practice, however, turned out
to be the problem of obtaining access to neutrons with a wave-
length short enough to permit the collection of high order data.
The D9 instrument at the Institut Max von Laue-Paul Langevin
(I.L.L) would have been ideal since this was mounted on a hot source
with wavelengths in the range $0.6-0.8\overset{o}{A}$ but demand for this instrument
was too great so that measurements eventually had to be made on the
D15 four circle diffractometer with a wavelength of $1.176\overset{o}{A}$.

Realisation that these difficulties might preclude a
decisive result on the symmetry question for $MgA\ell_2O_4$ led to

further consideration of the use of X-ray diffraction. However, facilities for the study of single crystals at Aston were severely limited so that collaboration with another crystallographic group had to be arranged. Fortunately, at this time, a group at the H.H.Wills Laboratory in the Physics Department, University of Bristol, under the direction of Dr.H.F.Kay were interested in the reproducibility of intensity data derived from their new Nonius four-circle, computer controlled, X-ray diffractometer, and were looking for single crystals with high symmetry (providing a large number of equivalent reflexions) as potential test specimens. A collaboration was therefore agreed whereby the Bristol group would carry out a program of measurements over half a hemisphere of reciprocal space using Molybdenum Kα radiation and a spherical single crystal to be provided by Aston who would also carry out an assessment of the data and the refinement of the structure parameters.

Thus, two sets of data were ultimately obtained, one set being through neutron diffraction and the other through the X-ray diffraction technique. The former are described in section 2.3 and the latter in 2.4 and a comparison of the results obtained is made in 2.5. But first we discuss the practical difficulties in more detail.

2.2) Practical difficulties.

2.2.1) Scattering form factors.

According to the kinematical theory of the diffraction of X-rays (James 1948) and neutrons (Bacon 1962) the integrated intensity of the h.k.ℓ planes from an infinitesimal volume δV is proportional to δV, thus,

$$\rho_{hk\ell} = Q \, \delta V \qquad\qquad 2.1$$

where Q is the well known reflexion coefficient which has the form,

$$Q = \left(\frac{e^2}{mc^2}\right)^2 N^2 \lambda^3 Lp \ |F_{hk\ell}|^2 \qquad 2.2$$

for X-rays and,

$$Q = N^2 \lambda^3 Lp \ |F_{hk\ell}|^2 \qquad 2.3$$

for neutrons. In these expressions e^2/mc^2 is the classical radius of the electron, N is the number of unit cells per unit volume and λ the wavelength of the incident radiation. The Lorentz factor L, is a function of the angle θ at which ρ is observed: it depends on the diffraction geometry and corrects for the different rates at which the reciprocal lattice points sweep through the Ewald sphere. The polarisation factor p, is another quantity which depends on the scattering angle θ, but in neutron diffraction there are no polarisation effects associated with nuclear Bragg scattering and p is unity.

In the usual formalism for X-ray scattering, the structure factors $F_{hk\ell}$ are related to the atomic form factor f_0 for each of the different atoms in the unit cell, where the latter in numerical calculations have been derived as a function of $Sin\theta/\lambda$ from a theoretical model of the electronic configurations of the atoms concerned. Such calculations should ideally take account of the fact that the innermost electrons can have binding energies comparable with the energy of the X-ray photon and thus resonant frequencies close to the frequency of the incident radiation. Though of lesser importance for the lighter elements, the X-ray scattering is modified by this effect so a more precise representation is achieved by writing

$$f = f_0 + \Delta f' + i \ \Delta f'' \qquad 2.4$$

where the dispersion corrections Δf and $\Delta f''$ arise from the

anomalous scattering and to a good approximation can be assumed
independent of the scattering angle. For the analysis of the
diffraction data from Spinel atomic form factors f_0 calculated
by Cromer and Waber (1965) for the Mg^{2+} and $A\ell^{3+}$ ions were used
together with those calculated by Tokonami (1965) for the O^{2-} ion.
Dispersion corrections calculated by Cromer (1965) were applied
to the Mg^{2+} and $A\ell^{3+}$ ions their values being 0.05, 0.07e for
Δf and $\Delta f''$ respectively for both ions. The dispersion correction
for the O^{2-} ion is negligible.

In neutron diffraction the expression for the structure
factors $F_{hk\ell}$ is identical to that in X-ray diffraction except that
each atomic form factor f is replaced by the coherent neutron
scattering length b, of the corresponding nucleus; there are
two important differences, however, arising from the latter. To
begin with, the coherent neutron scattering length, is independent
of the scattering angle θ since the nucleus is effectively a point
scattering source and secondly, because of inadequate theory,
neutron scattering lengths are experimentally determined quantities.

In the neutron diffraction analysis of Spinel the scatter-
ing lengths were taken from the International Tables Volumes 3 and 4
as follows:-

$$b_{Mg} = 0.52 \times 10^{-12} \text{ cm}$$
$$b_{A\ell} = 0.345 \times 10^{-12} \text{ cm}$$
$$b_O = 0.577 \times 10^{-12} \text{ cm}$$

There is no anomalous scatter from these nuclei, as is true for
most nuclei with a few notable exceptions such as Cd. For a
useful review of nuclear scattering lengths see Bacon 1962.

Now the description for both X-ray and neutron
scattering summarised above has tacitly assumed that the atoms
in the crystal are at rest whereas in reality they vibrate quite

vigorously about their mean positions and this must be taken into account before comparing theoretical and measured structure factors. If the atomic motions can be regarded as isotropic, for example, the form factors (atomic or nuclear) may be written

$$f \exp[-B \sin^2 \theta/\lambda^2] \qquad\qquad 2.5$$

where B is the isotropic Debye-Waller or temperature factor and is related to $\overline{u^2}$, the mean square displacement from the mean position of an atom perpendicular to the reflecting planes by,

$$B = 8\pi^2 \overline{u^2}. \qquad\qquad 2.6$$

More generally, the effect of temperature on the diffracted intensities is treated by introducing the possibility of anisotropic vibrations where the exponent of equation 2.5 is replaced by, (Cruickshank, 1956)

$$-(b_{11}h^2 + 2b_{12}hk + 2b_{13}h\ell + b_{22}k^2 + 2b_{23}k\ell + b_{33}\ell^2). \qquad 2.7$$

The anisotropic thermal motion of each atom may then be represented by a vibrational ellipsoid for which the temperature factors b_{11}, b_{12} etc. define the principal axes and their direction cosines. Note that the six parameters b_{11}, b_{12} form a 3×3 real symmetric matrix in which the number of independent parameters may be reduced by the symmetry of the environment of each atom. In particular, for the Spinel structure under consideration the following restrictions are imposed on these temperature parameters: the Magnesium ions are in sites of cubic symmetry, thus $b_{11} = b_{22} = b_{33}$, $b_{12} = b_{13} = b_{23} = 0$; while the Aluminium and Oxygen ions are in sites of trigonal symmetry thus, $b_{11} = b_{22} = b_{33}$, $b_{12} = b_{13} = b_{23}$. Finally it should be emphasized that equations 2.5 and 2.7 are valid only in the harmonic approximation, the effect of anharmonicity on the thermal parameters has been discussed by Dawson (1967) and Willis (1969).

2.2.2) <u>Absorption correction.</u>

An X-ray beam passing through a crystal of thickness
t is attenuated in accordance with the relation,

$$I = I_0 \exp(-\mu t).$$
2.8

where I_0 is the incident beam intensity and μ the linear attenuation
coefficient which can be evaluated from

$$\mu = \frac{1}{Vc} \sum \sigma_i ,$$
2.9

Vc being the volume of the unit cell in $\overset{o}{A}{}^3$, μ is in cm^{-1} and
σ_i is the total photon-atom interaction cross-section and is
measured in barns/atom. The summation is over all the atoms
in the unit cell.

Thus, the extent of the attenuation effect (loosely
referred to as absorption) depends not only on the atoms present,
but for a particular reflexion also on the total path length of
the X-rays through the crystal, that is, on the shape of the
crystal. Such effects thus can lead to systematic errors in
the observed intensities which are difficult to remove unless the
crystal is cylindrical or spherical in shape. In the latter case
the "absorption corrections " have been derived by Bond and are
tabulated in the International Tables Vol.2 as a function of μR
where R is the radius of the crystal.

In the case of the X-ray diffraction experiment on
Spinel μR was 0.28 for the small spherical crystal investigated
(Molybdenum Kα-radiation) which gave an absorption correction
(A*) varying by only 3% over the entire angular range i.e.
A* = 1.52 at θ = 0° to A* = 1.47 at θ = 90°. Nevertheless, the
correction was applied. No correction was necessary for the
neutron diffraction study, however, since all the nuclei in

$MgA\ell_2O_4$ have negligible neutron absorption.

2.2.3) Extinction.

Equation 2.1 is idealised in so far as it only applies to crystals of infinitesimal volume whereas in real crystals important physical processes arise which tend to modify the integrated intensity and introduce systematic error. One of these has already been discussed (section 2.2.2), but another factor first examined by Darwin (1914) often turns out to produce even more dramatic reductions in the intensity of the diffracted beam. This effect is known as extinction.

If the crystal is perfect so that all the atoms are positioned with perfect periodicity throughout the whole crystal volume then the reduction in the intensity of the diffracted beam due to Bragg reflexion is known as "primary extinction". In practice, real crystals usually possess irregularities in their atomic arrangement, like dislocations, point defects, stacking faults, etc, which tend, very slightly, to spoil the perfection of their periodicity. Real crystals were first imagined by Darwin (1914) to be composed of small mosaic blocks which in themselves are perfect and diffract the beam coherently. Between the mosaic blocks, however, he supposed that there is no coherence. In an extreme case it could be imagined that there is negligible primary extinction within the mosaic blocks and the crystal is then said to be "ideally mosaic".

Attenuation of the beam between mosaic blocks of identical orientation is known as "secondary extinction" and the extinction correction which is generally applied to X-ray or neutron data is usually that relating to this secondary process and is based on the diffraction theory proposed by Zachariasen

(1967) in which the integrated intensity ρ, of the diffracted beam is written as,

$$\rho = \rho_k y \qquad\qquad 2.10$$

where ρ_k is the kinematical integrated intensity of equation 2.1 and y is the extinction factor. To work out some functional form for y, the mosaic model of Darwin is idealised even further, in that the mosaic blocks, or domains, are assumed spherical and their misalignment is assumed to obey an isotropic angular Gaussian distribution,

$$w(\Delta) = \sqrt{2}\, g\, \exp(-2\pi^2 g^2 \Delta^2). \qquad\qquad 2.11$$

Thus, the extinction in real crystals, within the limits of the model is characterised by two parameters: the mean domain radius r, and the quantity g which is related to the mosaic spread η, by

$$\eta \approx \Delta_{\frac{1}{2}} = .332 g^{-1} \text{ radian} \qquad\qquad 2.12$$

where $\Delta_{\frac{1}{2}}$ is the half width of the angular distribution function for the orientation of the domains.

Zachariasen then derives the extinction factor as,

$$y = \left(1 + 2\, \frac{p2}{p1}\, x\right)^{-\frac{1}{2}} \qquad\qquad 2.13$$

where pn is the polarisation factor given by

$$pn = \tfrac{1}{2}\, (1 + \cos^{2n} 2\theta) \qquad\qquad 2.14$$

Now if the half width of the distribution function w is much greater than the angular width of a reflexion from a single domain, classified by Zachariasen as a type I crystal, (probably the case for many real crystals) then x is given by

$$x = g\, Q\, \bar{T} \qquad\qquad 2.15$$

and then the extinction depends on the mosaic spread parameter

$\Delta_{\frac{1}{2}}$. Whereas if the reverse is true (type II crystals) then x is given by,

$$x = r \, \lambda^{-1} \, Q \, \overline{T} \qquad\qquad 2.16$$

and the extinction depends on the mean domain radius and not on the mosaic spread. Zachariasen points out that real crystals might be expected to behave in between these two extremes but if the wavelength is constant then the form of the correction is not altered and equations 2.15 and 2.16 are degenerate, i.e. they apply identical corrections. Note that in these two expressions $\overline{T}$ is the total path length through the crystal for a particular crystal setting. The extinction correction thus depends on the shape of the crystal and consequently it is useful to have a spherical crystal for investigation, for then $\overline{T}$ can be considered as a constant.

In our X-ray data this secondary extinction correction was applied to Fcalc as a type I correction, the parameter g being refined in the least squares analysis. Whereas in the neutron data the extinction correction was applied to Fobs based on the above theory but following in the manner of Cooper, Rouse and Willis (1968) where the correction may be written

$$F \text{ corr} = F \text{obs} \, (1 + k \overset{2}{F} \text{obs} \; \text{Cosec} \; 2\theta)^{\frac{1}{4}}. \qquad\qquad 2.17$$

In this expression the corrected structure factor is Fcorr and k is a constant to be determined.

It should be emphasized that although Zachariasen's theory accounts reasonably well for the extinction properties of crystals it is nevertheless based on an idealized model of the crystal and at best can only be an approximation. The only really satisfactory way to ensure that extinction is removed from the data is to correct experimentally. One method, for example, involves collecting data from a range of crystals of various

diameters and with the intensities on an absolute scale it is possible to extrapolate to zero path length, but this would have involved carrying out still further measurements.

2.2.4) Multiple diffraction.

We have emphasized in the introduction to this thesis and also in this chapter that serious problems are encountered when trying to estimate the intensities of the weak forbidden reflexions, particularly at wavelengths which are suitable to reveal structural detail. This difficulty is not one of counting statistics which can, of course, be overcome, but is due to a real crystal effect known as "double diffraction", the occurrence of which in both X-ray and neutron diffraction is well known, and was first investigated by Renninger (1937). We recall here the essential features and principles which give rise to these effects.

Multiple reflexions occur whenever two or more reciprocal lattice vectors lie on the surface of the Ewald sphere simultaneously. One of these may be described as the operative reflexion (H,K,L) and the other as the cooperative reflexion (h,k,ℓ). The vector sum then produces a double diffracted beam which appears as the primary diffraction from the $(H+h,K+k,L+\ell)$ planes. The effect is observed experimentally by rotating about the $(H+h,K+k,L+\ell)$ scattering vector.

We present here, an analysis of double diffraction which gives rise to an observable intensity for the (002) reflexion from a single crystal of Spinel of volume 125 mm^3, by neutron diffraction. The measurements were taken on the four circle MkVI diffractometer at A.E.R.E Harwell with a neutron wavelength of $\lambda = 1.181\text{Å}$. The crystal orientation is shown in figure 2.1, and the multiple diffraction pattern was collected by rotating about the 002 scattering vector through the azimuthal or crystal angle ϕ, and is shown
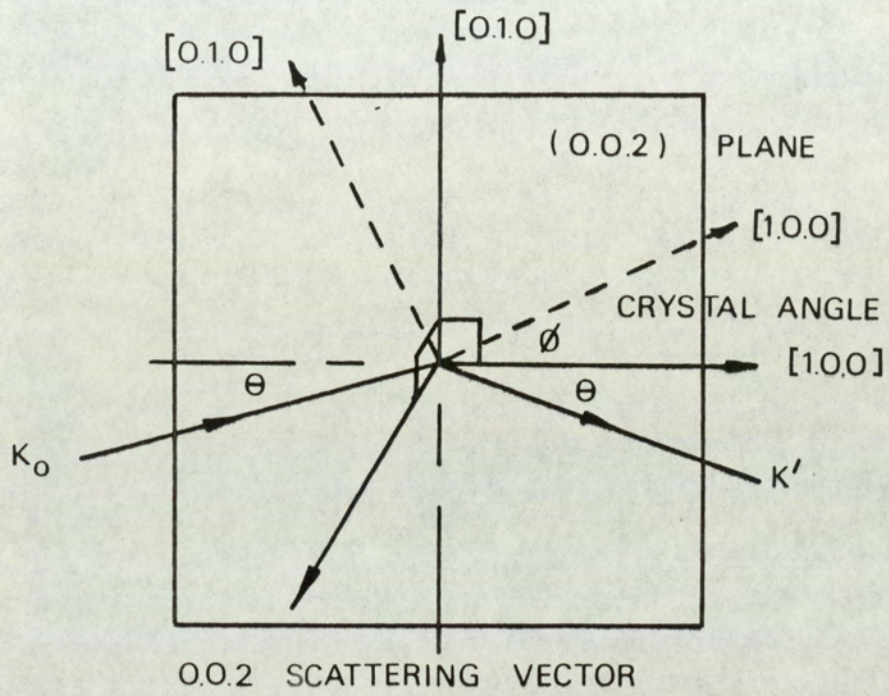
FIGURE 2.1   Crystal   orientation

in figure 2.2. It possesses the expected symmetry, being re-
flected through 0° and 45° and has been indexed in the manner of
Cole, Chambers and Dunn (1962), where the reference vector was
chosen to be (100). For clarity only some of the indices of
the operative reflexions are shown in the diagram.

Because of the large dispersion spread of monochromatized
neutron beams, some reflexions may remain in a condition to contri-
bute to the observed intensity over several degrees. Figure 2.2
demonstrates this quite clearly where a dispersion spread of
$\pm$ 1%, typical of neutron diffraction has been assumed. The
upper part of figure 2.2 shows the product of the structure factors
for the operative and cooperative reflexions at a mean wavelength
of 1.181Å and gives an indication of the observed intensity profile.
It must be emphasized that this is only a crude representation,
as the observed profile must be an integration over all the
reflexions at a particular crystal setting; an example of a more
complete analysis can be seen in the paper by Moon and Shull (1964).

These experimental results show that substantial double
diffraction occurs in Spinel at this wavelength and because of this
we cannot come to any definite conclusions concerning the obser-
vation of a genuine intensity for the 0.0.2 reflexion. Furthermore,
these effects are obviously not isolated to the 0.0.2 reflexion and
this must clearly imply that many of the other intensities suffer
from systematic error originating from this source.

Although it is possible to correct for this aberration
following the method of Moon and Shull, it would involve consider-
able numerical labour, especially when the wavelength of the
radiation is suitable to reveal a large number of reflexions. As
a result corrections of this nature are rarely applied.

FIGURE 2.2   ROTATION ABOUT 0.0.2. SCATTERING VECTOR
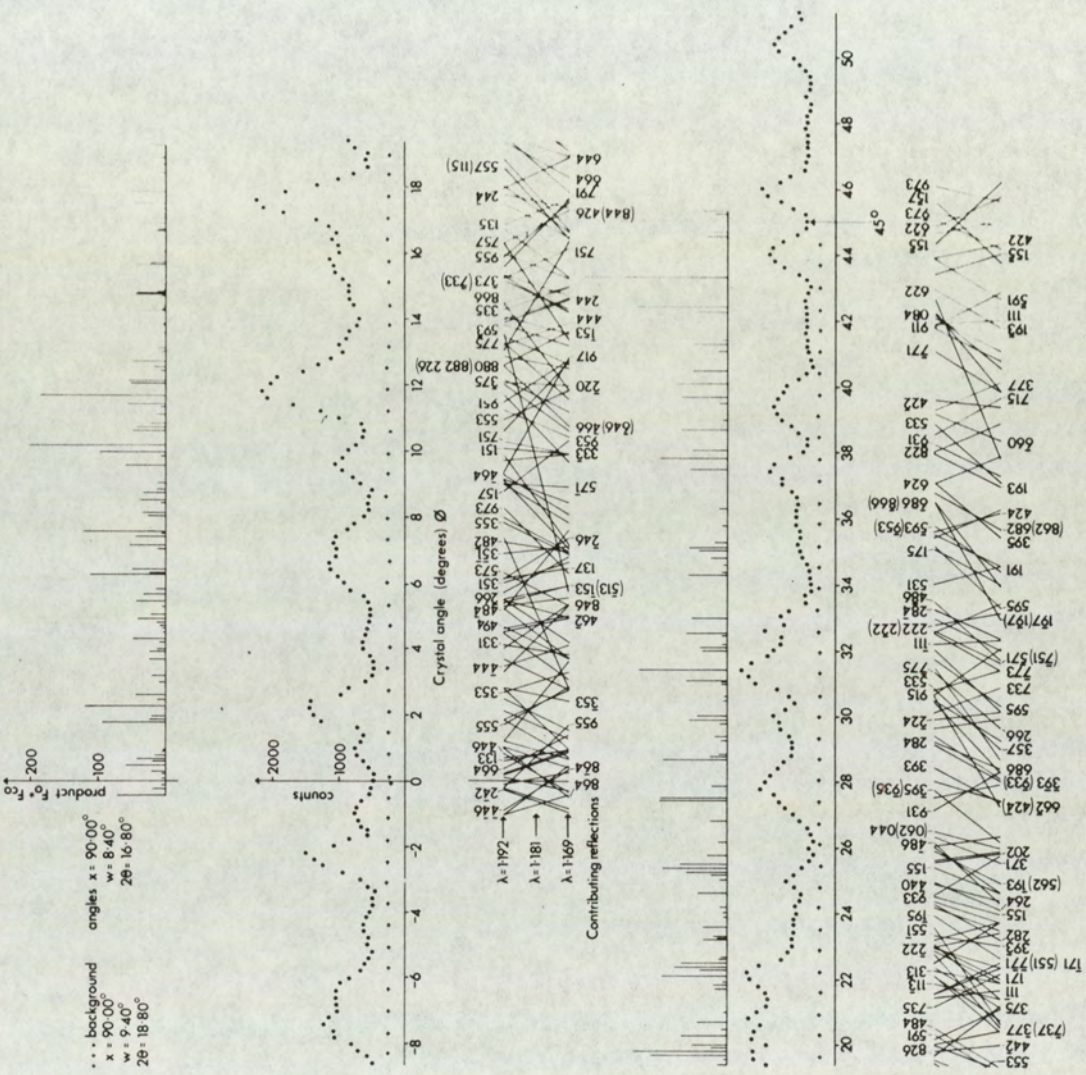
2.3) Results from the neutron diffraction study.

In the neutron diffraction experiment the sample chosen
for investigation was a small flux grown single crystal (kindly
supplied by Dr.E.A.D.White of Imperial College, London) which had
been ground with diamond powder into a sphere of diameter
$1.62 \pm .10$ mm.

The integrated intensities from this crystal were
obtained using the four-circle MkVI diffractometer (D15) on
the high flux nuclear reactor at the I.L.L Grenoble. With this
diffractometer a wavelength of $\lambda = 1.176\overset{\circ}{A}$, with a dispersion
spread $\delta\lambda/\lambda \sim 1\%$ is obtained by reflecting the collimated neutron
beam originating from the reactor core, from the 3.3.1 planes of
a copper monochromater with a take off angle $2\theta m = 90°$ and this gives a
neutron flux at the specimen of about $10^7 ns^{-1} cm^{-2}$. Focussing
then occurs at a detector angle of $\theta = \theta m$ after which the re-
solution deteriorates rapidly, [for a discussion of focussing
effects in neutron spectrometers and other aspects of the pro-
duction of monochromatic neutron beams see Arndt and Willis (1966)
and also E gelstaff (1965)].

The incident intensity of the neutron beam was monitored
by a ^{235}U fission chamber and the intensity of the Bragg peak of
each step in the scan was collected, by a BF_3 counter, for a time
corresponding to the collection of 20,000 monitor counts. This
lead to integrated intensities for the strong reflexions $\sim$ 200,000
counts while the very weak reflexions such as 1.3.7 were of the
order of a few 100, with backgrounds typically $0 \sim 20$ counts in each
step. The angular width of the scan over the peak was taken to
be five times the computed half width of the peak, and this was
varied in accordance with the resolution of the spectrometer. The
computed full width at half height (F.W.H.H) was derived from the

formula (in degrees)

$$F.W.H.H = 0.74 - 0.55 \tan\theta + 0.30 \tan^2\theta$$

and is shown as the dotted line in figure 2.3 which also shows
the bold line, the F.W.H.H of some of the observed peaks from
our Spinel crystal. As a result of this variable range over
which the Bragg peaks were collected the step size was altered so
that the number of steps in the peak was always maintained within
the range 40 to 70 steps, a procedure adopted to enhance experi-
mental efficiency. A standard intensity, in this case the 0.0.4
reflexion, was inserted after every ten reflexions and although
this varied by as much as 4% throughout the measurements no
systematic trend was observed.

Finally the data reduction was performed by the I.L.L
College V data reduction system (Lehmann and Wilson, 1975) which
was specially designed to deal with all the aspects which have
been mentioned above. Since there are no polarisation factors
associated with nuclear Bragg reflexions p was unity and the
Lorentz factor was $1/\sin 2\theta$ as normal beam geometry was employed to
collect the data.

Over the seven days of measurement 455 non-Friedel re-
lated integrated intensities, extending over three quadrants of
reciprocal space, were collected and these were subsequently reduced
to 66 independent reflexions. As in the X-ray data, which will be
discussed in the next section, large variations were observed in the
groups of equivalent reflexions, particularly amongst the strong re-
flexions. This data, however, appeared to have some systematic
trends correlated with patterns of hkl indicies, see for example
table 2.1 which shows the measured equivalent orders of the h,h,h
reflexions. The structure factors shown here are on the same scale
as those appearing in our final analysis given in table 2.2. Attempts
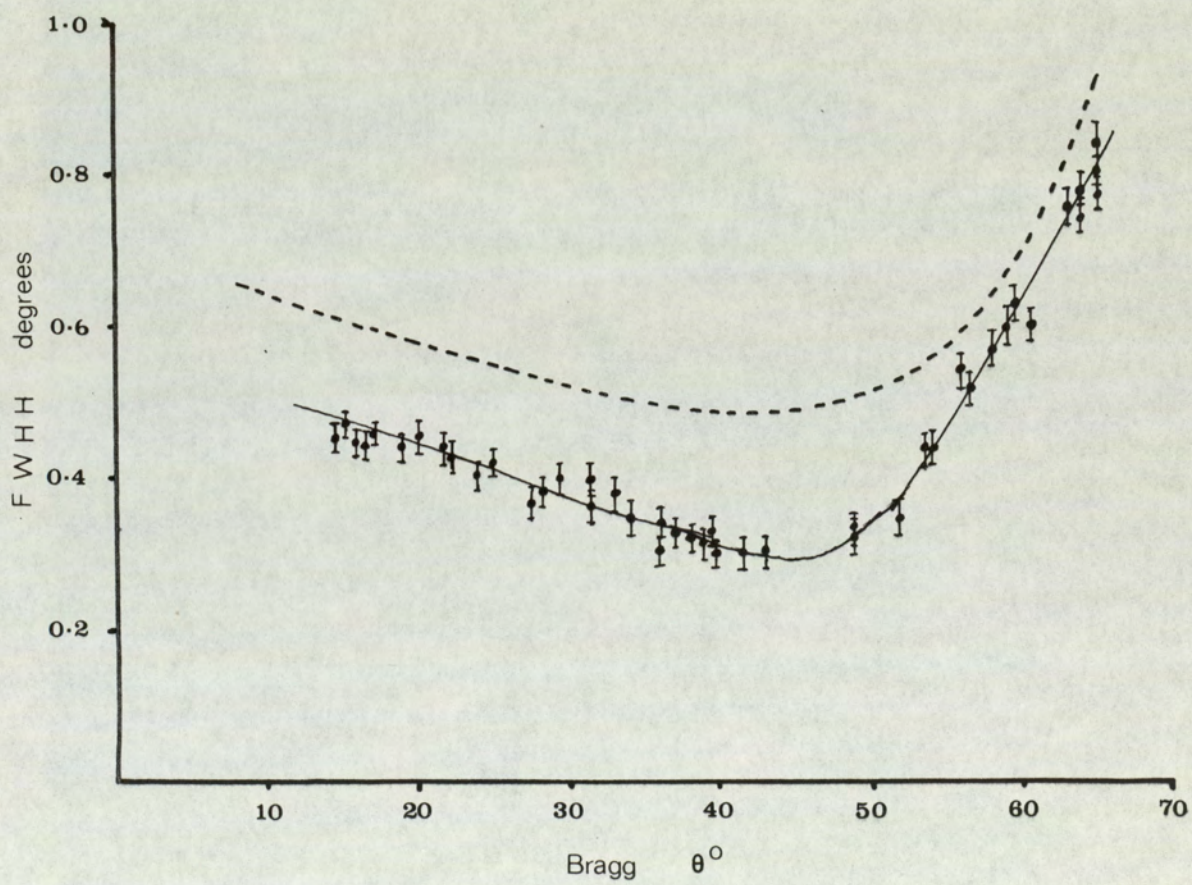
FIGURE 2.3   Resolution curve for D15 difractometer

to explain these variations on the basis of anisotropic extinction following the method of Coppens and Hamilton (1970) proved unsuccessful, and so the data which was used for refinement was selected by the same procedure which we used in the case of the X-ray data (to be described in the next section) and led to the rejection of approximately 20% of the individual measurements.

With all the intensities reduced to structure factors, a comparison was made between Fobs and Fcalc, for the two space groups Fd3m and $F\bar{4}3m$, by the method of least squares which minimizes the residual function

$$Res = \sum_{i=1}^{s} w_i \ (Fobs - Fcalc)^2 \qquad\qquad 2.19$$

where w_i is the weight applied to the ith observation and s is the number of independent observations (in the case of the neutron data 66 observed structure factors). For an account of the method of least squares applied to crystal structure determination, the reader is referred to the International Tables Volume 2 and to Lipson and Cochran (1966) where a useful comparison of both Fourier and least squares methods applied to structural analysis can be found. The method of least squares has the advantage over Fourier techniques in that it is readily adopted by computers and today several well established crystallographic least squares computer programmes are in operation. All the crystal structure analysis reported in this thesis was performed with the X-ray '72 system (1972) on the ICL 1906A/ CDC7600 computer at the University of Manchester.

Before any refinement was attempted with the neutron data the data was approximately corrected for extinction by fitting our measurements to twenty observed structure factors from some neutron powder data on $MgAl_2O_4$ kindly provided by Dr.Willis of A.E.R.E.Harwell.

Table 2.1   h.h.h equivalent orders from
neutron data

	h = 1	h = 2	h = 4	h = 5
Fobs (h,h,h)	1.95	6.78	9.36	8.69
Fobs ($\bar{h}$,h,h)	2.02	9.98	13.00	11.06
Fobs (h,$\bar{h}$,h)	1.95	7.24	9.42	8.61
Fobs ($\bar{h}$,$\bar{h}$,h)	-	9.27	12.39	10.90

This gave initial determinations of the relative scale factor and extinction parameter k of equation 2.17. Initial refinements of the data were then restricted to the space group Fd3m with the strong reflexions, those with Fobs > 10, removed from the analysis. This gave a better determination of the scale factor, although at the same time the structure parameters including three temperature factors were allowed to vary to give a first approximation to the structure. The strong Fobs were then fitted to the calculated structure factors by adjusting the extinction parameter, which increased by 2%, giving a final value for k of .0205 $\pm$ .0008 $\times$ 10^{24} cm^3. Further refinements with all the data produced little change in the parameters and reasonable agreement was obtained with the overall reliability index R defined as,

$$R = \frac{\Sigma \ |Fobs-Fcalc|}{\Sigma \ Fobs} \qquad\qquad 2.20$$

of 2.9 percent. Inversion was introduced by allowing the scattering lengths of the Mg and Aℓ nuclei to vary independently which produced the final refinement under Fd3m symmetry summarized in table 2.2 with an R-factor of 2.6 percent. This also gives, assuming the scattering length $b_{A\ell}$ is well established, an estimate of the magnesium scattering length in which there appears to be some slight uncertainty, since the value appearing in the International Tables Volume 3 is 0.54 $\pm$ .01 $\times$ 10^{-12} cm whereas the value initially derived by Bacon (1952) from measurements on MgO and MgAℓ_2O$_4$ powder is 0.52 $\pm$ .01 $\times$ 10^{-12} cm. which was also the value obtained by Sabine (1965) from studies on MgO a few years later. The inversion parameter i, and the magnesium scattering length can then be obtained from the solutions of the simultaneous equations representing the inversion

$$b_t = (1-i) \ b_{Mg} + ib_{AL} \qquad\qquad 2.21$$
$$2b_0 = (2-i) \ b_{A\ell} + ib_{Mg} \qquad\qquad 2.22$$

where b_t and b_0 are the refined values of the tetrahedral and

octahedral site neutron scatteringlengths and were found experi-
mentally to have values of $0.51 \pm .01 \times 10^{-12}$ cm and
$0.36 \pm .01 \times 10^{-12}$ cm respectively. This yielded an inversion
of $15 \pm 9\%$ and a coherent scattering length for Magnesium of
$0.54 \pm .02 \times 10^{-12}$ cm in agreement with the higher value of the
International Tables Volume 3.

Allowing the structure to refine on $F\bar{4}3m$, with individual
isotropic temperature factors and the neutron scattering lengths
fixed at b_o and b_t gave a slight improvement with R = 2.4%. The
results from this analysis are shown in table 2.2 next to the Fd3m
refinement. The final parameters deduced for the space groups
Fd3m and $F\bar{4}3m$ are compared with the corresponding parameters derived
from the X-ray results in tables 2.5 and 2.6 respectively and are
discussed in section 2.5.

2.4) <u>Results from the X-ray diffraction study</u>.

In the X-ray diffraction experiment the sample chosen was a
small melt grown single crystal of Spinel, supplied by R.R.E Malvern
and this was again shaped into a sphere of diameter $0.48 \pm .02$ mm by
grinding with diamond powder. As explained in 2.1 the measurements
on this crystal were obtained with a Nonius four-circle X-ray
diffractometer at the University of Bristol. The radiation employed
was β-filtered MoKα and was generated with the X-ray tube operating
at 40KV so as to eliminate harmonic contamination of the beam. The
radiation was also reflected from a pyrolytic graphite monochromator
at $\theta_m = 6.07°$ after reflexion from the crystal to minimise white
radiation background.

In all 3,968 non-Friedel related reflexions were collected
over a period of six weeks during which the diffractometer returned
after every tenth reflexion to measure a standard intensity which in
this case was the 4.2.2 reflexion. A systematic drift of several

Table 2.2:   Neutron structure factors in Spinel

(Fcalc and Fobs are in units of 10^{-12} cm)

h	k	ℓ	No. of Equiv	Fobs	Fcalc	Fcalc
					Fd3m	F$\bar{4}$3m
1	1	1	3	2.11	2.13	2.13
0	2	2	6	4.44	4.47	4.47
1	1	3	7	4.92	4.95	4.94
2	2	2	4	11.71	11.70	11.70
0	0	4	2	18.56	18.66	18.64
1	3	3	9	3.14	3.29	3.28
2	2	4	5	3.42	3.53	3.56
1	1	5	6	10.03	10.11	10.09
3	3	3	3	.40	.31	.35
1	3	5	18	1.93	1.88	1.90
2	4	4	8	1.60	1.59	1.59
0	2	6	7	2.61	2.65	2.62
3	3	5	8	4.94	5.10	5.10
2	2	6	6	9.41	9.27	9.26
4	4	4	4	15.48	16.03	15.98
1	1	7	9	3.15	3.19	3.19
1	5	5	5	6.61	6.49	6.46
2	4	6	18	4.52	4.84	4.83
1	3	7	9	.39	.17	.26
3	3	5	6	9.03	8.99	8.94
0	0	8	3	22.67	22.12	22.07
3	3	7	6	7.17	7.25	7.20
4	4	6	5	1.37	1.35	1.37
2	2	7	8	4.12	3.96	4.01
0	6	6	7	7.07	6.89	6.86
1	5	7	18	4.23	4.31	4.33
5	5	5	4	12.94	13.32	13.23
2	6	6	5	7.06	7.24	7.24

h	k	ℓ	No. of Equiv	Fobs	Fcalc	Fcalc
					Fd3m	F$\bar{4}$3m
0	4	8	7	13.64	13.67	13.59
1	1	9	6	6.33	5.98	5.94
3	5	7	14	2.21	2.21	2.22
2	4	8	12	2.74	2.75	2.74
4	6	6	5	.74	.58	.60
3	3	9	1	2.39	2.31	2.36
1	7	7	2	6.14	6.03	5.97
5	5	7	3	.83	.66	.84
0	2	10	3	5.02	5.10	5.06
2	6	8	4	2.58	2.63	2.64
1	5	9	4	12.12	12.04	11.92
3	7	7	2	2.88	3.17	3.14
2	2	10	2	5.51	5.30	5.32
6	6	6	2	5.74	5.55	5.60
3	5	9	6	4.89	4.73	4.68
4	6	8	7	2.32	2.32	2.34
2	4	10	6	1.86	1.89	1.86
5	7	7	4	1.76	1.66	1.75
0	8	8	3	16.95	17.55	17.38
1	7	9	6	1.41	1.32	1.42
0	6	10	6	1.04	1.11	1.13
6	6	8	6	5.75	5.61	5.55
2	8	8	3	4.94	4.74	4.71
4	4	10	2	.98	.94	1.03
3	7	9	11	5.46	5.25	5.28
3	3	11	2	2.55	2.58	2.57
2	6	10	9	3.97	3.93	4.00
1	5	11	3	2.91	2.84	2.87
7	7	7	2	8.61	8.66	8.56
2	2	12	2	3.07	3.03	3.05
4	6	10	8	6.63	7.30	7.22
5	7	9	13	6.82	6.38	6.35
3	5	11	4	1.19	1.17	1.38

R=2.6%   R=2.4%

percent was observed in this standard so all the integrated intensities were corrected for this drift by linear interpolation to the fixed reference.

Five attenuation filters were used throughout the experiment to reduce the intensity of the diffracted beam by different known ratios so as to enable a wide range of integrated intensities to be observed. The measurements were then scaled according to these various attenuation factors so that the whole range of measurements could be referred to a single relative scale. The integrated intensities were corrected for the angular dependence terms Lp, and as normal beam geometry was used for each measurement, the Lorentz factor has the value $L = 1/Sin2\theta$, but because of the presence of the monochromator the polarisation factor,

$$p = \tfrac{1}{2}(Cos^2\theta_m + Cos^2 2\theta) \qquad\qquad 2.23$$

was used.

Because Spinel belongs to the cubic crystal system many of the observed intensities are symmetry related i.e. equivalent, for example $I_{hk\ell} = I_{\overline{hk\ell}}$ etc. In our measurements, where one complete hemisphere of reciprocal space was examined, reflexions of the general type $hk\ell$ contained 24 equivalents, while hko and hhk contained 12, hho 6, hhh 4 and hoo only 3 equivalents. Thus the 3968 observed integrated intensities could be reduced to 242 independent reflexions including 20 forbidden reflexions of the type hko with $h+k = 4n \pm 2$. It should be emphasized here that these latter reflexions are extremely weak and although many were actually observed it was exceedingly difficult to eliminate double diffraction effects as a possible cause for their intensity (see section 2.2.4) and therefore it was thought best to exclude these reflexions from the structure refinements that follow.

The equivalent observations of each of the 242 independent reflexions were collected together into groups, and the results illustrate the difficulty in obtaining accurate intensities, for fairly large variations, typically 20 to 30%, were often observed among the equivalent reflexions within these groups. Now it is unlikely that these discrepancies can arise from counting statistics because a large number of counts were collected for most reflexions (i.e. typical intensities of the intermediate reflexions were about 100,000 ~ 200,000 counts) and, moreover, repeated measurements on the same $hk\ell$ reflexion over a period of time were always observed to lie well within the statistical counting uncertainties which surely indicates that the positioning of the various diffractometer shafts is not the cause. The explanation of these variations probably lies in the nature of real crystals and demonstrates the importance of effects such as anisotropic extinction and double diffraction, however, no evidence could be found of any systematic trends or patterns with particular values of $hk\ell$ indicies, within the groups of equivalents, as one might expect with these crystal effects.

Clearly some averaging process over the equivalent reflexions was necessary in order to obtain a data set with a high degree of internal consistency. For reflexions with 12 or more equivalents, the following procedure was adopted: the range of the observed intensity of each group was divided into a number of classes and a histogram was plotted with the frequency of occurrence of intensity I against the class width. Fairly typical reflexions analysed by this method are shown in figures 2.4a,b and as can be seen from these diagrams the intensity spread is very nearly represented by a Gaussian distribution, despite the small number of observations. The integrated intensities used in the analysis were therefore taken to be the mean of the intensities enveloped by the Gaussian curve. This method of

(4 , 4 , 8 ,) Planes

I obs = 2 410 052 ± 4 percent

(2 , 4 , 10 ,) Planes

I obs = 78978 ± 6 percent

(4 , 8 , 12 ,) Planes

I obs = 631399 ± 8 percent
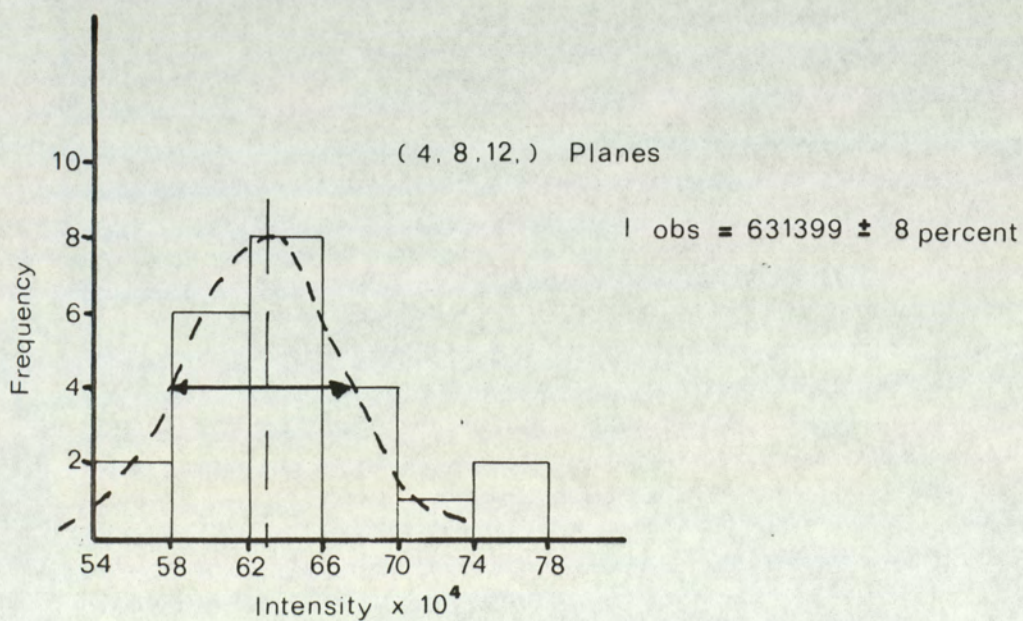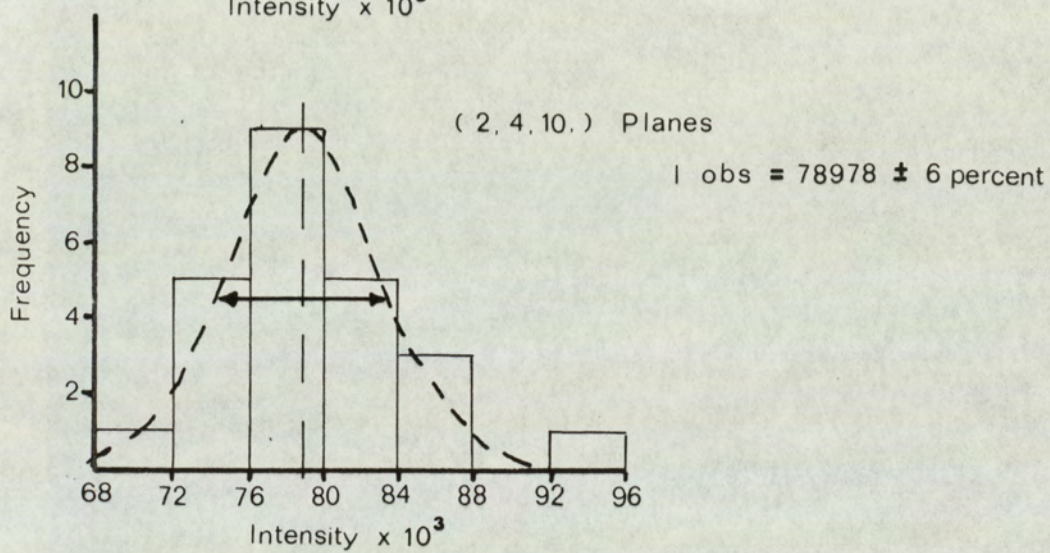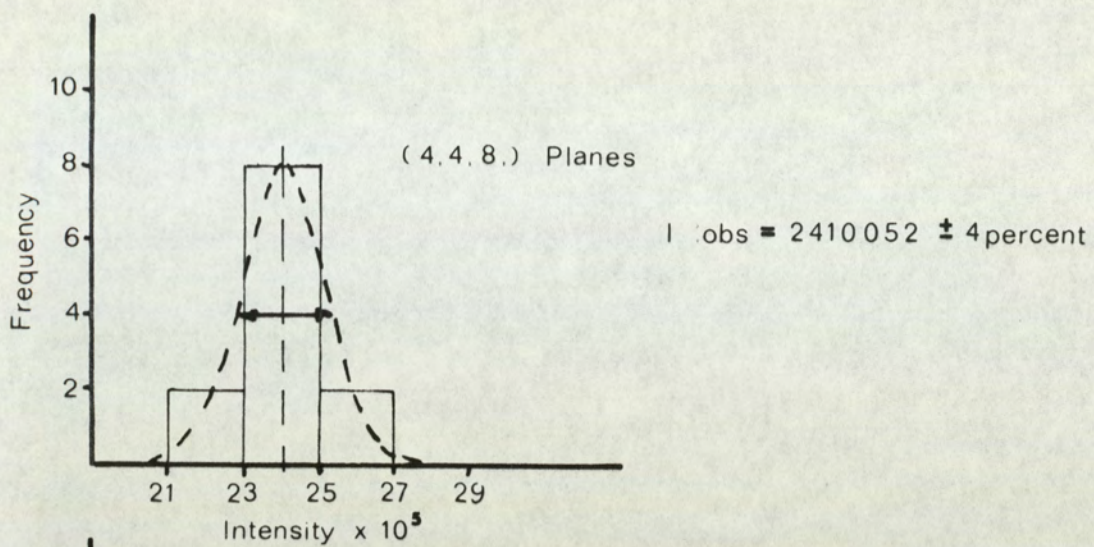
FIGURE 2.4a   Analysis of equivalent reflexions

(8 , 10 , 14 ,) Planes

I obs = 562 ± 60 percent

(4 , 10 , 12 ,) Planes

I obs = 5068 ± 6 percent
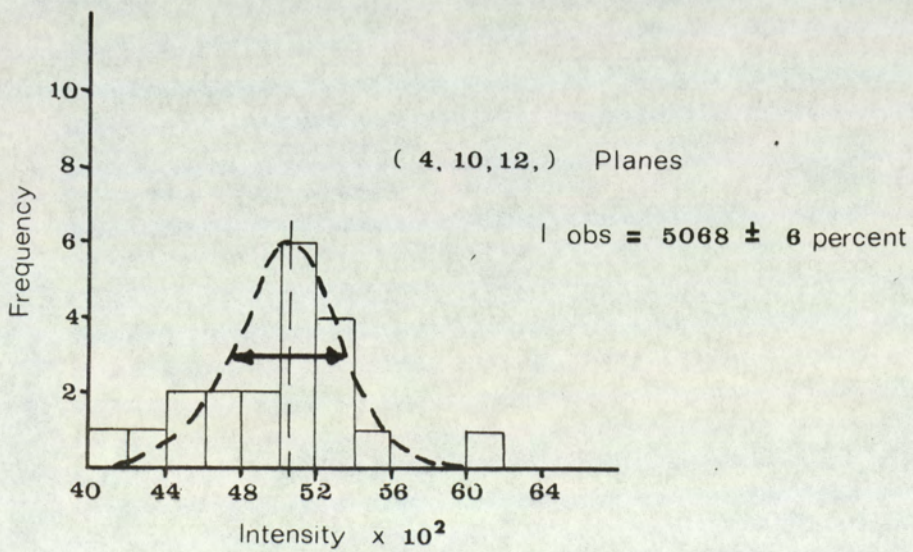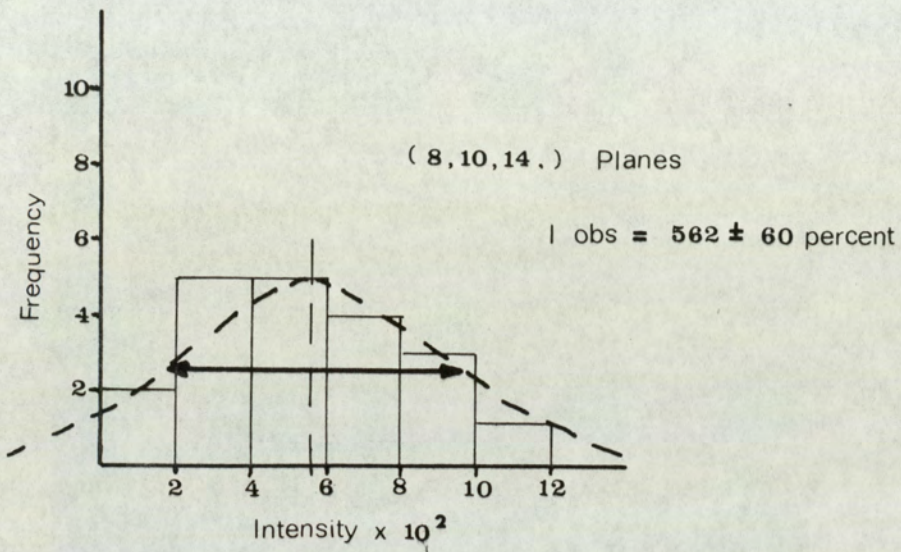
FIGURE 2.4 b

to the high angle data, which is where small atom shifts are expected to be more important, while at the same time down weighting the strong reflexions at low angles as these are seriously affected by extinction. Further refinements of all the parameters [six in this case] led to convergence of the least squares with an overall reliability index, R, of 2.8%.

With the same weighting scheme and with the scale and extinction parameters held constant the structure was then refined assuming the space group $F\overline{4}3m$ to be applicable. The number of structure parameters in this case was extended to eight, including three positional parameters and five temperature parameters. To enhance the sensitivity of the data to small shifts of the atoms we chose, from separate calculations of the geometric structure factors on the space group $F\overline{4}3m$, the 50 most sensitive reflexions, these inevitably turning out to be weak reflexions with Fobs generally below 30. With this group of selected data only the three parameters x_1, x_2 and x_3 were refined and this gave a first approximation to the atom positions. These values were then used as starting parameters for a refinement of all the model parameters with the complete data set and the R-factor dropped to 2.7%.

The effect of inversion was investigated by examining the behaviour of a different selected group of data, namely that with Fobs $\leqslant$ 30 and $Sin\theta/\lambda \leqslant$ .78. This region was chosen because it is practically insensitive to any other parameter, i.e. the low value of $Sin\theta/\lambda$ makes the effect of atom positions and temperature relatively unimportant,and similarly the lowish value of Fobs makes these reflexions fairly insensitive to the scale and extinction factors.

In taking account of inversion, the scattering factors are changed according to the inversion formulae, defined previously

data selection led to the rejection of more than 10% of the data.
Finally for reflexions with fewer equivalents a straight average
was taken except where there was an obvious foreign result . The
number of equivalents used to derive Iobs for each reflexion is
shown in column 2 of table 2.3. The integrated intensities shown
in column 3 of table 2.3 have the angular dependence terms L and
p removed and were reduced to structure factor by correcting for
absorption (see section 2.2.3).

Initial refinement of the data was restricted to the
space group Fd3m with the cations assumed to have their normal
arrangement, and only the intermediate intensities were used so that
an approximate value of the relative scale factor c, could be
derived together with the oxygen positional parameter and isotropic
temperature factors. With these factors then held constant the
extinction parameter g was refined separately as this is closely
correlated to both the scale factor and the temperature parameters.
Note, in the computer program CRYLSQ of the X-ray system the extinction
correction is applied to Fcalc following the method recommended by
Larson (1967) which is based on Zachariasen's theory of X-ray
diffraction and is formally identical to the latter except that the
correction is applied to F rather than I, the appropriate equation
being,

$$Fcalc = |F_c| \left(1 + 2 \frac{p2}{p1} x\right)^{-\frac{1}{4}} \qquad 2.24$$

where F_c is the kinematical structure factor and Fcalc the cal-
culated structure factor with extinction.

At this stage each observation was weighted according to
the expression $w_i = xy$ where x depends on $\sin\theta$ as follows:
if $\sin\theta > .7107$ then x = 1 otherwise x = $\sin\theta/.7107$ and y is
related to Fobs by: if Fobs > 30 then y = 30/Fobs otherwise y is
unity. This scheme was employed to try and establish a good fit

in equation 2.21 and 2.22 but with the neutron scattering lengths (b) replaced by the corresponding atomic form factors (f). The inversion was determined from plotting the R-factor against the percentage inversion which is shown in figure 2.5, and as can be seen there is a fairly well defined minimum in the neighbourhood of 17.5%. It should be emphasized that the inversion is not accurately determined in X-ray diffraction since the atomic form factors for the Mg^{2+} and Al^{3+} ions shown in figure 2.6, are very similar. To be realistic therefore the inversion is estimated to be $17.5 \pm 5\%$.

Introducing inversion into both space groups improved the overall R-factor by 0.1% in both cases and some further slight manual corrections of the order $\frac{1}{2} \sim 1\%$ were made to the scale and extinction parameters giving final values of c = 285.6 $\pm$ 1.5 and g = 3440 $\pm$ 50, to improve the overall appearance of the data. This gave a better balance between the positive and negative discrepancies (ΔF's) where ΔF is defined as $\Delta F = F_{obs} - F_{calc}$.

The calculated structure factors of the final refinement with isotropic temperature factors appear in columns I and II of table 2.3 for Fd3m (R = 2.7%) and $F\bar{4}3m$ (R = 2.6%) symmetry respectively. The introduction of anisotropic temperature parameters led to a better agreement between F_{obs} and F_{calc} for both space groups investigated and the results of these are shown in columns II and IV for Fd3m (R = 2.6%) and $F\bar{4}3m$ (R = 2.4%) respectively. The structure parameters from this analysis are compared in table 2.7.

During the analysis a breakdown of the R-factor into various categories in terms of F_{obs} and $Sin\theta/\lambda$ was found to be immensely helpful in that it highlighted certain regions of the observations which were not fitting particularly well. The final
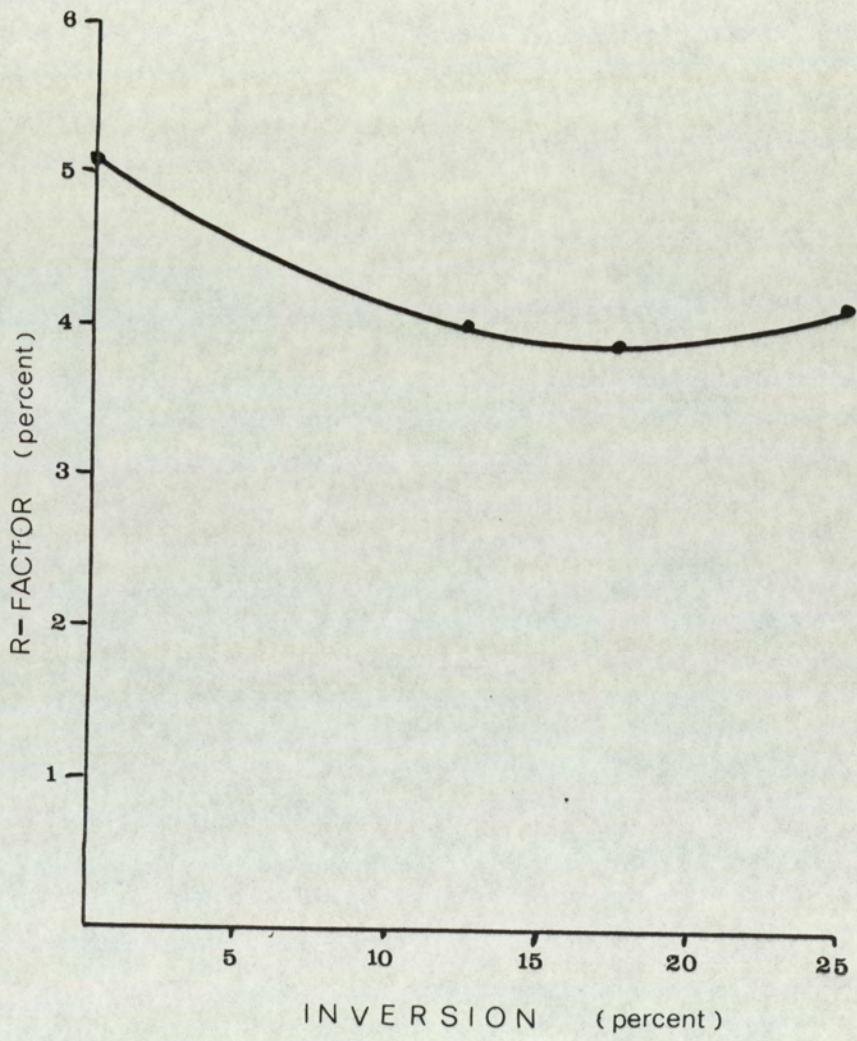
FIGURE 2.5   Inversion   v's   R - factor
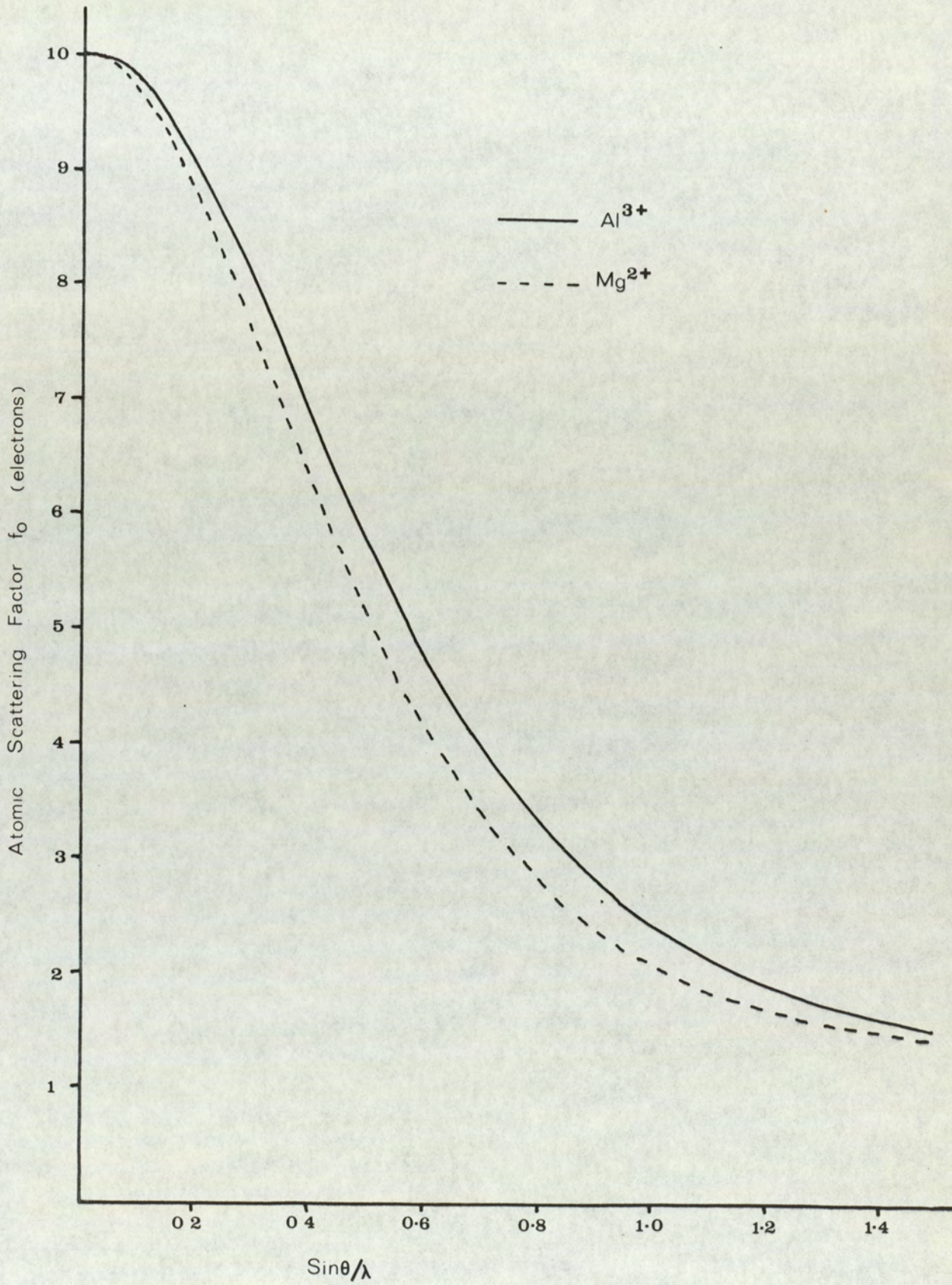
FIGURE 2.6   Atomic   form   factors   for   Al³⁺ & Mg²⁺

Table 2.3: X-ray results on Spinel

h	k	l	No of Equiv	Intensity obs	F obs	F calc I Fd3m	F calc II F$\bar{4}$3m	F calc III Fd3m	F calc IV F$\bar{4}$3m
0	0	4	2	3700163	139.86	139.67	139.63	139.68	139.66
0	0	8	2	3687998	139.69	140.54	140.53	140.57	140.42
0	0	12	3	491455	50.85	49.79	49.52	49.86	49.85
0	0	16	2	449576	48.43	48.40	48.53	48.53	48.36
0	2	2	4	892108	68.76	65.75	65.83	65.71	65.72
0	2	6	8	363396	43.82	42.10	42.05	42.24	42.11
0	2	10	8	213559	33.53	33.37	33.55	33.21	33.12
0	2	14	9	25529	11.55	11.29	11.35	11.44	11.28
0	2	18	8	34251	13.38	13.18	13.37	13.06	12.97
0	4	4	5	5105217	164.28	167.86	167.84	167.88	167.80
0	4	8	9	1273540	82.12	79.47	79.28	79.54	79.49
0	4	12	10	1223110	80.19	80.35	80.32	80.44	80.21
0	4	16	8	99226	22.74	22.74	22.48	22.87	22.93
0	6	6	5	442368	48.40	48.15	48.44	47.82	47.80
0	6	10	8	17038	9.46	9.28	9.18	9.69	9.47
0	6	14	10	123471	25.38	25.72	26.03	25.35	25.30
0	6	18		—	0.00	.46	.45	.26	.34
0	8	8	3	1810625	97.51	96.95	96.95	97.05	96.81
0	8	12	8	235342	35.04	34.54	34.34	34.71	34.70
0	8	16	9	270025	37.57	37.90	37.98	38.10	37.93
0	10	10	4	176662	30.37	32.16	32.53	31.68	31.64
0	10	14	8	4237	4.70	4.87	4.97	4.37	4.57
0	12	12	5	387069	44.93	44.30	44.42	44.53	44.32
1	1	1	4	531697	53.21	47.76	47.88	47.62	47.71
1	1	3	10	1552355	90.64	88.10	88.08	88.14	88.11
1	1	5	8	2204518	107.95	106.24	106.33	106.08	106.10
1	1	7	8	2258	3.45	1.94	2.55	2.07	2.94
1	1	9	9	236408	35.38	34.69	34.65	34.45	34.52
1	1	11	7	184321	31.11	31.06	31.11	31.16	31.20
1	1	13	9	479590	50.18	50.03	50.13	49.84	49.71
1	1	15	8	9522	7.05	6.62	7.12	6.54	6.77
1	1	17	9	59504	17.61	17.44	17.34	17.27	17.28
1	1	19	6	9024	6.84	6.40	6.82	6.45	6.86
1	3	3	9	7956	6.49	6.43	6.65	6.29	6.45
1	3	5	23	179667	30.82	29.52	29.52	29.52	29.61
1	3	7	20	513728	52.11	50.83	50.76	50.90	50.78
1	3	9	19	856624	67.30	67.18	67.29	67.18	67.11
1	3	11	15	10629	7.47	7.03	7.33	7.00	7.10
1	3	13	19	85771	21.20	20.66	20.64	20.65	20.73
1	3	15	18	27313	11.94	11.68	11.75	11.70	11.77
1	3	17	12	192877	31.72	30.43	30.66	30.43	30.37
1	3	19	17	6082	5.62	5.58	5.92	5.59	5.66
1	5	5	12	410992	46.60	45.92	45.96	45.53	45.65
1	5	7	23	664940	59.34	59.36	59.38	59.49	59.44
1	5	9	24	904791	69.00	70.29	70.36	69.92	69.83
1	5	11	13	600	1.78	.96	2.13	1.11	2.43
1	5	13	22	115203	24.53	24.56	24.44	24.20	24.23
1	5	15	21	38099	14.10	13.86	14.09	13.98	14.22
1	5	17	18	178698	30.56	30.47	30.57	30.19	30.08
1	5	19	16	4925	5.05	4.97	5.39	4.88	4.97
1	7	7	10	11908	7.92	7.61	7.81	7.60	7.66
1	7	9	23	38358	14.20	14.07	14.04	14.22	14.37
1	7	11	23	59060	17.61	18.06	18.10	18.05	18.04
1	7	13	14	226347	34.36	33.83	34.02	33.96	33.91
1	7	15	18	8579	6.69	6.60	6.84	6.63	6.70
1	7	17	18	26794	11.83	11.60	11.58	11.73	11.78
1	9	9	8	151760	28.24	28.06	27.95	27.60	27.64
1	9	11	21	134399	26.49	26.54	26.69	26.73	26.77

Table 2.3:   continued

h	k	l	No of Equiv	Intensity obs	F obs	F calc I Fd3m	F calc II F$\bar{4}$3m	F calc III Fd3m	F calc IV F$\bar{4}$3m
1	9	13	21	275803	37.93	37.95	38.00	37.54	37.41
1	9	15	17	756	1.99	1.03	1.77	.87	1.63
1	9	17	18	29273	12.32	13.08	12.93	12.75	12.76
1	11	11	11	9940	7.20	6.84	7.03	6.90	6.95
1	11	13	22	9877	7.18	6.61	6.55	6.81	6.95
1	11	15	22	18108	9.72	8.68	8.78	8.59	8.73
1	13	13	10	39782	14.41	14.50	14.35	14.11	14.12
2	2	2	4	186663	31.43	33.38	33.40	33.44	33.39
2	2	4	10	588604	55.78	53.18	53.20	53.23	53.19
2	2	6	11	154771	28.60	29.57	29.52	29.45	29.52
2	2	8	12	267841	37.66	37.35	37.44	37.30	37.19
2	2	10	12	150325	28.12	30.31	30.16	30.14	30.12
2	2	12	10	75988	19.99	19.94	20.07	19.98	19.86
2	2	14	10	92656	21.99	22.31	22.18	22.10	22.04
2	2	16	10	31143	12.74	12.27	12.47	12.24	12.28
2	2	18	8	78469	20.25	19.19	19.01	18.97	18.78
2	4	4	10	21387	10.63	9.40	9.58	9.63	9.71
2	4	6	24	414457	46.80	46.15	46.29	46.02	45.95
2	4	8	24	20599	10.44	10.02	10.25	10.30	10.41
2	4	10	23	78978	20.37	20.43	20.48	20.59	20.43
2	4	12	24	17277	9.53	9.23	9.41	9.47	9.50
2	4	14	22	68675	18.93	18.87	19.09	18.74	18.65
2	4	16	20	12123	7.95	7.62	7.78	7.79	7.85
2	4	18	20	8635	6.71	6.10	6.23	6.22	6.10
2	6	6	8	183193	31.15	33.22	33.07	33.05	33.07
2	6	8	22	116629	24.78	25.37	25.45	25.49	25.34
2	6	10	23	110610	24.12	26.05	25.91	25.83	25.85
2	6	12	17	66386	18.64	18.62	18.75	18.53	18.46
2	6	14	20	75538	19.85	20.13	19.90	19.87	19.78
2	6	16	18	20459	10.33	10.23	10.49	10.31	10.34
2	6	18	15	65065	18.38	17.73	17.54	17.47	17.31
2	8	8	11	39450	14.40	14.47	14.70	14.87	14.89
2	8	10	23	87900	21.49	21.96	22.14	21.83	21.75
2	8	12	24	44105	15.15	14.94	15.19	15.29	15.34
2	8	14	23	16978	9.41	9.02	9.22	9.16	9.07
2	8	16	18	30643	12.66	12.60	12.80	12.88	12.90
2	10	10	12	75032	19.79	20.62	20.35	20.33	20.28
2	10	12	23	24867	11.39	11.03	11.24	11.15	11.09
2	10	14	18	59078	17.55	17.28	17.04	16.95	16.88
2	10	16	18	17661	9.58	9.51	9.87	9.41	9.63
2	12	12	11	54123	16.80	16.18	16.42	16.54	16.56
2	12	14	23	26328	11.72	11.00	11.34	10.88	10.96
3	3	3	4	683474	60.11	57.18	57.00	57.20	57.06
3	3	5	9	1162499	78.37	77.29	77.34	77.43	77.34
3	3	7	11	38139	14.21	13.97	14.07	13.89	13.96
3	3	9	9	78390	20.33	20.03	20.03	20.21	20.26
3	3	11	9	73340	19.64	19.84	19.90	19.75	19.84
3	3	13	10	326697	41.34	41.56	41.75	41.70	41.57
3	3	15	10	18189	9.74	9.65	9.97	9.73	9.83
3	3	17	9	47360	15.72	15.04	15.01	15.15	15.15
3	3	19	8	7980	6.43	5.78	6.29	5.69	6.23
3	5	5	12	1280184	82.26	82.64	82.68	82.54	82.50
3	5	7	21	6653	5.93	5.80	5.82	6.00	6.23
3	5	9	22	124914	25.62	25.75	25.64	25.58	25.66
3	5	11	24	140602	27.20	27.64	27.69	27.80	27.75

Table 2.3: continued

h	k	l	No of Equiv	Intensity obs	F obs	F calc I Fd3m	F calc II F$\bar{4}$3m	F calc III Fd3m	F calc IV F$\bar{4}$3m
3	5	13	21	315591	40.59	41.04	41.13	40.89	40.81
3	5	15	22	3311	4.16	3.74	4.11	3.64	3.83
3	5	17	20	37019	13.91	13.68	13.60	13.56	13.63
3	7	7	11	107028	23.73	24.84	24.80	24.66	24.66
3	7	9	22	318252	40.91	42.33	42.46	42.56	42.46
3	7	11	24	29978	12.53	12.67	12.94	12.86	12.83
3	7	13	21	33655	13.25	13.11	13.10	13.34	13.38
3	7	15	18	9359	6.99	6.57	7.00	6.39	7.00
3	7	17	18	122249	25.25	25.10	25.33	25.29	25.18
3	9	9	7	373448	44.28	46.44	46.45	46.20	46.12
3	9	11	19	4238	4.70	4.50	4.50	4.72	4.96
3	9	13	21	46100	15.51	15.52	15.36	15.27	15.35
3	9	15	18	41039	14.64	14.61	14.67	14.76	14.76
3	9	17	18	87999	21.35	21.92	22.02	21.74	21.70
3	11	11	11	10921	7.55	7.23	7.55	7.00	7.56
3	11	13	20	102845	23.16	22.61	22.77	22.84	22.76
3	11	15	16	8802	6.77	7.08	7.41	7.33	7.46
3	13	13	7	111353	24.10	23.50	23.54	23.26	23.21
4	4	4	4	2111353	104.86	104.32	104.20	104.37	104.32
4	4	6	8	6781	5.99	5.45	6.17	5.60	6.40
4	4	8	12	2410052	112.79	116.78	116.76	116.85	116.63
4	4	10	7	1774	3.05	2.85	2.90	2.91	3.08
4	4	12	10	332681	41.76	41.27	41.03	41.41	41.38
4	4	14	6	656	1.85	1.29	1.78	1.29	1.78
4	4	16	9	356001	43.08	42.66	42.69	42.82	42.64
4	6	6	11	85975	21.33	21.39	21.32	21.73	21.53
4	6	8	20	10879	7.56	7.40	7.49	7.60	7.63
4	6	10	22	182155	30.96	32.20	32.49	31.82	31.77
4	6	12	19	11267	7.67	7.45	7.58	7.63	7.72
4	6	14	22	1537	2.83	1.91	1.95	2.28	2.11
4	6	16	20	7781	6.37	6.25	6.55	6.39	6.50
4	8	8	11	487767	50.66	51.13	50.93	51.27	51.21
4	8	10	20	4522	4.87	4.51	4.71	4.60	4.88
4	8	12	21	631399	57.39	58.70	58.76	58.88	58.64
4	8	14	19	1453	2.75	2.21	2.49	2.14	2.45
4	8	16	16	54453	16.87	17.30	17.11	17.51	17.57
4	10	10	8	589	1.75	.35	.46	.43	.34
4	10	12	21	5068	5.14	4.85	5.12	4.93	5.08
4	10	14	16	108268	23.78	24.24	24.59	23.75	23.73
4	10	16	18	3575	4.31	4.11	4.18	4.20	4.25
4	12	12	9	91183	21.81	21.34	21.19	21.58	21.60
5	5	5	4	1393203	85.90	87.64	87.76	87.18	87.15
5	5	7	11	40727	14.65	14.37	14.25	14.45	14.59
5	5	9	12	211498	33.33	34.86	34.84	34.30	34.38
5	5	11	7	143904	27.49	28.66	28.72	28.80	28.84
5	5	13	7	346458	42.51	45.07	45.17	44.61	44.47
5	5	15	8	2375	3.52	3.35	4.00	3.21	3.55
5	5	17	10	46749	15.62	16.38	16.26	15.99	16.01
5	7	7	9	221907	34.14	35.80	35.88	35.98	35.89
5	7	9	23	304206	40.00	41.83	41.87	41.87	41.81
5	7	11	22	1048	2.34	1.65	1.93	1.52	2.05
5	7	13	20	27787	12.04	11.89	11.75	11.91	11.99
5	7	15	20	31143	12.74	12.70	12.79	12.77	12.81
5	7	17	16	87353	21.30	21.58	21.72	21.63	21.56
5	9	9	11	466643	49.41	52.32	52.43	51.77	51.63
5	9	11	17	3777	4.44	4.10	4.07	4.24	4.54

Table 2.3: continued

h	k	l	No of Equiv	Intensity obs	F obs	F calc I Fd3m	F calc II F$\overline{4}$3m	F calc III Fd3m	F calc IV F$\overline{4}$3m
5	9	13	17	78864	20.28	21.71	21.63	21.21	21.21
5	9	15	17	26647	11.80	11.86	12.00	12.03	12.13
5	11	11	12	44913	15.30	15.42	15.54	15.52·	15.53
5	11	13	19	71751	19.36	19.02	19.12	19.17	19.14
5	11	15	21	289	1.22	.54	.69	.53	1.09
5	13	13	10	142113	27.16	28.19	28.35	27.75	27.63
6	6	6	3	142209	27.3	29.47	29.38	29.26	29.33
6	6	8	11	154423	28.49	29.39	29.57	29.10	29.05
6	6	10	12	83885	20.98	22.69	22.47	22.43	22.40
6	6	12	11	21721	10.64	10.99	11.17	11.25	11.12
6	6	14	10	61641	17.93	18.43	18.28	18.14	18.09
6	6	16	10	25501	11.32	11.08	11.33	10.87	11.06
6	8	8	11	25895	11.67	11.48	11.68	11.77	11.88
6	8	10	19	10193	7.30	7.36	7.45	7.72	7.55
6	8	12	20	27743	12.03	12.21	12.42	12.48	12.54
6	8	14	19	64216	18.30	18.78	19.07	18.44	18.43
6	8	16	20	21202	10.50	10.35	10.52	10.58	10.64
6	10	10	10	58706	17.50	18.75	18.63	18.44	18.45
6	10	12	22	5067	16.25	16.19	16.41	15.87	15.93
6	10	14	16	49711	16.12	16.16	15.84	15.83	15.69
6	12	12	10	35570	13.64	13.29	13.49	13.58	13.63
7	7	7	3	69929	19.18	15.76	16.05	16.06	16.03
7	7	9	10	10606	7.45	7.59	7.62	7.85	8.02
7	7	11	10	8658	6.72	6.70	7.00	6.38	6.97
7	7	13	11	140146	27.03	27.46	27.69	27.71	27.64
7	7	15	9	15794	9.09	9.76	10.12	10.06	10.12
7	7	17	7	24532	11.27	11.04	10.99	11.25	11.26
7	9	9	10	26898	11.85	11.72	11.51	11.68	11.77
7	9	11	23	87564	21.37	21.97	22.12	22.18	22.15
7	9	13	19	106860	23.61	23.82	23.84	23.77	23.71
7	9	15	19	923	2.19	1.83	1.63	1.95	2.16
7	11	11	10	22906	10.93	11.87	12.24	12.25	12.25
7	11	13	16	12276	8.01	7.56	7.47	7.77	7.84
7	13	13	8	7221	6.12	5.75	5.55	5.68	5.74
8	8	8	4	883219	67.94	69.07	69.12	69.24	68.98
8	8	10	10	12007	7.01	7.36	7.49	7.50	7.59
8	8	12	11	119287	24.94	25.18	25.03	25.41	25.42
8	8	14	11	3392	4.21	3.51	3.51	3.55	3.64
8	8	16	10	189610	31.34	30.76	30.88	30.98	30.84
8	10	10	10	93990	22.14	22.95	23.32	22.49	22.50
8	10	12	23	13452	8.38	7.99	8.07	8.15	8.22
8	10	14	19	562	1.71	1.64	1.86	1.18	1.67
8	12	12	11	254451	36.40	35.16	35.30	35.40	35.24
9	9	9	4	112619	24.24	25.80	25.77	25.23	25.22
9	9	11	8	67864	18.81	19.32	19.35	19.42	19.41
9	9	13	9	162490	29.14	32.69	32.88	32.20	32.05
9	9	15	9	859	2.11	1.62	1.97	1.44	1.58
9	11	11	10	2460	3.59	3.49	3.37	3.64	3.81
9	11	13	13	1789	3.05	2.89	2.65	3.00	3.05
10	10	10	3	46500	15.57	16.37	16.07	16.04	15.93
10	10	12	10	2411	3.55	3.01	3.43	3.43	3.58
10	12	12	6	16715	9.31	8.74	8.96	8.94	9.09
11	11	11	4	2581	3.66	2.32	3.64	1.85	3.71

Table 2.4: Analysis of the R-Factor

Breakdown of the R-factor in percent in terms of F obs

Group F obs	No of planes	Refinement I	Refinement II	Refinement III	Refinement IV
0-5	26	18.6	12,7	18.0	9.5
5-10	37	4.4	3.6	4.5	3.3
10-15	34	2.3	2.2	2.4	2.3
15-20	26	2.9	2.8	2.6	2.8
20-25	25	2.9	3.0	2.5	2.4
25-30	14	3.6	3.8	3.3	3.3
30-35	13	3.4	3.4	3.1	3.2
35-40	6	1.4	1.5	1.6	1.7
40-45	10	2.8	3.0	2.5	2.5
45-50	5	1.9	1.8	2.0	2.0
50-55	5	3.3	3.2	3.4	3.4
55-60	3	2.3	2.3	2.4	2.3
60+	18	1.7	1.7	1.6	1.6

Breakdown of the R-factor in percent in terms of $\sin\theta/\lambda$

Group $\sin\theta/\lambda$	No of planes	Refinement I	Refinement II	Refinement III	Refinement IV
0-.13	1	10.2	10.0	10.5	10.3
.13-.26	4	2.3	2.3	2.3	2.3
.26-.39	7	3.1	3.1	3.1	3.0
.39-.52	12	1.6	1.4	1.6	1.5
.52-.65	21	2.5	2.4	2.4	2.3
.65-.78	24	2.9	2.9	2.7	2.7
.78-.91	36	2.4	2.4	2.3	2.1
.91-1.04	42	2.9	2.6	2.6	2.2
1.04-1.17	54	3.1	3.0	3.0	2.9
1.17-1.30	21	4.7	4.0	4.5	2.5

breakdown of the R-factor, shown in table 2.4, also illustrates
a number of interesting features which will be discussed in the
next section where we examine the results of the neutron and
X-ray diffraction.

2.5) Discussion.

The parameters for the space group Fd3m with individual
isotropic temperature factors derived from the neutron and X-ray
diffraction analysis, shown in table 2.5, agree within the standard
derivations, estimated from the least squares refinement on these
parameters. The derived oxygen position parameter is also in
agreement with previous estimates (Fischer, 1967; Rouse, Thomas
and Willis, 1976).

On the other hand, only some of the parameters derived
for the space group F$\bar{4}$3m with the neutron results are in agree-
ment with those estimated from the X-ray data, see table 2.6,
namely the oxygen position parameters (x_2 and x_3) and the tem-
perature factors $B_{A\ell}$, B_{OX1}, B_{OX2}. The aluminium position parameter
(x_1) for both sets of data agree only because of the larger error
on this parameter with the neutron data. The temperature factors
for the magnesium atoms, however, exhibit anomalous behaviour in that
completely different results were found for these parameters from
the neutron diffraction. It seems highly unlikely that this is
associated with a real physical difference in the vibrations of the
nuclei and electrons for these atoms since the magnesium vibrational
parameters for the two sets of data are in excellent agreement when
we refine the results with the space group Fd3m. We can possibly
attribute the difference to two causes, firstly the number of
reflexions used to derive the structure with neutron diffraction
was only 66 which may be too few to determine the parameters
accurately. Secondly, and more likely, these two parameters might

Table 2.5: Structure parameters in
Spinel with space group Fd3m

	X-ray data	Neutron data
Anion u-parameter	.3876 ± .0001	.3874 ± .0003
B_{Mg}	$.36 \pm .01\text{Å}^2$	$.40 \pm .06\text{Å}^2$
$B_{A\ell}$	$.32 \pm .01\text{Å}^2$	$.36 \pm .06\text{Å}^2$
B_{OX}	$.48 \pm .01\text{Å}^2$	$.54 \pm .06\text{Å}^2$
b_{Mg}	–	$.54 \pm .02*10^{-12}\text{cm}$
$b_{A\ell}$	–	–
i	$17.5 \pm 5\%$	$15 \pm 9\%$
R	2.7%	2.6%

well be correlated in the least squares analysis since the unit
cell contains relatively few magnesium nuclei, i.e. 8 compared
with 16 aluminium and 32 oxygen nuclei; thus the nuclear scatter-
ing is dominated by the oxygen. For the relatively few reflexions
where the scattering is predominantly from the magnesium the two
temperature factors in the neutron data have similar effects. In
contrast, in the X-ray data, although some correlation between
these two parameters may be present it is likely to be less serious
since there were many more reflexions used in the analysis and the
main contribution to the structure factors originates from the
metal ions.

The best agreements between Fobs and Fcalc for both
space groups was obtained from the X-ray analysis with anisotropic
temperature factors and the final parameters are shown in table
2.7. The overall R-factor was only 0.2% better for $F\bar{4}3m$ but it
should be noted that most of this difference arises from an
improved fit to the weak and high order structure factors where one
would expect small atom movements to be of greater importance. This
is best illustrated by a breakdown of the R-factor into various
groups of $Sin\theta/\lambda$ and Fobs as shown in table 2.4 for all the X-ray
refinements. The differences between refinements III and IV are
also demonstrated by figure 2.7 where we have plotted this division
of the R-factor analysis as a histogram where the number of reflexions
in each category are given above the class widths. The group
$Sin\theta/\lambda$ = 0 to 0.13 contains only the 111 reflexion and the large
discrepancy between Fobs and Fcalc is attributed, at least in part
together with similar discrepancies to a few other low angle re-
flexions such as 220 and 113 to an overestimate of the integrated
intensity. Such effects arise because the absorption edge in the
β-filtered $MoK\alpha$ emission spectrum is so close to the Bragg peak that
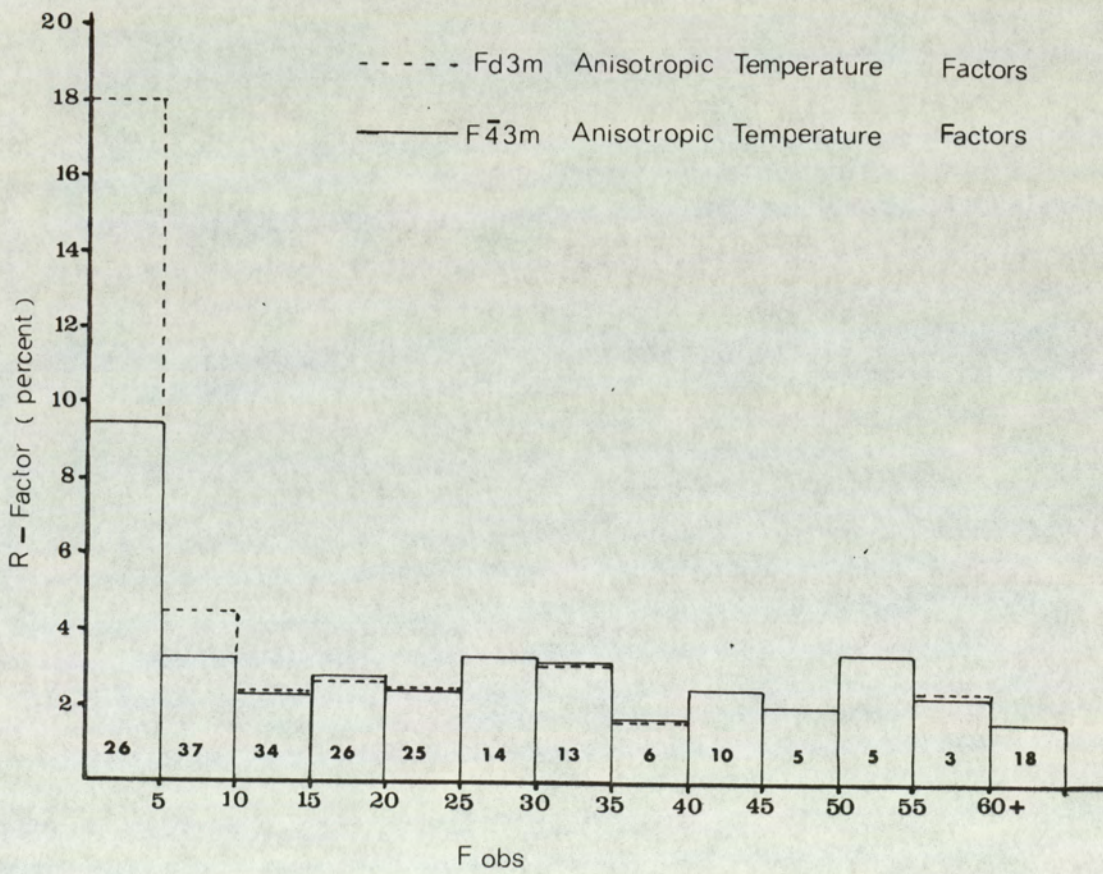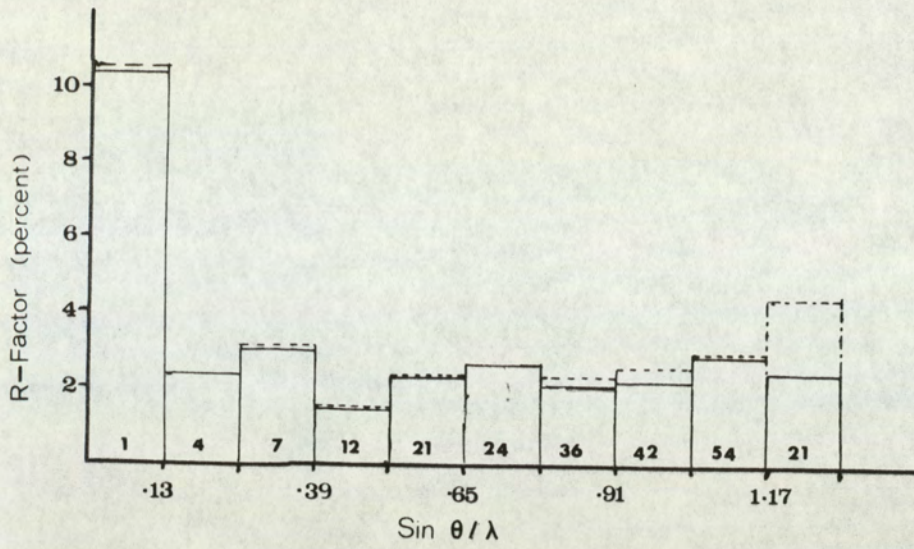the background tends to be underestimated. No attempt has been made

FIGURE 2.7   Analysis of R

Table 2.6: Structure parameters in Spinel
with space group F$\bar{4}$3m

	X-ray Data	Neutron Data
Position parameters		
$U_{A\ell}$ (x_1)	.6247 $\pm$ .0002	.626 $\pm$ .001
U_{OX1} (x_2)	.3888 $\pm$ .0002	.3885 $\pm$ .0005
U_{OX2} (x_3)	.8633 $\pm$ .0002	.8637 $\pm$ .0005
Temperature parameters		
$B_{Mg1}(0,0,0)$	.28 $\pm$ 02$\overset{o}{A}^2$	.63 $\pm$ .20$\overset{o}{A}^2$
$B_{Mg2}(\frac{1}{4},\frac{1}{4},\frac{1}{4})$	.43 $\pm$ .02$\overset{o}{A}^2$	.24 $\pm$ 15$\overset{o}{A}^2$
$B_{A\ell}$ $(x_1x_1x_1)$	.33 $\pm$ .02$\overset{o}{A}^2$	.38 $\pm$ .05$\overset{o}{A}^2$
$B_{OX1}(x_2x_2x_2)$	.52 $\pm$ .02$\overset{o}{A}^2$	.61 $\pm$ .10$\overset{o}{A}^2$
$B_{OX2}(x_3x_3x_3)$	.42 $\pm$ .02$\overset{o}{A}^2$	.48 $\pm$ .10$\overset{o}{A}^2$
INVERSION	17.5%	15%
R	2.6%	2.4%

Table 2.7: Structure parameters deduced from the X-ray results with anisotropic temperature factors

SPACE GROUP Fd3m

Thermal parameters

b_{ij} (these values have been multiplied by 10,000)

	b_{11}	b_{22}	b_{33}	b_{12}	b_{13}	b_{23}
Mg (0,0,0)	139(2)	139(2)	139(2)	0	0	0
Al ($\frac{5}{8},\frac{5}{8},\frac{5}{8}$)	124(2)	124(2)	124(2)	−6(2)	−6(2)	−6(2)
O (u,u,u)	186(3)	186(3)	186(3)	4(2)	4(2)	4(2)

Oxygen position parameter $u = .3876 \pm .0001$

Inversion = 17.5 percent

SPACE GROUP F$\bar{4}$3m

Thermal parameters

b_{ij} these values have been multiplied by 10,000)

	b_{11}	b_{22}	b_{33}	b_{12}	b_{13}	b_{23}
Mg1 (0,0,0)	169(11)	169(11)	169(11)	0	0	0
Mg2 ($\frac{1}{4},\frac{1}{4},\frac{1}{4}$)	118(10)	118(10)	118(10)	0	0	0
Al (X_1,X_1, X_1)	125(2)	125(2)	125(2)	−6(2)	−6(2)	−6(2)
O1 (X_2,X_2,X_2)	210(8)	210(8)	210(8)	−12(9)	−12(9)	−12(9)
O2 (X_3,X_3,X_3)	159(7)	159(7)	159(7)	14(8)	14(8)	14(8)

Position parameters

Al $X_1 = .6247 \pm .0002$

O1 $X_2 = .3887 \pm .0002$

O2 $X_3 = .8635 \pm .0002$

Inversion = 17.5 percent

to correct for this effect, which is only significant at low angles, although following the recent work of Nelmes (1975) in retrospect it might have been desirable to have done this.

We emphasize also that the discrepancy of the high order reflexions in Fd3m are unlikely to originate from thermal diffuse scatter (T.D.S), which peaks under the Bragg peak, and can lead to an underestimation of the intensity since an approximate correction for T.D.S, requiring a knowledge of the elastic constants, introduced by Pryor (1966) and discussed in the book by Pryor and Willis (1975), accounts for only 1% of the intensity. Thus, despite the problems of obtaining reliable intensity measurements of the weak reflexions it seems likely in view of the result that $F\bar{4}3m$ symmetry consistently improves the weak and high angle reflexions that the change of space group is significant.

In the refinement of any crystal structure the introduction of extra variables into the least squares analysis will normally lead to a better agreement between the observed and calculated structure factors simply because there are fewer restraints on the model. Since we wish to distinguish between two structures which are similar it is necessary to ask the question; Is the gain in the R-factor significant or is it just a manifestation of the introduction of extra parameters? This is a difficult question to answer, but a solution can be obtained from the R-factors using the statistical significant levels derived by Hamilton (1965), who tests the R-factor ratio R_1/R_0*, by linear hypothesis tests (Hamilton 1964). In this ratio

---

*This analysis should strictly be based on the generalised R-factors which are defined as $R = \{\Sigma w_i (|F_0|_i - |F_c|_i)^2 / \Sigma w_i |F_0|_i^2\}^{\frac{1}{2}}$ but Hamilton emphasizes that the ratio R_1/R_0 is insensitive to the method by which the R-factor is computed and that the conventional R-factor is adequate for most purposes.

R_1 is the R-factor for the unrestrained model and R_0 is the R-factor for the model containing fewer parameters. With this approach, it turns out that we can reject the hypothesis that the space group cannot be $F\bar{4}3m$, with at least 99.50% certainty which means that the gain in R-factor when the X-ray data is refined under $F\bar{4}3m$ symmetry must be considered very significant indeed. Similar tests with the two neutron refinements, however, shows that the above hypothesis can only be rejected in this case with 90% certainty.

The bond lengths between the atoms can be evaluated from the formulae derived in table 2.8, where the δ parameters defined describe the shifts from the ideal configuration. The actual estimates of the bond lengths in Magnesium Aluminate from refinements III and IV together with the standard deviations derived from the least squares analysis are shown in table 2.9. As can be seen the bond lengths differ by about .010 ~ .030Å from the corresponding values in Fd3m, the bond lengths in the latter case being evaluated by constraining the equations of table 2.8 with $\delta_1 = 0$ and $\delta_2 = \delta_3 = \delta = u - {}^3/_8$.

We can compare these bond lengths with the numerical significance levels suggested by Cruickshank (1949), who gives the following criterion.

If P represents the probability that a bond length d_1 having standard deviation $\sigma(d_1)$ could be observed greater than a bond length d_2 having standard deviation $\sigma(d_2)$ by $\delta\ell$ by chance: then

       if   P > 5% $\delta\ell$ is not significant

       if   5% $\geqslant$ P > 1% $\delta\ell$ is of possible significance

       if   1% > P > 0.1% $\delta\ell$ is significant, and

       if   P $\leqslant$ 0.1% $\delta\ell$ is said to be highly significant.

Table 2.8 Bond Lengths for $F\bar{4}3m$

Mg1–O2	$d = \sqrt{3}\, a\, (^1/_8 + \delta_3)$
Mg2–O1	$d = \sqrt{3}\, a\, (^1/_8 + \delta_2)$
Al–O1	$d = a\sqrt{[3(\delta_1{}^2 + \delta_2{}^2) - 2\delta_1\delta_2 - \frac{1}{2}(\delta_1 + \delta_2) + {}^1/_{16}]}$
$\approx$	$a/_4 \{1 - 4(\delta_2 + \delta_1) + 16(\delta_2{}^2 + \delta_1{}^2) - 32\delta_1\delta_2 + \cdots\}$
Al–O2	$d = a\sqrt{[3(\delta_1{}^2 + \delta_3{}^2) + 2\delta_1\delta_3 - \frac{1}{2}(\delta_3 - \delta_1) + {}^1/_{16}]}$
$\approx$	$^a/_4 \{1 - 4(\delta_3 - \delta_1) + 16(\delta_3{}^2 + \delta_1{}^2) + 32\delta_1\delta_3 + \cdots\}$
O1–O1	$d = a\sqrt{2}\,(\frac{1}{4} - 2\delta_2)$
O1–O1	$d = a\sqrt{2}\,(\frac{1}{4} + 2\delta_2)$
O2–O2	$d = a\sqrt{2}\,(\frac{1}{4} - 2\delta_3)$
O2–O2	$d = a\sqrt{2}\,(\frac{1}{4} + 2\delta_3)$
O1–O2	$d = a\sqrt{[3(\delta_2{}^2 + \delta_3{}^2) - 2\delta_2\delta_3 + {}^1/_8]}$
$\approx$	$\dfrac{a_0}{2\sqrt{2}} \left\{1 + 24(\delta_1{}^2 + \delta_3{}^2) - 8\delta_2\delta_3 + \cdots\right\}$

a	$=$	lattice constant	O1 = OX1$(x_2 x_2 x_2)$
δ_1	$=$	$^5/_8 - x_1$	O2 = OX2$(x_3 x_3 x_3)$
δ_2	$=$	$x_2 - {}^3/_8$	
δ_3	$=$	$^7/_8 - x_3$	

Table 2.9 Bond lengths in Spinel

Fd3m			F$\bar{4}$3m		
Bond	Distance $\overset{o}{A}$	σ $\overset{o}{A}$	Bond	Distance $\overset{o}{A}$	σ $\overset{o}{A}$
Mg–0	1.926	0.002	Mg1–02(d_t)	1.912	0.003
			Mg2–01(d_t')	1.942	0.003
Aℓ–0	1.924	0.002	Aℓ–01(d_o)	1.914	0.004
			Aℓ–02(d_o')	1.934	0.004
0–0	2.570	0.003	01–01(d_1)	2.545	0.005
			02–02(d_2)	2.593	0.005
0–0	2.865	0.001	01–02(d_3)	2.865	0.001
0–0	3.146	0.003	01–01(d_1')	3.171	0.005
			02–02(d_2')	3.123	0.005

a* = 8.083 $\pm$ .001$\overset{o}{A}$

* estimated by Bristol
  group from diffractometer
  control matrix.

The probability P due to random errors is given by the normal error curve as,

$$P = \tfrac{1}{2}[1 - \text{erf}(x)]$$

where $x = \delta\ell/(2\sigma^2(d_1)+2\sigma^2(d_2))^{\frac{1}{2}}$.

Applying these to the differences between the bond lengths calculated from Fd3m and $\overline{F43}m$ space groups we obtain the following results:

	Bond	Bond Difference($\overset{o}{A}$)	x	P
d_t	Mg1-02	.014	2.75	< .1%
d_t'	Mg2-01	.016	3.14	< .1%
d_o	$A\ell$-01	.010	1.57	1.3%
d_o'	$A\ell$-02	.010	1.57	1.3%
d_1	01-01	.025	3.05	< .1%
d_2	02-02	.023	2.80	< .1%
d_1'	01-01	.025	3.05	< .1%
d_2'	02-02	.023	2.80	< .1%

Thus, all the bond differences on Cruickshank's criterion are highly significant except for the $A\ell$-O bonds and these border on the possibly significant/significant categories. Once again, therefore, analysis supports the contention that the structure of $MgA\ell_2O_4$ is more correctly described by the space group $\overline{F43}m$.

The structure factors of the forbidden reflexions calculated from the best X-ray and neutron diffraction data refinements under the space group $\overline{F43}m$ are shown in table 2.10. In the X-ray case about $\tfrac{1}{2}$ of the forbidden reflexions within the angular range of the diffractometer are well below the minimum detectable limit which was optimistically estimated to be approximately 1.2 electrons. Of the remainder the 0.0.6 reflexion is the strongest and possibly offers the best chance of an unequivocal observation of a "forbidden reflexion". In the neutron data the 0.0.6 is the

only reflexion above the minimum detectable limit which in this case appeared to be about 0.4×10^{-12} cm.

An estimate of the intensity of the forbidden reflexions, excluding the $0.0.\ell$'s, was obtained by the same procedure used to derive the intensities of the other reflexions (section 2.4). Two types of histogram were observed and are shown below. If the pattern was of type I then the intensity was thought to be below the detectable limit of the diffractometer and was given the value zero. If, on the other hand, the distribution was of type II, then the intensity was given the value corresponding to the mean of the "Gaussian" distribution. Table 2.10
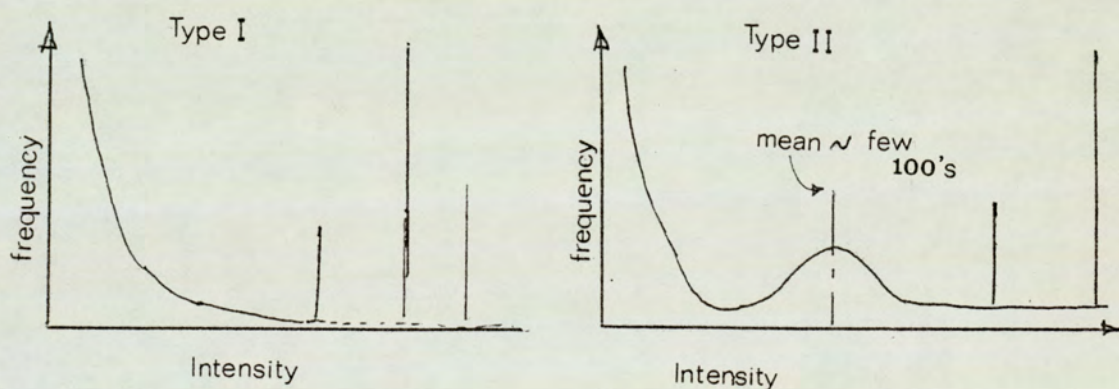
compares these estimates of the forbidden relfexions with the calculated values. In most cases there is a fair correspondence between these values which is remarkable considering how very weak they are and the considerable double diffraction effects.

Finally, the small atom movements giving rise to the $F\bar{4}3m$ symmetry are shown in figures 2.8 and 2.9. The former figure indicating both tetrahedral sites while the latter shows the surroundings of the octahedral ion which is normally at $\frac{5}{8},\frac{5}{8},\frac{5}{8}$ (cross-hatched in the diagram). Note that these diagrams are drawn for the ideal configuration with the origin at an oxygen site and the arrows indicate the senses of the <111> displacements

Table 2.10: Forbidden Reflexions

h	k	l	No of Equiv	Intensity obs	F obs	F calc Refinement II	F calc Refinement IV	F43m Neutron data F calc in 10^{-12} cm
0	0	2	–	–	–	3.81	3.93	0.16
0	0	6	3	–	–	4.91	4.88	0.45
0	0	10	2	–	–	1.98	1.97	0.12
0	0	14	2	–	–	2.12	1.72	
0	0	18	2	–	–	1.22	1.47	
0	2	4	8	∼0	0	2.33	2.41	0.18
0	2	8	10	∼0	0	0.20	0.04	0.20
0	2	12	12	500	1.62	0.87	0.92	
0	2	16	11	∼0	0	1.22	0.90	
0	4	6	10	∼0	0	2.32	2.52	0.06
0	4	10	12	∼350	1.36	2.99	2.85	0.31
0	4	14	8	∼0	0	0.15	0.23	
0	6	8	10	∼400	1.45	1.91	2.06	0.17
0	6	12	12	∼550	1.70	1.13	0.62	
0	6	16	11	∼0	0	0.12	0.45	
0	8	10	8	∼0	0	0.23	0.05	
0	8	14	11	∼0	0	0.80	0.61	
0	10	12	9	∼0	0	0.37	0.59	
0	10	16	11	∼400	1.44	2.07	1.45	
0	12	14	12	∼300	1.25	1.87	1.60	

∼ 0   Intensity thought to be below the observable limit

–   No estimate was made, because there are too few equivalents

corresponding to $F\bar{4}3m$ symmetry. The diagrams also show the origin of all the distances given in table 2.9. Figure 2.10 shows how two sections labelled A and B of the structure are fitted together to complete one unit cell of Spinel.
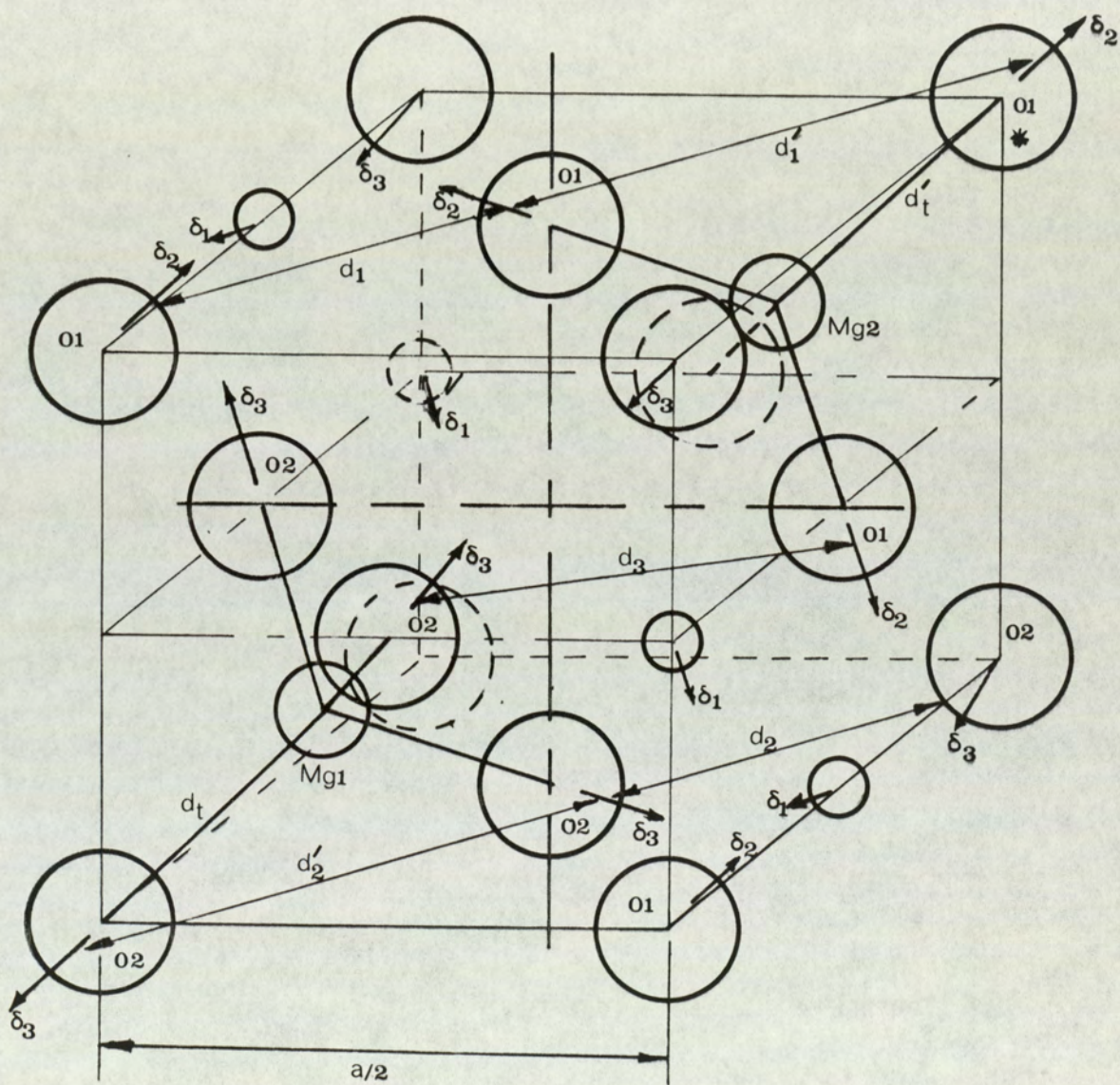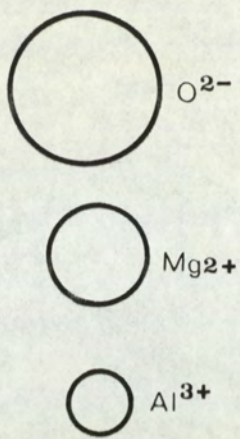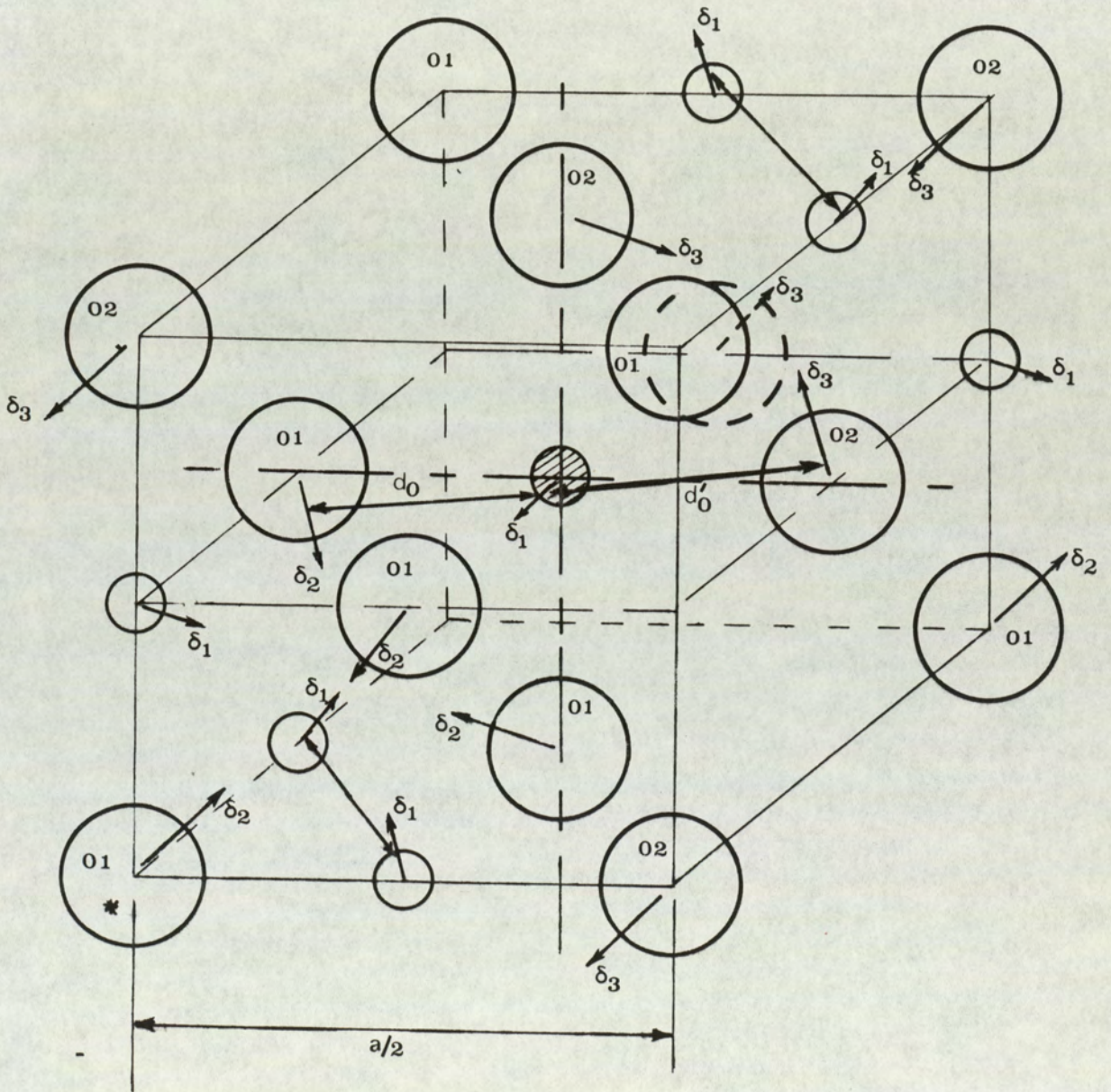
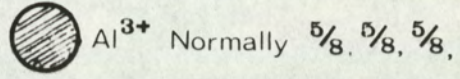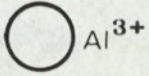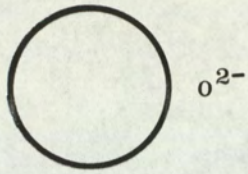FIGURE 2.8 Section A of the Spinel structure

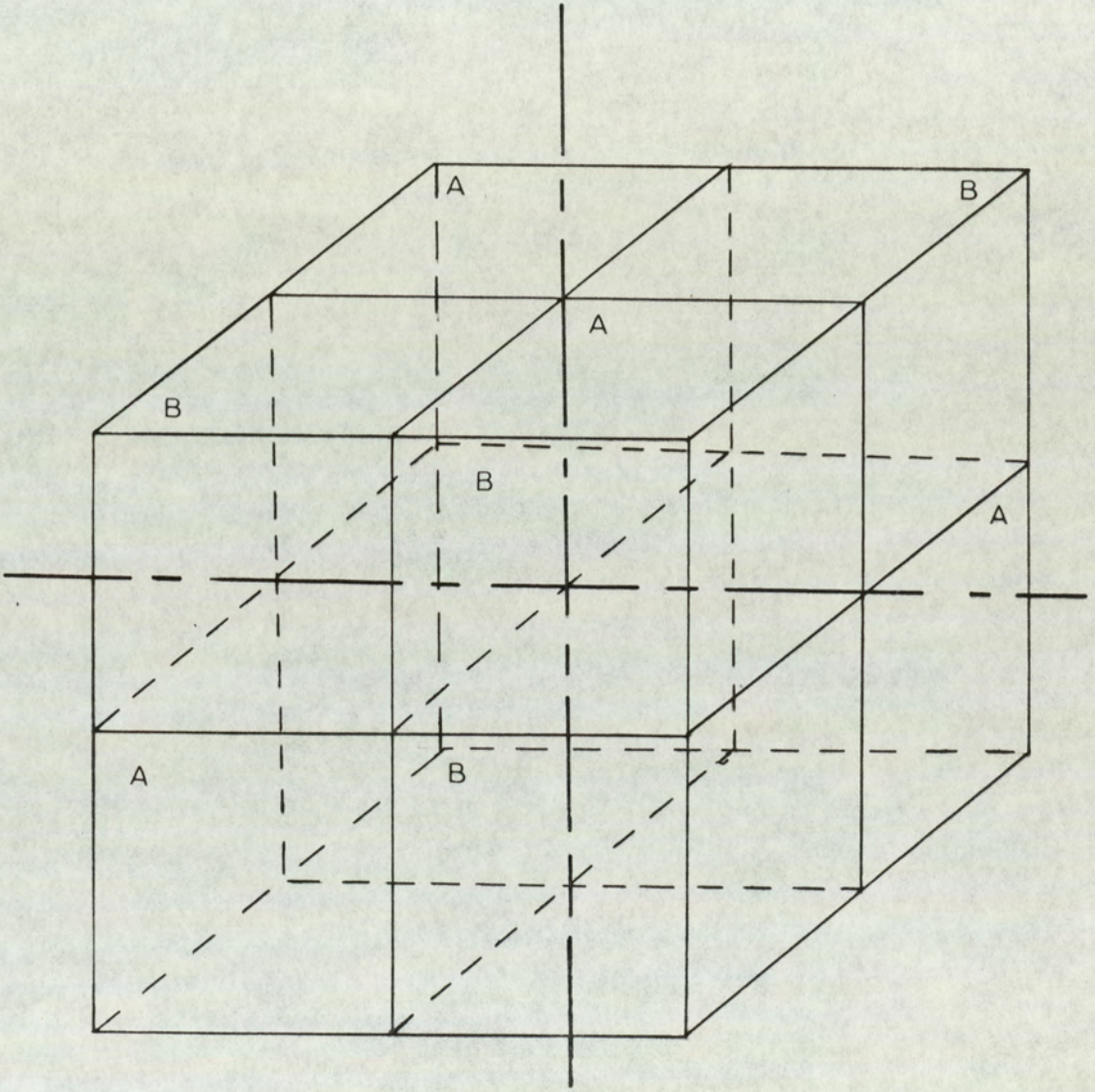FIGURE 2.9   Section B   of   the   Spinel structure

FIGURE 2.10 A unit cell of Spinel

CHAPTER 3

LATTICE DYNAMICS IN THE HARMONIC APPROXIMATION.

3.1) Born von Karman Theory of Lattice Dynamics.

3.1.1) Basic theory.

Although for many purposes a crystalline solid may be regarded as an idealised elastic continuum it is now generally recognised that the vibrational spectrum of a real crystal can differ appreciably and that this distinction can only be satisfactorily explained along the lines first suggested by Born and von Kármán (1912,1913). The theory which they developed takes account of the discrete nature of crystal structures and is the foundation upon which all recent work on lattice dynamics, including that presented here, is based. A brief outline of the essential ideas is therefore given in this chapter; the standard work of reference is that of Born and Huang (1954). The theory is based on a number of assumptions of which the most important are:-

i) the crystal structure is periodic and infinite in extent,

ii) the harmonic approximation and

iii) the adiabatic approximation.

In an infinite three dimensional periodic lattice the position of the kth nucleus in the ℓth unit cell can be expressed as,

$$\underline{r}(\ell k) = \underline{r}(\ell) + \underline{r}(k) \qquad 3.1$$

where the suffix $k = 1,2 \ldots n$, there being n atoms in the primitive unit cell and the lattice vector $\underline{r}(\ell)$ is defined as

$$\underline{r}(\ell) = \ell_1 \, \underline{a}_1 + \ell_2 \, \underline{a}_2 + \ell_3 \, \underline{a}_3 \qquad 3.2$$

ℓ_1, ℓ_2 and ℓ_3 being integer, and $\underline{a}_1, \underline{a}_2, \underline{a}_3$ are the basis vectors of the primitive unit cell.

Each nucleus is displaced from its equilibrium position and such displacements are represented by the vectors $\underline{u}(\ell k)$. If the displacements are small then the total potential energy of the crystal ϕ, may be expanded as a series in powers of the displacements, using the multivariable Taylor series expansion:

$$\phi = \phi_0 + \phi_1 + \phi_2 + \dots \qquad\qquad 3.3$$

Since ϕ_0 is merely a reference potential, the reference may be chosen as zero. The term ϕ_1 expressed as,

$$\phi_1 = \sum_{\ell k \alpha} \left. \frac{\partial \phi}{\partial u_\alpha(\ell k)} \right|_0 u_\alpha(\ell k) \qquad\qquad 3.4$$

involves only terms of the first differential and as these de-rivatives are evaluated at the equilibrium positions of the atoms, this term is also zero.

In the harmonic approximation the series is truncated after the second term so that small vibrations are controlled by the second differential of the potential, through the term ϕ_2 which is,

$$\phi_2 = \tfrac{1}{2} \sum_{\ell k \alpha} \sum_{\ell' k' \beta} \left. \frac{\partial^2 \phi}{\partial u_\alpha(\ell k)\, \partial u_\beta(\ell' k')} \right|_0 u_\alpha(\ell k) u_\beta(\ell' k') \qquad 3.5$$

For most purposes a second order theory such as this is adequate even though ideally harmonic crystals have zero thermal expansion, no thermal conductivity, elastic constants which are independent of temperature and pressure, and other properties not exhibited by real crystals. Higher order or anharmonic theories where interactions between normal modes of vibration can be accounted for, are required to understand the more realistic behaviour. For a discussion of anharmonic theories see Maradudin and Flinn (1963). Finally, it is implicitly assumed that the electrons instantaneously take up the configuration of the displaced nuclei, which is probably reasonably valid providing that the electronic band gap is very much greater than the vibrational energies of the lattice. This is the adiabatic approximation believed to be most closely satisifed by ionic crystals.

Now, the α-component of the force acting on atom (ℓk) is,

$$F_\alpha(\ell k) = -\frac{\partial \phi}{\partial u_\alpha(\ell k)}. \qquad 3.6$$

Substituting 3.5 into 3.6 and differentiating, the equation of motion is obtained as,

$$M_k \ddot{u}_\alpha(\ell k) = -\sum_{\ell' k' \beta} \phi_{\alpha\beta}(\ell k \ell' k') u_\beta(\ell' k') \qquad 3.7$$

where $\left. \dfrac{\partial^2 \phi}{\partial u_\alpha(\ell k) \partial u_\beta(\ell' k')} \right|_o$ has been written as $\phi_{\alpha\beta}(\ell k, \ell' k')$, and M_k is the mass.

The quantities, $-\phi_{\alpha\beta}$'s, correspond to force constants giving the α component of the force exerted on atom (ℓk) when atom $(\ell' k')$ is given unit displacement in the β-direction. The symmetry properties of the crystal lattice impose restrictions on the indices in the expressions for ϕ_1, ϕ_2, ϕ_3 etc, and limit the number of independent force constants. In addition, the structural periodicity of an ideal crystal requires that if the lattice is translated by a vector $\underline{r}(\ell)$ then the lattice once more coincides with itself. Under such a translation, physical quantities such as potential, polarisability, electric field, etc. must be invariant. The force constants $-\phi_{\alpha\beta}(\ell k, \ell' k')$ can then only depend on the relative cell indices $\ell-\ell'$, and not on ℓ or ℓ' independently.

Consider the effect when the nuclei are displaced by the same vector, say $\underline{\epsilon}$, from their equilibrium positions, this represents a translation of the lattice as a whole. The derivative $\partial \phi / \partial u_\alpha(\ell k)$ is given by,

$$\phi_\alpha(k) + \sum_{\ell' k' \beta} \phi_{\alpha\beta}(\ell k, \ell' k') \epsilon_\beta . \qquad 3.8$$

Since the potential energy of the lattice is unchanged by this

uniform translation, the value of the derivative $\partial\phi/\partial u_\alpha(\ell k)$ must be independent of $\underline{\epsilon}$ and must therefore vanish. This leads to relations of the type,

$$\sum_{\ell' k'} \phi_{\alpha\beta}(\ell k, \ell' k') = \sum_{\ell k} \phi_{\alpha\beta}(\ell k, \ell' k') = 0 \qquad 3.9$$

and thus one defines a "self-force constant" involving only atom (ℓk) as,

$$\phi_{\alpha\beta}(\ell k, \ell k) = -\sum_{\ell' k'}{}' \phi_{\alpha\beta}(\ell k, \ell' k') \qquad 3.10$$

the prime on the summation indicates that the term $\ell' k' = \ell k$ is omitted. This term is known as translational invariance and has important consequences when numerical calculations are attempted.

The equations of motion 3.7 represent a set of simultaneous linear differential equations infinite in number. But because of the periodicity of the lattice we can introduce the normal modes of vibration which decouple the equations and reduce their number. Hence, assuming a plane wave solution of the type,

$$u_\alpha(\ell k) = M_k^{-\frac{1}{2}} U_\alpha(k, \underline{q}) \exp(i\underline{q}\cdot\underline{r}(\ell k) - i\omega(\underline{q})t) \qquad 3.11$$

where $\underline{q} = 2\pi/\lambda$ is the wave vector for a travelling wave of wavelength λ and angular frequency $\omega(\underline{q})$ and $\underline{r}(\ell k)$ the vector previously defined (3.1), the equation of motion becomes

$$\omega^2(\underline{q}) U_\alpha(k, \underline{q}) = \sum_{k'\beta} D_{\alpha\beta}(kk', \underline{q}) U_\beta(k', \underline{q}) \qquad 3.12$$

which in matrix notation may be written

$$\omega^2 \underline{U} = [D]\underline{U} \qquad 3.13$$

The dynamical matrix, D, is then given by

$$D_{\alpha\beta}(kk',\underline{q}) = (M_k M_{k'})^{-\frac{1}{2}} \sum_{\ell'} \phi_{\alpha\beta}(\ell k, \ell' k') \exp[i\underline{q} \cdot \{\underline{r}(\ell' k') - \underline{r}(\ell k)\}] \quad 3.14$$

If there are n atoms in the primitive unit cell equation 3.13 is a set of 3n linear equations, with a condition for solubility which is,

$$\left| D_{\alpha\beta}(kk',\underline{q}) - \omega^2 \, \delta_{\alpha\beta} \, \delta_{kk'} \right| = 0 \qquad\qquad 3.15$$

This is an equation of $3n^{th}$ degree in ω^2, the squared normal mode angular frequencies, the 3n solutions being the eigenvalues $\omega^2(\underline{q}, j)$ for each value of which there are a set of values for the displacements $U_\alpha(k\underline{q}, j)$. The eigenvectors of matrix D, $\underline{e}(k\underline{q}, j)$ can be chosen orthogonally and are related to $\underline{U}$ for they determine the pattern of nuclear displacements when the wave of angular frequency ω is propagated through the lattice. The index j takes integer values only i.e. j = 1,2 ... 3n and is used to label and identify the branch of the dispersion system to which the phonon or normal mode $\omega(\underline{q}, j)$ belongs.

Newton's third law implies that the force constants are invariant for permutations of the indices, so that

$$\phi_{\alpha\beta}(\ell k, \ell' k') = \phi_{\beta\alpha}(\ell' k', \ell k) \qquad\qquad 3.16$$

and as a result it follows that,

$$D^*_{\alpha\beta}(kk',\underline{q}) = D_{\beta\alpha}(k'k,\underline{q}), \qquad\qquad 3.17$$

where $D^*_{\alpha\beta}(kk',\underline{q})$ is the complex conjugate of $D_{\alpha\beta}(kk',\underline{q})$. Therefore $D_{\alpha\beta}(kk',\underline{q})$ defines a 3n * 3n Hermitian matrix and accordingly all the eigenvalues are real. In order that ω^2 should be positive, so that the normal mode frequencies are real, the principle minors of matrix D must all be positive, which is the condition to produce a stable crystal lattice.

As $q \to 0$, $\omega \to 0$ for 3 of the 3n normal modes of vibration. These are the acoustic modes, and in the limit $q \to 0$ correspond to

elastic waves in the solid. The remaining 3n-3 vibrational modes have finite frequencies as q → 0. These are the optic modes and some may couple to infra-red radiation, providing certain conditions are met, and in the case of Spinel will be discussed later.

3.1.2) The force constants.

Before any numerical calculations can be attemped to examine dispersion relations, and physical properties of crystals, it is necessary to determine the force constants - $\phi_{\alpha\beta}$. This is the central problem in calculations of the dynamics of atoms in crystal lattices, and can sometimes prove difficult, for in the most part, the interatomic potential has no unique mathematical form, and consequently the forces acting between atoms are unknown. The problem is sometimes overcome by refining directly the $\phi_{\alpha\beta}$'s as independent parameters to obtain a fit with the experimental dispersion curves. This has been carried out mainly for covalent crystals, such as Germanium (Pope 1963), where nineteen independent force constants were fitted to forty-seven observed phonon frequencies taken from the results of Brockhouse and Iyengar (1957). Alternatively a functional form for the potential may be assumed and parameters describing this potential, through the independent interactions can be refined. This has been successfully applied to the problem of the solid inert gases, see for example, Horton and Leech (1963).

As a result of the difficulty concerning force constants several theoretical approximations have been developed, the most successful being the shell model of Dick and Overhauser (1958) in which the electron clouds surrounding the nuclei are represented by rigid shells. Since the forces between electrons and nuclei, electrons and electrons can then be represented it is possible to a certain extent to reconcile the polarisation effects of the various

atoms. Historically, this model was first applied to the alkali halides (Cochran, 1959b , Woods et al. 1960) but more recently has also been applied to covalent materials like Germanium (Cochran 1959c ; Dolling 1963) and to other ionic crystals like the Perovskites, an example of which is $SrTiO_3$ (Stirling,1972).

The theory of lattice dynamics in ionic crystals is somewhat simpler than that for covalent and other crystals, for at least the form of part of the interionic potential namely, the Coulomb potential is well known. But, whichever model is employed to describe the vibrational behaviour of this type of solid the repulsive contribution to the potential function is always represented by a function of a number of adjustable parameters. Shell models have produced superior descriptions of the vibrational properties of ionic compounds than those provided by the less sophisticated but simpler Rigid Ion model of Kellermann(1940). However it must be emphasized that substantial information can be obtained from the latter and models of this type often offer a very good first approximation to the phonon dispersion curves in structures like Spinel where numerical calculations have not previously been attempted. In a later chapter we treat the vibrations of Spinel under this approximation, so the essential features of the Rigid Ion model will now be described.

3.2) Ionic Crystals in the Rigid Ion Approximation.

If it can be assumed following Kellermann (1940) that the ions in an ionic crystals are rigid, spherical and do not overlap, that is, that they can be treated as point charges, then the crystal potential can be expressed as.

$$\phi = \frac{1}{2} \sum_{\ell k} \sum_{\ell' k'} \left[\frac{e^2 Z_k Z_{k'}}{r} + v(r) \right] \qquad 3.18$$

where $r = |\underline{r}(\ell'k') - \underline{r}(\ell k)|$ and the ionic charge on the kth ion has been written as eZ_k. The overlap potential $v(r)$ may be approximated by mathematical forms such as br^{-n} or $\lambda \exp(-r/\rho)$ and is usually restricted to nearest neighbour ions only. The parameters b and n, or λ and ρ are then adjustable parameters which may be refined directly.

The crystal potential, is split into Coulomb and re-pulsive (overlap) parts and correspondingly the force constants are also divided by writing,

$$\phi_{\alpha\beta}(\ell k, \ell' k') = \phi_{\alpha\beta}^{C}(\ell k, \ell' k') + \phi_{\alpha\beta}^{R}(\ell k, \ell' k'), \qquad 3.19$$

where the suffix C and R represent the Coulomb and repulsive components respectively. Similarly, the dynamical matrix divides so that,

$$D_{\alpha\beta}(kk', \underline{q}) = D_{\alpha\beta}^{C}(kk, \underline{q}) + D_{\alpha\beta}^{R}(kk', \underline{q}). \qquad 3.20$$

In this expression the Coulomb contributions are normally written as,

$$D_{\alpha\beta}^{C}(kk', \underline{q}) = (M_k M_{k'})^{-\frac{1}{2}} \frac{e^2}{V_a} Z_k Z_{k'} C_{\alpha\beta}(kk', \underline{q}) - \delta_{kk'} \frac{e^2}{V_a} \frac{Z_k}{M_k} \sum_{k''} Z_{k''} C_{\alpha\beta}(kk'', 0) \qquad 3.21$$

where the $C_{\alpha\beta}(kk', \underline{q})$ are the dimensionless coefficients introduced by Kellermann which depend only on the crystal structure, and V_a is the volume of the primitive unit cell. The second term arises from the translational invariance property. The Coulomb force constants are now defined as

$$\phi_{\alpha\beta}^{C}(\ell k, \ell' k') = Z_k Z_{k'} \frac{\partial^2 r^{-1}}{\partial u_\alpha(\ell k) \partial u_\beta(\ell' k')} \qquad 3.22$$

and the self force constant as,

$$\phi_{\alpha\beta}(\ell k, \ell k) = - e^2 Z_k \sum_{\ell' k'} Z_{k'} \frac{\partial^2 r^{-1}}{\partial u_\alpha(\ell k) \partial u_\beta(\ell' k')} \qquad 3.23$$

Hence,

$$C_{\alpha\beta}(kk',\underline{q}) = \sum_{\ell'} \frac{\partial^2 \ r^{-1}}{\partial u_{\alpha}(\ell k) \partial u_{\beta}(\ell'k')} \ \exp[i\underline{q}.\underline{r}] \ . \qquad 3.24$$

This slowly convergent Coulomb series is transformed by Ewald's transformation (Ewald 1921) into two rapidly convergent series, one a sum in real space the other in reciprocal space.

The repulsive contribution to the dynamical matrix is expressed as

$$D_{\alpha\beta}(kk',\underline{q}) = (M_k M_{k'})^{-\frac{1}{2}} \sum_{\ell'} \phi_{\alpha\beta}(\ell k, \ell'k') \ \exp(i\underline{q}.\underline{r}) \qquad 3.25$$

and is reduced to the dimensionless coefficients of Kellerman by introducing two parameters defined as,

$$A = \frac{2V_a}{e^2} \frac{\partial^2 \phi}{\partial r^2}\bigg|_{\parallel} \quad , \quad B = \frac{2V_a}{e^2} \ \frac{\partial^2 \phi^R}{\partial r^2}\bigg|_{\perp} \qquad 3.26$$

where A is evaluated parallel to the line joining the interacting particles and B perpendicular to this line, both derivatives being evaluated at the equilibrium positions of the ions. The repulsive contribution can then be written thus,

$$D^R_{\alpha\beta}(kk',\underline{q}) = (M_k M_k)^{-\frac{1}{2}} \frac{e^2}{V_a} \ R_{\alpha\beta}(kk',\underline{q}) \qquad 3.27$$

where;

$$R_{\alpha\beta}(kk',\underline{q}) = -\frac{1}{2} \sum_{\ell} \left[\frac{r_{\alpha}(\ell k, \ell'k') r_{\beta}(\ell k, \ell'k')}{|r(\ell k, \ell'k')|^2} A(\ell k, \ell'k') + \right.$$

$$\left. + B(\ell k, \ell'k')\left\{ \delta_{\alpha\beta} - \frac{r_{\alpha}(\ell k, \ell'k') r_{\beta}(\ell k, \ell'k')}{|r(\ell k, \ell'k')|^2} \right\} \right] \times$$

$$\times \exp[i\underline{q}.\{\underline{r}(\ell'k') - \underline{r}(\ell k)\}] \qquad 3.28$$

and the sum of ℓ' extends over nearest neighbours of the same type only. The self force constant is derived from the translational invariance and is

$$R_{\alpha\beta}(kk,q) = - \sum_{k'}' R_{\alpha\beta}(kk',0) \qquad 3.29$$

where the prime on the summation indicates the term $k = k'$ is omitted.

Finally the dynamical matrix in matrix notation, excluding translational invariance is

$$[D] = \frac{e^2}{V_a} [M^{-\frac{1}{2}}] \left\{ [Z] [C] [Z] + [R] \right\} [M^{-\frac{1}{2}}] \qquad 3.30$$

Note: the translational invariance has to be added to this matrix before diagonalisation to obtain the normal mode angular frequencies. Matrix R is parameterised in terms of the A's and B's for each independent interaction involved with the structure under consideration. Matrix Z is diagonal and contains the ionic charges which can also be regarded as parameters of the model, and which by adjustment can be used to compensate, rather inadequately, for polarization effects. This was first pointed out by Szigeti (1949) who showed in particular that the static dielectric constant in NaCℓ is comparable with the experimental value providing the ionic charge is slightly less than its nominal value, i.e. Zeff = .74 These parameters then are also at our disposal to effect a fit with the experimental dispersion curves.

It should be emphasized that in the description given so far, the harmonic vibrations of a crystal lattice have been considered in the rigid ion approximation for wave vectors greater than zero. The long wavelength limit has not been discussed in any detail, because of certain mathematical difficulties which arise from the divergence of the series 3.25 as $q \to 0$. Nevertheless, the latter region is of some importance as it is in this region that the macroscopic properties of the crystal are directly comparable with the theory. We therefore outline in the next section how the elastic and dielectric properties of ionic crystals may be accommodated

within the dynamical theory.

3.3) Elastic and Dielectric properties.

In the long wavelength limit the vibrations of the atoms calculated from the dynamical theory must represent elastic waves in the crystal, but in ionic crystals mathematical difficulties arise as $q \to 0$. As a consequence equation 3.12 has to be solved .by a perturbation method due to Born (Born and Huang 1954) which involves expanding the dynamical matrix with respect to the wave-vector q. The details of this method will not be given here, but since some of the results are needed for Spinel we briefly indicate their origin.

In classical elasticity theory Hooke's Law relates stress and strain tensors by the elasticity tensor, according to the relation,

$$S_{\alpha\gamma} = \sum_{\beta\lambda} C_{\alpha\gamma,\beta\lambda} \, s_{\beta\lambda} \qquad\qquad 3.31$$

where S,s,C are the stress,strain and elasticity tensors respectively. The equation of motion for a plane elastic wave of wavevector q, is given by, (see Born and Huang)

$$\rho\omega^2 u_{\alpha} = \sum_{\beta} \left[\sum_{\gamma\lambda} C_{\alpha\gamma,\beta\lambda} \, q_{\gamma} q_{\lambda} \right] u_{\beta} \qquad\qquad 3.32$$

u being the displacement and ρ the mass density. In the perturbation method developed by Born quantities appear which can be identified with the square bracket term, and hence the elements of the elasticity tensor can be evaluated in terms of the parameters of the model employed, describing the dynamics. For ionic crystals, however, equation 3.32 is incorrect as electrical effects produced by the motion of the ions cannot be divorced from the mechanical effects so that true elastic waves do not exist in this case. This

problem is overcome in Born's treatment by regarding all ionic crystals as piezoelectric. Thus in ionic crystals associated with the plane elastic wave

$$u_\alpha(\underline{x},t) = \overline{U}_\alpha \exp(\ell \underline{q} \cdot \underline{x} - i\omega t)$$

there is an electric field whose amplitude is given by,

$$E_\alpha(\underline{x},t) = \overline{E}_\alpha \exp(\ell \underline{q} \cdot \underline{x} - i\omega t),$$

and the stress is related by the tensor equation,

$$S_{\alpha\gamma} = \sum_{\beta\gamma} C_{\alpha\gamma,\beta\lambda} \, s_{\beta\lambda} - \sum_\beta e_{\beta,\alpha\gamma} E_\beta. \qquad\qquad 3.33$$

Similarly, the dielectric polarisation is given by the tensor equation,

$$P_\alpha = \sum_{\beta\gamma} e_{\alpha,\beta\gamma} \, s_{\beta\gamma} + \sum_\beta a_{\alpha\beta} E_\beta, \qquad\qquad 3.34$$

where $a_{\alpha\beta}$ is an element of the dielectric susceptibility tensor $e_{\beta,\alpha\gamma}$ a component of the piezoelectric tensor and $\underline{E}$ is the macroscopic electric field. The true equation of motion for a plane wave is therefore,

$$\rho\omega^2 u_\alpha = \sum_\beta \left[\sum_{\gamma\lambda} C_{\alpha\gamma,\beta\lambda} \, q_\gamma q_\lambda \right] \overline{u}_\beta + i \sum_\beta \left[\sum_\gamma e_{\beta,\alpha\gamma} q_\gamma \right] \overline{E}_\beta \qquad 3.35$$

and from the perturbation theory quantities can be identified with the terms in the square brackets to give the components of the elastic, dielectric and piezoelectric tensors.

In general a crystal structure will contain more than one atom per lattice point, and when such a structure is deformed the resulting strain at a point arises from two sources, called internal and external strain. The external strain is identified with the strain of classical elasticity theory and arises when the structure is deformed homogeneously. (A homogeneous deformation is defined as one in which the lattice remains as a perfect Bravais lattice.)

Internal strain, on the other hand, arises from the relative movements of the atoms within a single unit cell. The additional energy per cell due to a general deformation therefore depends on both of these contributions. In equilibrium the energy of the lattice must be a minimum, therefore it follows that the external strain determines the size and shape of a unit cell, whereas the internal strain defines the relative positions of the atoms within the cell.

Normally then, the elastic constants of a given structure will have contributions from both internal and external sources and will be given by,

$$C_{\alpha\beta,\gamma\lambda} = [\alpha\beta,\gamma\lambda] + [\beta\gamma,\alpha\lambda] - [\beta\lambda,\alpha\gamma] + (\alpha\gamma,\beta\lambda) \qquad 3.36$$

where the square bracket terms correspond to external strain and the round brackets to internal strain. These terms can be derived from the perturbation method and for the details of the expressions see Born and Huang (1954) and also the remarks by Cowley (1962). For crystals where every atom is at a centre of symmetry the contribution from the internal strain is zero.

Finally, the elements of the dielectric constant tensor in the long wavelength can be evaluated from,

$$\epsilon_{\alpha\beta} = \delta_{\alpha\beta} + \frac{4\pi^2}{V_a} e^2 \sum_{kk'} \frac{Z_k Z_{k'}}{(M_k M_{k'})^{\frac{1}{2}}} \Gamma_{\alpha\beta}(kk') \qquad 3.37$$

where the matrix Γ is related to the dynamical matrix at $q = 0$, see Born and Huang, and $\epsilon_{\alpha\beta}$ the static dielectric tensor. As a consequence of assuming the ions to be unpolarizable the high frequency dielectric constant is unity, for the Clausius-Mossotti relationship can be expressed as,

$$\frac{\epsilon - 1}{\epsilon + 1} = \frac{4\pi}{3} \sum_i N_i \alpha_i \qquad 3.38$$

there being N_i ions each of polarizability α_i per unit volume. Strictly speaking, this relationship is only true providing every

ion is at a site of cubic symmetry and thus experiences the

Lorentz field.   However, even if this is not so the above result

for ϵ = 1 is not affected since the polarisation in a crystal

may be expressed approximately as the product of the polarizabilities

of the ions times the local electric field (E_{loc}),

$$\text{i.e.} \quad P = \sum_i N_i \alpha_i E_{loc}(i),$$

and in a isotropic cubic medium the dielectric constant relative

to vacuum is defined as ϵ = $1+4\pi\chi$, where the susceptibility,

χ, is P/E.   Thus, if α_i = 0 then ϵ = 1.

CHAPTER 4

EXPERIMENTAL DISPERSION CURVES FOR $MgAl_2O_4$

4.1) <u>Neutron Inelastic Scattering</u>.

4.1.1) <u>The neutron spectrum</u>.

The neutron flux in a reactor is in thermal equilibrium with a moderator at temperature T so that there will be a velocity distribution with the form of a Maxwellian spectrum. The peak of this spectrum in terms of neutron wavelength normally occurs at approximately 1 Å but is given more explicitly by,

$$\lambda_{peak} = h/(5kTm)^{\frac{1}{2}} \qquad\qquad 4.1$$

where h = Planck's constant

      k = Boltzmann's constant

      m = neutron mass.

Only a narrow range from this distribution is normally usefully utilized in diffraction experiments. A narrow band of wavelengths can be selected by Bragg reflexion from a single crystal with a suitable interplanar spacing, and the choice of a crystal mono-chromator is governed by the particular experimental requirements. For example, resolution, range of incident neutron energies, intensity of the incident beam, are among the factors which may be considered.

In this non-relativistic region, the wavelength of a neutron is related to its velocity and energy by,

$$\lambda = 3.96/v = 9.044/\sqrt{E} \ \text{Å} \qquad\qquad 4.2$$

when the neutron velocity v is in kms^{-1} and the energy, E, in meV. Thus, the thermal neutrons with a wavelength in the neighbourhood of 1 Å have energies and momenta comparable to those of lattice vibrations in crystals. They are therefore usefully exploited for the experimental examination of phonon dispersion curves.

4.1.2) <u>Neutron-Phonon Interaction</u>.

The scattered wave from any given nucleus may be described as a spherical wave of wavevector k given by,

$$\psi_s = -\frac{b}{r} e^{-i\underline{k}\cdot\underline{r}} \qquad\qquad 4.3$$

where the scattering length, b, is characteristic of that nucleus. The phase of the scattered wave depends on the precise position of the scattering nucleus, and as the velocity of the nucleus is comparable to the neutron velocity the neutron wave equation is unlike the classical wave equation. In particular, the expected scattering power differs from that of the normal optical Huygen's construction, in that Doppler shifts change the scattered frequencies. Each nucleus is at every instant a potential source of a spherical wave coherent in phase with the incident wave, and the scattered waves interfere so that at a large distance from the sample the outgoing wavefront represents neutrons of various energies and momenta. Two cases then need to be considered namely, that the nuclei are at rest or alternatively, that the nuclei are in motion. In the former case, only elastic scattering, that is, nuclear Bragg scattering is possible. In the latter, where the nuclei are in motion, the scattered neutrons can have their energy changed by $\hbar\omega$ and their momenta by $\hbar Q$. The scattering system has then changed its dynamic state by just these quantities, and this corresponds to inelastic scattering.

The scattering length, b, has two components a coherent and an incoherent part, as a consequence of the details of the nuclear structure. They may be thought of crudely as arising as follows: suppose the nucleus has spin S so that the compound nucleus formed by reaction with the incident neutron has spin $s \pm \frac{1}{2}$. Then some random time delay can occur before the neutron gains enough energy

to be re-emitted. In this case therefore, it is emitted incoherently. Alternatively, the neutron may be scattered instantaneously from the nucleus with no discontinuity in its motion and then it is scattered coherently. If the solid contains one nucleus per unit cell then the cross section for coherent processes is

$$\sigma_{co} = 4\pi \; \frac{1}{N^2} \sum_{\substack{nm \\ n \neq m}}^{NN} b_m b_n = 4\pi \; \bar{b}^2 \qquad 4.4$$

where $\bar{b}$ is the coherent scattering length and N is the number of unit cells in the crystal. Fortunately most nuclei are good coherent point sources, with notable exceptions such as vanadium and hydrogen.

In any neutron diffraction experiment the quantity actually observed is the differential scattering cross section, which is defined as the number of neutrons per sec scattered into solid angle $\partial\Omega$, having an energy between E and E+dE, in the direction of the nuclear detector, normalised to the incident flux. For one-phonon coherent scattering the differential scattering cross-section is given by, (see for example Egelstaff (1965)), in the harmonic approximation,

$$\frac{\partial^2 \sigma}{\partial\Omega\partial E} = \frac{(2\pi)^3}{V} \sum_{q,s} \frac{k}{k_0} \; \delta(h\omega \pm hf) \times \sum_{d^*} \delta(Q \pm q - d^*) \times$$

$$\times \; h \; (n+\tfrac{1}{2} \pm \tfrac{1}{2})/2f \times$$

$$\times \; \left| \sum_k \bar{b}_\kappa \; e^{iQ \cdot \mathcal{L}_k} Q \cdot e^k \; M_k^{-\frac{1}{2}} e^{-W_k} \right|^2 \qquad 4.5$$

The first δ function here takes account of the conservation of energy, while the second incorporates the crystal momentum conservation law. These two conditions define the scattering surfaces

in reciprocal space. The next factor gives the phonon population
as the probability of finding a phonon with energy hf at a tem-
perature T and is given by the Bose distribution,

$$n = \left[\exp(hf/kT) - 1\right]^{-1} \qquad\qquad 4.6$$

The final term in the equation is the "dynamic structure factor"
and this takes account of the amplitudes and phases of the various
vibrating nuclei through the polarisation vectors $\underline{e}^k$, $\dot{W}_k$ is the
Debye-Waller factor, $\underline{k}$ and $\underline{k}_0$ are the diffracted and incident
wave vectors, $\underline{Q}$ is the scattering vector, r_k is a vector in
real space giving the position of the ith nucleus of mass M_k
in the unit cell. The summation of k extends over the unit cell,
$\underline{q}$ is the phonon wavevector and s is a label giving the number of
states with the same $\underline{q}$, V is the volume of the crystal and $\underline{d}^*$ is a
vector of the reciprocal lattice. The dynamical structure factor
has important consequences when experiments are attempted since
this quantity can alter very rapidly in reciprocal space. It is
therefore essential to ensure that the dynamical structure factor
has a favourable value for the measurement of a given phonon.

Even though each Brillouin zone contains the same infor-
mation about the phonons in the crystal, the neutron-phonon inter-
action varies throughout reciprocal space but repeats with a
periodicity given by,

$$e^{i\underline{d}^* \cdot \underline{r}_j} = 1, \quad \text{for all } r_j \text{ of the unit cell} \qquad 4.7$$

and this periodicity is known as the "structure factor zone". In
the case of Spinel with $\delta = 0$, this is a cube bounded by the
reciprocal vectors $(8,0,0)$; $(0,8,0)$; $(0,0,8)$.

4.1.3) Experimental observation of phonons.

Three functions must be performed in convential in-
elastic scattering experiments. Firstly, neutrons in a small
velocity interval have to be selected from the incident beam; this
can be achieved with suitable monochromators and collimators.
Secondly, an energy analysis must be performed in order to
establish the energy exchange and finally, the angle of scatter-
ing with respect to the incident beam and with respect to the
sample orientation must be measured to determine the momentum
exchange. These conditions are satisfied by triple axis spectro-
meters and also by time of flight spectrometers. In the former
the incident neutron beam, of wavevector k_0, is selected by a
crystal monochromater and the beam scattered by the sample in a
direction k' is energy analysed by an analyser crystal. At the same
time the angular relationship between k_0, k' the final wavevector,
and the scattering vector $(Q = d^* \pm q = k_0 - k')$ can be measured to
determine the momentum change. In the latter a narrow range of
neutron velocities is selected by a curved slot rotor, rotating
crystal, etc. this defines the incident wavevector k_0 and a
neutron pulse in time. An energy analysis is performed by timing
the neutrons over a predetermined distance. Similarly, the angular
relationship between the counters and the sample can be measured,
establishing the momentum change. Time of flight spectrometers
usually consist of a large number of counters which are equally
spaced and move as a rigid body. At one particular setting each
counter has a set angular relationship to the incident beam, which
defines the direction for the scattered neutron beam, k'. The
magnitude of k' is proportional to the square root of the energy
of the scattered beam, and when the two δ functions of equation 4.5
are satisfied the ends of the k' vectors trace out a portion of the
scattering surface in reciprocal space [Schmunk, Brugger and

Randolph, 1967]. The phonon energy and momenta can be deter-
mined for phonons in symmetry directions by interpolation, pro-
viding the scattering surface crosses a symmetry axis. Since
this time of flight technique was used to measure the phonon
dispersion curves in Magnesium Aluminate with the use of a rotating
crystal spectrometer, this particular apparatus will now be
discussed in more detail.

4.2) The R.X.S.Spectrometer.

The three conditions mentioned above are satisfied in
the rotating crystal spectrometer, (Brockhouse ,1958) where
pulses of neutrons are produced by Bragg reflexion from a single
crystal rotating at high angular velocities. In the work to be
described the Rotating Crystal Spectrometer at A.W.R.E Aldermaston
on the 5MW Swimming Pool Reactor was used (Carlise, 1973)   This
spectrometer shares the neutron beam from a H_2/D_2 cold source with
a curved slot rotor time of flight spectrometer and is shown
schematically in figure 4.1.

When the neutrons are in thermal equilibrium with the
liquid H_2/D_2 cold source the peak of the Maxwellian distribution
occurs at approximately 4.4Å. A cylindrical single crystal of
lead of diameter 50mm is rotated about the [211] direction, at a
frequency of 167Hz, giving two 111 reflexions per revolution, equally
spaced in time, and a neutron flux at the sample of approximately
10^4 ns^{-1} cm^{-2}. From the Bragg condition,

$$2d \, Sin\theta = \lambda \qquad\qquad 4.8$$

a wavelength of 4Å is selected at $2\theta = 90°$, second and higher order
contamination being removed by the Beryllium filter which removes
neutrons with energies greater than 5meV.

On the R.X.S. spectrometer the detector consists of eight
adjacent ^3He proportional counters, at a pressure of 4 atms, each

Detector

Collimators. C_1, C_2.

Beryllium
Filter

Sample

C_2

Liquid H_2/D_2
Cold Source

C_1

Rotating
Crystal

Reactor Face

Fig 4. 1. Schematic View of R. X. S.

Intensity
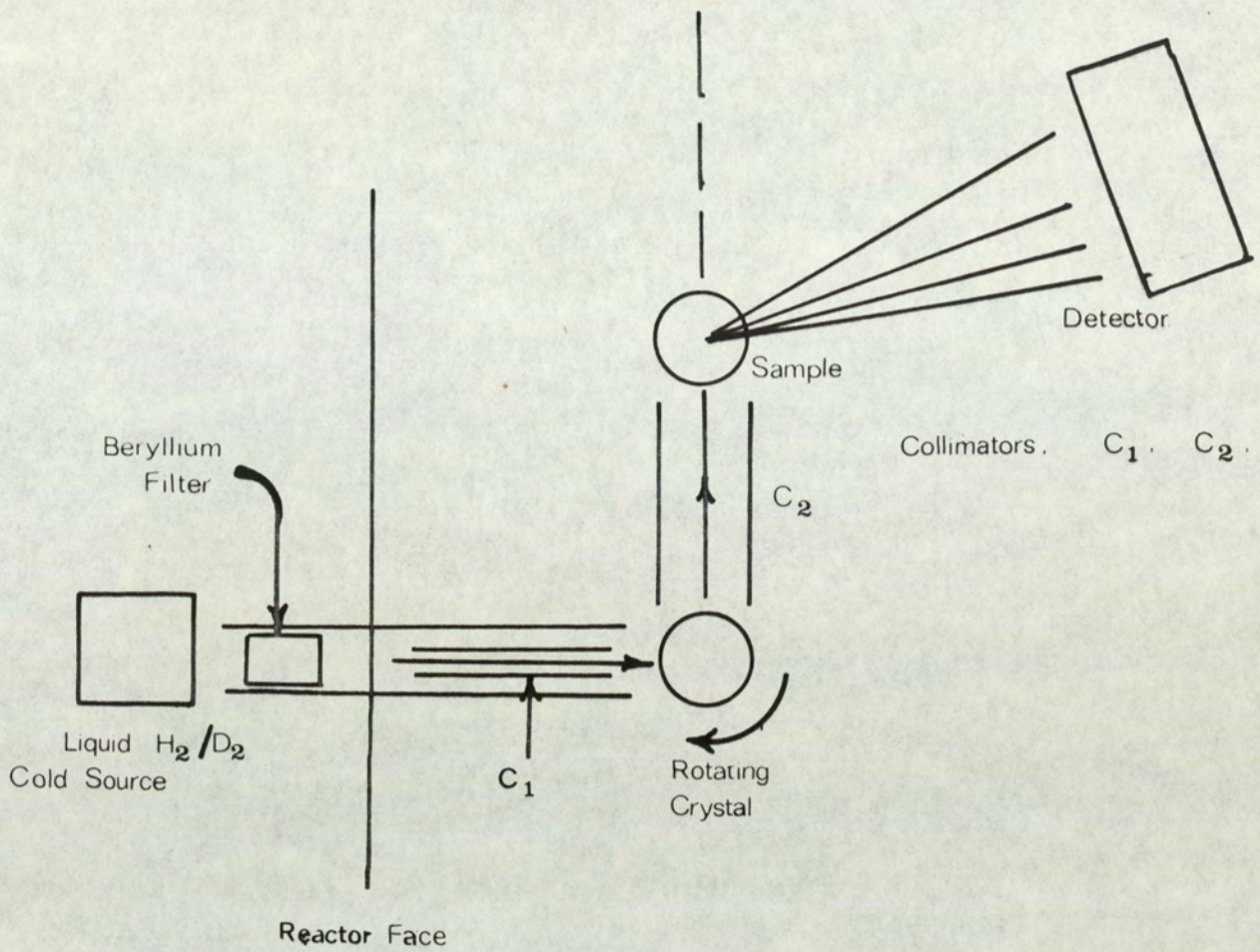
3000 µs

T_1

T_0 T_{IE} T_E T_0 Time
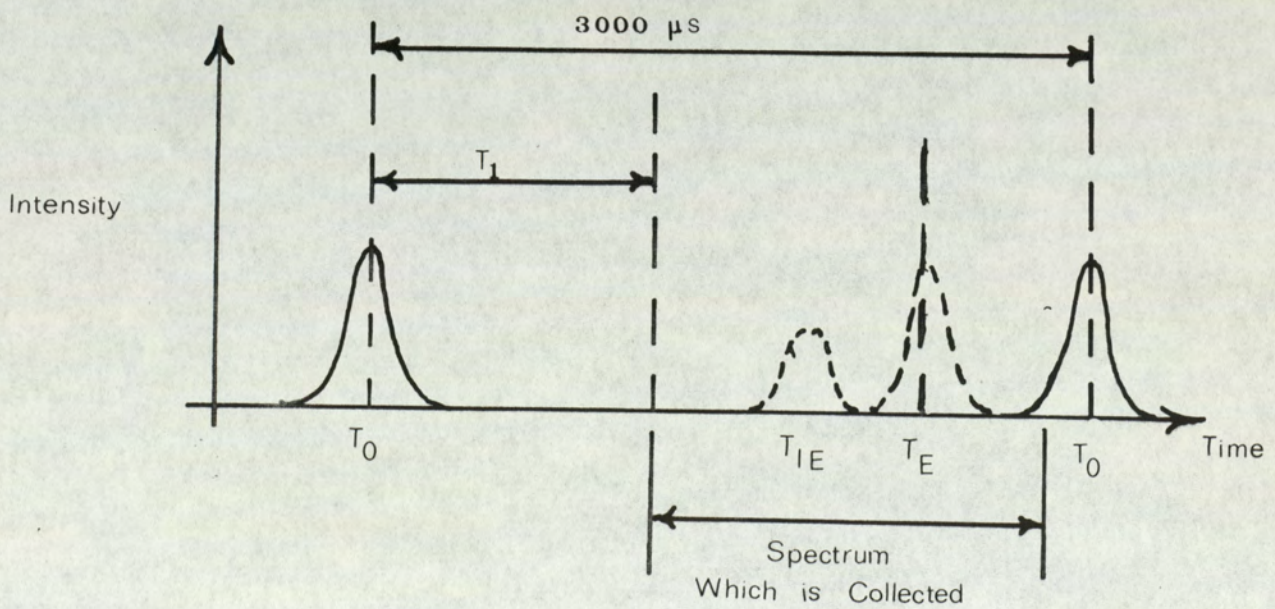
Spectrum
Which is Collected

Fig 4. 2. Time of Flight Spectrum

with dimensions 25mm diameter and 200mm in length, the long dimension being perpendicular to the scattered beam and parallel to the rotation axis of the crystal. Now, each neutron pulse is defined in time, there being approximately 3000 μs between each pulse, see figure 4.2. A time delay T_1 is introduced electronically to allow the neutrons ample time to reach the sample position, before a time analysis begins. The detectors are then divided electronically into n time channels of m μs per channel and thus an energy analysis can be performed.

Neutrons which are scattered elastically through the system will arrive at the detector at a time T_E. This determines the zero energy exchange, whereas those scattered inelastically by gaining energy from the sample, will increase in velocity, and therefore arrive at the detector earlier, with a time T_{IE}. Hence, $T_{IE} < T_E$ since only upscattering can be usefully employed in this type of spectrometer. The spectrum in each counter is collected over a period of time; for our experiments this was typically two or three days, and stored by a PDP8 computer. Unfortunately only 4 counters could be used simultaneously and only 128 channels were available. Hence the amount of data which could be collected in any one particular analysis was severely limited.

An important feature of the R.X.S. spectrometer, arising from the relatively high angular velocity of the rotating crystal, is that the diffracted neutrons have their velocities shifted by the Doppler effect, (A discussion of neutron diffraction by moving crystals can be found in Buras and Giebullowiez, 1972). Consequently if the direction of rotation is suitably chosen so that the slower neutrons are reflected first then time focussing occurs (Meister, 1967). For the A.W.R.E spectrometer the focal length is 2.86m and the total flight path is 3m (Ross and Carlisle 1975). The spectrometer therefore possesses good focussing properties. Other

factors governing the energy and momentum resolution are
discussed by Ross and Carlile (1975), who show in particular,
that $\delta E/E$ varies from 3% up to 10% for an energy exchange between
0 and 30 meV but deteriorates rapidly for higher energy exchanges.

In the present experiments the value of the initial time
of flight was measured by timing the neutrons over a standard
flight path, and a value of $1018 \pm 3 \mu sm^{-1}$* obtained corresponded
to an energy of 5 meV or a wavelength of $4.03\overset{o}{A}$ which is in good agree-
ment with previous measurements (Carlile 1973). The flight path,
(the sample detector distance) was also measured and found to be
$1.999 \pm .005m$ with negligible variation over the angular range of
the detector.

4.3) Phonons in Magnesium Aluminate.

Although the neutron-phonon interaction produces finite
measurable intensity, it must be emphasized that it is not a
particularly strong interaction and this factor coupled with the
relatively low intensity of neutron beams, makes the observation
of phonons time consuming. Enhancement of the experimental
efficiency can be achieved by the use of large single crystals,
since the one-phonon differential scattering cross-section depends
on the phonon density of states, which in turn is dependent on
the crystal volume. In the present experiments, for example, the
specimen of Magnesium Aluminate used to investigate the phonon
spectra was a large single crystal (purchased from the Radar Research
Establishment, Malvern) with an approximate volume of 5×10^4 mm^3.
The shape was roughly cylindrical, as the crystal had been pulled
from a melt, the growth axis being a [110] direction.

In investigating the phonon dispersion curves in Spinel

*the units normally used in time of flight spectrometry are μsm^{-1}
which is the reciprocal neutron velocity.

a number of necessary preliminary calibration experiments were performed each time the crystal was positioned on the spectrometer, and these will now be described. In each case, a [110] crystallographic direction was aligned along the goniometer axis.

The zero crystal angle θ_{so}, which was defined to be the angle which makes $\underline{d}^*_{220}$ and $\underline{k}o$ coincident, was determined from a rock-scan or ω-scan on the 220 planes. For this, the R.X.S was operated as a normal single crystal spectrometer with the four proportional counters (1,2,3,4) coupled together, and a typical result is shown in figure 4.3. The zero angle was derived from the expression,

$$\theta_{so} = \omega_{220} - Cos^{-1} \left[\frac{1}{4} d^*_{220} | / 2 | ko | \right] \qquad 4.9$$

where the positive rotation direction is defined in figure 4.6.

With the crystal set at ω_{220} the detector bank was scanned over the 220 reflexion and in this manner the angular separation of the four counters was determined together with the angular position of the detector centre, θ_c, see figure 4.4. This allowed the detector zero θo to be defined by,

$$\theta_0 = \theta_c + 2\theta_{220} \qquad 4.10$$

where the positive rotation direction of the detector is also defined in figure 4.6. Finally, with the instrument operating as a time of flight spectrometer the zero energy exchange was determined by the following procedure: using the Bragg 220 reflexion to scatter nuetrons elastically through the system the time of flight spectra in each of the four counters was collected. These are shown in figure 4.5. The mean channel number, $\bar{I}$, was determined statistically from the expression,

$$\bar{I} = \frac{\sum\limits_{I} N_I I}{\sum\limits_{I} N_I} \qquad 4.11$$

where N_I is the number of counts in channel I. This expression may
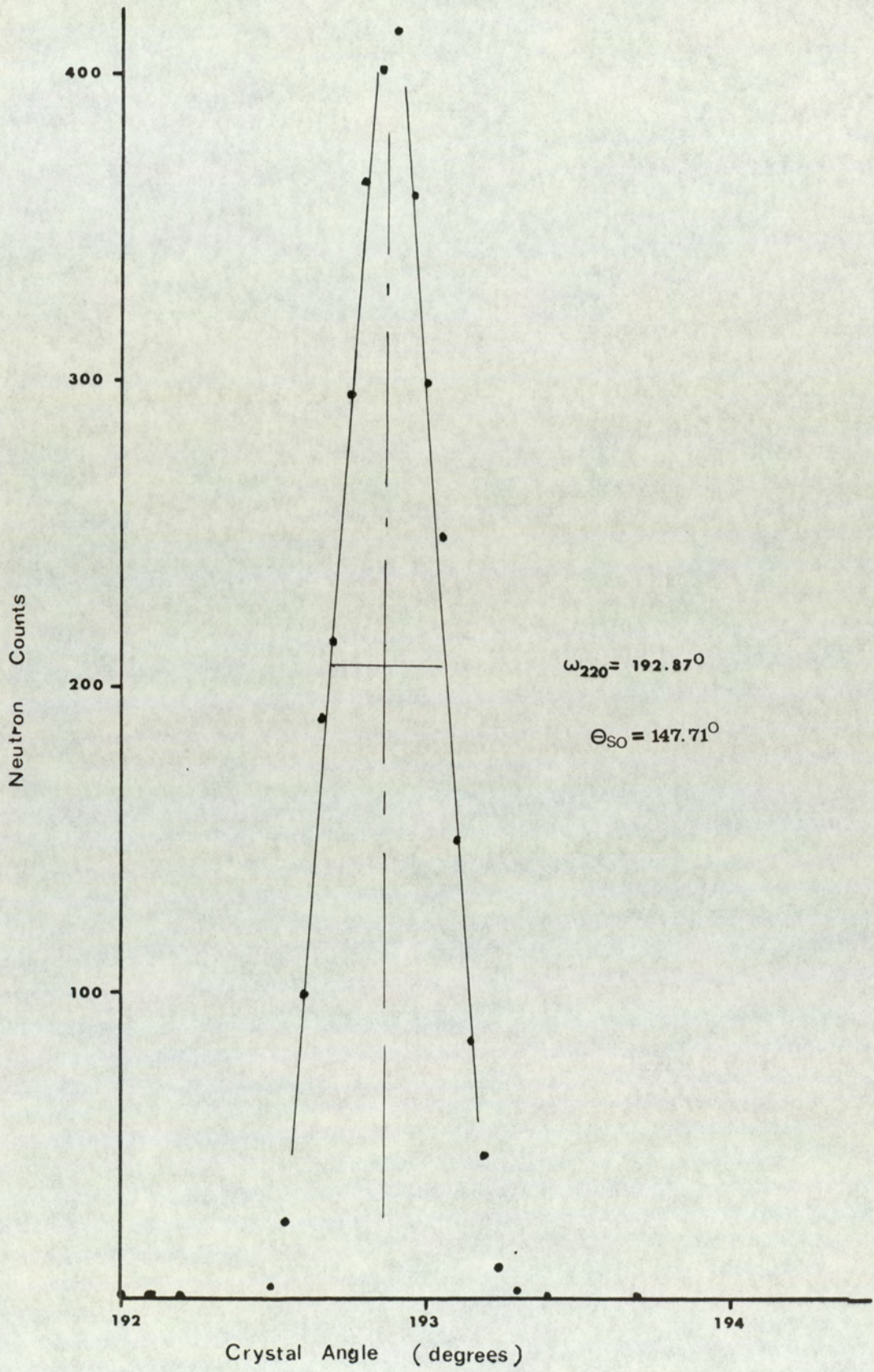
FIGURE 4.3   ω - Scan on 220 Planes

FIGURE 4.4 Mean Position of each Counter

Channel Width 18 μs

Counter Nº 1

$\bar{I} = 115.13$

on 18 μs scale $\bar{I} = 172.7$

Counts

Channel Nº

Counter Nº 2

$\bar{I} = 115.02$

on 12 μs scale $\bar{I} = 172.53$

Counts

Channel Nº

Counter Nº 3

$\bar{I} = 115.07$

on 12 μs scale $\bar{I} = 172.61$

Counts

Channel Nº

Counter Nº 4

$\bar{I} = 115.0$

on 12 μs scale $\bar{I} = 172.5$

Counts

Channel Nº

FIGURE 4.5   Calibration of Zero

Energy Exchange

be used because the background count is negligible. Since the
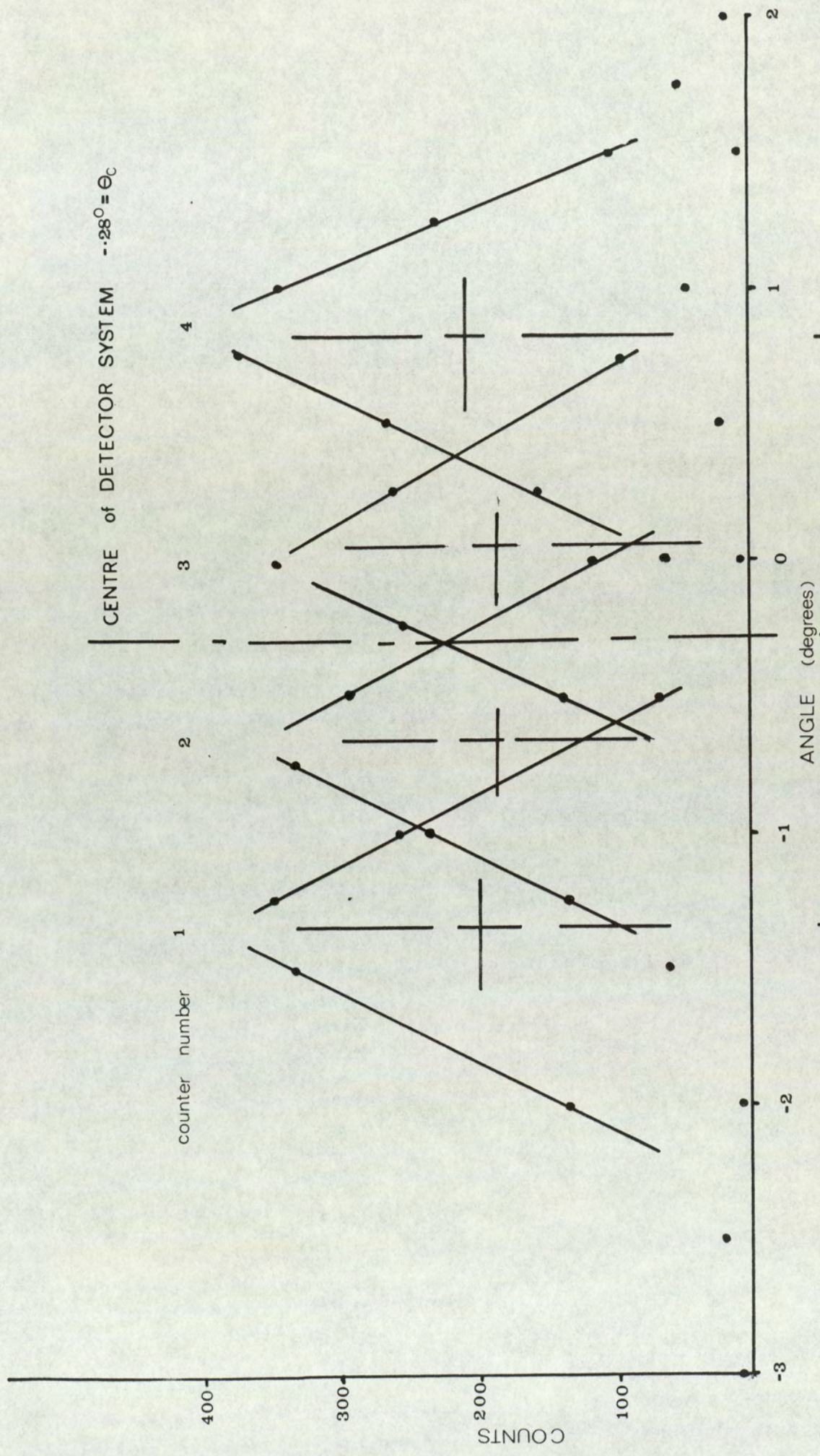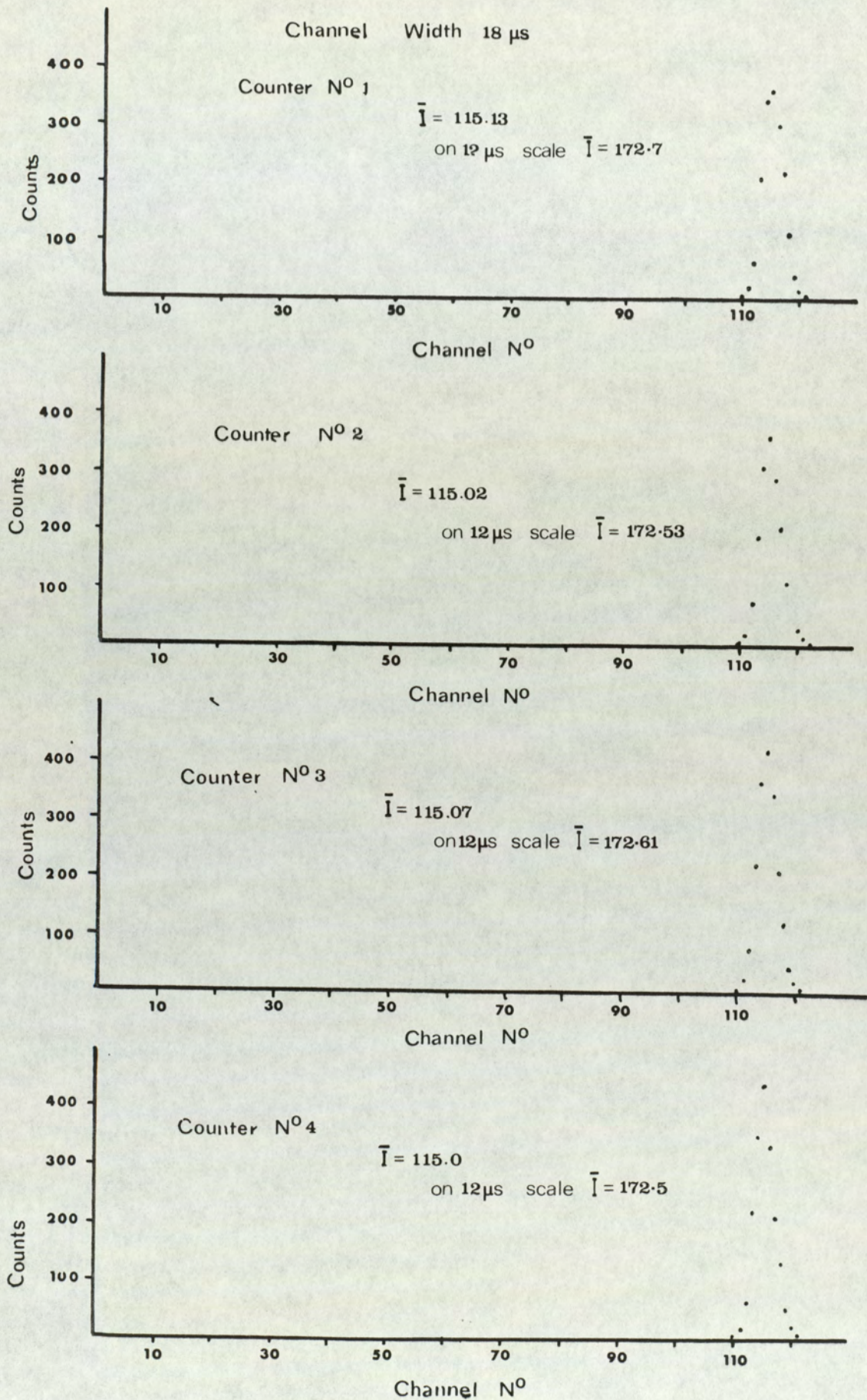channel width is n μs and this peak corresponds to a time of
flight of 1018 μsm^{-1} we must therefore have,

$$1018 = n\,\overline{I}/\ell \qquad\qquad 4.12$$

where ℓ is the flight path which is 2m. So in the example shown
in figure 4.5 for the counter No.1 the peak corresponds to a time
of flight of 1036.2 μs, but since this must equal 1018 μs a
correction of 18.2 μs was subtracted from the whole spectrum
in this particular counter, and similarly for all other counters.
Figure 4.5 also shows what the mean channel would be if the channel
width were 12 μs and not 18 μs. This is significant for some of
the experiments which were performed, see section 4.5.

In carrying out measurements of the phonons according to
this technique, and with this particular spectrometer, it should be
understood that it is a prerequisite to have some prior knowledge
of the phonon energies and their polarisations, in order that a
suitable region of reciprocal space may be chosen where the dynamic
structure factor favours their observation. With this knowledge,
the spectrometer was set up to measure a phonon of energy, Ep, and
wavevector, $\underline{q}$, by the following procedure: since the energy of the
scattered neutron beam from the sample En = Ep + Eo where Eo is the
energy of the incident beam, the corresponding wavevector magnitude
may be determined from,

$$|k'| = \sqrt{\left(\frac{2mEn}{h^2}\right)} \qquad\qquad 4.13$$

The scattering vector $\underline{Q}$ is shown in figure 4.6 where it is shown
firstly on the right hand side of this diagram with the crystal
set at the zero angle θ_{so}, as $\underline{Q} = \underline{d}^* + \underline{q}$. It can be brought into
the correct position, shown on the left hand side of the diagram,
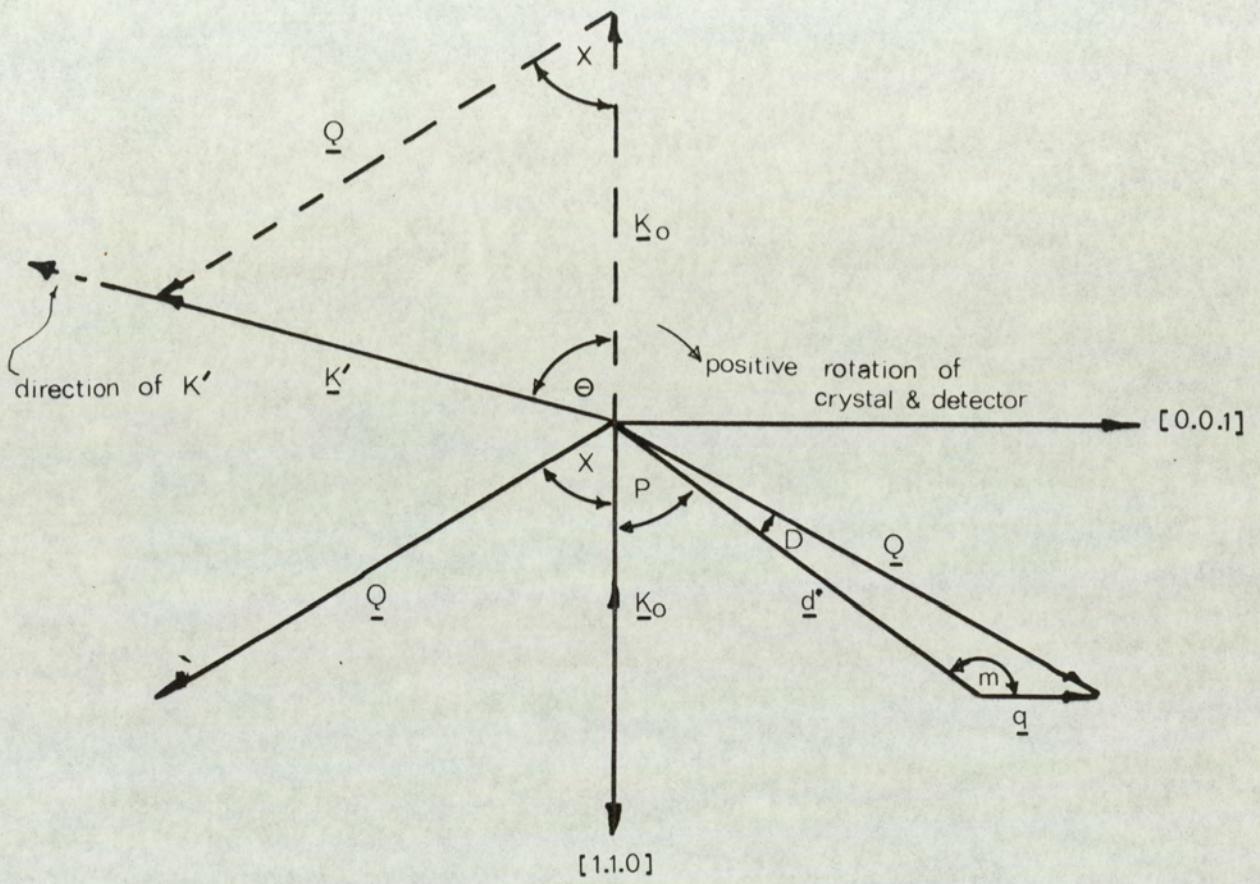by rotating the crystal through the angle X+P+D. Movement of the

FIGURE   4.6 $\underline{K}o$ $\underline{K}'$ $\underline{Q}$ Triangle

detector to $\theta_D = \theta_o - \theta$ completed the momentum triangle $\underline{k}'$, $\underline{k}_0$, $\underline{Q}$. The magnitude of these vectors and the angles shown in figure 4.6 are calculable from the following formulae,

$$\theta = \cos^{-1}[(k_0{}^2+k'{}^2 - Q^2)/2k_0k']$$

$$X = \cos^{-1}[(k_0{}^2+Q^2 - k'{}^2)/2k_0Q]$$

$$P = \cos^{-1}[h+k/(\sqrt{2}.\sqrt{(h^2+k^2+\ell^2)})]$$

$$Q = |\underline{q}||d*|\cos m;$$

$$D = \sin^{-1}(|q|/|Q| \times \sin m) \qquad\qquad 4.14$$

Measurements on the phonon dispersion curves in Spinel were restricted to the acoustic phonons, and for small, q, an estimate of the phonon energy was obtained from classical elasticity theory as this gave the initial gradients of the acoustic dispersion branches. The elastic wave velocities depend on the elastic constants (see for example Kittel, 1969) and for cubic symmetry in particular these sound velocities are given in table 4.1. The density ρ of Magnesium Aluminate is 3.581 gcm^{-3}, and the elastic constants are also known to good accuracy, see Chapter 5.

In the acoustic modes particularly those of long wave-length the polarisation vectors e^ℓ in the dynamic structure factor of expression 4.5 do not vary rapidly and furthermore for very long wavelengths all the atoms in most unit cells will be moving in phase. In this case it is fair approximation to take the term $\underline{Q}.\underline{e}^\ell$ from under the summation sign so that the dynamic structure factor becomes proportional to,

$$|\underline{Q}.\underline{e}_s F_{hk\ell}|^2 \qquad\qquad 4.15$$

where $F_{hk\ell}$ is the structure factor and e_s is the polarisation of the phonon. Now, since the elastic continuum theory specifies the polarisations of the particular modes of vibration as longitudinal (L) and transverse (T) in table 4.1, it becomes possible to establish which Brillouin zone offers a maximum for the observation of a long

wavelength acoustic phonon. In table 4.2 we have divided the acoustic phonons in Spinel according to the Brillouin zone where maximum intensity can be obtained and once the dispersion branches were located they were, as far as possible, followed out to the zone boundary by successive measurements.

However, because of the limitations of the instrument employed it was not always possible to achieve these ideal conditions, shown in table 4.2. In particular, measurements in the (440) zone were not possible until the energy exchange reached at least 20 meV. Therefore the T[001] mode could not be measured in this zone. Of the possible alternatives the 222 zone was the most desirable, but even here the intensity obtained from the phonons was far from ideal and consequently less reliability is placed on the measurements of this dispersion branch.

A selection of the results obtained are shown in figures 4.7 to 4.12. Each figure is divided into three parts, part (a) shows the time of flight spectrum, where the scale has been converted to phonon frequency, part (b) the section of the scattering surfaces traced out by the ends of the k' vectors, and part (c) shows the interpolation on these scattering surfaces to obtain phonons in the symmetry directions.

4.4) Discussion of the Results.

As explained previously, the phonon dispersion surfaces can be represented by two δ functions but whenever measurements are attempted, these phonons will always be convolved with the instrumental resolution function. Invariably therefore the peaks actually observed in practice are Gaussian, and a statistical analysis is needed to derive the mean and standard deviation, the latter providing a measure of the uncertainty in the mean. To obtain reliable results it is desirable to have a good estimate of the background intensity, and a peak which is well resolved, conditions not always achieved in

Table 4.1: Elastic wave velocities in cubic crystals.

[001] direction	[110] direction	[111] direction
T: $v = \sqrt{\left(\dfrac{C_{44}}{\rho}\right)}$	T1: $v = \sqrt{\left(\dfrac{C_{11}-C_{12}}{2\rho}\right)}$	T: $v = \sqrt{\left(\dfrac{C_{11}-C_{12}+C_{44}}{3\rho}\right)}$
L: $v = \sqrt{\left(\dfrac{C_{11}}{\rho}\right)}$	T2: $v = \sqrt{\left(\dfrac{C_{44}}{\rho}\right)}$	L: $v = \sqrt{\left(\dfrac{C_{11}+2C_{12}+4C_{44}}{3\rho}\right)}$
	L: $v = \sqrt{\left(\dfrac{C_{11}+C_{12}+2C_{44}}{2\rho}\right)}$	

Table 4.2: Favourable zones for the observation of acoustic phonons.

Crystal Orientation [$\bar{1}$10]	
(0.0.4) Zone	(4.4.0) Zone
T_2 [110]	T [001]
L [001]	L [110]
T [111]	L [111]

time of flight spectrometers. Usually, because of the nature
of the experiments, the conditions for one phonon coherent scatter-
ing are satisfied simultaneously for more than one dispersion branch
at a time and often the observed peaks are not clearly resolved. In
view of this difficulty it was decided that the mean phonon energies
were best obtained by a visual estimate but where possible the mean
was determined by bisecting the full width of half height (F.W.H.H)
of the peak and by these methods it was possible to estimate the
mean peak position in the time of flight spectrum to about plus or
minus one channel number which gives an uncertainty in the scattered
neutron time of flight, from this source, of about 12 μs.

The effects of the dynamic structure factor (section 4.1.2)
were often observed. For example, the time of flight spectra shown
in 7(a) shows a peak which decreases in intensity as one scans from
counter 4 to 2 and in counter 1 this peak has disappeared. This can
be understood by examination of figure 7(b) which shows how the "tips"
of the k' vectors trace out a portion of the scattering surface. The
peak referred to above corresponds to the dispersion surface closest
to the centre of the 0.0.4 zone. This small section of the scatter-
ing surface crosses the [111] symmetry direction and was interpolated
in 7(c) as a longitudinal [111] acoustic phonon. When we trace this
scattering surface back towards the [110] direction the vector dot
product $\underline{Q} \cdot \underline{e}_s$ in equation 4.15 tends to zero, thus the observed peak
decreases in intensity.

In figures 9(a) to 12(a) the spectra had been shifted in
frequency from those shown in figures 7(a) and 8(a), in order that
a larger energy exchange could be observed. This was achieved by
determining the elastic peak with 18 μs channels and then switching
to 12 μs channels. Several normalisation experiments were per-
formed by observing the same inelastic peak with both configurations
and no correction was necessary. In all these spectra a general

plateau of intensity was observed between 10 TH$_z$ and 30 TH$_z$. This intensity almost certainly corresponds to one-phonon coherent scattering from some of the 39 optic phonon branches, but unfortunately the resolution of the spectrometer in this region is too poor to resolve any detailed information, but it does give an indication of the maximum phonon frequency, which appeared to be typically about 30 TH$_z$.

Finally, because only upscattering can be usefully employed in this type of spectrometer, and because of the relatively high energy (compared with kT) of the acoustic phonons in Spinel it was necessary to heat the crystal. This improves the count rate since it ensures that the phonon states are highly populated. The results were therefore collected at different temperatures, i.e. 273 $\pm$ 5°K, 523 $\pm$ 10°K and 673 $\pm$ 10°K, with the majority of measurements being performed at 523°K. These measurements are tabulated in table 4.3 and as far as experimental errors would permit, no "softening" of the observed phonon modes was detected. The results are displayed graphically in figure 5 where our calculations of the normal modes of vibration from the rigid ion model are compared with the experimental values. In this diagram the dashed lines at the origin represent the velocities of sound.

Table 4.3: Phonon measurements in Spinel

Transverse 00ξ	
ξ	Frequency (THz)
.22 ± .01	1.95 ± .10*
.25 ± .01	2.12 ± .10*
.36 ± .02	3.22 ± .15†
.56 ± .03	4.55 ± .25†

Transverse $\xi\xi 0$	
ξ	Frequency (THz)
.19 ± .01	2.35 ± .15*
.25 ± .01	2.70 ± .15*
.27 ± .01	3.15 ± .15*
.28 ± .01	2.90 ± .15†
.40 ± .02	4.40 ± .20†
.44 ± .03	4.90 ± .25†
.45 ± .03	4.90 ± .25*
.55 ± .03	5.82 ± .30†

Transverse $\xi\xi\xi$	
ξ	Frequency (THz)
.17 ± .01	2.05 ± .10*
.18 ± .01	2.15 ± .10*
.25 ± .01	2.65 ± .15†
.31 ± .02	3.10 ± .15†
.34 ± .02	3.50 ± .15†
.35 ± .02	3.60 ± .15†
.43 ± .02	4.30 ± .20*
.44 ± .02	4.20 ± .20*
.46 ± .02	4.25 ± .20
.47 ± .02	4.30 ± .20†

Longitudinal 00ξ	
ξ	Frequency (THz)
.14 ± .01	1.80 ± .10†
.20 ± .01	2.15 ± .10†
.28 ± .02	3.35 ± .15†
.30 ± .02	3.70 ± .15†
.36 ± .02	4.28 ± .20†
.46 ± .02	5.35 ± .25†
.57 ± .02	6.30 ± .30†
.76 ± .03	7.85 ± .35†
.87 ± .04	8.60 ± .40†
.91 ± .04	9.50 ± .50†

Longitudinal $\xi\xi 0$	
ξ	Frequency (THz)
.14 ± .01	2.75 ± .15†
.30 ± .02	5.35 ± .20
.34 ± .02	5.95 ± .30
.40 ± .03	6.80 ± .30†

Longitudinal $\xi\xi\xi$	
ξ	Frequency (THz)
.09 ± .01	2.85 ± .10*
.17 ± .01	4.65 ± .20†
.22 ± .02	5.50 ± .25†
.24 ± .02	6.25 ± .35
.29 ± .02	7.55 ± .35†
.46 ± .03	9.95 ± .60†

Others $\xi\xi 0$	
ξ	Frequency (THz)
.84 ± .04	8.60 ± .45†
.86 ± .04	8.80 ± .45†
.95 ± .04	9.00 ± .45†
.58 ± .03	8.40 ± .40†

Optic mode $\xi\xi\xi$	
ξ	Frequency (THz)
.30 ± .03	6.40 ± .35
.36 ± .03	6.60 ± .40†
.46 ± .03	6.60 ± .40

ξ Reduced wavevector

* Results at 293 °K

† Results at 523 °K

No symbol Results at 673 °K
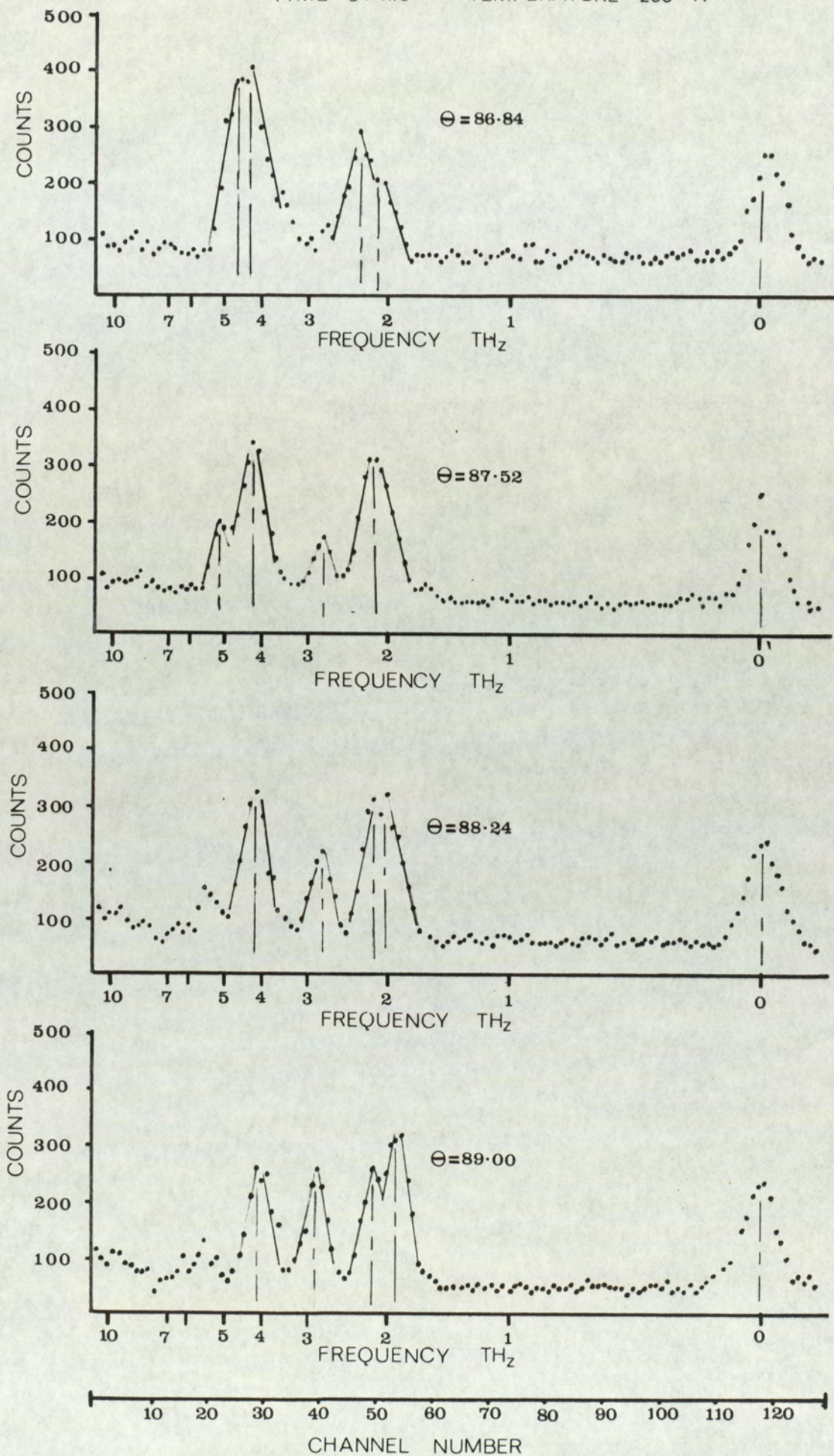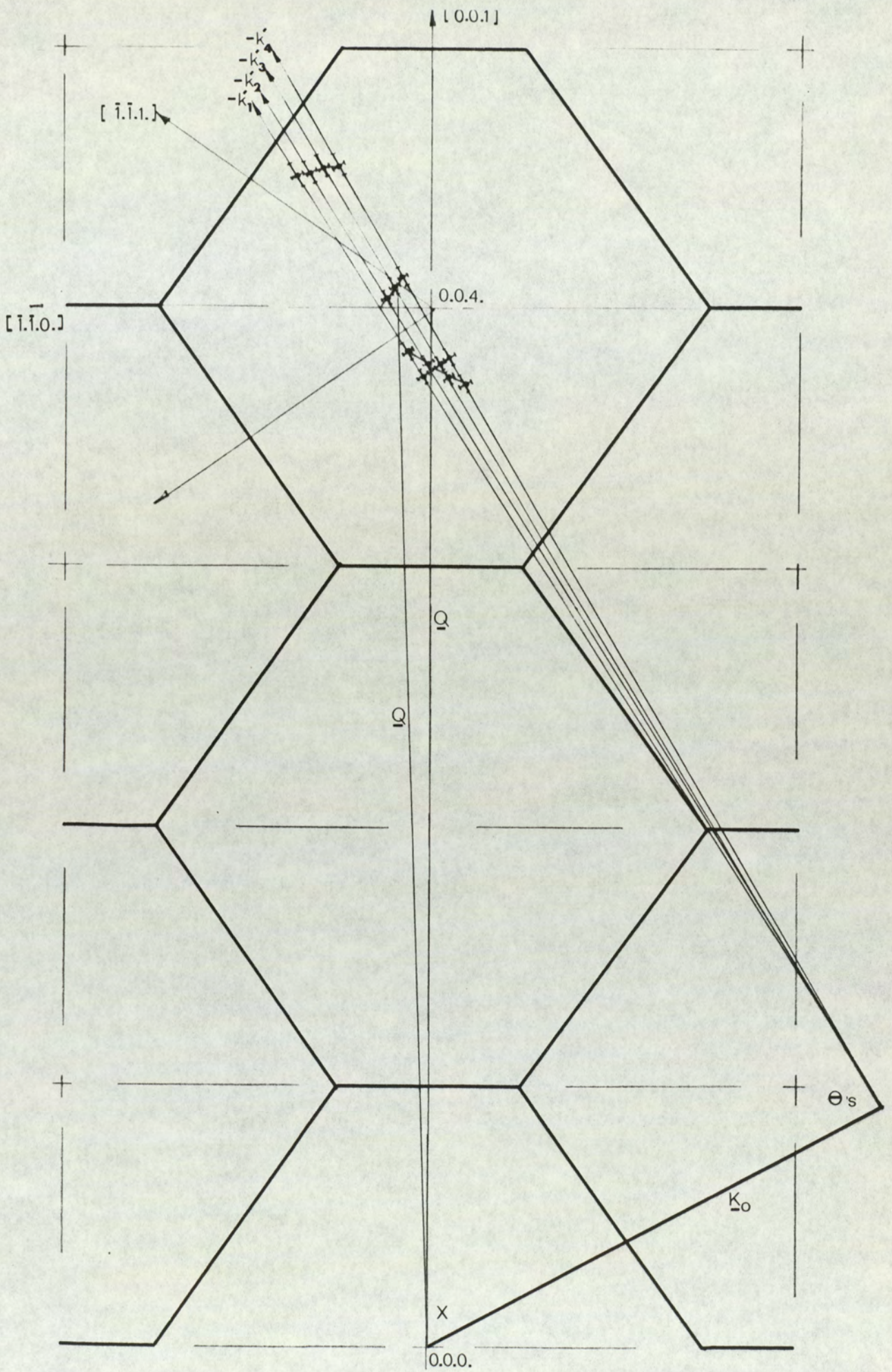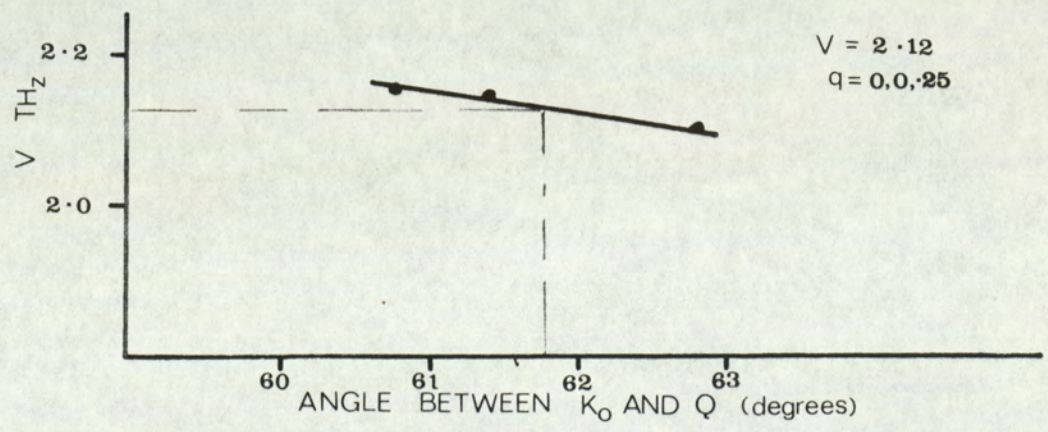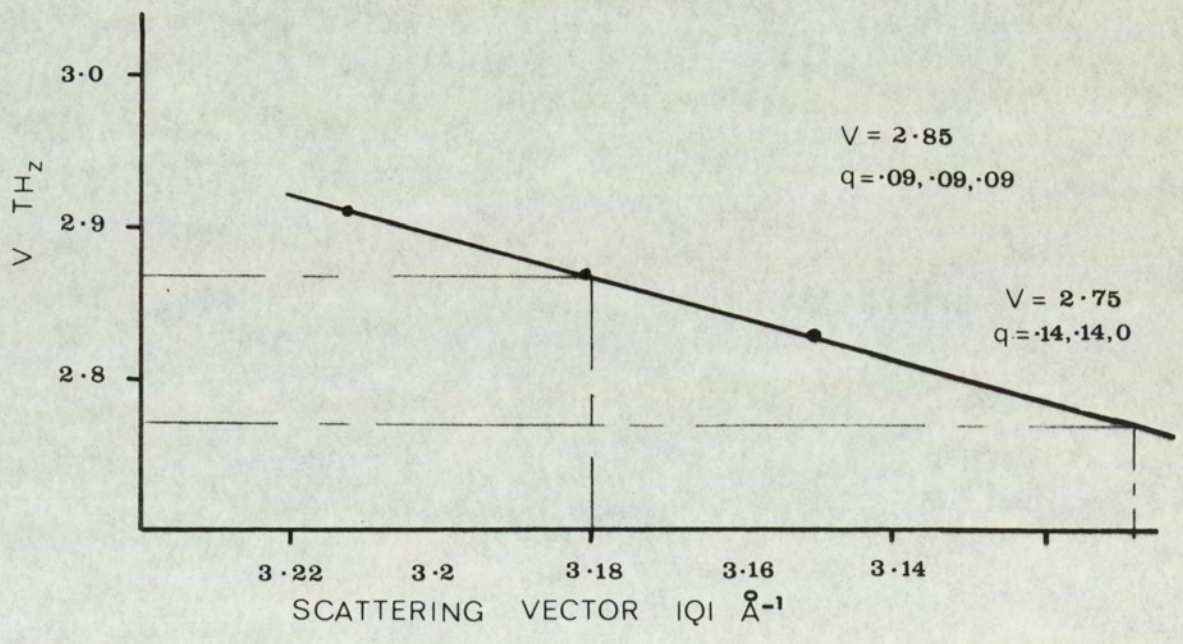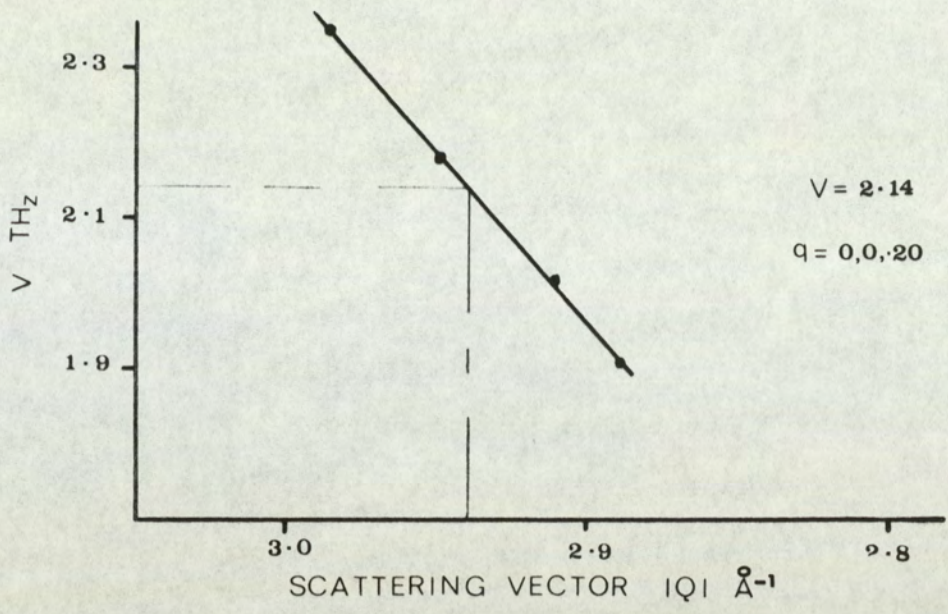
Fig 4.7 a

Fig 4.7 b

Fig 4.7 c

Fig 4.8 a

Fig 4.8 b

Fig 4.8c

TIME 52 hrs   TEMPERATURE 293°K

Θ = 83·8°

Θ = 84·48°

Θ = 85·24°

Θ = 86°
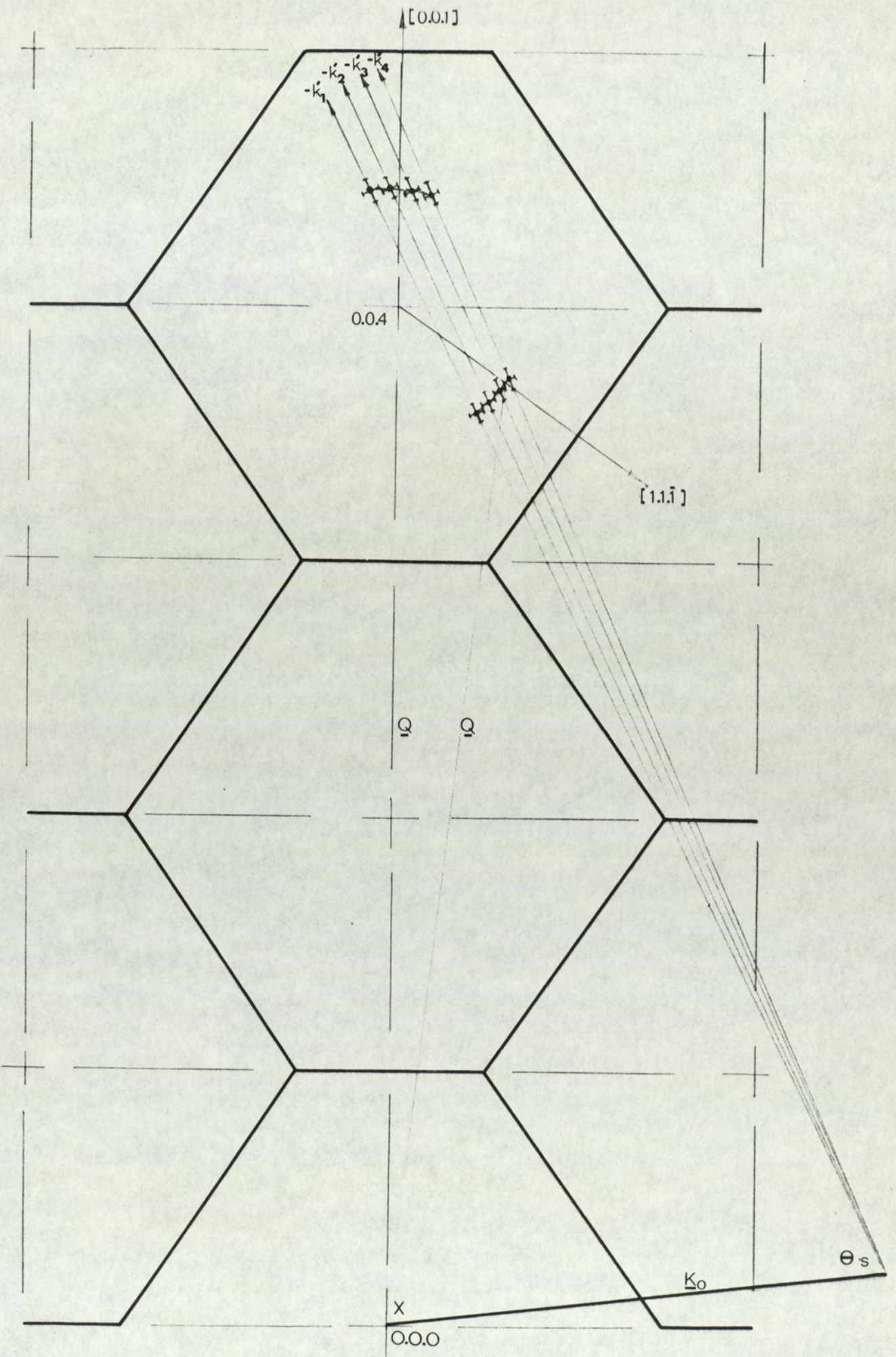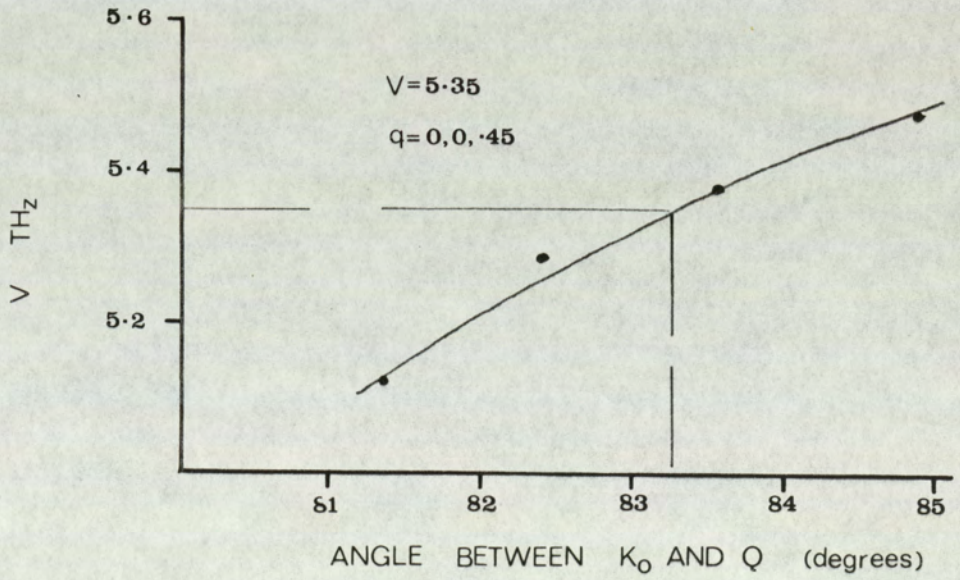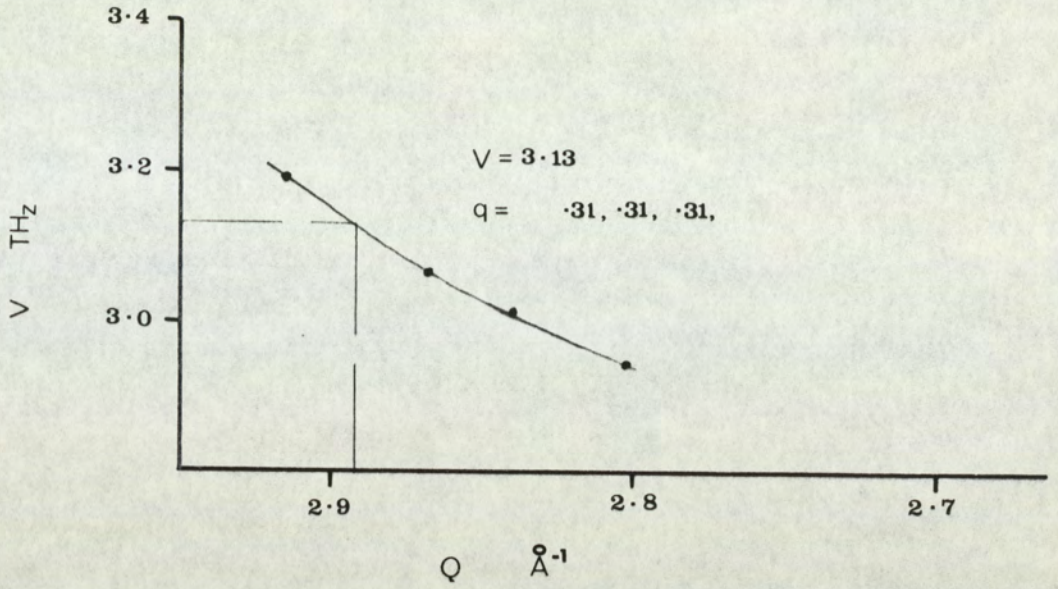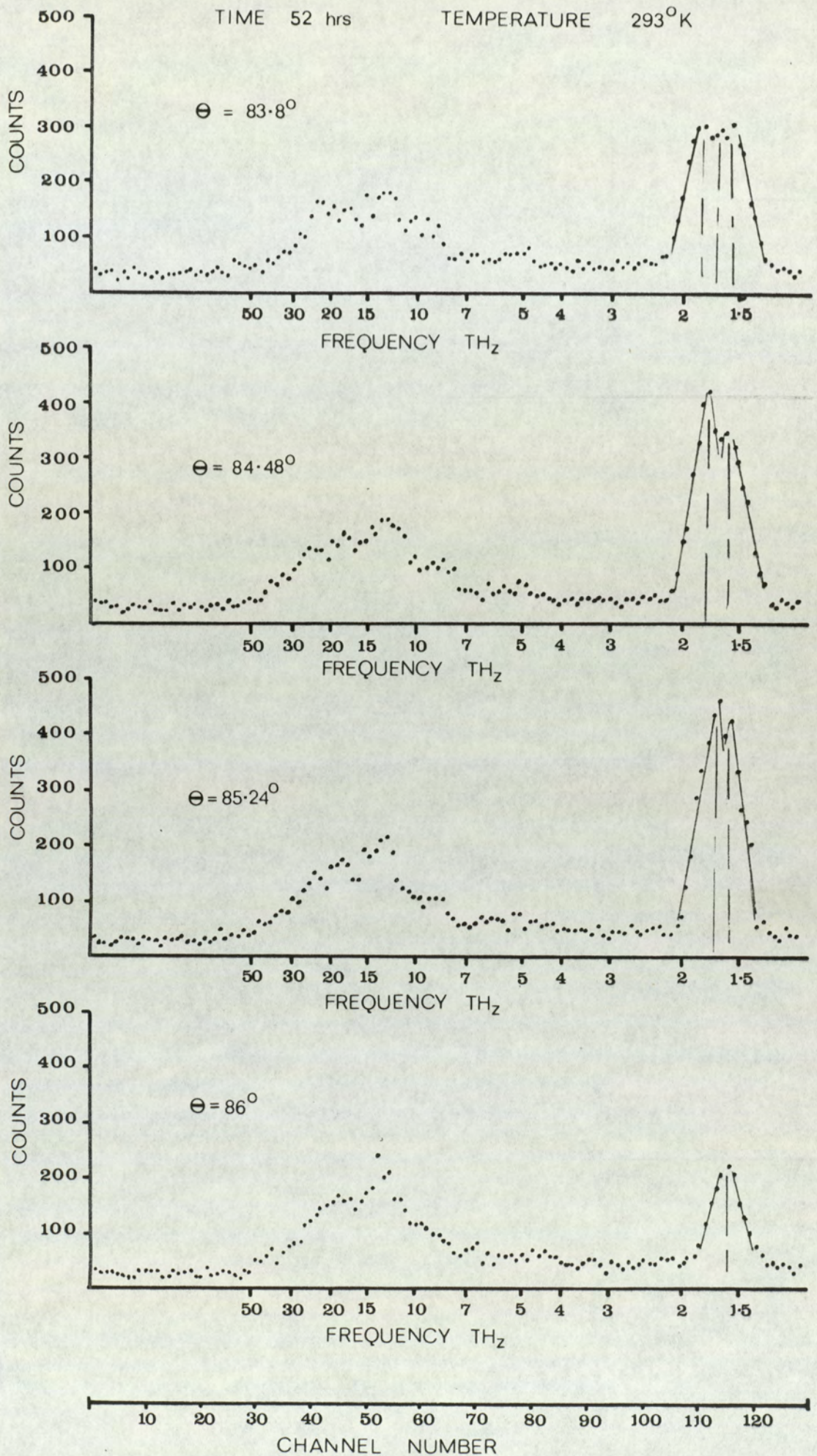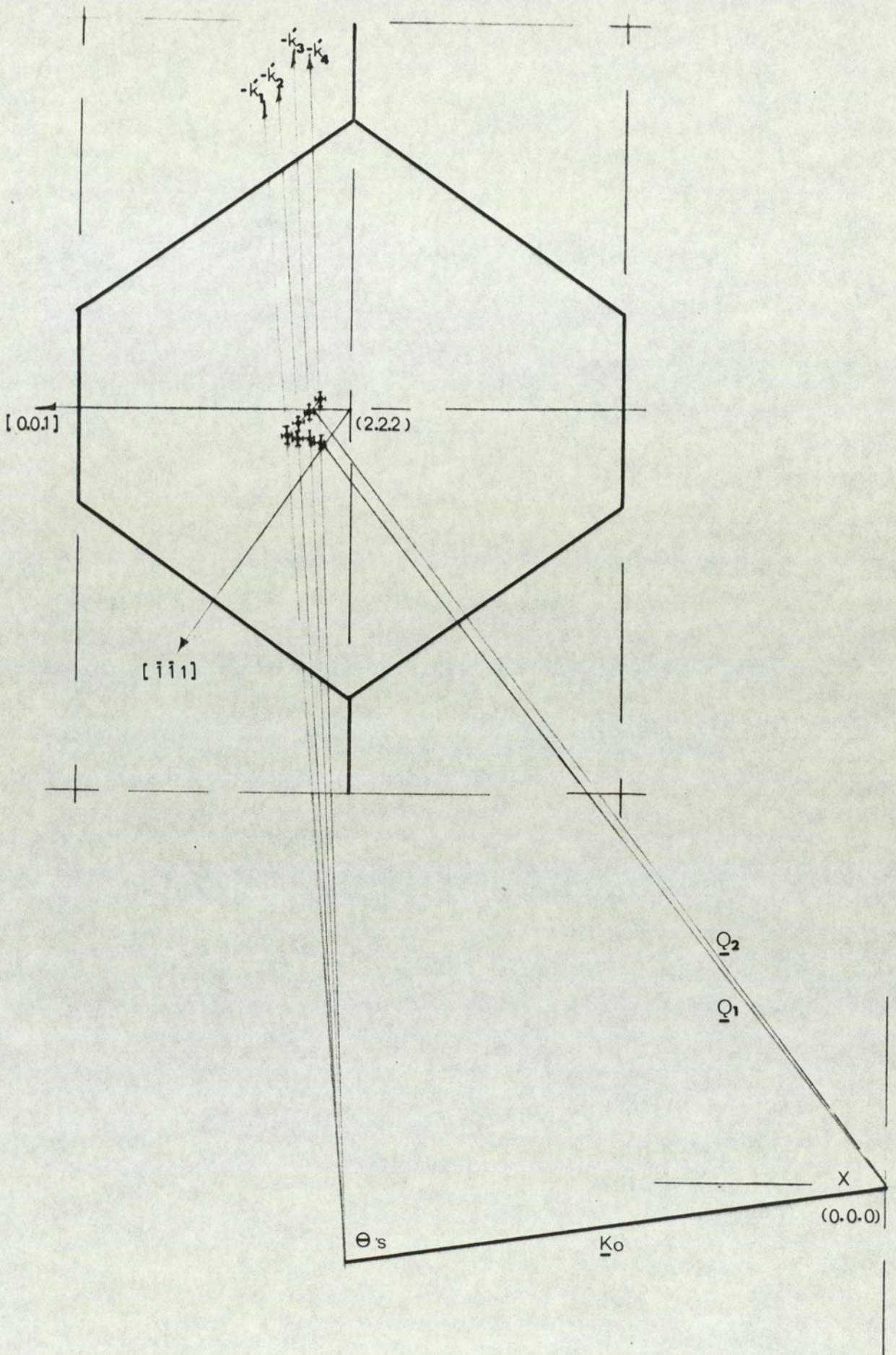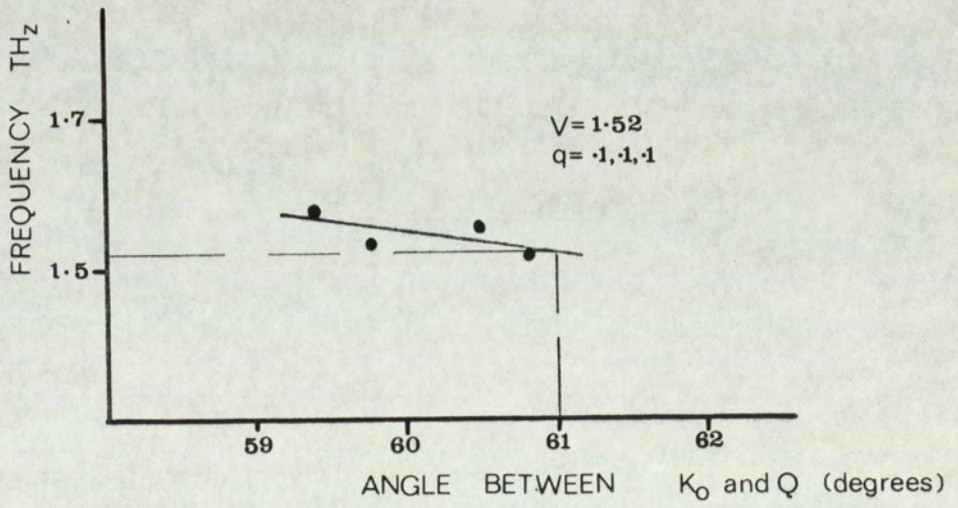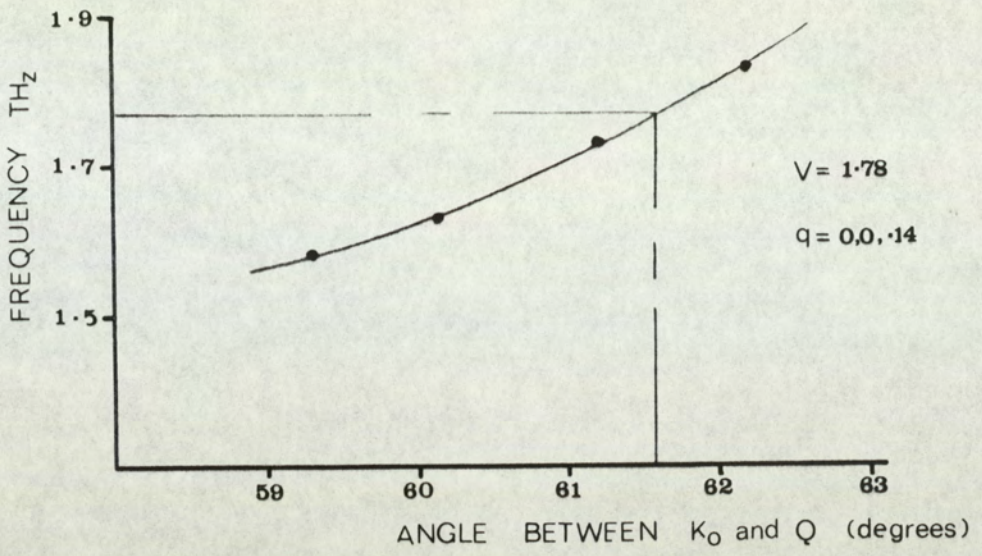
Fig 4.9 a

Fig 4.9b

Fig 4.9c
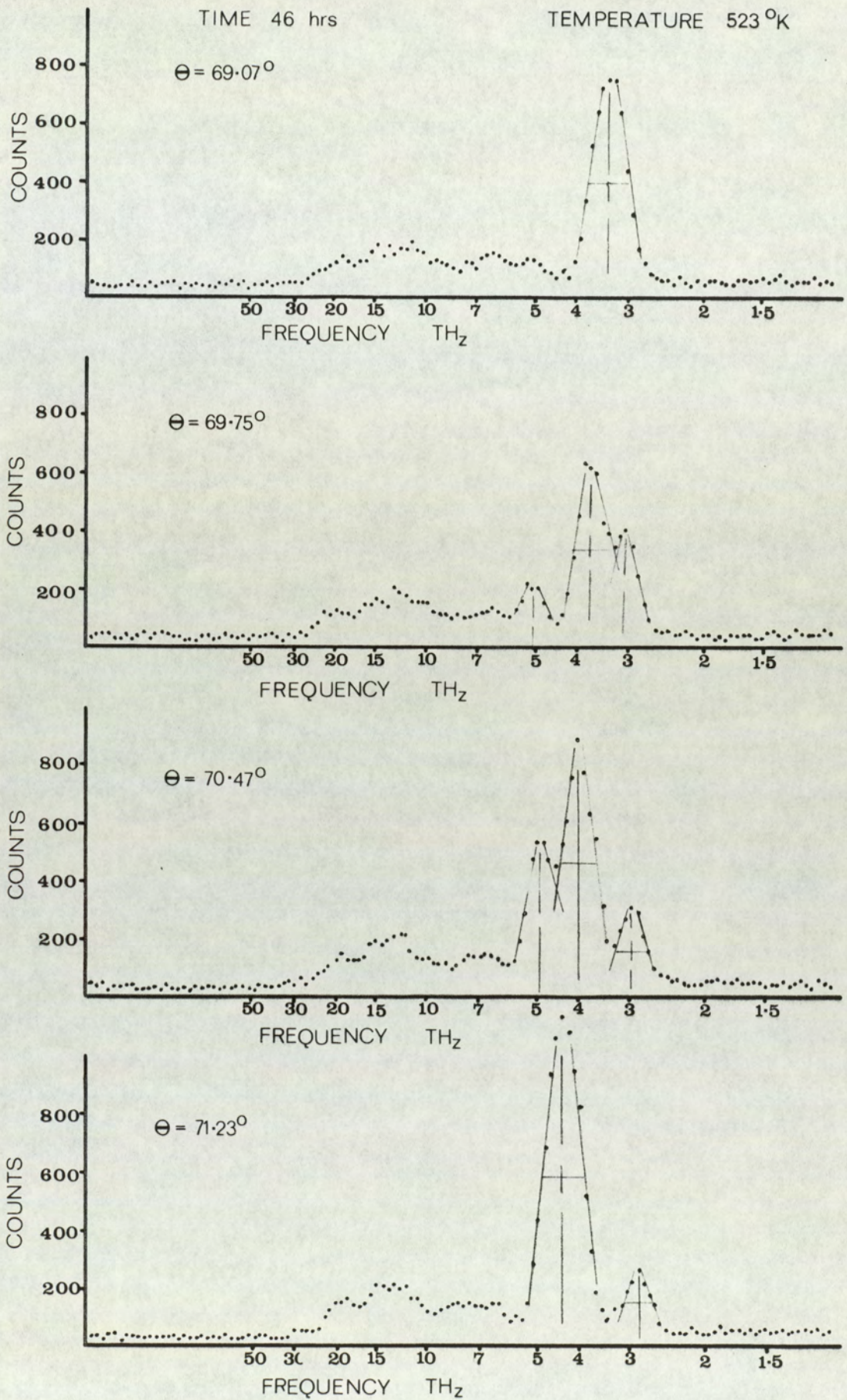
Fig 4·10a
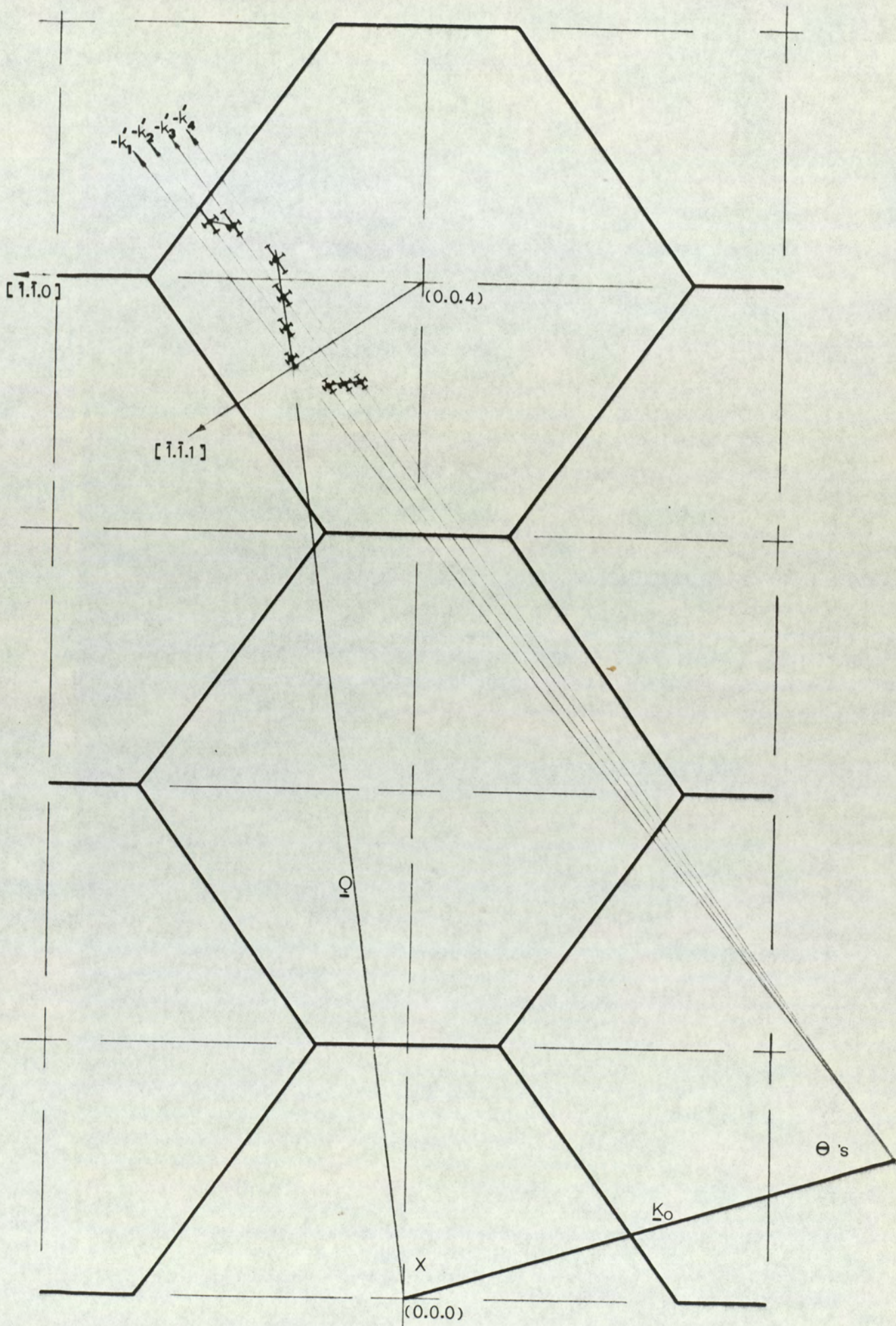
Fig 4.10 b
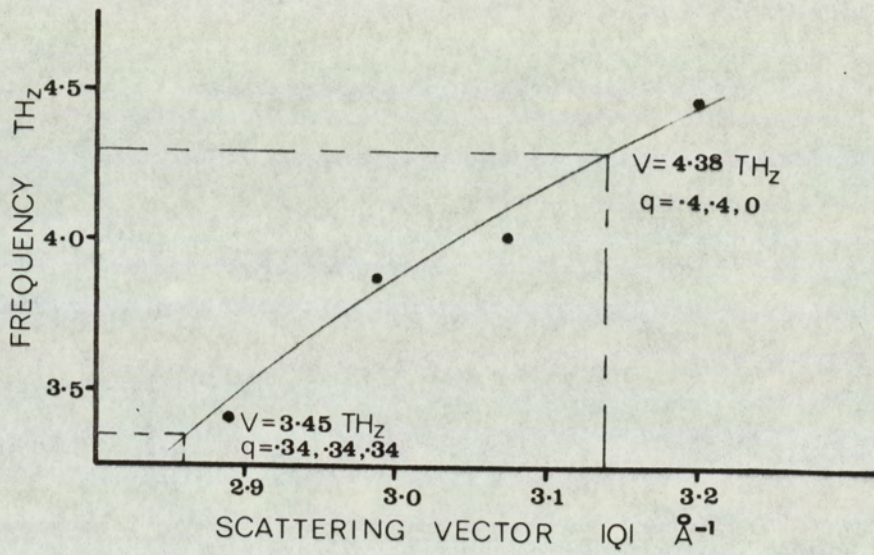
Fig 4.10c
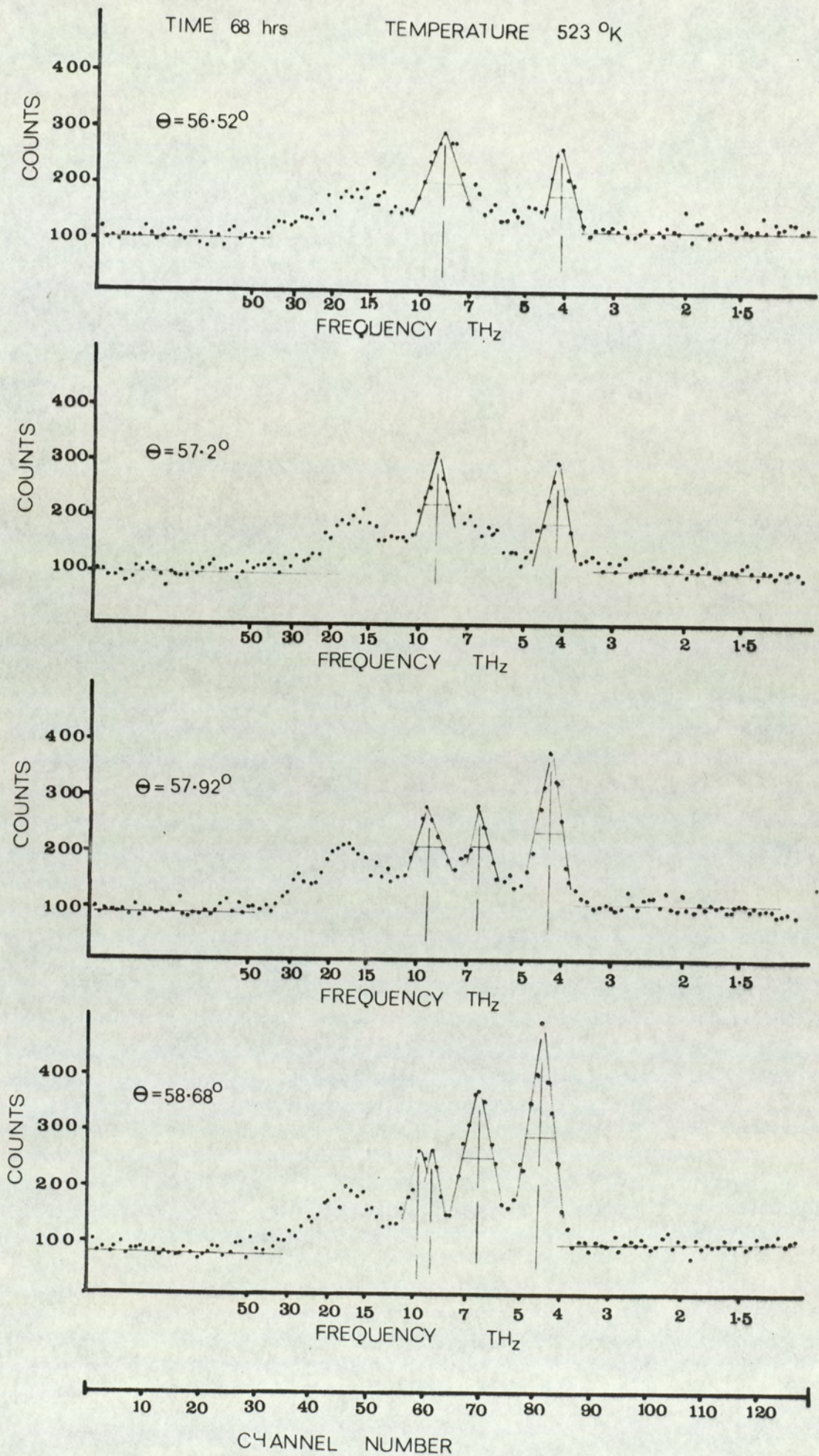
Fig 4.11a

Fig 4.11 b

Fig 4.11c

TIME 49 hrs   TEMPERATURE 673°K

Θ = 87.02°

Θ = 87.7°

Θ = 88.42°

Θ = 89.18°

FREQUENCY TH$_z$

CHANNEL NUMBER
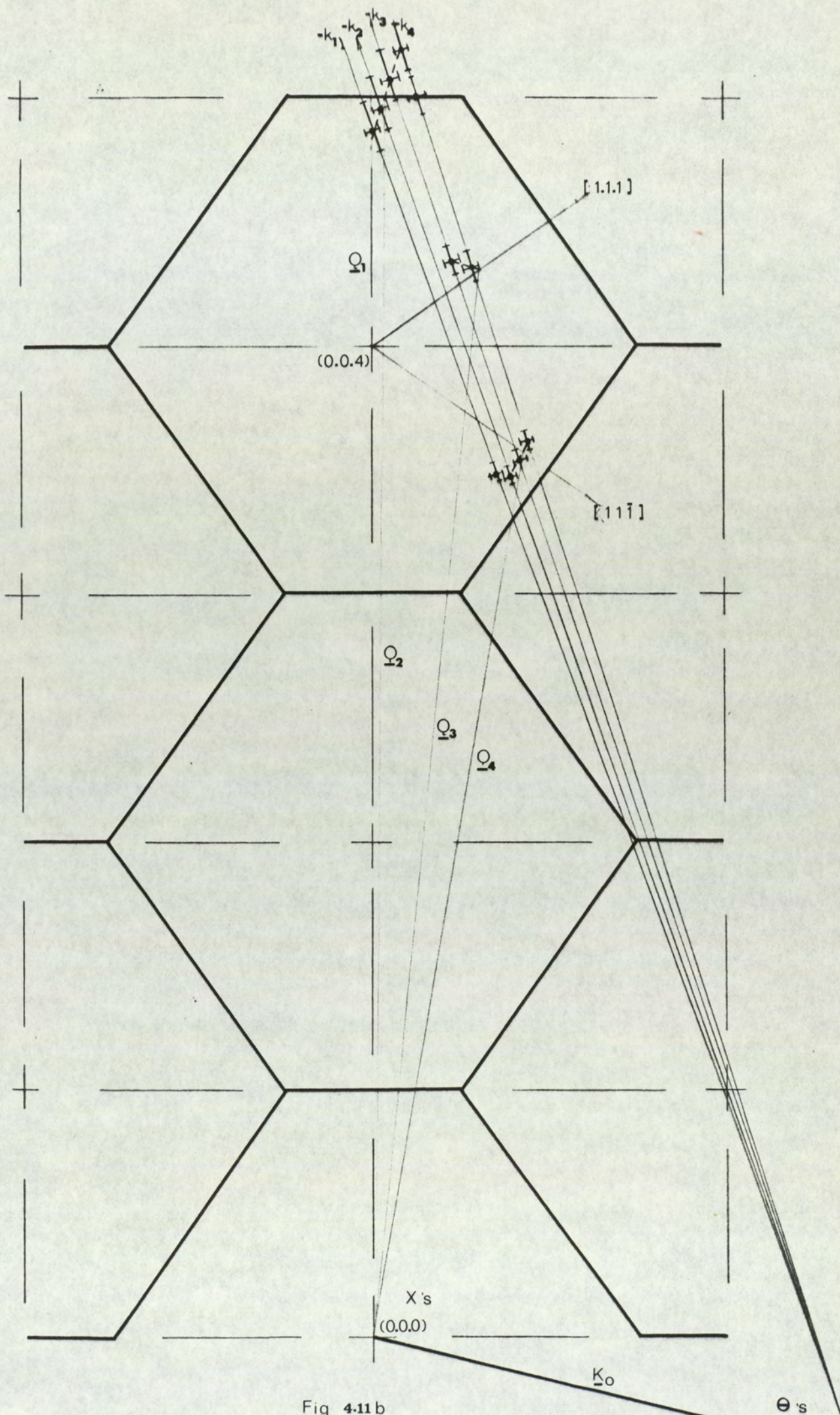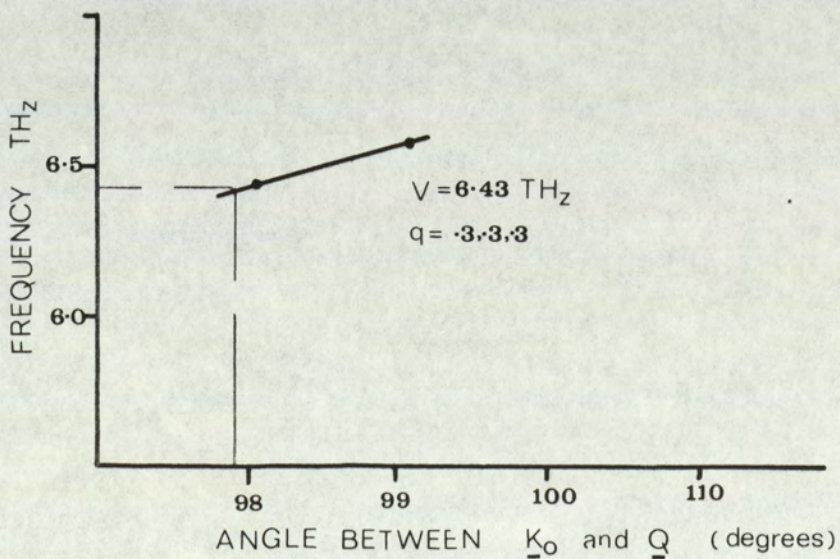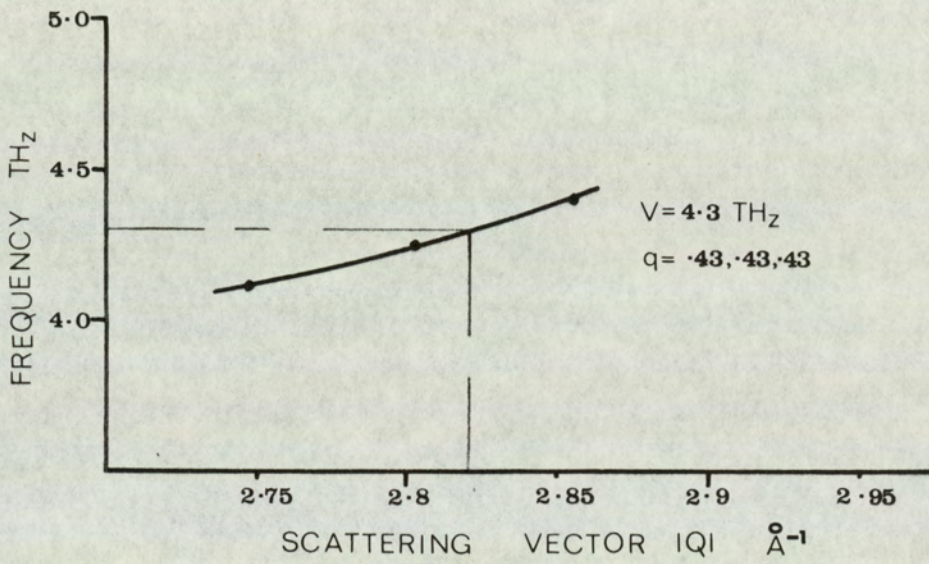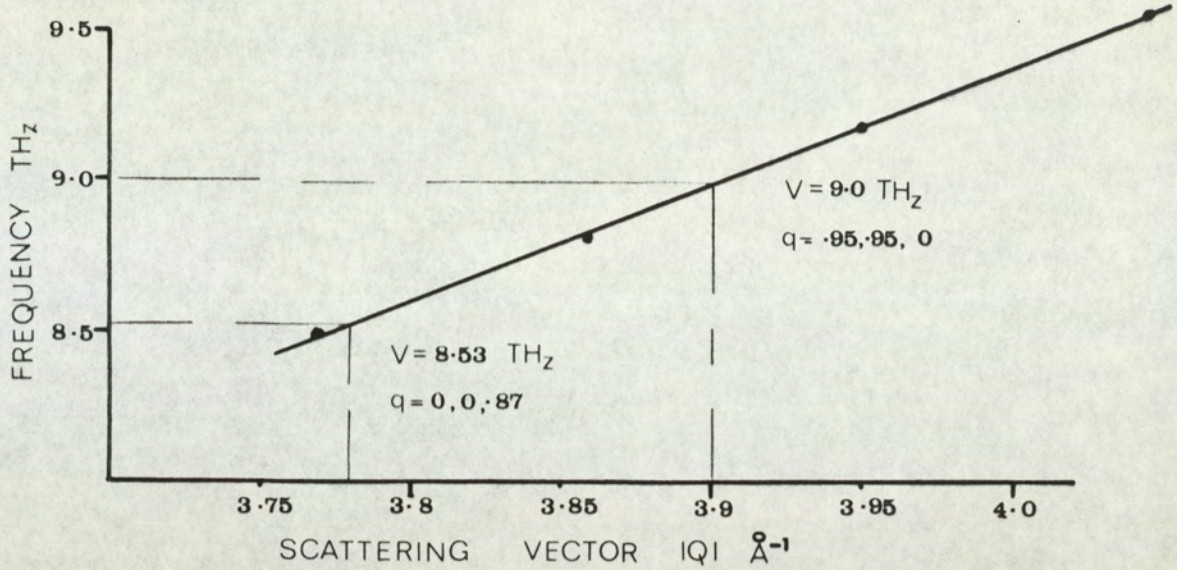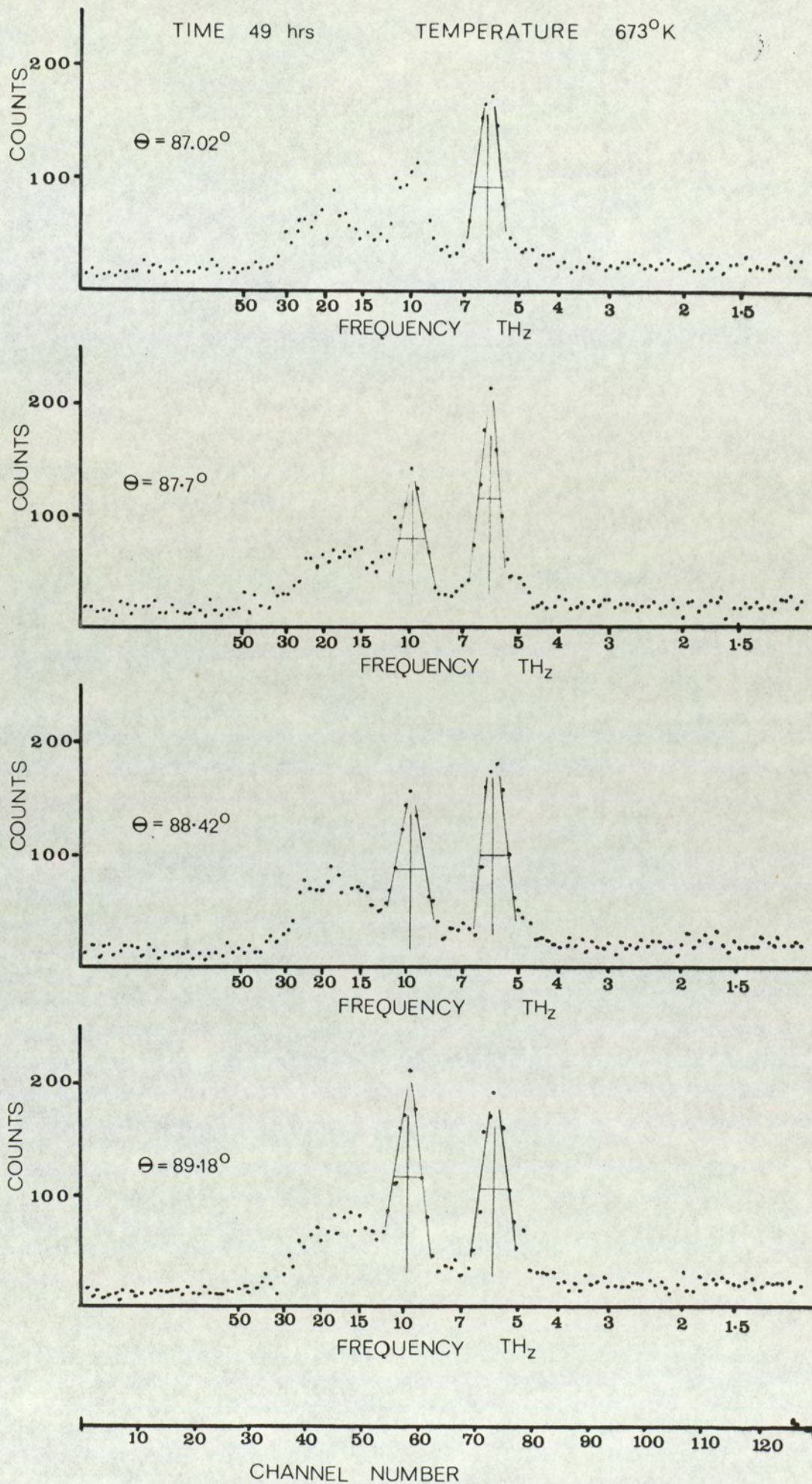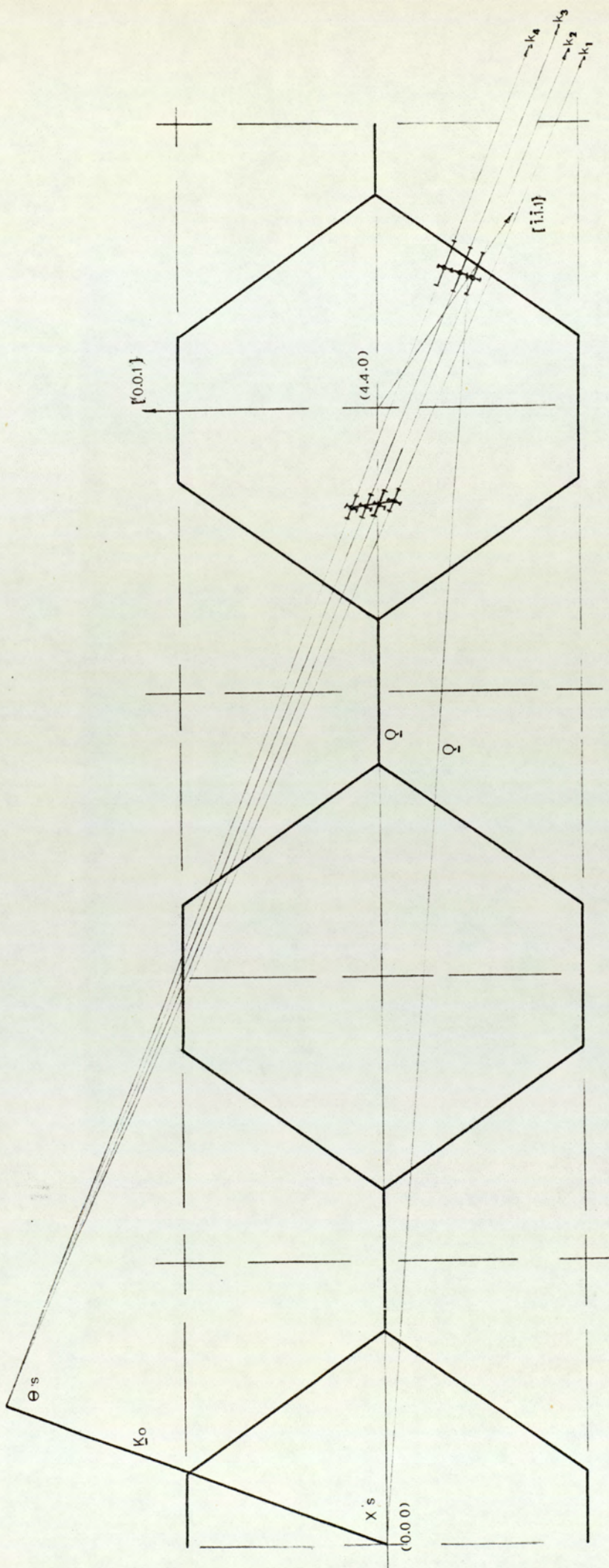
Fig 4.12a

Fig 4.12b
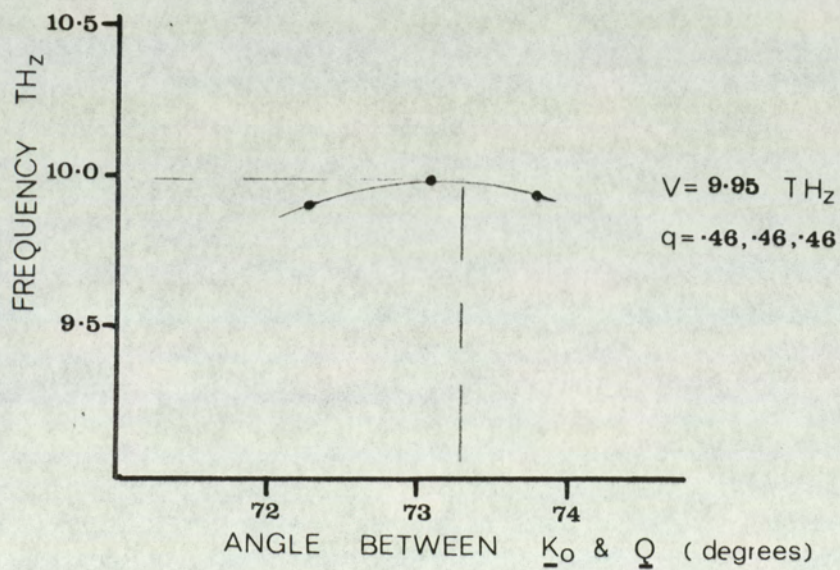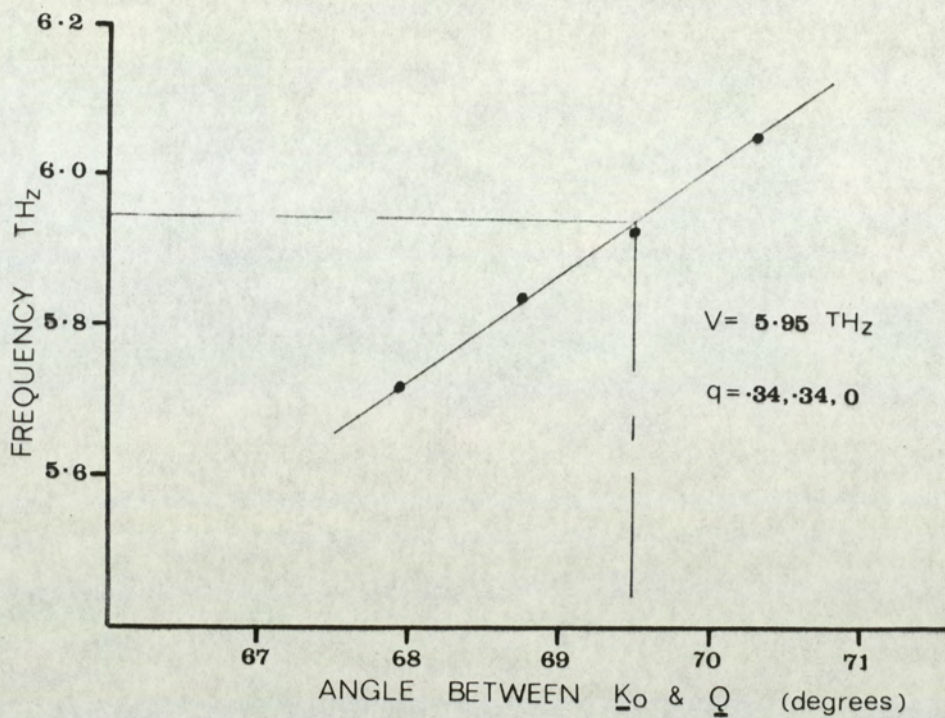
Eig 4.12 c

CHAPTER 5

A THEORETICAL MODEL FOR THE DYNAMICAL BEHAVIOUR OF SPINEL AND MAGNETITE.

5.1) Introduction.

As explained in Chapter 1, the physical behaviour of the cubic ionic spinels is not consistent with the conventionally assumed crystallographic space group Fd3m. Similarly, in Chapter 2, new and very precise diffraction evidence was presented to show that small atom shifts to the octahedral cations and oxygen arise in $MgAl_2O_4$, so that this structure is more correctly referred to the symmetry $F\bar{4}3m$. Nevertheless, since the lattice dynamics of a spinel had never previously been examined theoretically, it seemed advisable that initial investigations should be based on a minimum number of adjustable parameters. Therefore, in the dynamical calculations to be described in this chapter, the spinel structure was assumed to correspond to the space group Fd3m.

At the present time, adequate experimental data on the low energy phonon dispersion system is only available for two members of the spinel family, namely, $MgAl_2O_4$ itself, for which some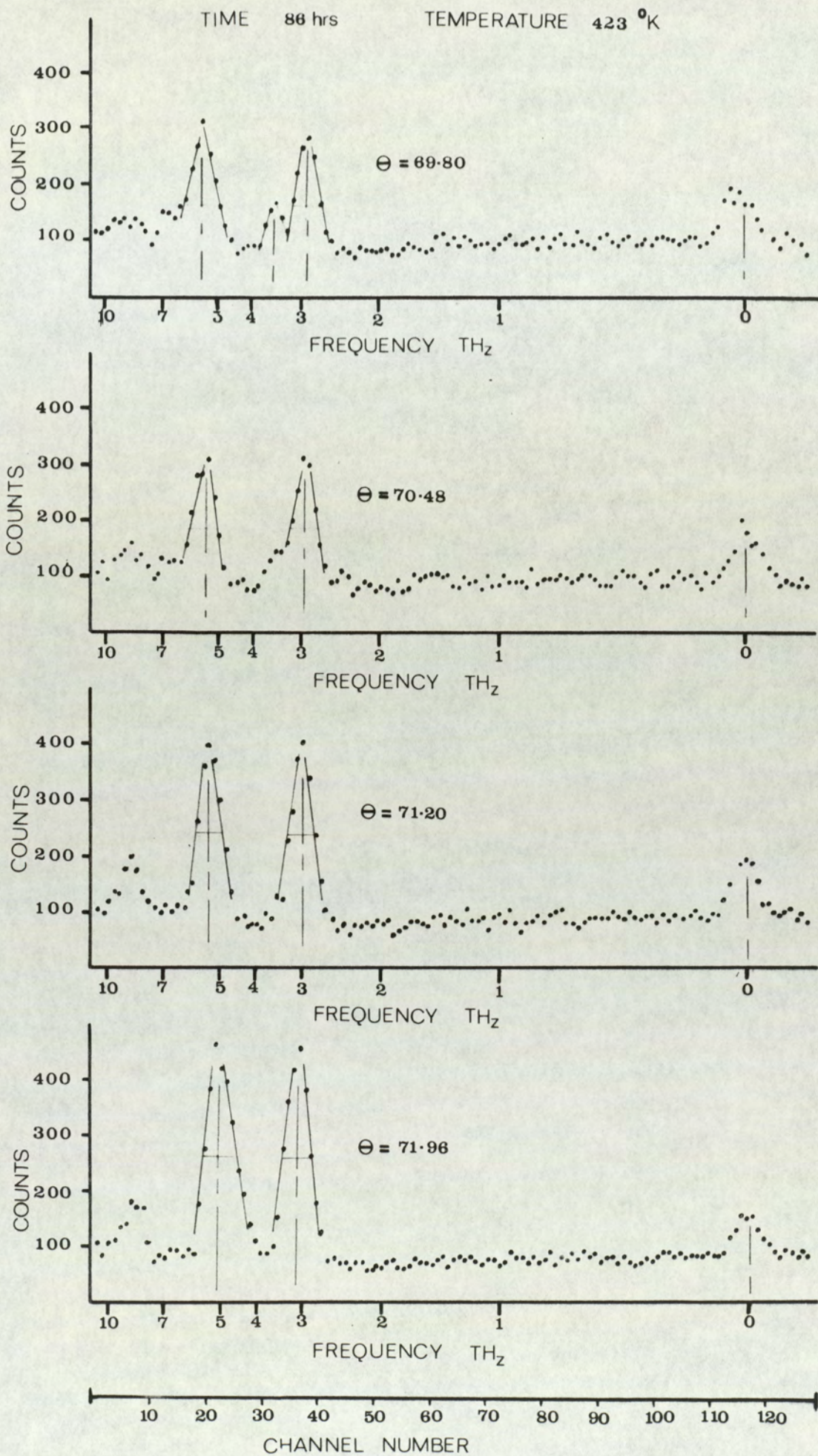 measurements have been obtained in this study, and Magnetite, Fe_3O_4, for which Samuelsen and Steinsvoll (1974) have carried out a similar limited investigation. These two materials are interesting to compare, however, in so far that the former corresponds quite closely to the normal cation arrangement (for simplicity it will be assumed to be ideally normal with u = 0.387 or δ = 0.012) while Magnetite is known to be an almost completely inverse spinel (Shull, Wollan and Kochler, 1951; Hamilton 1958) with oxygen position parameter u = 0.379 (δ = 0.004). In both cases, the materials will be treated as ionic which should be a good approximation for Spinel at least. Magnetite, on the other hand, has quite a good electrical conductivity at room temperature. Nevertheless, since the mechanism responsible for this property is thought to be associated with electrons hopping from Fe^{2+} to Fe^{3+} ions on neighbouring octahedral sites, (Verwey, Haagman and Romiejn, 1947) the

ionic approximation may be reasonable. Finally, it should be noted that magnetic exchange interactions arise in Magnetite which might also be expected to have some influence on the dynamics through magnon-phonon coupling, but again, for reasons of simplicity, this has been neglected.

Assuming, then, that the space group is Fd3m, the rhombohedral primitive unit cell must contain fourteen dynamically independent ions, and these have been labelled according to table 5.1 with positions as shown in figure 5.1. The corresponding dynamical matrix is thus of order 42 and the elements of this matrix were arranged in 9 sub matrices of order 14 according as α and β become the x,y and z components in turn giving xx, xy, xz etc, and within each sub matrix k and k' have values 1 to 14 increasing monotonically with k for the rows and k' for the columns. The diagonal matrices M and Z of equation 3.30 contain the masses and ionic charges respectively arranged along the leading diagonal in corresponding order. For example, the first fourteen diagonal elements of Z comprise of the two tetrahedral charges followed by four octahedral charges and then the eight anion charges, this pattern being repeated three times to complete the Z array.

5.2) The Coulomb coefficients.

The Coulomb coefficients, as explained in Chapter 3, are reduced to the dimensionless form of Kellermann and these are the elements of matrix C in equation 3.24. Each element was evaluated by the Ewald transformation (Ewald 1921) which enables the elements of matrix C to be expressed as a summation of two series one in real space, and the other in reciprocal space, both of which are arranged to be rapidly convergent. The result may be written
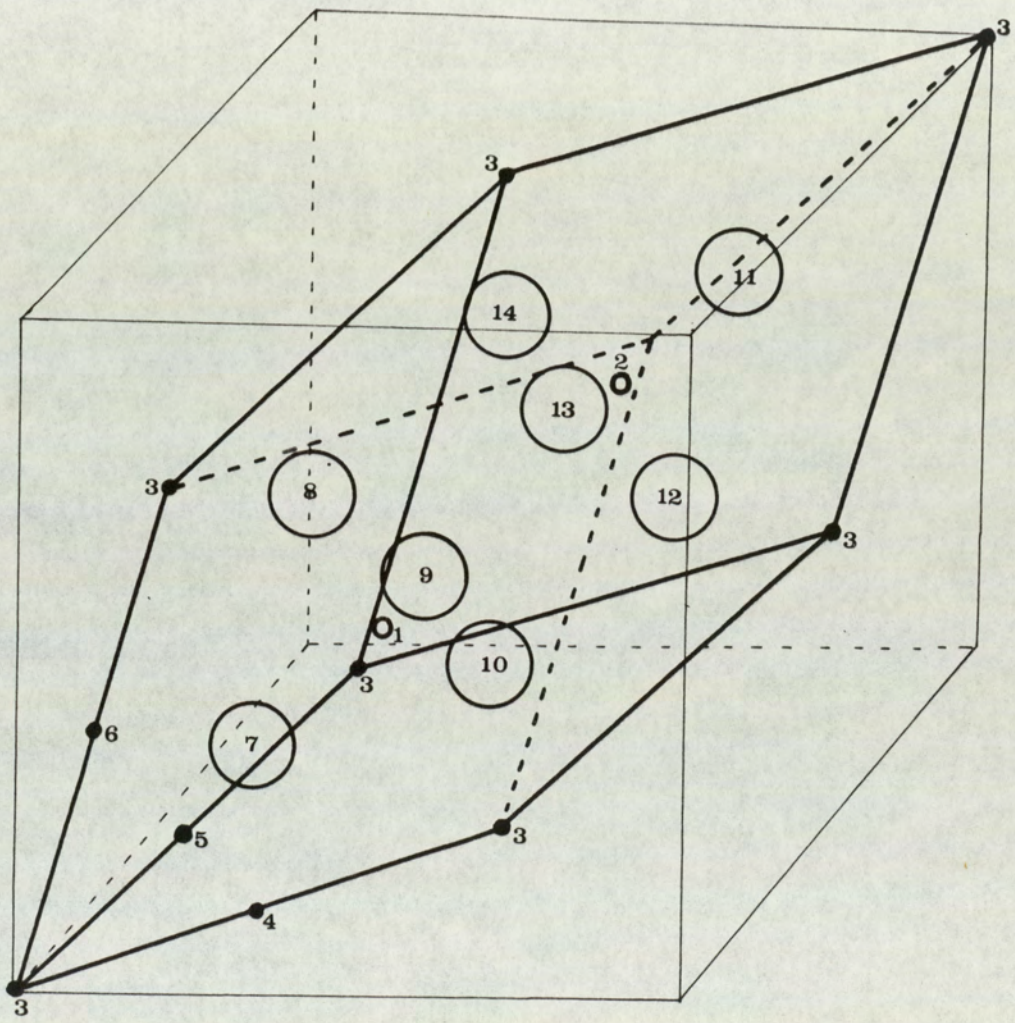
FIGURE 5.1 The Primitive Unit Cell of Spinel

Table 5.1: Labelling of the ions in the primitive unit cell.

Label k	Ions	Site Symmetry	Position
1	Mg, Fe^{3+}	$\bar{4}3m$	$\frac{3}{8}, \frac{3}{8}, \frac{3}{8}$
2	Mg, Fe^{3+}	$\bar{4}3m$	$\frac{\bar{3}}{8}, \frac{\bar{3}}{8}, \frac{\bar{3}}{8}$
3	Aℓ, $Fe^{2\frac{1}{2}+}$	$\bar{3}m$	$0, 0, 0$
4	Aℓ, $Fe^{2\frac{1}{2}+}$	$\bar{3}m$	$0, \frac{1}{4}, \frac{1}{4}$
5	Aℓ, $Fe^{2\frac{1}{2}+}$	$\bar{3}m$	$\frac{1}{4}, 0, \frac{1}{4}$
6	Aℓ, $Fe^{2\frac{1}{2}+}$	$\bar{3}m$	$\frac{1}{4}, \frac{1}{4}, 0$
7	0	$3m$	$\frac{1}{4}-\delta, \frac{1}{4}-\delta, \frac{1}{4}-\delta$
8	0	$3m$	$\frac{1}{4}-\delta, \delta, \delta$
9	0	$3m$	$\delta, \frac{1}{4}-\delta, \delta$
10	0	$3m$	$\delta, \delta, \frac{1}{4}-\delta$
11	0	$3m$	$\delta-\frac{1}{4}, \delta-\frac{1}{4}, \delta-\frac{1}{4}$
12	0	$3m$	$\delta-\frac{1}{4}, -\delta, -\delta$
13	0	$3m$	$-\delta, \delta-\frac{1}{4}, -\delta$
14	0	$3m$	$-\delta, \delta-\frac{1}{4}, -\delta$

$$C_{\alpha\beta}(kk',\underline{q}) = 4\pi\sum_{d^*} \frac{(d^*_\alpha+q_\alpha)(d^*_\beta+q_\beta)}{|\underline{d}^*+\underline{q}|^2} \exp(-|\underline{d}^*+\underline{q}|^2/4R^2 \times$$

$$\times \exp i\underline{d}^*.[\underline{r}(k)-\underline{r}(k')] + \Delta_{\alpha\beta}(kk',\underline{q}) \qquad 5.1$$

where $\underline{d}^*$ is a vector of the reciprocal lattice, and in the case of Spinel the reciprocal lattice is body centred cubic and $\underline{d}^*$ is given by $\underline{d}^* = \frac{2\pi}{a}(h,k,\ell)$. The phonon wavevector, $\underline{q}$, is also a vector of this space given by, $\underline{q} = \frac{2\pi}{a}(q_x,q_y,q_z)$.

The function $\Delta_{\alpha\beta}(kk',\underline{q})$ is a complicated expression in crystal space given by,

$$-2\epsilon^3 \sum_{\ell'} H_{\alpha\beta}(\epsilon\underline{\ell}) \exp(i\underline{q}.\underline{r}) \qquad 5.2$$

in this expression, the vector $\underline{\ell}$ is related to the vector, r, in the spinel structure by,

$$\underline{\ell} = \underline{r}(\ell k, \ell' k')/a \qquad 5.3$$

where a is the lattice constant. It has components x,y,z the x-component being,

$$x = \ell x/2 - x_k + x_{k'} \qquad 5.4$$

ℓx, ℓy and ℓz being integers generating the face centred cubic symmetry, and x_k and $x_{k'}$, the fractional coordinates of the ions.

The function $H_{\alpha\beta}(\underline{r})$ is,

$$\frac{\partial}{\partial x \partial y} \frac{\phi(r)}{r} \text{ with } \phi(r) = 1 - \frac{2}{\sqrt{\pi}} \int_0^r e^{-\rho^2} d\rho \qquad 5.5$$

where α and β are the x,y and z coordinates in turn. For the term $\ell = 0$ in equation 5.2 $\phi(r)$ is replaced by,

$$\phi(r) = \frac{-2}{\sqrt{\pi}} \int_0^r e^{-\rho^2} d\rho \qquad 5.6$$

So,

$$Hxy(\epsilon\underline{\ell}) = -a(\epsilon\ell)\delta xy + b(\epsilon\ell) \frac{xy}{\ell^2} \qquad 5.7$$

where
$$a(\epsilon\ell) = \frac{\phi(\epsilon\ell)}{\epsilon^3\ell^3} + \frac{2}{\sqrt{\pi}\epsilon^3\ell^2}\ \exp(-\epsilon^2\ell^2)$$
5.8

and
$$b(\epsilon\ell) = \frac{3\phi(\epsilon\ell)}{\epsilon^3\ell^3} + \frac{6}{\sqrt{\pi}\epsilon^2\ell^2}\ \exp(-\epsilon^2\ell^2) + \frac{4}{\sqrt{\pi}}\ \exp(-\epsilon^2\ell^2)$$
5.9

From these expressions the elements of $C_{\alpha\beta}(kk',\underline{q})$ defined by equation 5.1 can be evaluated. The parameter R in 5.1 is related to ϵ by $R = \epsilon/a$, ϵ being a pure number which controls the convergence of each series. When both series have converged, the elements of $C_{\alpha\beta}(kk',\underline{q})$ are independent of ϵ and the value of ϵ is adjusted until this condition has been achieved. In the present calculations, a value for ϵ of 3.0 was found to provide convergence at about the same rate in the real and reciprocal series for both Spinel and Magnetite. The Coulomb translational invariance term of equation 3.21 can also be evaluated from expression 5.1 but in this case the term $d^* = 0$ must be excluded from the summation of the reciprocal series.

5.3) The repulsive coupling coefficients.

In the rigid ion model, the short-range repulsive forces are parameterised in terms of two constants A and B, defined by equation 3.26, per interaction of the same type, and are often restricted to the interaction between nearest neighbours. For the spinel compounds we therefore consider nearest neighbour interactions between the tetrahedral ion and its surrounding oxygen ions, and the octahedral ion and its nearest oxygens. Figures 5.2 and 5.3 show the oxygen ions which are the nearest neighbours to the tetrahedral and octahedral ions respectively. The latter gives only one B-site, whereas the former shows both AO_4 tetrahedra which occur in the primitive unit cell. In addition, because of the comparatively large size of the oxygen ion (radius $\sim 1.4\text{Å}$) it seemed likely that
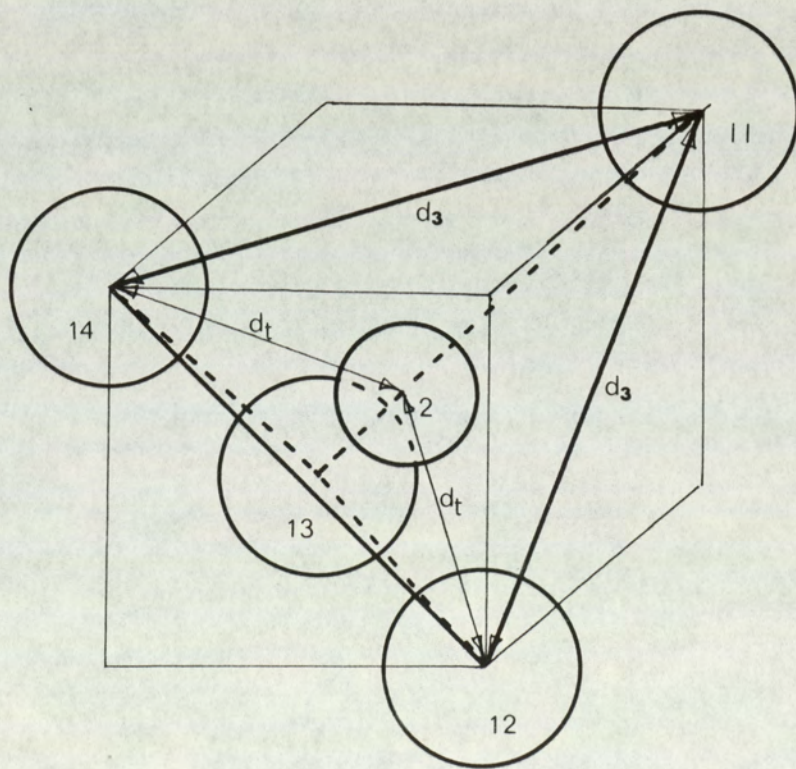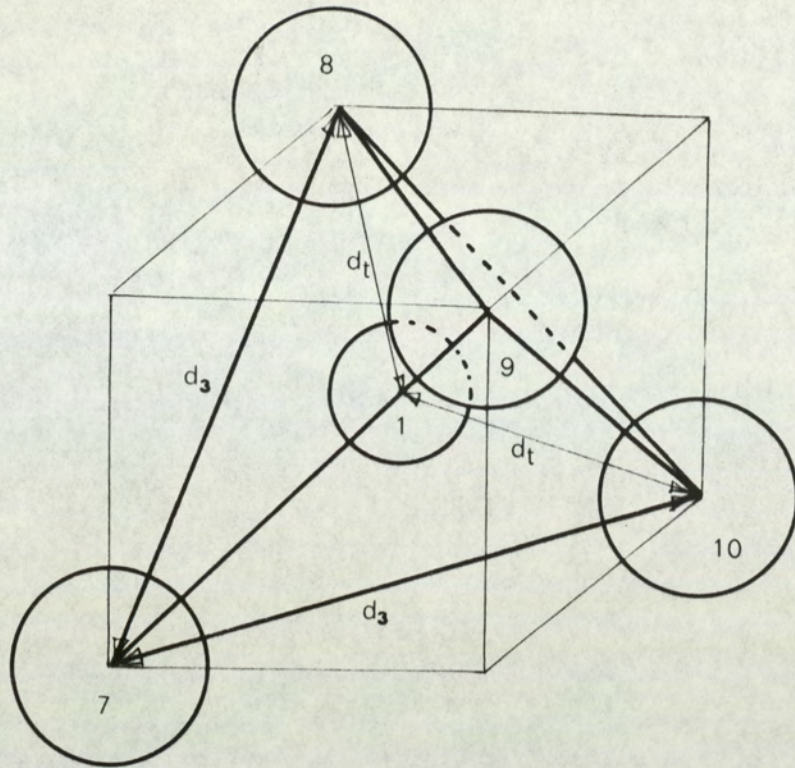
FIGURE 5.2   Tetrahedral Ion Environment
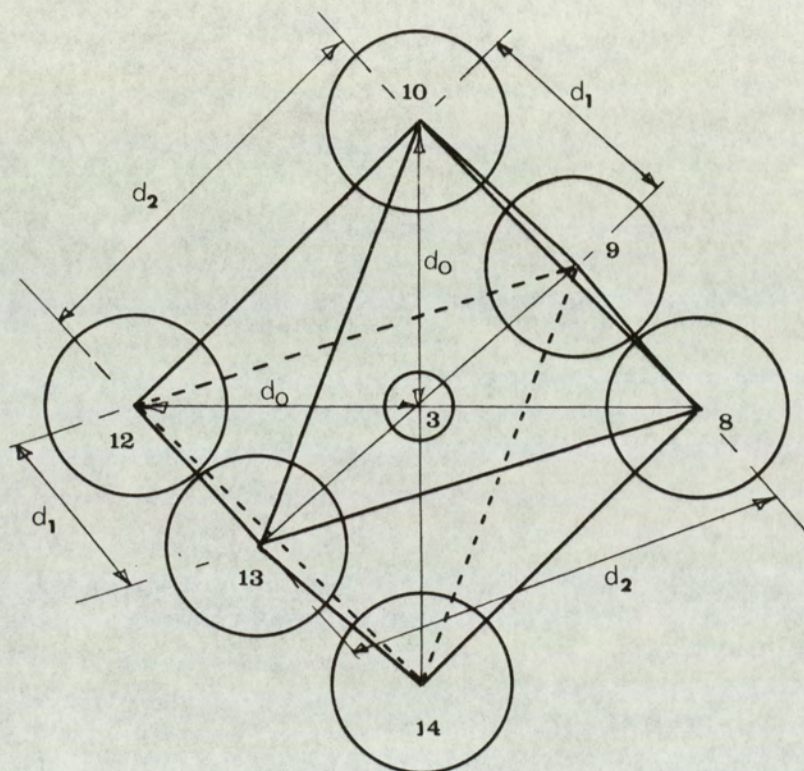
FIGURE 5.3 Octahedral Ion Enviroment

considerable interaction between neighbouring oxygen ions would
occur even though these are second nearest neighbours. These
next nearest neighbour interactions have therefore been included
in the analysis.

Now, in an ideal spinel each oxygen ion is surrounded by
twelve neighbouring oxygen ions all at the same distance, but in
practice, as a result of the displacements of the anions from their
perfect configuration, the oxygen-oxygen separations divide into three
groups. Three different anion-anion interactions must therefore be
considered and these may be characterised by the three separation
distances d_1, d_2 and d_3, from the shortest to the longest respectively,
as shown in figure 5.4, with reference to the oxygen ion which we
have labelled number 7. This ion has three neighbouring oxygen
ions of the type 8,9,10 at a distance d_1; six neighbouring oxygens
at a distance d_2, i.e. two ions of each type 12,13,14; and finally,
three at a distance d_3 which are ions of the type 8,9,10. The five
different types of repulsive interaction incorporated into the
present model may therefore be summarised as in table 5.2.

The ten short range parameters corresponding to these
repulsive interactions must be specified before the elements of the
repulsive matrix (matrix R) can be evaluated through equation
3.28, for each element depends upon some combination of the repulsive
parameters as well as a phase factor related to q. At q = 0, for
example, the independent elements are as shown in table 5.3 which also
gives the elements of $C_{\alpha\beta}(kk',0)$.

In the dynamical model then, there are a total of twelve
parameters, ten describing the short range interactions and two
ionic charges (the third charge being fixed by the necessity for
electrical neutrality) available for adjustment to fit the experimental
dispersion curves.

Further assumptions can be invoked which limit the number
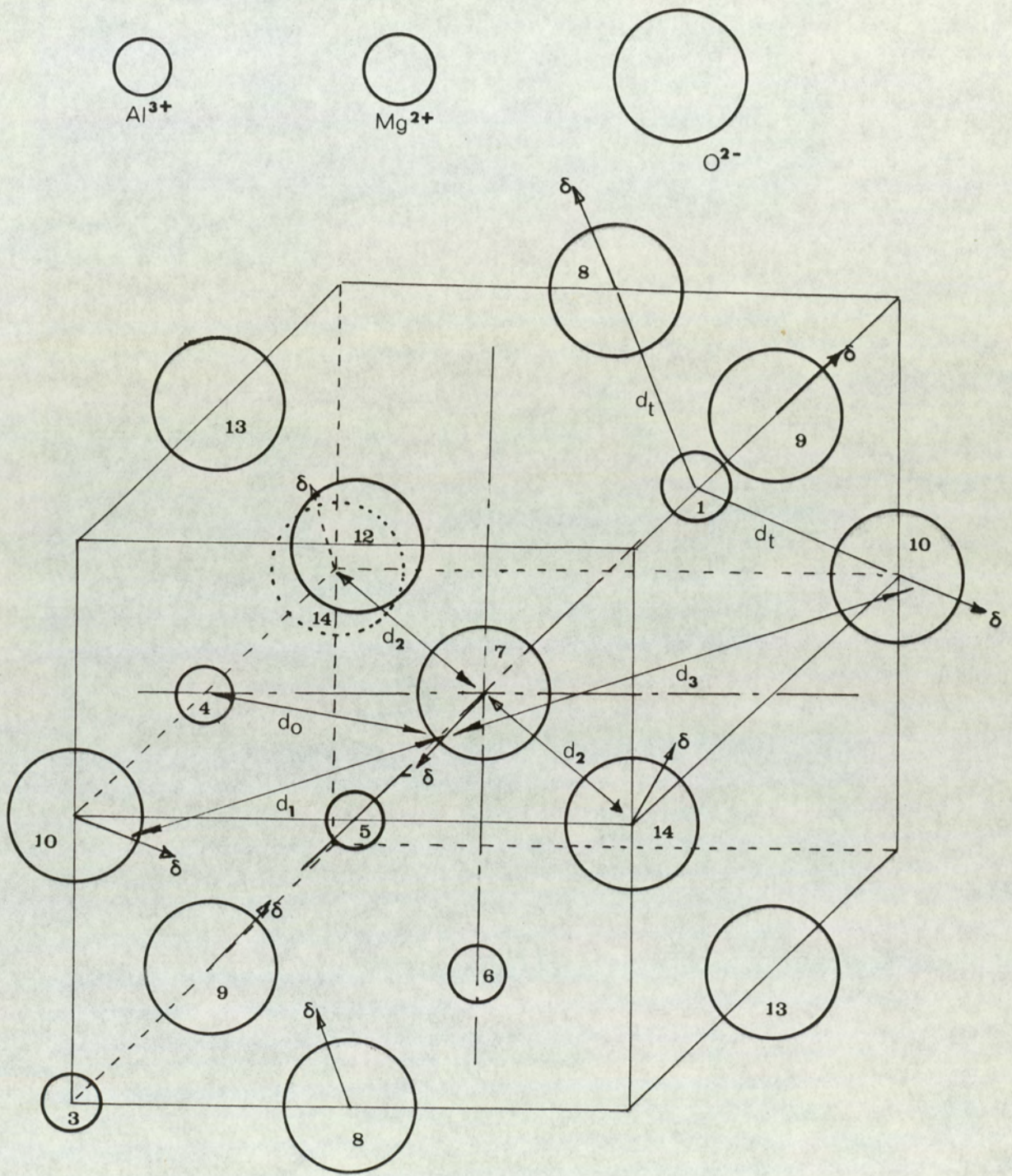
FIGURE 5.4 Oxygen Ion environment

of independent parameters, for example, if the short range inter-
actions can be described by central forces, then certain relation-
ships between the five B parameters can be deduced from the
equilibrium conditions of the spinel structure (see Chapter 6). Also,
a considerable reduction in the number of parameters, can be achieved
if the overlap potential of the oxygen-oxygen interaction could be
described by a mathematical functional form such as λr^{-n} or
$b \exp(-r/\rho)$, for then only two parameters describe all three anion-
anion interactions. However, this is probably an oversimplification,
and it was perhaps hardly surprising that initial attempts to refine
models of this type proved unsuccessful, in many cases producing
negative normal mode squared angular frequencies which correspond
to theoretical instability. Only when the model was given its
complete freedom, all twelve parameters being treated independently,
could a satisfactory fit to the experimental dispersion curves be
obtained for Magnetite and Spinel (see later).

5.4) Numerical calculations.

Computer programs were written to calculate the elements
of matrix R and C, these being evaluated with the CDC7600/ICL 1906A
computer at the University of Manchester Regional Computer Centre.
The 1764 elements of matrix C were evaluated for all three principal
crystallographic cubic directions $[0.0.\xi]$, $[\xi.\xi.0]$ and $[\xi.\xi.\xi]$
at intervals of reduced wavevector $\Delta\xi = .1$ from $\xi = .1$ to the
Brillouin zone boundaries, for both Magnetite and Magnesium Aluminate.
Since spinel has a face-centred cubic lattice, the Brillouin zone
has identical symmetry to that of NaCℓ and is shown in figure 5.5a
The results of these calculations were then stored on magnetic tape
and used throughout the refinement of the model parameters. The
independent elements are given as a function of q in the Appendix.
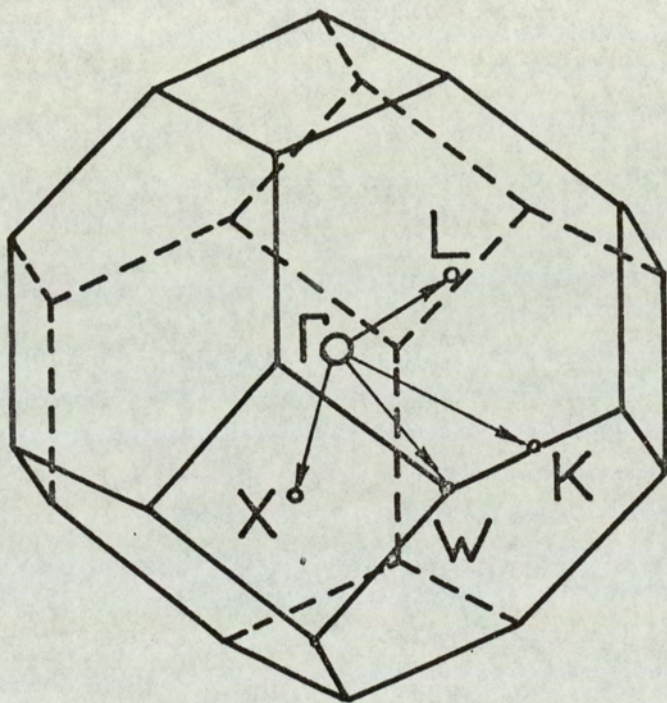
FIGURE 5.5a Brillouin zone for the F.C.C. lattice

Table 5.2: Summary of the short range interactions.

Interaction	Parameters	Separation distance
Tetrahedral site		
Mg–O	B_t, A_t	$d_t = \sqrt{3}\,(\frac{1}{8} + \delta)a$
Fe^{3+}–O		
Octahedral site		
Al–O	B_0, A_0	$d_0 = a\sqrt{3\delta^2 - \delta/2 + {}^1/_{16}}$
$Fe^{2\frac{1}{2}+}$–O		$\approx (\frac{1}{4} - \delta)a$
Anion		
O1–O1	B_1, A_1	$d_1 = \sqrt{2}(\frac{1}{4} - 2\delta)a$
O2–O2	B_2, A_2	$d_2 = [\frac{1}{2}\sqrt{2(1+16\delta^2)} + \ldots]a$
O3–O3	B_3, A_3	$d_3 = \sqrt{2}(\frac{1}{4} + 2\delta)a$

a = lattice constant $\delta = u - {}^3/_8$

Table 5.3: Contributions to the sub matrices Rxx, Rxy, Cxx,Cxy at q = 0

K	K'	elements of $Rxx(kk',0)$	elements of $Cxx(kk',0)$ $\delta = .004$	$\delta = .012$
1	1	$\frac{2}{3}(A_t+2B_t)$	-4.189	-4.189
1	2	0	-4.189	-4.189
1	3	0	-4.189	-4.189
1	7	$-\frac{1}{6}(A_t+2B_t)$	-4.189	-4.189
1	11	0	-4.189	-4.189
3	3	$\approx (A_0 +2B_0)$	-4.189	-4.189
3	4	0	4.479	4.479
3	5	0	-8.523	-8.523
3	7	0	-4.189	-4.189
3	8	$-A_0/2$	-35.387	-39.006
3	9	$-B_0/2$	11.653	13.220
7	7	$\approx \frac{1}{2}(A_1+A_3+B_1+B_3)+A_2+2B_2+\frac{1}{2}(B_1+B_3)+$ $+ \frac{1}{6}(A_t+2B_t) + A_0/2 + B_0$	-4.189	-4.189
7	8	$-\frac{1}{2}(B_3+ B_1)$	4.553	5.158
7	9	$-\frac{1}{4}(A_1+A_3+B_1+B_3)$	-8.560	-8.862
7	11	0	-4.189	-4.189
7	12	$-B_2$	4.454	4.257
7	13	$-\frac{1}{2}(A_2+B_2)$	-8.510	-8.411

Table 5.3: Continued

K	K'	elements of Rxy(kk,0)	elements of Cxy(kk',0)	
			$\delta = .004$	$\delta = .012$
1	1	0	0	0
1	3	0	3.374	3.374
1	7	$-\frac{1}{16}(A_t - B_t)$	-22.368	-18.604
3	3	$\approx 2\delta(A_0 - B_0)/(\frac{1}{4} - \delta)$	0	0
3	4	0	0	0
3	6	0	-14.461	-14.461
3	8	$\delta/2(A_0 - B_0)/(\frac{1}{4} - \delta)$	-.852	-2.868
3	10	≈ 0	-.011	-.124
3	7	0	-.312	-.965
7	7	$\approx +\frac{1}{16}(A_t - B_t) + \delta(A_0 - B_0)/(\frac{1}{4} - \delta) + \\ +\frac{1}{4}(A_1 - B_1 + A_3 - B_3) - \frac{1}{2}(A_2 - B_2)$	0	0
7	8	≈ 0	0	0
7	10	$-\frac{1}{4}(A_1 - B_1 + A_3 - B_3)$	-14.568	-15.446
7	11	0	.020	.183
7	14	$+\frac{1}{2}(A_2 - B_2)$	14.436	14.242

Matrix R was generated for each set of the ten parameters describing the overlap forces as these were adjusted together with two independent ionic charges to effect a fit with the experimental dispersion curves. Initial refinement was performed for $\xi = .1$ in all three directions, and when satisfactory results were obtained, the calculation was then extended in steps of $\Delta\xi = .1$ to the zone boundaries for further refinement in the $[0.0.\xi]$ and $[\xi.\xi.\xi]$ directions. Refinement of the model calculations in the $[\xi.\xi.0]$ direction was only continued out to $\xi = .3$ in Magnetite and $\xi = .4$ in Spinel, as the LA[110] dispersion branch is then confused with the low lying optic modes, and mode identification becomes a severe problem. This problem is alleviated to a certain extent in the other directions as an immediate classification can be made into transverse and longitudinally polarised modes of vibration, for the former are twofold degenerate. It is, therefore, possible in the majority of cases to identify each mode, as they are sufficiently well separated in terms of energy, by displaying the results graphically.

The refinement of the twelve model parameters in Magnetite was based on the experimental results shown in table 5.4. These are some of the results of Samuelsen and Steinsvoll but as the actual numerical values were not given, the values appearing in table 5.4 were derived by interpolation from a large scale graph, and possibly some accuracy may have been lost.

The model parameters for Spinel itself have been derived from the experimental measurements of the previous chapter and the observations used in the analysis are given in table 5.5.

Full matrix diagonalisation of the dynamic matrix D was employed, and was performed using the computer programs of the Nottingham algorithms group libraries (Nag Library). The routines used were FO2AWA, FO2AXA, the former giving only the eigenvalues of matrix D, whereas the latter also produces the eigenvectors of

matrix D but is somewhat slower in its operation. Both routines reduce D to a tridiagonal matrix and the diagonalisation is performed by the QL algorithm (see Bowdler, Martin and Reinsch 1968; Peters and Wilkinson 1970).

Care must be taken to ensure that the Coulomb translation invariance terms are added before diagonalisation. Therefore the elements of $C_{\alpha\beta}(kk',0)$ were calculated and stored on magnetic tape. The independent elements of this matrix are given in table 5.3. Prior to diagonalisation of D, the summation of the second term in 3.21 was performed by recalling the elements of $C_{\alpha\beta}(kk',0)$. This is then added to D in form defined by equation 3.30.

The refined parameters derived by fitting the theory to the experimental low energy dispersion curves is shown in table 5.6. The errors appearing in this table were deduced from examining the deterioriation in the fit to the dispersion curves as each parameter was varied in turn. The optic modes and transverse acoustic modes are sensitive to changes in the B parameters, ionic changes and the parameter A_2, i.e. a reduction of around 5~10% in the B-parameters resulted in a drop in the lowest optic mode frequency of about 5%. On the other hand, the acoustic modes, especially the longitudinal acoustic vibrations, were found to depend primarily on the A parameters and alterations of about 15% gave approximately 5% variation to these frequencies at intermediate phonon wavevectors. In Spinel itself because of the almost complete absence of useful data on the optical modes of vibration we could not identify with certainty which optic mode should belong to the observed optic phonon branch in the $[\xi.\xi.\xi]$ direction and as a result the errors given in table 5.6 may not reflect the true uncertainties in the model parameters (especially when one considers the recent results on UO_2 (Dolling, Cowley and Woods, 1965) where it has been shown that two totally different sets of parameters produce equally good descriptions of the phonon

Table 5.6) <u>Refined values of the adjustable parameters.</u>

Parameter	Fe_3O_4	$MgA\ell_2O_4$
B_t	$-9.0 \pm .5$	-17.5 ± 1.0
A_t	96 ± 10	190 ± 2.0
B_o	$-16 \pm .5$	-42 ± 2
A_o	337 ± 30	425 ± 35
B_1	$5.5 \pm .5$	$-5 \pm .5$
A_1	46 ± 5	135 ± 15
B_2	$-6.5 \pm .5$	-9 ± 1
A_2	28 ± 5	-10 ± 1
B_3	$-4.5 \pm .5$	$-4 \pm .5$
A_3	30 ± 5	43 ± 5
Z_t	$1.30 \pm .05$	$1.14 \pm .05$
Z_o	$1.15 \pm .05$	$2.95 \pm .05$
Z_{ox}	-0.90	-1.76

$e\ Z_t$ = Tetrahedral charge

$e\ Z_o$ = Octahedral charge

$e\ Z_{ox}$ = Oxygen charge
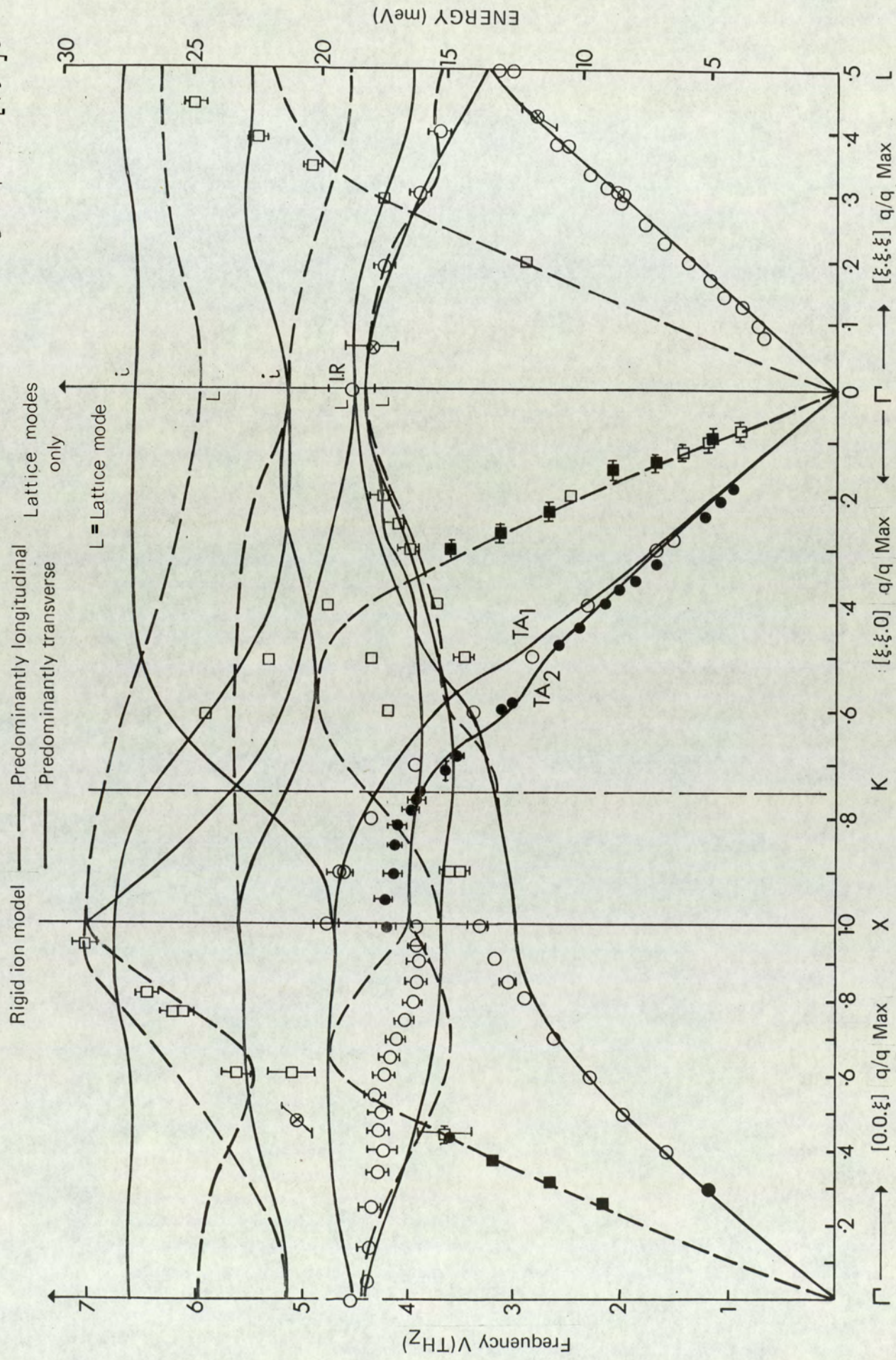
FIGURE 5.5 LOW ENERGY PHONON DISPERSION SURFACES IN MAGNETITE
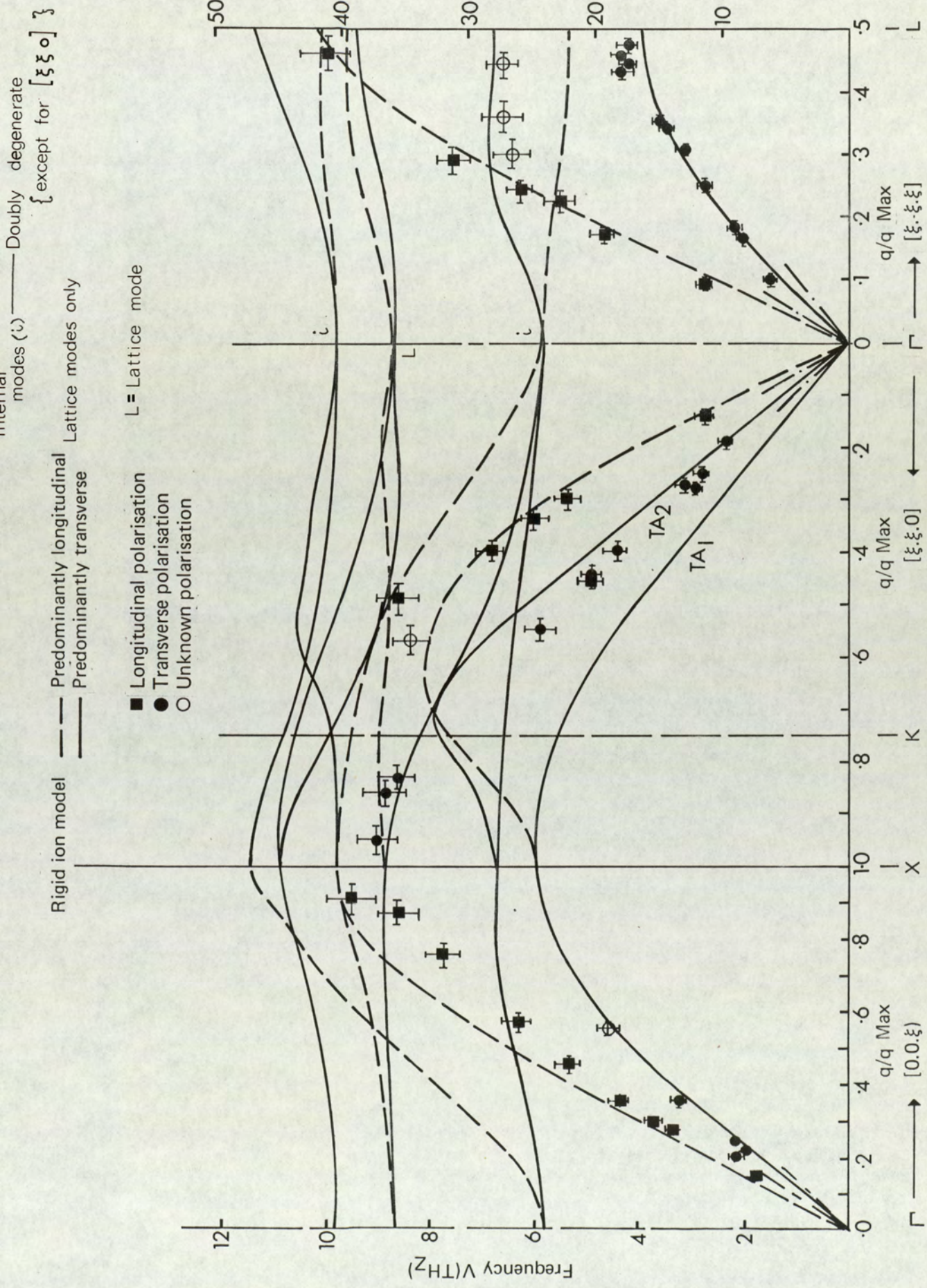
FIGURE 5.6 LOW ENERGY PHONONS IN SPINEL
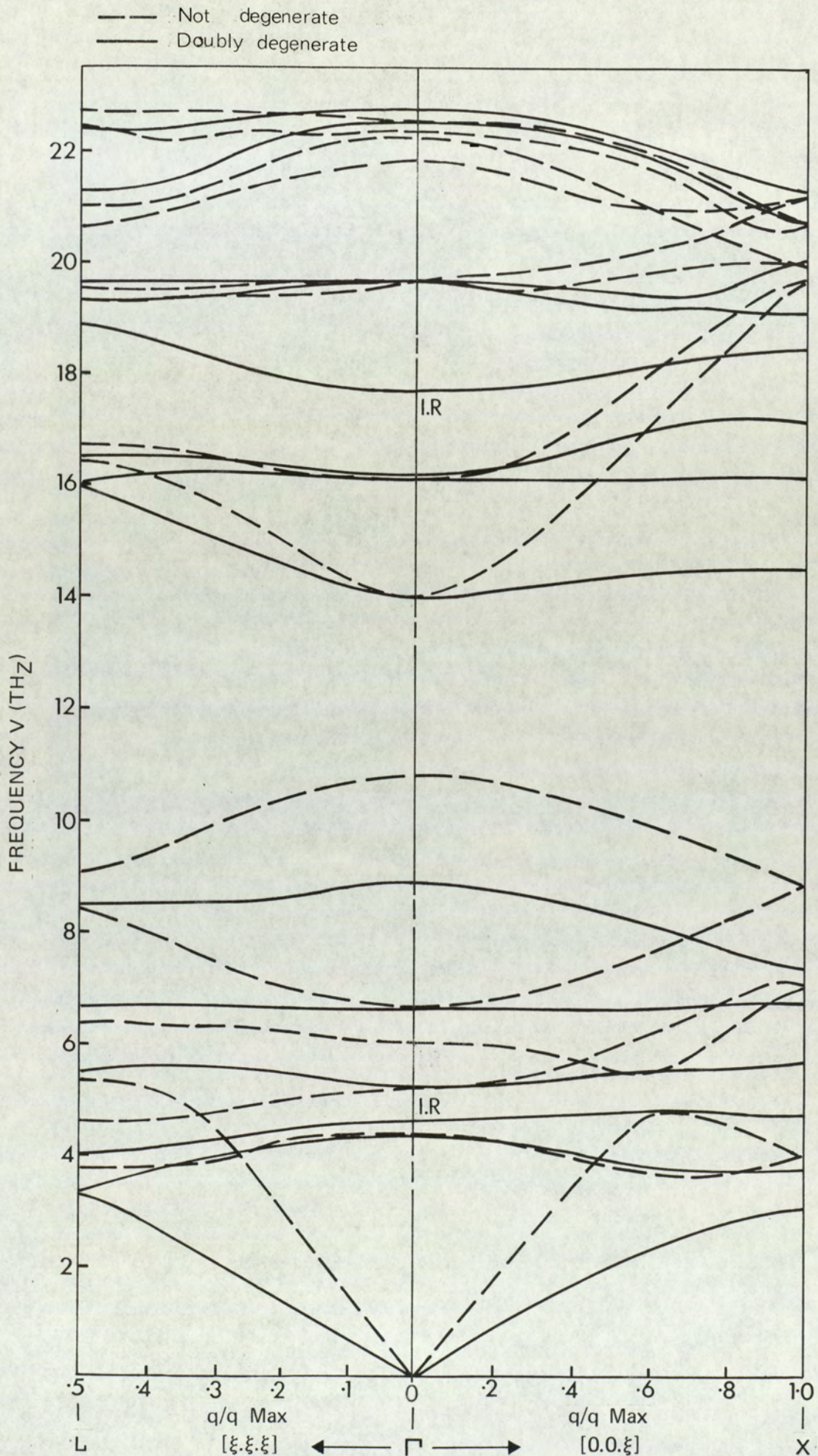
FIGURE 5.7   THEORETICAL PHONON DISPERSION SURFACES IN
MAGNETITE IN THE RIGID ION MODEL
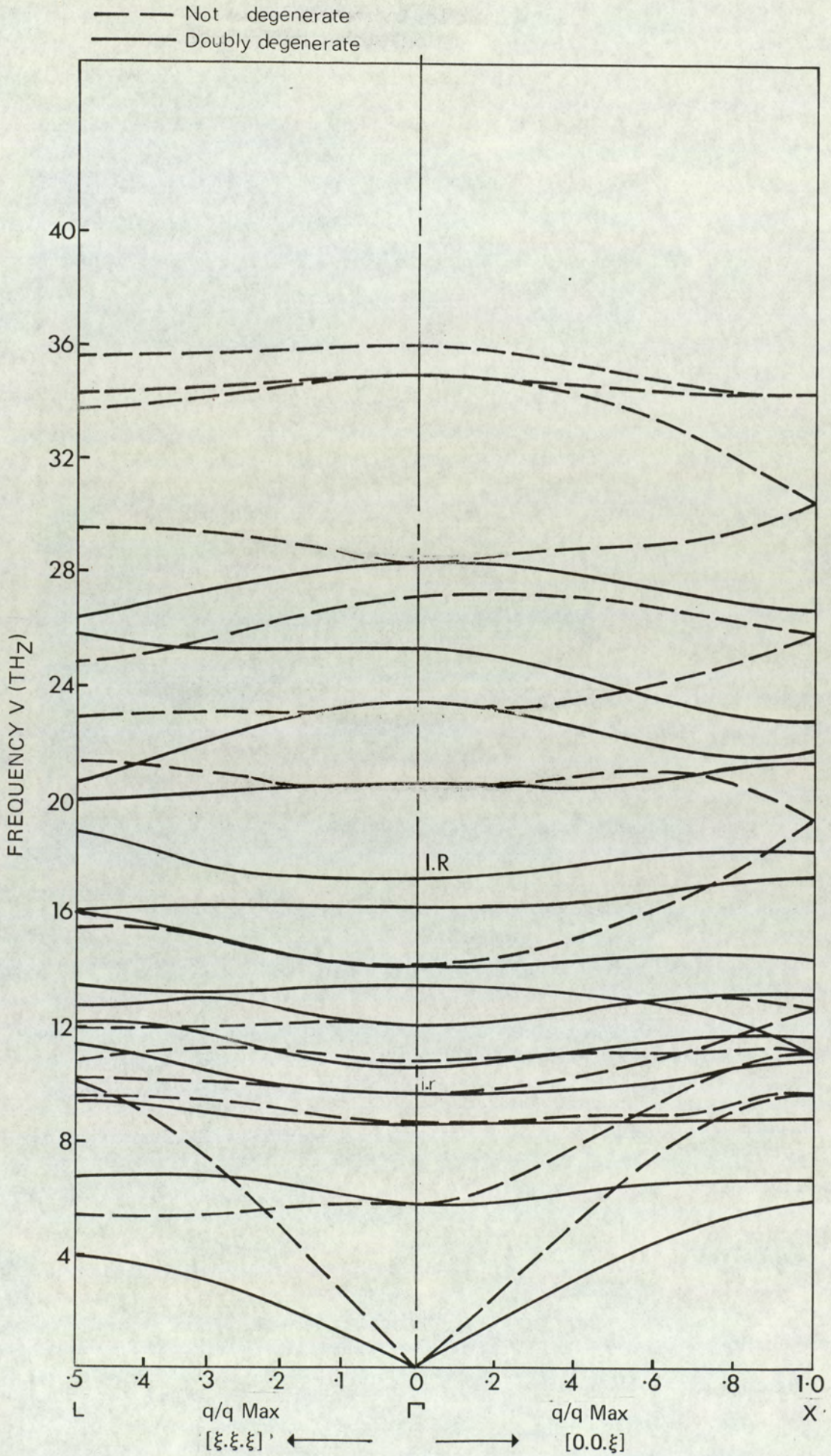
FIGURE 5.8 THEORETICAL PHONON DISPERSION CURVES IN
SPINEL IN THE RIGID ION MODEL

dispersion curves.)

Diagrams of the low energy dispersion system for Magnetite and Spinel are shown in figures 5.5 and 5.6 respectively, where the model calculation on these compounds are compared with the experimental values. The modes of vibration, particularly in the $[\xi.\xi.0]$ direction were tracked through the zone with help from the eigenvectors. To give an indication of the total dispersion system, the phonon curves have been plotted in $[0.0.\xi]$ and $[\xi.\xi.\xi]$ directions in figures 5.7 and 5.8. Following Samuelsen and Steinsvoll, in figure 5.5 the open symbols are measurements performed with the crystal orientated along a [110] axis, whereas the closed symbols are measurements in the [001] orientation. The square symbols correspond to longitudinal modes and the circular symbols to transverse modes.

5.5) The elastic constants.

In cubic structures there are three independent elastic constants and in the dynamical theory developed by Born are given by equation 3.36, which reduce in this case to,

$$C_{11} = [\alpha\alpha,\alpha\alpha] + (\alpha\alpha,\alpha\alpha) \qquad\qquad 5.10$$

$$C_{12} = 2[\alpha\beta,\alpha\beta] - [\alpha\alpha,\beta\beta] + [\alpha\alpha,\beta\beta] \qquad 5.11$$

$$C_{44} = [\alpha\beta,\alpha\beta] + [\alpha\beta,\alpha\beta] \qquad\qquad 5.12$$

The explicit expressions for the bracketed terms are given by Born and Huang (equations 31.38 and 31.39) and discussed by Cowley (1962). The external strain contribution to the elastic constants can be divided into two parts, i.e. $C_{11}{}^{R}$ and $C_{11}{}^{C}$ etc. where the suffices R and C represent the repulsive and Coulomb contributions respectively. The internal strain contributions, in the round brackets, involve rather complicated summations which include a matrix related to the inverse of $\overline{D}_{\alpha\beta}(kk',0)*$ and therefore cannot be separated in

---

*The elements of this matrix have the contributions associated with the macroscopic electric field removed.

Table 5.4: Observed phonons in Magnetite (after Samuelsen and Steinsvoll)

$[o.o.\xi]$

q/q_{max}	TA ν, TH$_z$	LA ν, TH$_z$	TO ν, TH$_z$	LO ν, TH$_z$
.1	.40 ± .05	.85 ± .05	4.45 ±.10	
.2	.85 ± .05	1.70 ± .05	4.40 ±.10	
.3	1.20 ± .05	2.55 ± .05	4.40 ±.10	
.4	1.60 ± .10	3.35 ± .05	4.35 ±.10	
.5	1.95 ± .05	4.25 ± .10	4.30 ±.10	
.6	2.35 ± .05	5.05 ± .20	4.25 ±.10	5.65 ± .15
.7	2.65 ± .05		4.10 ±.10	5.7 ± .15
.8	2.90 ± .10		4.00 ±.10	6.25 ± .15
.9	3.15 ± .05		8.90 ±.10	6.90 ± .15
1.0	3.30 ± .10		3.90 ±.10	7.00 ± .15

$[\xi.\xi.0]$

q/q_{max}	TA$_1$ ν, TH$_z$	TA$_2$ ν, TH$_z$	LA ν, TH$_z$	LO ν, TH$_z$
.1	.50 ± .05	.50 ± .05	1.20 ± .05	4.40 ± .10
.2	1.05 ± .05	1.05 ± .05	2.50 ± .05	4.25 ± .10
.3	1.60 ± .05	1.70 ± .05	3.60 ± .05	4.0 ± .10

$[\xi.\xi.\xi]$

q/q_{max}	TA ν, TH$_z$	LA ν, TH$_z$	LO ν, TH$_z$
.1	.70 ± .05	1.50 ± .05	4.40 ± .20
.2	1.40 ± .05	2.90 ± .05	4.25 ± .10
.3	2.05 ± .05	4.25 ± .10	3.90 ± .10
.4	2.65 ± .05	5.45 ± .10	3.65 ± .10
.5	3.05 ± .10	6.15 ± .10	3.15 ± .10

Table 5.5 Observed phonons in Spinel.

$[0.0.\xi]$

q/q_{max}	TA $\nu,$ TH$_z$	LA $\nu,$ TH$_z$	
.1	.90 ± .10	1.8 ± .10	
.2	1.90 ± .10	2.5 ± .10	
.3	2.70 ± .10	8.7 ± .15	
.4	3.70 ± .15	4.7 ± .25	
.5	4.20 ± .20	5.8 ± .30	
.6		6.7 ± .35	
.7		7.6 ± .35	
.8		8.2 ± .40	
.9		8.8 ± .40	
1.0		8.9 ± .40	

$[\xi.\xi.0]$

q/q_{max}	TA$_2$ $\nu,$ TH$_z$	LA $\nu,$ TH$_z$	
.1	1.2 ± .10	2.0 ± .10	
.2	2.4 ± .10	4.0 ± .20	
.3	3.5 ± .15	5.4 ± .25	
.4	4.5 ± .20		

$[\xi.\xi.\xi]$

q/q_{max}	TA $\nu,$ TH$_z$	LA $\nu,$ TH$_z$	Unknown Polarisation $\nu,$ TH$_z$
.1	1.2 ± .10	2.8 ± .15	
.2	2.3 ± .10	4.2 ± .20	
.3	3.2 ± .15	7.6 ± .35	6.4 ± .35
.4	4.0 ± .20	9.3 ± .45	6.6 ± .35
.5	4.2 ± .20	10.2 ± .50	6.6 ± .35

the same manner.

The repulsive contributions from the external strain components are then given by the following expressions:-

$$C_{11}{}^R = \frac{2e^2}{V_a a} \left[\frac{8}{3} A_t (\tfrac{1}{8}+\delta)^2 + \frac{16}{3} B_t (\tfrac{1}{8}+\delta)^2 + 4A_0 (\tfrac{1}{4}-\delta)^2 \right.$$
$$+4A_1 (\tfrac{1}{4}-2\delta)^2 + 4B_1 (\tfrac{1}{4}-2\delta)^2 + A_2/4 + B_2/4$$
$$\left. +4A_3 (\tfrac{1}{4}+2\delta)^2 + 4B_3 (\tfrac{1}{4}+2\delta)^2 \right] \qquad\qquad 5.13$$

$$C_{12}{}^R = \frac{2e^2}{V_a a} \left[\frac{8}{3} A_t (\tfrac{1}{8}+\delta)^2 - 8B_t (\tfrac{1}{8}+\delta)^2 - 8B_0 (\tfrac{1}{4}-\delta)^2 \right.$$
$$+2A_1 (\tfrac{1}{4}-2\delta)^2 - 10B_1 (\tfrac{1}{4}-2\delta)^2 + A_2/4 - B_2/4$$
$$\left. + 2A_3 (\tfrac{1}{4}+2\delta)^2 - 10B_3 (\tfrac{1}{4}+2\delta)^2 \right] \qquad\qquad 5.14$$

$$C_{44}{}^R = \frac{2e^2}{V_a a} \left[\frac{8}{3} A_t (\tfrac{1}{8}+\delta)^2 - \frac{8}{3} B_t (\tfrac{1}{8}+\delta)^2 + 2A_1 (\tfrac{1}{4}-2\delta)^2 \right.$$
$$-2B_1 (\tfrac{1}{4}-2\delta)^2 + A_2/8 - B_2/8 + 2A_3 (\tfrac{1}{4}+2\delta)^2$$
$$\left. + 2B_3 (\tfrac{1}{4}+2\delta)^2 \right] \qquad\qquad 5.15$$

These expressions are only approximate as they ignore terms beyond the second order in δ but should yield values correct to four significant figures.

The Coulomb contribution to the square bracket terms may be reduced to a sum of terms involving products of the charges as the Ewald transformation permits the expansion (Cowley, 1962)

$$C_{xy}{}^C = \frac{2e^2}{V_a a} \left[k_1 Z_t{}^2 + k_2 Z_0{}^2 + k_3 Z_{ox}{}^2 + k_4 Z_0 Z_t + \right.$$
$$\left. + k_5 Z_t Z_{ox} + k_6 Z_0 Z_{ox} \right] \qquad\qquad 5.16$$

where the coefficients k_1 etc. depend only on the structural arrangement of the ions and eZ_t, eZ_0 and eZ_{ox} are the tetrahedral, octahedral and anion charges respectively. The coefficients k_1, k_2 and k_4 are constant for any spinel since they are independent of the internal parameter δ because they involve only the A and B-site ions which are in fixed positions, while k_3, k_5 and k_6 involve the anion positions and therefore δ.

All of the coefficients were evaluated from the expressions given by Cowley and the values of the fixed constants were found to be,

	k_1	k_2	k_4
$C_{11}{}^C$	-2.018	-4.450	2.529
$C_{12}{}^C$	-0.782	-1.987	-3.503
$C_{44}{}^C$	0.118	0.127	-2.395

the constants k_3, k_5 and k_6 are given as a function of δ for the elastic constants $C_{11}{}^C$, $C_{12}{}^C$, $C_{44}{}^C$ in table 5.7 a,b and c respectively.

Unfortunately the internal strain contribution cannot be separated in this manner for the reasons given. The detailed calculations in this case were carried out using the parameters of table 5.6 for Magnetite and Spinel respectively and the results from the internal contributions to the elastic constants are shown in table 5.8. The final values for the theoretical elastic constants obtained after adding the contributions from internal and external strain together are also compared with the experimental values in this table.

The fit to the elastic constants in Spinel is poor and may be due to the uncertainties in the refined parameters for this model. Nevertheless, the calculated values are similar to the experimental values, in so far as Cauchy's condition is nearly satisfied and C_{11} is greater than C_{12}. The agreement between the elastic constants in Magnetite at 300°K, however, is much better despite the considerable discrepancy between different sets of experimental measurements. The results of Moran and Luthi (1969) obtained through ultrasonic measurements of sound velocities are probably much more accurate than those of Doraiswami (1947) whose results were based on elastic measurements from natural crystals of

Table 5.7: Coulomb contributions to the elastic constants.

(a) Contributions to C_{11}^c

δ	k_3	k_5	k_6
− .008	−7.767	−5.504	12.718
− .004	−7.633	−4.899	12.830
.000	−7.587	−4.301	12.879
.004	−7.628	−3.712	12.844
.008	−7.756	−3.134	12.710
.012	−7.971	−2.570	12.459
.016	−8.270	−2.021	12.077
.020	−8.652	−1.491	11.547

(b) Contributions to C_{12}^c

δ	k_3	k_5	k_6
− .008	−8.248	2.444	−22.818
− .004	−8.387	1.746	−22.598
.000	−8.432	1.083	−22.265
.004	−8.388	.448	−21.798
.008	−8.253	− .155	−21.173
.012	−8.028	− .731	−20.371
.016	−7.708	−1.279	−19.364
.020	−7.296	−1.798	−18.137

(c) Contributions to C_{44}^c

δ	k_3	k_5	k_6
− .008	−2.178	2.609	−8.216
− .004	−2.283	2.107	−8.079
.000	−2.319	1.624	−7.903
.004	−2.288	1.157	−7.681
.008	−2.189	.709	−7.405
.012	−2.023	.278	−7.069
.016	−1.788	− .135	−6.665
.020	−1.486	− .529	−6.186

Table 5.8 <u>Elastic constants in Spinel and Magnetite.</u>

Elastic Constants in Spinel in units of 10^{11} dyns cm^{-2}

Elastic Constant	c_{xy}^{R}	c_{xy}^{C}	c_{xy}(Int)	Theoretical	Experiment [Ref.C]
C_{11}	59.40	−38.08	1.0	22.32	27.9
C_{12}	24.51	− 5.29	−0.7	18.52	15.3
C_{44}	12.67	9.97	−3.9	18.74	15.3

Elastic Constants in Magnetite in units of 10^{11} dyns cm^{-2}

Elastic Constant	c_{xy}^{R}	c_{xy}^{C}	c_{xy}(Int)	c_{xy} Theoretical	Experiment Ref[A]	Ref[B]
C_{11}	35.53	− 10.88	0.1	24.75	23.6	26.73
C_{12}	11.51	− 2.72	−0.05	8.74	−	10.60
C_{44}	6.79	0.57	−0.2	7.16	7.06	9.71

Ref A: Moran and Luthi   (1969)

Ref B: Doraiswami   (1947)

Ref C: Lewis   (1966)

Magnetite. The calculated values certainly fit the ultrasonic measurements better than the static measurements. Unfortunately Moran and Luthi did not measure any sound velocity which is dependent on the elastic constant C_{12}. Nevertheless, it is probably not unreasonable to suppose that this constant might be lower than the value quoted by Doraiswami and so the calculated value for C_{12} seems a fair figure.

CHAPTER 6

DISCUSSION

6.1) <u>The dispersion curves for Fe_3O_4 and $MgA\ell_2O_4$.</u>

The fit to the experimental dispersion curves shown in figures 5.5 and 5.6 is reasonably good, particularly in the case of Magnetite. However, it is typical of the physically unrealistic rigid ion model in that when the acoustic modes have been fitted at small values of the phonon wavevector $\underline{q}$, they deviate from the experimental observations near to the Brillouin zone boundaries. The theoretical predictions for Magnetite, nevertheless reveal a number of remarkable features. For example, Samuelsen and Steinsvoll from their measurements of the dispersion in LA [001] reasonably assumed that this mode passes through the point $q = 0.6$, $\nu = 5.2$ TH_z, and continues on to meet the zone boundary at X, at $7TH_z$. In contrast, the present calculations indicate that this dispersion branch bends over severely at $q = 0.5$ to join the $TA_2[110]$, at the critical point X. The higher energy phonons identified by Samuelsen as belonging to the LA[001] are fitted instead quite nicely by one of the longitudinal optic branches. Evidently, further experimental work is needed to clarify this discrepancy.

The agreement between experiment and theory in the [110] direction appears superficially to be better than it actually is, for theoretically the two transverse acoustic branches in this direction cross over at about [0.3, 0.3, 0], so that TA_2 apparently fits the experimental TA_1 branch and vice-versa. It seems unlikely that confusion between these modes could occur experimentally, as the dynamic structure factor would be expected to make the neutron-phonon interaction negligible for TA_1 with the crystal orientation in a (110) zone and negligible for TA_2 in the (001) zone. Nevertheless, Samuelsen et al. make only tentative assignments to the higher energy phonons from these branches so that some uncertainty concerning the true situation here must remain until

further experimental investigation has been carried out. The
longitudinal acoustic [110] branch fits quite well, however, at
least out to [0.3, 0.3, 0] and also reproduces, though not very
faithfully, the bending feature in the neighbourhood of
[0.5, 0.5, 0].

In the case of magnesium aluminate, $MgA\ell_2O_4$, there
is really insufficient data on which to base a dynamical model
with twelve parameters, in so far that, so little detail of the
lower lying optic modes has been uncovered that there is some
uncertainty as to whether the correct optic mode has been fitted.
This chiefly affects the B parameters and to some extent the ionic
charges as the remainder are to all intents determined by the
measured data from the acoustic branches. Apart from this slight
uncertainty the theoretical fit seems to be quite satisfactory,
in the present context.

6.2) Madelung constants for Spinels.

Before embarking on a discussion of the equilibrium
conditions in spinels and their connection with the repulsive
parameters, an expression for the Coulomb potential of the Spinel
structure is required, and this is conveniently expressed in terms
of the Madelung constant per formula unit.

Madelung constants in spinels have been derived previously
by Verwey and Heilmann (1947) and Verwey, de Boer and van Santen
(1948) but recently, calculations by Striefler and Barsh (1972)
on $MgA\ell_2O_4$ have shown that the earlier results may be in error by
about 3% for $\delta > 0$. The calculations of the Madelung constants
for a range of different spinel compounds was thereford repeated
as a precaution before undertaking the more detailed investigations
of the lattice dynamics.

The electrostatic energy per formula unit can be generally

expressed as

$$\phi^C = - \frac{e^2 M}{a} \qquad\qquad 6.1$$

where, a, is the lattice constant, M the Madelung constant and e, the electronic charge. M can be evaluated from the series

$$M_{cell} = \frac{1}{2} \sum_{k} \sideset{}{'}\sum_{\ell'k'} \frac{a\, Z_k\, Z_{k'}}{|r(\ell'k')-r(\ell k)|} \qquad\qquad 6.2$$

where the prime on the summation indicates that the terms $\ell'k' = \ell k$ are excluded, the rest of the symbols having their usual meaning. The expression 6.2 gives the Madelung constant per conventional unit cell and as this contains eight molecules, the Madelung constant per formula unit is a half of M_{cell}. The series 6.2 is transformed by Ewald's method to improve its convergence (see Appendix II of Born and Huang), and in the present case is then divided according to the possible combinations of the products of the ionic charges in the same manner as for the elastic constants of the previous chapter. The final result is obtained in the form,

$$M = 1.091\, Z_t^2 - 0.079 Z_o^2 - 3.076 Z_o Z_t + k_1 Z_{ox}^2 +$$
$$+ k_2 Z_t Z_{ox} + k_3 Z_o Z_{ox} \qquad\qquad 6.3$$

where eZ_o, eZ_t and eZ_{ox} are the octahedral cation, tetrahedral cation, and anion charges respectively. The coefficients k_1, k_2 and k_3 then depend on the anion positions and are tabulated as a function of $\delta = u - {}^3/_8$ in table 6.1 which covers a wide range of observed u-parameters for the spinel compounds. The variation of the coefficients k_1, k_2 and k_3 is also shown graphically in figures 6.1, 6.2 and 6.3 respectively.

In table 6.2 the results of the present calculations are compared with those of Verwey, and as can be seen they agree well at $\delta = 0$ but are slightly lower for $\delta > 0$. In each case the anion

Table 6.1: Coefficients for partial sums contributing
to the Madelung constant

Delta	k_1	k_2	k_3
- .010	-7.528	-12.664	-19.841
- .008	-7.448	-12.353	-20.122
- .004	-7.342	-11.766	-20.695
0	-7.306	-11.221	-21.284
.004	-7.341	-10.716	-21.885
.008	-7.446	-10.246	-22.497
.012	-7.624	- 9.809	-23.118
.016	-7.875	- 9.403	-28.744
.020	-8.204	- 9.024	-24.373

Table 6.2: __Madelung constants in spinels.__

δ	2 - 3	Ref	3 - 2½	Ref	4 - 2	Ref
-.010	124.71		131.33		143.10	
-.008	125.55		131.19		142.05	
-.004	127.06		130.96		140.07	
0	128.56	128.6	130.78	130.8	138.21	138.2
.004	130.01	130.8	130.61	130.9	136.44	136.3
.008	131.38	132.9	130.43	131.1	134.70	134.5
.012	132.65	135.0	130.20	131.3	132.98	132.7
.016	133.77		129.89		131.23	
.020	134.72		129.45		129.40	

Ref = Verwey, de Boer and van Santen (1948).
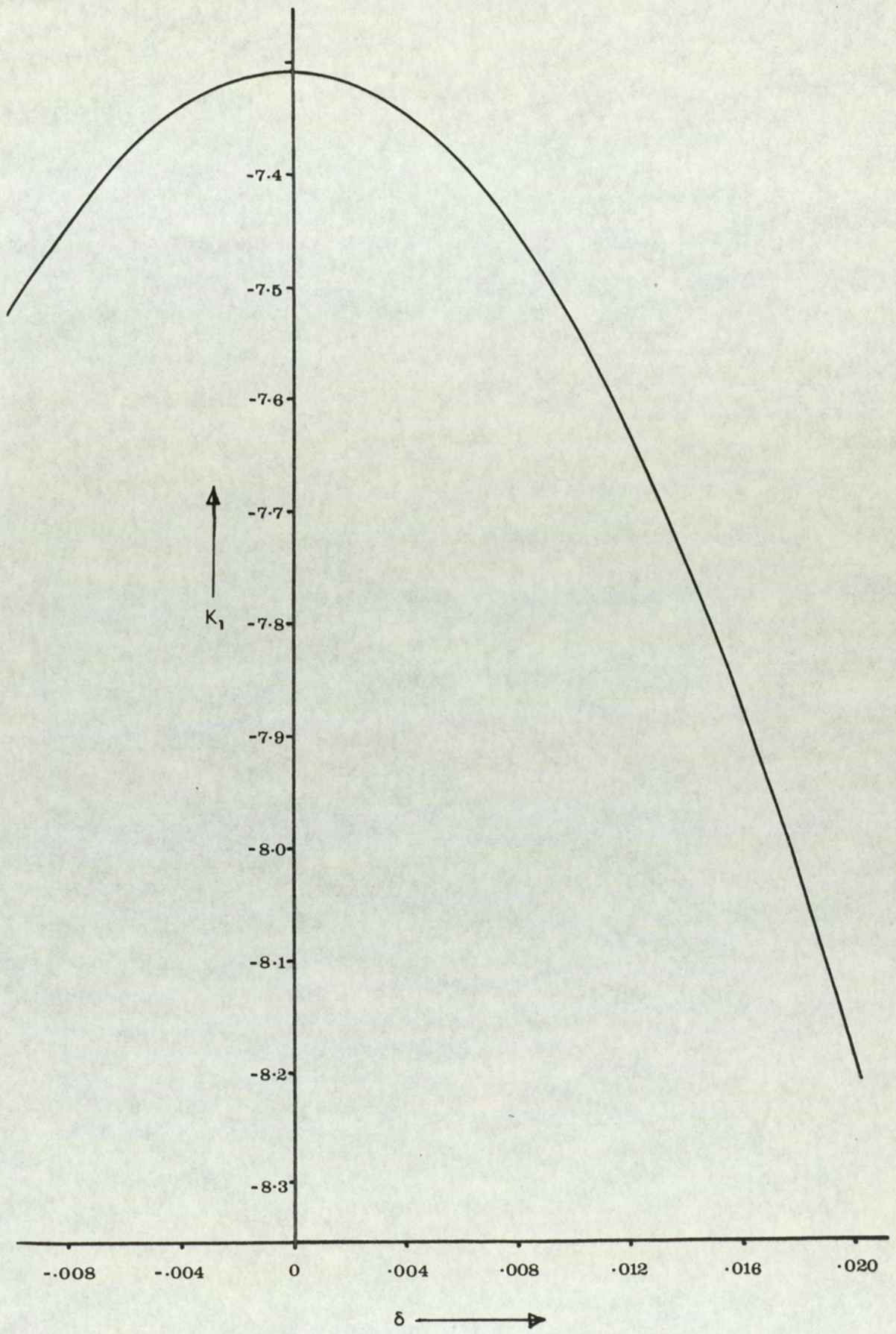
FIGURE 6.1 Contribution to Madelung constant from Z_{ox}^2
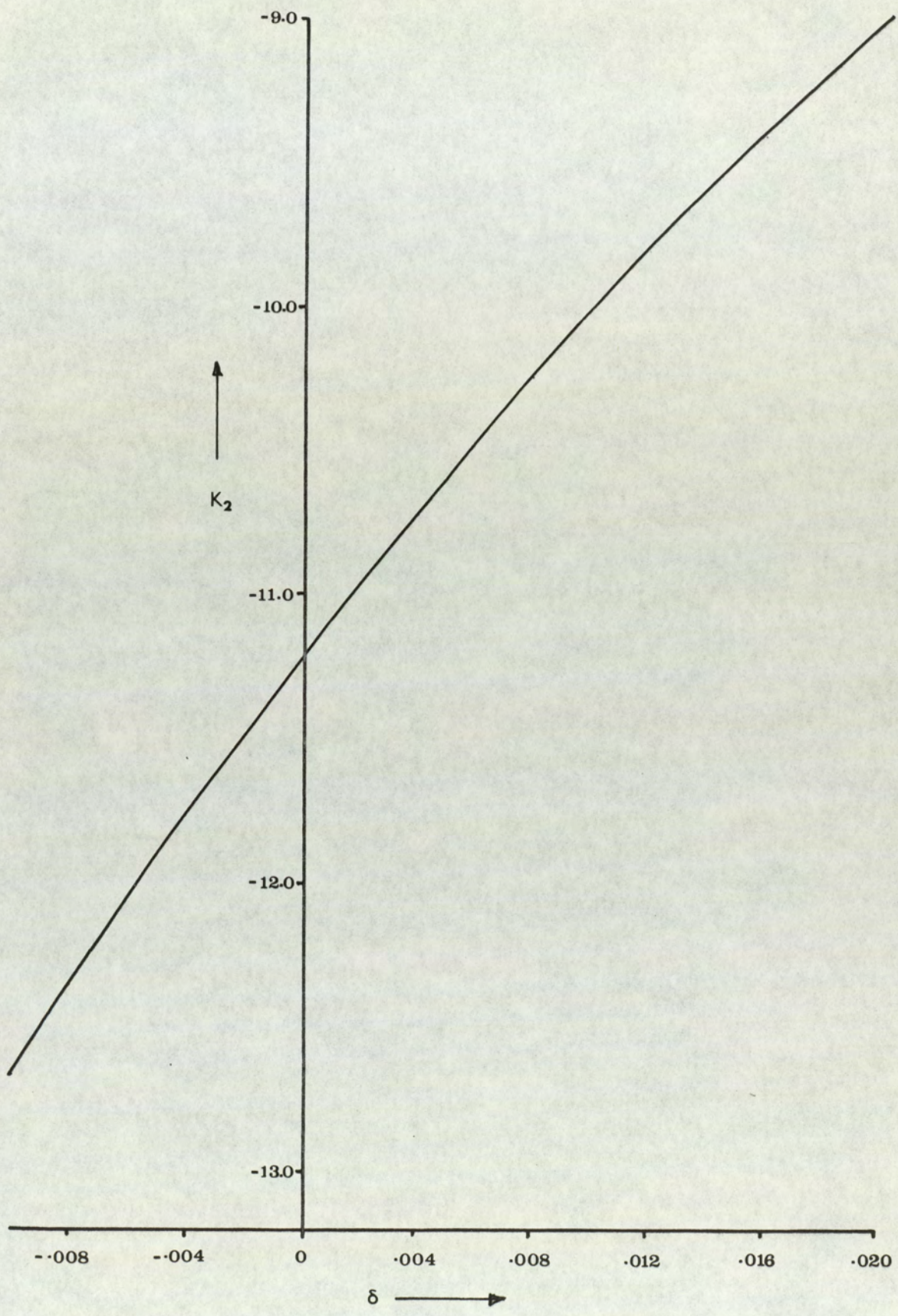
FIGURE 6.2   Contribution to Madelung constant from $Z_t Z_{ox}$
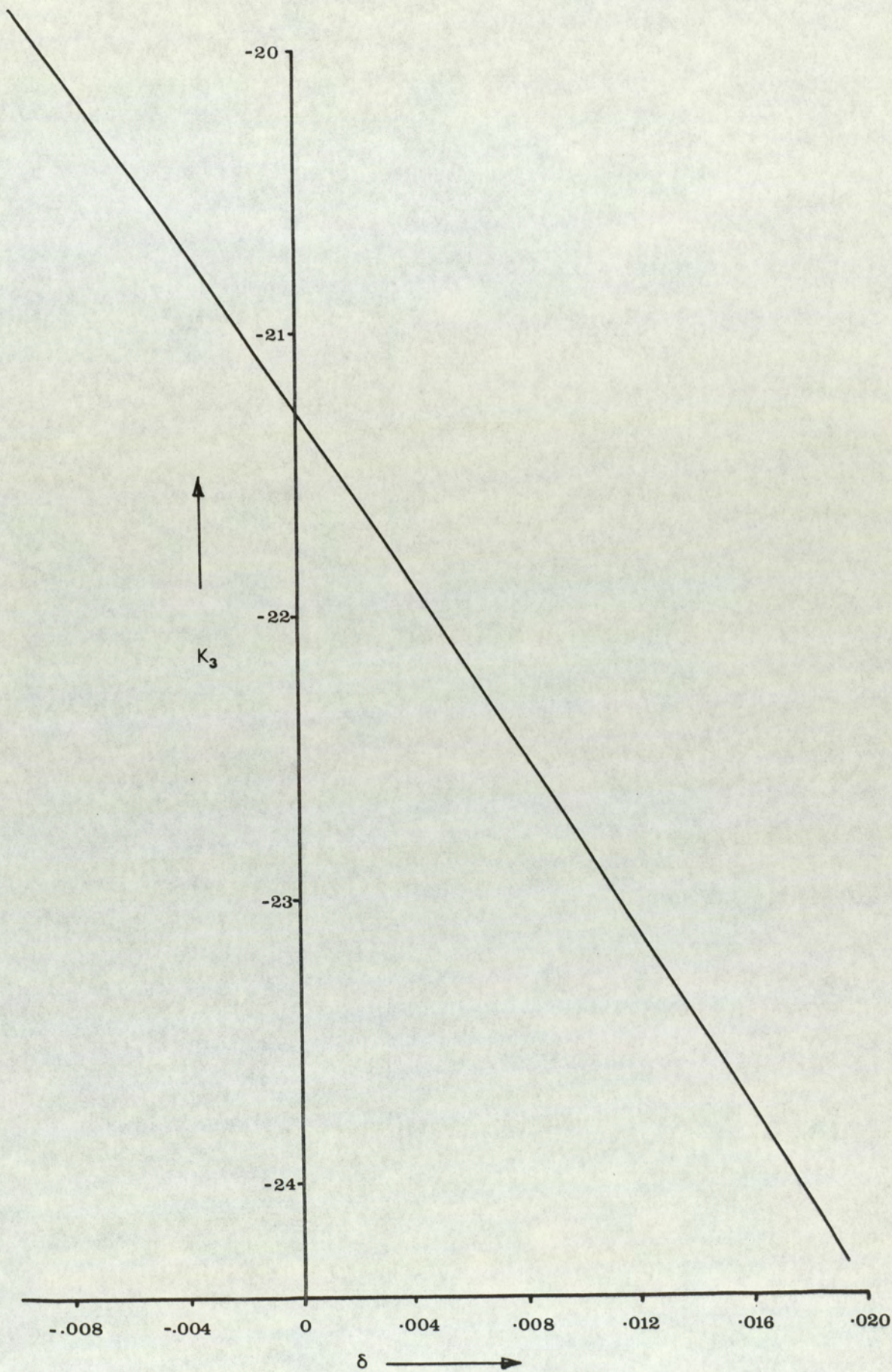
FIGURE 6.3 Contribution to Madelung constant from $Z_O Z_{OX}$

charge is assumed to be -2, and the tetrahedral and octahedral cation charges are as given at the column heading, e.g. 2-3 indicates $Z_t = 2$, $Z_o = 3$. The calculations agree well with the results of Streifler and Barsh who found M to be 132.65 with the normal arrangement of cation in Spinel with δ = .012.

Finally, it should be emphasized that the form of the results for M given here, i.e. equation 6.3, is valid for any arrangement of the cations within the space group Fd3m. Thus the Madelung constant may be evaluated to two decimal places immediately for any spinel for which the cation distribution, and therefore the effective tetrahedral and octahedral charge, is known.

6.3) Equilibrium conditions in Spinel.

Clearly, since crystals with spinel structure exist, the attractive Coulomb forces must balance the repulsive forces to produce positions of stable equilibrium for the ions. In the spinel structure, referred to the space group Fd3m, the total potential energy per molecule ϕ, is described by the two parameters a and δ. The equilibrium conditions then lead to two conditions which must be satisfied given by,

$$\frac{\partial \phi}{\partial a}\bigg|_o = 0 \quad ; \quad \frac{\partial \phi}{\partial \delta}\bigg|_{\delta_o} = 0 \quad ; \quad \quad 6.4$$

In these expressions the Coulomb component of the potential ϕ, can be found from the Madelung constant, i.e. from the previous section, as

$$\phi^C = -\frac{e^2}{a} M \quad \quad 6.5$$

The overlap contribution to the total potential per molecule was first given by Striefler and Barsh (1972) as,

$$\phi^R = 4\phi_t(r) + 12\phi_0(r) + 6\phi_1(r) + 12\phi_2(r) + 6\phi_3(r) \qquad 6.6$$

where ϕ_t represents the tetrahedral-oxygen interation, ϕ_0 the octahedral-oxygen interaction, and ϕ_1, ϕ_2 and ϕ_3 represent the three different oxygen-oxygen interactions. Thus the two conditions 6.4 lead to the equations

$$\frac{e^2}{a^2} M + 4 \left.\frac{\partial\phi_t(r)}{\partial r}\right|_{r=r_t} + 12\left.\frac{\partial\phi_0(r)}{\partial r}\right|_{r=r_0} + 6\left.\frac{\partial\phi_1(r)}{\partial r}\right|_{r=r_1} +$$

$$+ 12\left.\frac{\partial\phi_2(r)}{\partial r}\right|_{r=r_2} + 6\left.\frac{\partial\phi_3(r)}{\partial r}\right|_{r=r_3} = 0 \qquad 6.7$$

and

$$-\frac{e^2}{a^2}\left.\frac{\partial M}{\partial \delta}\right|_{\delta_0} + 4\left.\frac{\partial\phi_t(r)}{\partial \delta}\right|_{\delta_0} + 12\left.\frac{\partial\phi_0(r)}{\partial \delta}\right|_{\delta_0} + 6\left.\frac{\partial\phi_1(r)}{\partial \delta}\right|_{\delta_0}$$

$$+ 12\left.\frac{\partial\phi_2(r)}{\partial \delta}\right|_{\delta_0} + 6\left.\frac{\partial\phi_3(r)}{\partial \delta}\right|_{\delta_0} = 0 \qquad 6.8$$

In this form, the equilibrium conditions are not particularly useful, however, for in the formulation of the general theory of lattice dynamics due to Born and von Kármán, the vibrations of the atoms are controlled solely through the second and higher order differentials of the potential, and the first differential is completely eliminated. This difficulty was resolved by Born by introducing the boundary condition that in the long wavelength limit $q \to 0$ the acoustic modes must correspond to elastic waves in the crystal, and this condition leads to the translational invariance terms in the expression for the Dynamical matrix.

Thus the equilibrium conditions 6.7 and 6.8 cannot be easily built into the equations of motion unless it is assumed that the repulsive interactions can be described by central

forces (not necessarily valid in the spinel compounds), for then the B parameters of equation 3.26 can be written as,

$$B = \frac{2V_a}{e^2} \cdot \frac{1}{r} \left. \frac{\partial \phi(r)}{\partial r} \right|_0 \qquad 6.9$$

In this form, the B-parameters can be substituted into equations 6.7 and 6.8 and the expressions first derived by Striefler and Barsh obtained,

$$M + 8f_t^2 B_t + 24f_o^2 B_o + 12f_1^2 B_1 + 24f_2^2 B_2 + 12f_3^2 B_3 = 0 \qquad 6.10$$

and

$$\left. \frac{\partial M}{\partial \delta} \right|_{\delta_o} - \frac{24}{\sqrt{3}} f_t B_t + 24W\left(1 - \frac{2\delta}{W}\right) B_o + 24\sqrt{2} f_1 B_1 -$$

$$- 96\delta B_2 - 24\sqrt{2} f_3 B_3 = 0 \qquad 6.11$$

where the little f's represent r/a for each interaction (i.e. $f_t = r_t/a$, $f_o = r_o/a$ etc, and $W = \frac{1}{4} - \delta$).

For these expressions the Madelung constant M can be calculated from equation 6.3 and $\partial M/\partial \delta$ evaluated from the variation of M in the neighbourhood of δ for the spinel concerned. A good approximation to the latter quantity can also be obtained by taking the gradient graphically from figures 6.1, 6.2 and 6.3, in which case the major source of error arises from $\partial k_1/\partial \delta$ as k_2 and k_3 are nearly linear functions of δ. However, the error in $\partial k_1/\partial \delta$ can be minimised by noting that k_1 is very closely described by a parabolic function of δ and can be approximated by the equation,

$$-k_1 \approx 2210\delta^2 + 7.306 \qquad 6.12$$

and hence $\partial k_1/\partial \delta \approx -4420\delta$. With this procedure,

$$\left. \frac{\partial M}{\partial \delta} \right|_{\delta = .012} \approx .53.04\, z_{ox}^2 + 105.38 z_t z_{ox} - 155.88 z_o z_{ox} \qquad 6.13$$

which yields a value of 301.6 as compared with 300.16 according

to the calculation described by Striefler and Barsh for
$MgA\ell_2O_4$.

From a substitution of M and $\partial M/\partial \delta$ into 6.10 and 6.11
corresponding equilibrium conditions can be found for both Spinel
and Magnetite. It is found, however, that in neither case can
these conditions be satisfied by the B-parameters which have
been derived from fitting the experimental dispersion curves.
They are satisfied more closely when M and $\partial M/\partial \delta$ are calculated
with the effective ionic charges but there is a substantial
discrepancy even then which lies significantly outside experi-
mental uncertainty. This should not be viewed as a contradiction
of the theory for the equilibrium conditions 6.10 and 6.11 are
founded on a central force approximation to the overlap component
of the interaction between the ions. The present result may be
indicative, however, that within the context of the rigid ion model
the repulsive forces are indeed more correctly described by non-
central interactions between the ion cores.

It should be emphasized here that severe limitations
are inevitably imposed on any interpretation based on comparisons
with the physically unrealistic rigid ion model, for it is well
known that the electronic polarization of the ions plays an important
role in determining the shape and features of phonon dispersion
curves. To illustrate this one need only examine an analysis of
the dispersion curves for the alkali halides, a typical example of
which is given in the work of Woods, Cochran and Brockhouse (1960)
on NaI. In this case, a simple shell model was employed to take
account of the polarizability of the iodine ion only, and their
results show that this simple shell model produces a much improved
fit to the dispersion curves compared with the corresponding rigid
ion model. It is interesting to note, however, that in simple
compounds of this type, where every atom is at a centre of symmetry

that the expressions for the elastic constants are unaffected by the polarizabilities of the ions (Woods, Cochran and Brockhouse, 1960; Szigeti, 1950). This, of course, may not be true for the spinels as only the B-site ion is   at a centre of symmetry (within the space group Fd3m) and significantly the Cauchy condition is violated by many spinel compounds, including Fe_3O_4 (see Grimes 1973b for a useful collection of elastic constant data for the spinel compounds).

6.4) Discussion of the model parameters.

6.4.1) Repulsive parameters.

As shown in table 5.6 the repulsive parameters which describe the overlap forces between the ions are found to be very similar in Magnetite and Spinel. In both of these compounds the octahedral A_0 parameter has the highest value, the next highest being the tetrahedral parameter A_t, and so on. The oxygen-oxygen overlap parameters are particularly interesting. Intuitively one might have expected the oxygen-oxygen iteraction to fall off rapidly with the separation between these ions so that, for example, $A_1 > A_2 > A_3$ corresponding to the sequence $d_1 < d_2 < d_3$. This is not the case, however, for instead, both $MgA\ell_2O_4$, and Fe_3O_4 have $A_1 > A_3 > A_2$, this pattern being more prominent in the former compound where the range of d-values is wider (see table below).

	Bond distance $\overset{o}{A}$	
	$MgA\ell_2O_4$	Fe_3O_4
O1 - O1 (d_1)	2.583	2.873
O2 - O2 (d_2)	2.864	2.968
O3 - O3 (d_3)	3.132	3.063

Note: O-O contact distance = 2.76 $\overset{o}{A}$

Now, as the largest ion in the spinel structure, O^{2-}
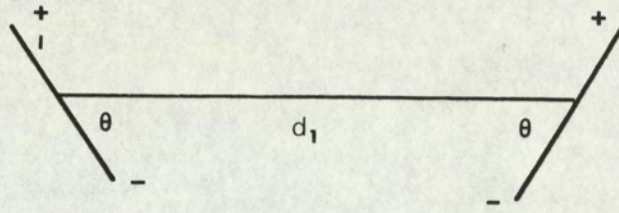
(a) Dipole – Dipole O1 - O1 Interaction
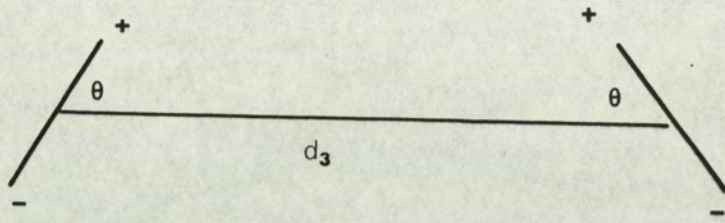
(b) Dipole – Dipole O3 - O3 Interaction
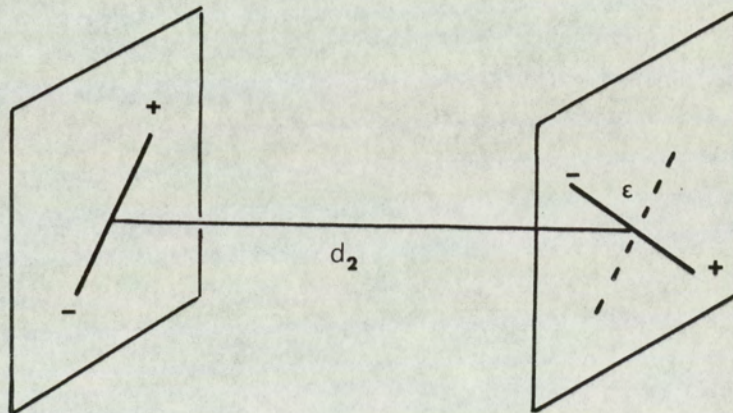
(c) . Dipole – Dipole O2 - O2 Interaction

FIGURE 6.4   Dipole – Dipole Interactions

between the O^{2-} Ions

is also the most polarizable and it is generally supposed (see
for example Hudson and Whitfield, 1967) that for symmetry
reasons the dipole moment is orientated with the axis along the
[111] direction joining each oxygen to its nearest neighbour
tetrahedral cation and directed in the same sense. Thus, the
dipole arrangement is similar for O1-O1 and O3-O3 interactions
where each pair of dipoles lie in one plane and tilted towards
one another (see figures 6.4a and b) but totally different for
the O2-O2 interaction (figure 6.4c). In the latter case the two
dipoles lie in parallel planes but rotate relative to each other
through an angle ϵ and this difference, presumably, is the
qualitative explanation for the anomalous value of the A_2
parameters in $MgA\ell_2O_4$ and Fe_3O_4.

6.4.2) The ionic charges.

It is often the case, when refining parameters describing
the inter-atomic forces within the context of the rigid ion model,
to allow the charge on the ions to take values different from their
nominal values, and normally this improves the agreement between
theoretical and experimental dispersion curves. A procedure such
as this is justified on the grounds that the electrons surrounding
the nuclei of the ions extend over a finite region of space, and that
local distortions of the ionic cores occur in the regions of overlap
between neighbouring ions, giving rise to dipole moments. So in
general ions must be treated as polarizable, but this is not possible
within the rigid ion model and the introduction of an adjustment
to the ionic charges effectively provides some compensation for this
theoretical imperfection.   The rigid ion model is still, however,
inadequate for a satisfactory description of the high q and optical
parts of the phonon dispersion system and in particular is totally
inadequate with regard to the dielectric properties of ionic crystals.

This is inevitable for assuming the ions to be unpolarizable
automatically fixed the high frequency dielectric constant as
unity (see section 3.3). In practice the high frequency dielectric
constant for $MgAl_2O_4$ is 2.92 (Wang and Zanzucchi, 1971) and this
can be theoretically accounted for almost entirely by the polarizability
of the oxygen, through the Clausius-Mossotti relation. At low fre-
quencies, however, the rigid ion model should be more reliable and
in fact a static dielectric constant of 4.71 was found which
compares quite favourably with the lowest frequency measurement to
date of 8.42 at 100 H_z, (Wang and Zanzucchi, 1971).

Usually, the refined charges give values lower than the
nominal charges on the ions, and the present calculations on
Spinel and Magnetite are consistent with this. In the case of
Spinel, for example, the effective charges turning out to be
$z_t = 1.14$, $z_0 = 2.95$ and $z_{ox} = -1.76$ as compared with the nomial
values of $z_t = 2$, $z_0 = 3$ and $z_{ox} = -2$. Thus, the octahedral charge
within the errors of the refinement (see table 5.6), is virtually
maintained at its nominal value, and this is, of course, consistent
with Al^{3+} being the smallest ion in this particular compound, and
therefore least polarizable.

On the other hand, the oxygen ion is 12% below the
nominal value, a reduction similar to that observed with O^{2-} in
$SrTiO_3$, by Stirling (1972). This ion is the most polarizable in
Spinel as it is the largest, and the outermost electrons are
expected to be more loosely bound than those in the metal ions.
One might therefore have expected this charged to be modified.
Not much significance should be attached to the value of the
tetrahedral charge z_t, for this is linked to the charge on the
oxygen through the requirement of charge neutrality.

The effective charges found for Magnetite are rather
interesting, as these values viz. $z_t = 1.30$, $z_0 = 1.15$ and

$z_{ox} = -0.9$ are very low compared with their nominal values of $z_t = 3$, $z_o = 2.5$ and $z_{ox} = -2$. As the overlap parameters A and B for the different repulsive interactions are so similar to those of $MgAl_2O_4$, it seems most likely that these unusual charge discrepancies arise from treating Magnetite as a purely ionic compound. It may be significant, for example, that the reduction in the tetrahedral charge as a fraction of the nominal charge at this site is almost the same in $MgAl_2O_4$ and Fe_3O_4, i.e. the additional reduction in z_{ox} is primarily associated with the change in the octahedral cation charge z_o. If this interpretation is correct, then it would appear that the presence of electron hopping conductivity is equivalent to giving an enhanced polarizability to the octahedral metal ions.

6.5) The infra-red spectrum.

Normally, the treatment of the absorption of infra-red radiation in crystals is considered in terms of the generation of single phonons. In a "one-phonon process", like this the conservation laws require that the energy of the photon is the same as the energy of the phonon, so that $\nu_{photon} = \nu_{phonon}$. In addition, the conservation of momentum requires that $\underline{q}_{photon} = \underline{q}_{phonon}$. However, the wavelength of the infra-red photon is very long compared with the dimensions of the unit cell and thus its wavevector may be effectively set to zero. Therefore, "one-phonon processes" can only occur at the centre of the Brillouin zone, that is, at the critical point Γ. Furthermore, a change of dipole moment must be produced, so that for example, in an optic vibration one type of sublattice must effectively move as a rigid body relative to the other ions, in order to satisfy this condition, and thus be infra-red active.

To establish the optical vibrations which can be infra-red active, from the dynamical theory for Spinel, we require the phonon

frequencies at zero wavevector, and also the pattern of the ionic displacements, so that we can identify from the 39 possible optical modes of vibration those which can produce a change of dipole moment. The phonon frequencies at the critical point Γ are obtained from the diagonalisation of $\bar{D}_{\alpha\beta}^{*}(kk',0)$ and these are shown in table 6.3 for Magnetite and Spinel. For comparison, the eigenvalues at the critical points X and L, evaluated from diagonalisation of $D_{\alpha\beta}(kk',\underline{q})$ with the appropriate q, are also listed in tables 6.4 and 6.5 and could be used to predict the frequencies of the two phonon absorption bands when the selection rules are known.

Examination of the eigenvectors at q = 0 shows that only two patterns of displacement, corresponding to two 3-fold, degenerate modes can produce a change of dipole moment. This pattern is similar in Spinel and Magnetite and is shown in table 6.6 which gives details for one of each degeneracy. The details of the other two related modes may be derived from a cyclical permutation of the X,Y and Z coordinates. The frequencies to which these modes of vibration correspond are marked with an asterisk in table 6.3.

It should be emphasized here, that in calculating the elements of $D_{\alpha\beta}^{C}(kk',0)$ from equation 5.1 the term associated with the macroscopic electric field is excluded since this term does not possess a unique limit as q → 0. However, the macroscopic electric field has important consequences when considering vibrations in which the rative motion of the ions creates a dipole moment, for then the ions experience a force exerted by the macroscopic electric field when they are vibrating longitudinally (i.e. parallel to $\underline{q}$) and thus the longitudinal modes have a higher frequency than the corresponding transverse modes (see Born and Huang). As a result the

*The elements of $\bar{D}_{\alpha\beta}(kk,0)$ are the modified coefficients of Born and Huang which exclude terms associated with the macroscopic electric field.

degeneracy of the two 3-fold modes, marked with the asterisk in table 6.3 is in part removed and the frequency of the longitudinal mode has been obtained by interpolation back to zero q from $q = \frac{2\pi}{a} (0,0,\cdot 1)$ and is therefore shown in brackets.

The dynamical model for Magnetite thus predicts two infra-red active modes of vibration, one predominantly involving the motion of the tetrahedral cation sublattice relative to the rest of the structure, which is vibrating to a lesser extent in antiphase (type I), and one where the octahedral cation and oxygen sublattices vibration in antiphase with the tetrahedral ion sublattice stationary (type II).

It is interesting to note the observations of Preudhomme and Tarte (1971) who investigated the effects of isotopic substitution on the infra-red spectrum for a range of normal 2-3 spinels. Their observations show that when the tetrahedral cation is substituted by a heavier isotope only the two lowest frequency modes shift, whereas when the octahedral cation is substituted for a heavier isotope the frequency of all four infra-red bands decreases slightly. This is inconsistent with the one-phonon absorption spectra of type I and type II vibrations predicted from the dynamical theory, for the latter corresponds to the two high frequency bands.

When the calculated values are compared with the experimental values for the observed infra-red absorption frequencies (tabe 6.7) for both Magnetite (Grimes and Collett, 1971b) and $MgA\ell_2O_4$ (O'Horo, Frisillo and White, 1973) the agreement is found to be poor. We can probably attribute the discrepancies to two reasons. Firstly, the optical vibrations are very sensitive to changes in the parameters of the model, and it may be possible by further adjustments of these parameters to improve the fit with the experimental infra-red frequencies without deteriorating the

fit to the other modes. Secondly, the rigid ion model is well known to produce errors of as much as 30-40% for some optic vibtations in relatively simple structures, such as the alkali halides, see for example, Woods, Cochran and Brockhouse (1960).

Finally, the model predicts only two modes of vibration which are infra-red active, whereas four absorption peaks are normally observed the two higher frequencies being the stronger. Therefore, the model provides additional support for a change of space group and/or indicates that the interpretation of the infra-red spectra in terms of one-phonon processes is incorrect.

Table 6.3: <u>Phonon frequencies at the critical point Γ</u>

	<u>MgAl_2O$_4$</u>		<u>Fe$_3$O$_4$</u>	
<u>Frequency</u> ν TH$_z$	<u>Degeneracy</u>		<u>Frequency</u> ν TH$_z$	<u>Degeneracy</u>
L 0	3		L 0	3
5.84	3		L 4.42	3
L 8.68	3		L 4.51* (5.97)	3
9.77	3		5.16	3
L 10.62* (11.04)	3		6.62	3
12.09	3		8.88	2
13.56	2		10.79	1
14.09	3		14.07	3
16.30	2		16.08	3
L 17.26* (36.04)	3		16.23	2
20.66	3		L 17.76* (21.76)	3
23.45	3		19.68	3
25.44	2		19.71	3
27.38	1		22.24	1
28.41	3		22.37	1
34.93	1		22.52	3
34.99	1		22.78	2

L = Lattice mode

Table 6.4: <u>Phonon frequencies at the critical point X.</u>

MgAℓ$_2$O$_4$		Fe$_3$O$_4$	
<u>Frequency</u>	<u>Degeneracy</u>	<u>Frequency</u>	<u>Degeneracy</u>
ν TH$_z$		ν TH$_z$	
5.93	2	3.01	2
6.70	2	3.70	2
8.87	2	4.01	2
9.75	2	4.69	2
10.95	2	5.58	2
11.27	2	6.72	2
11.47	2	7.03	2
11.74	2	7.34	2
12.83	2	8.85	2
13.28	2	14.52	2
14.55	2	16.16	2
17.26	2	17.24	2
18.29	2	18.55	2
19.34	2	19.11	2
21.33	2	19.61	2
21.84	2	19.96	2
22.90	2	20.12	2
25.92	2	20.73	2
26.83	2	20.76	2
30.87	2	21.18	2
34.40	2	21.30	2

Table 6.5: <u>Phonon frequencies at critical point L.</u>

$MgA\ell_2O_4$		Fe_3O_4	
<u>Frequency</u>	<u>Degeneracy</u>	<u>Frequency</u>	<u>Degeneracy</u>
ν TH$_z$		ν TH$_z$	
3.90	2	3.25	2
5.31	1	3.34	2
6.75	2	3.76	1
9.36	2	3.97	2
9.56	1	4.59	1
10.03	1	5.32	1
10.16	1	5.50	2
10.84	1	6.34	1
11.35	2	6.67	2
11.96	1	8.32	1
12.22	2	8.50	2
12.77	2	9.06	1
13.50	2	15.90	2
15.59	1	15.97	2
16.05	2	16.42	1
16.10	2	16.51	2
18.92	2	16.71	1
19.67	2	18.88	2
20.75	2	19.28	2
21.36	1	19.28	1
23.02	1	19.51	1
25.04	1	19.62	2
25.91	2	20.66	1
26.36	2	21.00	1
29.56	1	22.40	2
		21.16	2
33.84	1	22.44	1
34.42	1	22.67	1
35.68	1		

<u>Type I - lowest mode frequency</u>

Atom type (K)	X	Y	Z
1	-.031	-.015	-.613
2	-.031	-.015	-.613
3	.040	.035	.196
4	-.020	.032	.193
5	.038	-.026	.195
6	-.019	-.023	.192
7	.005	.003	.105
8	.005	.003	.105
9	.005	.003	.105
10	.005	.003	.105
11	.005	.003	.105
12	.005	.003	.105
13	.005	.003	.105
14	.005	.003	.105

<u>Type II - higher I-R band</u>

Atom type (K)	X	Y	Z
1	0	0	-.010
2	0	0	-.010
3	-.053	-.069	.296
4	.055	-.068	.297
5	-.058	.044	.292
6	.060	.044	.292
7	-.050	-.040	-.268
8	.048	-.040	-.268
9	-.054	.063	-.273
10	.053	.062	-.273
11	-.050	-.040	-.268
12	.048	-.040	-.268
13	-.054	.063	-.273
14	.053	.062	-.273

Table 6.7: Comparison of experimental and theoretical
infra-red frequencies

$MgA\ell_2O_4$
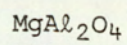
Infra-Red absorption peaks in cm^{-1}

Experiment[1]	Theory (type of vibration)
305	
428	
485	354 (I) T
670	575 (II) T

Fe_3O_4

Infra-Red absorption peaks in cm^{-1}

Experiment[2]	Theory (type of vibration)
178	
268	
390	150 (I) T
570	592 (II) T

T = Transverse,

[1] O'Horo Frisillo and White (1975)

[2] Grimes and Collett (1971b)

CHAPTER 7

SUMMARY OF CONCLUSIONS AND SUGGESTIONS FOR
FURTHER WORK.

7.1) <u>Summary of conclusions</u>.

It has been shown for both Spinel and Magnetite that the simple rigid ion model can account quite well for the acoustic modes of vibration at small and intermediate values of the phonon wavevectors, and thus provides a fair correlation with the observed elastic constants. In order to obtain this fit it was necessary to allow the dynamical model its complete freedom, which corresponds to describing the ion core interactions by non-central, axially symmetry, forces. The interaction between the oxygen ions separated by the intermediate distance appears to be quite different in character from the other two types of oxygen-oxygen interaction, and this is apparently connected with the orientation of the dipole moments which would be created when the electron clouds surrounding the oxygen nuclei are deformed. Compensation for the polarisation of the constituent ions is also accomplished by a reduction in the ionic charges, where the effective charges are lower than their nominal values.

In many respects, the theoretical model for Magnetite provides a better description of the dynamical behaviour of this compound than the corresponding model for Spinel, which is surprising when one considers the added complications in the former. Firstly, the electronic configurations of the ferrous and ferric are not closed shell configurations and therefore would be expected to deviate more from a point charge approximation than the Mg^{2+} and $A\ell^{3+}$ ions. Secondly, there is the added complexity of the electrical conductivity of Fe_3O_4. Nevertheless, the results are encouraging for they seem to indicate that the crystal cohesion in Magnetite is predominantly ionic in character, and similar to Spinel itself. It appears that the electrical conductivity is accommodated in the rigid ion model through a drastic reduction in the effective ionic charge of the ion occupying the octahedral site. It is, however, difficult to separate this effect

from the reduction in the effective charge due to the compensation for the polarizability of the anions. It seems likely that electron hopping creates a localized charge in the neighbourhood of the octahedral site which is loosely bound to the nuclei and thus very polarizable. Models where the polarizability of the ions can be directly taken into account may provide a more complete under-standing of this point, but because of the additional parameters which would be introduced in this type of model more experimental data than that presented here is necessary.

It has also been shown that the rigid ion model, for the two spinel compounds investigated, provides an interpretation of the infra-red spectrum in terms of one-phonon processes. Two infra-red active modes are predicted for Magnetite and Spinel, but the actual derived frequencies do not agree with those observed. Also, the ion movements are inconsistent with the frequency shifts of the various modes observed through isotopic substitution.

Finally, the detailed analysis of the X-ray and neutron diffraction patterns from Magnesium Aluminate has revealed that there is a significant gain in the overall fit when the data is refined under $F\bar{4}3m$ symmetry. In view of this it is difficult to escape the conclusion that the symmetry of Spinel is more correctly described by the space group $F\bar{4}3m$. If this is the case, then the change of symmetry must influence the lattice dynamics of this compound as the overlap forces depend sensitively on the separation distances of the ions.

7.2) Suggestions for further work.

The eigenvectors giving the sense of the ion displace-ments for the infra-red active modes can be used to locate which Brillouin zone offers a high intensity from the neutron-phonon

interaction for the observation of these modes using neutron
inelastic scattering. One might thus be able to correlate the
neutron measurements with infra-red measurements to establish more
precisely whether the infra-red spectrum could be described$\underset{\wedge}{}$ at least in part by one-
phonon processes.

An obvious extension of the dynamical model in Spinel
would be to include the polarizability of the oxygen ion through
a rigid shell approximation. This should provide the possibility
of a better physical description of the phonon dispersion curves.
However, a model of this type would involve many more parameters
and there seems little point in extending the description in this
way until more experimental information on the dispersion system
is available. Introduction of the polarizability of the oxygen
ion through the rigid shell approximation in Magnetite could
provide a more precise explanation of how the electrical con-
ductivity is accommodated within the dynamical representation,
since at least part of the reduction in the ionic charges associated
with the polarization effects is then removed.

Because the cubic spinel compounds are all related by a
common structure, in the long term they offer a unique opportunity
for studying the repulsive forces acting between metal ions and
oxygen ions. For example, one could investigate an aluminate
series such as $MeA\ell_2O_4$ or the octahedral cation could be
substitute creating compounds like say $MgMe_2O_4$. It would therefore
be possible to investigate ineractions between different cations
and the anions under very similar circumstances. A remarkable
feature of the spinel compounds from a dynamical viewpoint is the
presence of three oxygen-oxygen interactions in the same relatively
simple material and this gives the possibility of investigating the
O-O interaction in the same conditions over a fairly wide range of
interatomic distances (i.e. between about $2.5\overset{o}{A}$ and $3.5\overset{o}{A}$).

Finally, in view of the very precise diffraction evidence for $MgAl_2O_4$ which shows that the structure of Spinel is more correctly described by $F\bar{4}3m$ symmetry, it seems likely that most cubic spinels do not accurately conform to $Fd3m$ symmetry. This must clearly have implications concerning the interpretation of the magnetic behaviour of spinel ferrites since the magnetic exchange interactions depend sensitively on the separation between the magnetic ions. This will, of course, also affect the interpretation of the dynamical behaviour of Spinel which has been presented here. Moreover, if the mechanism for creating off-centre ions (i.e. potential maxima at the B-sites) is correct , then the corresponding forces might be expected to have considerable anharmonic components. To be physically realistic one should then consider a dynamical description based on $F\bar{4}3m$ symmetry with anharmonic terms and polarizability of the various constituent ions included. However, this may be impractical at the present time as the experimental and computational labour would be enormous and it is doubtful, indeed, whether very much more would really be learnt from such a monumental effort.

APPENDIX

Indpendent   Coulomb   coefficients $C_{\alpha\beta}(kk'\underline{q})$

for   Spinel

Elements of $C_{xx}(kk',q)$ for Spinel

in the 0.0.1 direction

k	k'	$q/q_{max}=.1$ real	imag	$q/q_{max}=.3$ real	imag	$q/q_{max}=.5$ real	imag	$q/q_{max}=.7$ real	imag	$q/q_{max}=.9$ real	imag
1	1	-4.143	0.000	-3.793	0.000	-3.210	0.000	-2.605	0.000	-2.220	0.000
1	2	-4.136	0.000	-3.723	0.000	-2.944	0.000	-1.884	0.000	-0.648	0.000
1	3	-4.204	-0.575	-4.317	-1.698	-4.482	-2.730	-4.595	-3.594	-4.535	-4.209
1	7	-4.147	0.086	-3.822	0.270	-3.231	0.498	-2.483	0.817	-1.704	1.272
1	11	-4.125	0.581	-4.409	1.711	-4.178	2.737	-4.992	3.575	-5.086	4.143
3	4	4.423	0.000	3.982	0.000	3.147	0.000	2.016	0.000	0.693	0.000
3	5	-8.417	0.000	-7.584	0.000	-6.008	0.000	-3.850	0.000	-1.325	0.000
3	6	-8.510	0.000	-8.413	0.000	-8.257	0.000	-8.046	0.000	-8.009	0.000
3	7	-4.176	-0.040	-3.727	-0.121	-2.954	-0.206	-1.903	-0.296	-0.676	-0.393
3	8	-38.985	-0.276	-38.826	-0.830	-38.564	-1.395	-38.292	-1.975	-38.103	-2.571
3	9	13.212	0.091	13.147	0.275	13.044	0.465	12.940	0.662	12.870	0.866
3	10	13.078	2.723	11.964	7.962	9.832	12.572	6.864	16.105	3.038	18.150
7	8	5.101	-0.411	4.649	1.214	3.793	-1.951	2.615	-2.569	1.221	-3.103
7	9	-8.756	0.217	-7.921	0.646	-6.340	1.067	-4.178	1.484	-1.648	1.900
7	10	-8.849	0.000	-8.746	0.000	-8.581	0.000	-8.416	0.000	-8.314	0.000
7	11	-4.265	-0.182	-4.837	-0.529	-5.778	-0.824	-6.741	-1.038	-7.349	-1.126
7	12	4.203	0.000	3.784	0.000	2.993	0.000	1.915	0.000	0.659	0.000
7	13	-8.307	0.000	-7.485	0.000	-5.939	0.000	-3.8000	0.000	-1.308	0.000
7	14	-8.397	-0.103	-8.292	-0.313	-8.119	-0.532	-7.938	-0.779	-7.807	-1.042

Elements of $C_{zz}(kk',\underline{q})$ for Spinel

in the 0.0.1 direction

k	k'	$q\,q_{max}=.1$ real	imag	$q\,q_{max}=.3$ real	imag	$q\,q_{max}=.5$ real	imag	$q\,q_{max}=.7$ real	imag	$q\,q_{max}=.9$ real	imag
1	1	8.284	0.000	7.858	0.000	6.420	0.000	5.210	0.000	4.439	0.000
1	2	8.272	0.000	7.446	0.000	5.889	0.000	3.768	0.000	1.295	0.000
1	3	8.408	1.150	8.663	3.396	8.964	5.460	9.190	7.187	9.069	8.418
1	7	8.293	-0.172	7.643	-0.539	6.463	-0.996	4.966	-1.634	3.408	-2.545
1	11	8.430	-1.162	8.819	-3.421	9.435	-5.474	9.995	-7.149	10.172	-8.286
3	4	3.994	0.000	3.602	0.000	2.858	0.000	1.835	0.000	0.632	0.000
3	6	17.019	0.000	16.827	0.000	16.516	0.000	16.207	0.000	16.017	0.000
3	7	8.273	0.079	7.452	0.241	5.908	0.411	3.804	0.593	1.352	0.785
3	8	25.774	0.184	25.679	0.555	25.520	0.930	25.352	1.313	25.234	1.705
3	10	-26.157	-5.445	-23.927	-15.924	-19.663	-25.144	-13.278	-32.210	-6.616	-36.30
7	8	3.655	0.195	3.271	0.568	2.547	0.883	1.563	1.084	0.424	1.113
7	10	17.697	0.000	17.492	0.000	17.161	0.000	16.832	0.000	16.628	0.000
7	11	8.531	0.364	9.674	1.058	11.556	1.648	13.482	2.063	14.698	2.252
7	12	4.104	0.000	3.701	0.000	2.936	0.000	1.884	0.000	0.649	0.000
7	14	16.979	0.206	16.858	0.622	16.238	1.073	15.876	1.558	15.615	2.085

Elements of $C_{xy}(kk',\underline{q})$ for Spinel

in the 0.0.1 direction

k	k'	$q/q_{max}=.1$ real	imag	$q/q_{max}=.3$ real	imag	$q/q_{max}=.5$ real	imag	$q/q_{max}=.7$ real	imag	$q/q_{max}=.9$ real	imag
1	1	0.000	0.000	0.000	0.000	0.000	0.000	0.000	0.000	0.000	0.000
1	2	0.000	-1.575	0.000	-4.617	0.000	-7.306	0.000	-9.356	0.00	-10.475
1	3	3.398	0.595	3.583	1.745	3.879	2.771	4.157	3.580	4.267	4.089
1	7	-18.567	1.917	-18.259	5.681	-17.592	9.223	-16.478	12.374	-14.824	14.972
1	11	3.032	-0.463	3.203	-1.357	3.478	-2.156	3.743	-2.786	3.862	-3.188
3	6	-14.561	0.000	-14.976	0.000	-15.792	0.000	-16.504	0.000	-16.993	0.000
3	7	-0.967	-1.569	-0.975	-4.599	-0.979	-7.280	-0.953	-9.325	-0.821	-10.448
3	8	-2.872	-0.025	-2.906	-0.074	-2.962	-0.122	-3.019	-0.168	-3.054	-0.211
3	10	-0.122	-0.025	-0.122	-0.072	-0.092	-0.114	-0.064	-0.145	-0.031	-0.164
7	10	-15.505	0.000	-15.949	0.000	-16.684	0.000	-17.440	0.000	-17.918	0.000
7	11	0.184	0.005	00.196	0.015	0.216	0.024	0.235	0.032	0.248	0.036
7	12	0.000	0.298	0.000	0.872	0.000	1.376	0.000	1.757	0.000	1.963
7	14	14.301	0.299	14.744	0.887	15.474	1.445	16.215	1.945	16.663	2.363

Elements of $C_{xz}(kk', \underline{q})$ for Spinel

in the 0.0.1 direction

k	k'	$q/q_{max}=.1$ real	imag	$q/q_{max}=.3$ real	imag	$q/q_{max}=.5$ real	imag	$q/q_{max}=.7$ real	imag	$q/q_{max}=.9$ real	imag
1	1	0.000	0.000	0.000	0.000	0.000	0.000	0.000	0.000	0.000	0.000
1	2	0.000	0.000	0.000	0.000	0.000	0.000	0.000	0.000	0.000	0.000
1	3	3.325	-0.453	2.945	-1.221	2.216	-1.612	1.221	-1.489	0.120	-0.861
1	7	-18.528	1.330	-17.918	3.995	-16.695	6.666	-14.876	9.318	-12.545	11.869
1	1	2.965	0.442	2.622	1.187	1.965	1.551	1.077	1.400	0.109	0.753
3	4	0.000	0.000	0.000	0.000	0.000	0.000	0.000	0.000	0.000	0.000
3	5	-14.301	0.000	-13.029	0.000	-10.507	0.000	-6.856	0.000	-2.386	0.000
3	7	-0.955	-0.078	-0.876	-0.228	-0.717	-0.358	-0.485	-0.460	-0.196	-0.525
3	8	-2.863	0.519	-2.826	1.364	-2.752	1.688	-2.650	1.331	-2.539	0.395
3	9	-0.124	-0.010	-0.125	-0.025	-0.127	-0.032	-0.129	-0.029	-0.131	-0.017
3	10	-2.837	-0.375	-2.592	-1.091	-2.115	-1.712	-1.441	-2.182	-0.626	-2.463
7	9	-15.285	-0.570	-13.999	1.703	-11.449	2.812	-7.755	3.865	-3.221	4.803
7	10	0.000	-0.058	0.000	-0.154	0.000	-0.195	0.000	-0.161	0.000	-0.062
7	11	0.180	-0.119	0.158	-0.315	0.116	-0.394	0.063	-0.323	0.009	-0.126
7	12	0.000	-0.168	0.000	-0.488	0.000	-0.756	0.000	-0.949	0.000	-1.050
7	13	14.085	0.000	12.832	0.000	10.346	0.000	6.753	0.000	2.351	0.000

Elements of $C_{xx}(kk',\underline{q})$ for Spinel

in the 1.1.0 direction

k	k'	$q/q_{max}=.1$ real	imag	$q/q_{max}=.3$ real	imag	$q/q_{max}=.5$ real	imag	$q/q_{max}=.7$ real	imag	$q/q_{max}=.9$ real	imag
1	1	2.047	0.000	1.630	0.000	0.669	0.000	-0.766	0.000	-1.980	0.000
1	2	2.042	0.000	1.655	0.000	1.035	0.000	0.424	0.000	0.050	0.000
1	3	2.061	0.580	1.813	1.833	1.381	3.306	0.851	4.899	0.286	6.063
1	4	2.159	1.702	2.678	4.501	3.700	5.667	5.033	4.685	6.077	1.816
1	7	2.078	-0.079	1.944	-0.086	1.670	0.300	1.249	1.094	0.664	1.867
1	8	2.026	-0.257	1.485	-0.777	0.443	-1.777	-0.881	-1.140	-1.901	-0.482
1	11	2.077	-0.587	1.948	-1.862	1.746	-3.387	1.516	-5.066	1.210	-6.327
1	12	2.165	-1.720	2.736	-4.544	3.866	-5.715	5.310	-4.720	6.415	-1.829
3	4	10.679	0.000	9.978	0.000	8.406	0.000	5.750	0.000	2.065	0.000
3	5	-2.275	0.000	-2.490	0.000	-2.581	0.000	-2.084	0.000	-0.817	0.000
3	6	-2.037	0.000	-0.484	0.000	2.262	0.000	5.421	0.000	7.671	0.000
3	7	2.050	0.039	1.725	0.103	1.222	0.129	0.754	0.096	0.481	0.000
3	8	-32.376	-5.714	-29.596	16.620	-24.033	-26.103	-15.822	-33.423	-5.543	-37.609
3	9	19.336	2.886	17.946	7.985	14.930	11.364	10.066	12.762	3.578	12.917
3	10	19.481	0.275	19.312	0.826	19.022	1.377	18.693	1.931	18.434	2.498
7	8	11.355	-0.410	10.632	-1.169	9.016	-1.795	6.304	-2.315	2.565	-2.849
7	9	-2.613	0.195	-2.818	0.588	-2.900	1.007	-2.406	1.481	-1.143	1.941
7	10	-2.375	0.412	-0.811	1.222	1.959	1.974	5.164	2.547	7.516	2.672
7	11	2.169	0.184	2.776	0.595	4.009	1.111	5.665	1.703	6.983	2.155
7	12	10.457	0.203	9.762	0.554	8.212	0.738	5.607	0.660	2.008	0.283
7	13	-2.165	-0.102	-2.383	0.275	-2.486	-0.359	-2.016	-0.307	-0.792	-0.121
7	14	-2.219	0.000	-2.945	0.000	-4.364	0.000	-6.206	0.000	-7.647	0.000
8	9	-2.669	-0.023	-3.387	-0.096	-4.798	-0.193	-6.639	-0.220	-8.083	-0.100
8	12	2.175	0.539	2.828	1.422	4.147	1.782	5.908	1.467	7.307	0.567
8	13	-1.931	0.000	-0.419	0.000	2.258	0.000	5.344	0.000	7.595	0.000

Elements of $C_{zz}(kk',g)$ for Spinel

in the 1.1.0 direction

k	k'	$q/q_{max}=.1$ real	imag	$q/q_{max}=.3$ real	imag	$q/q_{max}=.5$ real	imag	$q/q_{max}=.7$ real	imag	$q/q_{max}=.9$ real	imag
1	1	−4.049	0.000	−3.261	0.000	−1.338	0.000	1.531	0.000	3.959	0.000
1	2	−4.084	0.000	−3.309	0.000	−2.070	0.000	−0.848	0.000	−0.100	0.000
1	3	−4.123	−1.160	−3.625	−3.251	−2.761	−6.612	−1.702	−9.799	−0.572	−12.126
1	4	−4.318	0.000	−5.356	0.000	−7.400	0.000	−10.067	0.000	−12.155	0.000
1	7	−4.156	0.158	−3.888	0.173	−3.340	−0.599	−2.497	−2.188	−1.329	−3.734
7	8	−4.053	0.000	−2.970	0.000	−0.887	0.000	1.762	0.000	3.801	0.000
1	11	−4.153	1.173	−3.896	3.724	−3.493	6.774	−3.032	10.132	−2.420	12.655
1	12	−4.331	0.000	−5.472	0.000	−7.712	0.000	−10.620	0.000	−12.890	0.000
3	4	−8.404	0.000	−7.488	0.000	−5.825	0.000	−3.667	0.000	−1.248	0.00
3	6	4.074	0.000	0.968	0.000	−4.525	0.000	−10.841	0.000	−15.341	0.000
3	7	−4.100	−0.078	−3.450	−0.207	−2.444	−0.257	−1.508	−0.191	−0.961	0.000
3	8	13.040	2.829	11.650	8.635	9.103	14.738	5.756	20.661	1.965	24,968
3	10	−38.962	−0.551	−38.624	−1.652	−38.045	−2.754	−37.387	−3.863	−36.868	−4.996
7	8	−8.742	0.214	−7.814	0.581	−6.117	0.788	−3.898	0.833	−1.422	0.908
7	10	4.751	−0.824	1.623	−2.443	−3.917	−3.947	−10.328	−5.094	−15.033	−5.343
7	11	−4.337	−0.369	−5.552	−1.919	−8.018	−2.221	−11.330	−3.503	−13.965	−4.311
7	12	−8.293	−0.102	−7.380	−0.279	−5.727	−0.379	−3.591	−0.353	−1.217	−0.163
7	14	4.438	0.000	5.889	0.000	8.728	0.000	12.412	0.000	15.294	0.000
8	9	5.337	0.000	6.777	0.000	9.597	0.000	13.278	0.000	16.165	0.000
8	12	−4.349	0.000	−5.656	0.000	−8.924	0.000	−11.815	0.000	−14.613	0.000

Elements of $C_{xy}(kk'\underline{q})$ for Spinel

in the 1.1.0 direction

k	k'	$q/q_{max}=.1$ real	imag	$q/q_{max}=.3$ real	imag	$q/q_{max}=.5$ real	imag	$q/q_{max}=.7$ real	imag	$q/q_{max}=.9$ real	imag
1	1	6.225	0.000	5.669	0.000	4.265	0.000	2.100	0.000	0.279	0.000
1	2	6.363	0.000	6.988	0.000	8.148	0.000	9.518	0.000	10.483	0.000
1	3	9.503	-0.917	8.342	-2.704	6.337	-4.288	3.896	-5.406	1.307	-5.911
1	4	2.948	0.000	3.269	0.000	3.973	0.000	4.988	0.000	5.836	0.000
1	7	-12.082	2.662	-10.259	8.206	-7.016	13.344	-2.978	18.013	1.202	20.727
1	8	24.824	0.000	24.322	0.000	23.375	0.000	22.184	0.000	21.268	0.000
1	11	9.125	0.894	7.867	2.614	5.717	4.062	3.160	4.948	0.536	5.128
1	12	3.281	0.000	3.366	0.000	3.695	0.000	4.335	0.000	4.953	0.000
3	4	6.198	0.000	5,538	0.000	4.328	0.000	2.736	0.000	0.934	0.000
3	6	-7.623	0.000	-3.437	0.000	3.645	0.000	11.262	0.000	16.347	0.000
3	7	5.416	-0.158	6.184	-0.491	2.585	-0.862	9.214	-1.235	10.351	-1.514
3	8	3.387	0.140	3.143	0.168	2.604	-0.456	1.739	-1.722	0.613	-2.883
3	10	6.035	-0.020	5.072	-0.073	3.354	-0.148	1.402	-0.201	0.042	-0.135
3	11	5.146	0.158	6.184	0.491	7.585	0.863	9.214	1.235	10.351	1.519
3	12	3.387	-0.140	3.143	-0.168	2.604	0.456	1.739	1.722	0.613	2.883
7	8	6.198	-0.057	5.541	-0.123	4.326	-0.074	2.722	0.057	0.918	0.093
7	10	-8.601	1.136	-4.355	3.306	2.858	5.331	10.711	6.232	16.190	6.061
7	11	6.273	-0.240	4.879	-0.666	2.788	-0.908	0.960	-0.833	-0.042	-0.398
7	12	6.202	-0.170	5.576	-0.535	4.429	-0.953	2.919	-1.405	1.198	-1.810
7	14	20.449	0.000	19.881	0.000	18.932	0.000	17.843	0.000	17.021	0.000
8	9	21.652	0.000	21.077	0.000	20.102	0.000	19.932	0.000	18.113	0.000
8	12	5.919	0.000	4.614	0.000	2.691	0.000	1.090	0.000	0.366	0.000
8	13	-7.413	0.000	-3.294	0.000	3.679	0.000	11.183	0.000	16.196	0.000

Elements of $C_{xz}(kk',\underline{q})$ for Spinel

in the 1.1.0 direction

k	k'	$q/q_{max}=.1$ real	imag	$q/q_{max}=.3$ real	imag	$q/q_{max}=.5$ real	imag	$q/q_{max}=.7$ real	imag	$q/q_{max}=.9$ real	imag
1	1	0.000	0.000	0.000	0.000	0.000	0.000	0.000	0.000	0.000	0.000
1	2	0.000	-1.562	0.000	-4.264	0.000	-5.701	0.000	-5.073	0.000	-2.076
1	3	3.400	0.136	3.558	0.365	3.589	0.503	2.942	0.556	1.186	0.567
1	4	-3.301	1.045	-2.770	2.867	-1.932	3.866	-1.121	3.467	-0.632	1.425
1	7	-18.416	3.229	-16.885	9.204	-13.662	13.861	-8.447	16.663	-1.369	17.407
1	8	18.566	0.588	18.289	1.693	17.870	2.450	17.483	2.370	17.260	1.018
1	11	3.036	-0.015	3.188	-0.025	3.236	-0.018	2.680	-0.076	1.123	-0.287
1	12	-2.943	-0.903	-2.458	-2.489	-1.649	-3.374	-0.954	-3.046	-0.508	-1.257
3	4	-0.121	0.000	-0.967	0.000	-2.053	0.000	-2.397	0.000	-1.078	0.000
3	5	-14.362	0.000	-13.545	0.000	-11.703	0.000	-8.340	0.000	-3.102	0.000
3	7	-0.959	-1.633	-0.905	-4.451	-0.745	-5.937	-0.391	5.283	0.200	-2.209
3	8	2.838	-0.399	-2.606	-1.154	-2.142	-1.785	-1.439	-2.234	-0.513	-2.267
3	9	-0.131	-0.034	-0.185	-0.091	-0.246	-0.124	-0.237	-0.133	-0.102	-0.132
3	10	-2.877	0.504	-2.937	1.532	-2.998	2.347	-2.943	2.309	-2.684	0.795
7	8	-0.118	-0.060	-0.944	-0.194	-2.005	-0.327	-2.292	-0.352	-1.502	-0.160
7	9	-15.344	0.568	-14.503	1.663	-12.617	2.678	-9.203	3.669	-3.918	4.710
7	11	0.185	-0.116	0.196	-0.332	0.203	-0.480	0.171	-1.460	0.076	-0.195
7	12	0.118	0.297	0.941	0.843	1.987	1.239	2.237	1.380	0.933	1.213
7	13	14.145	0.296	13.336	0.813	11.516	1.102	8.199	1.008	3.045	0.436
7	14	0.000	0.129	0.000	0.366	0.000	0.520	0.000	0.536	0.000	0.209
8	12	-0.178	0.126	-0.146	0.360	-0.096	0.518	-0.048	0.494	-0.017	0.211
8	13	0.000	0.462	0.00	1.234	0.000	1.587	0.000	1.351	0.000	0.536

Elements of $C_{xx}(kk',\underline{q})$ for Spinel

in the 1.1.1 direction

k	k'	$q/q_{max}=.1$		$q/q_{max}=.2$		$q/q_{max}=.3$		$q/q_{max}=.4$		$q/q_{max}=.5$	
		real	imag	real	imag	real	imag	real	imag	real	imag
1	1	0.000	0.000	0.000	0.000	0.000	0.000	0.000	0.000	0.000	0.000
1	2	0.000	0.000	0.000	0.000	0.000	0.000	0.000	0.000	0.000	0.000
1	3	0.000	0.000	0.000	0.000	0.000	0.000	0.000	0.000	0.000	0.000
1	4	0.191	2.265	0.720	4.292	1.462	5.858	2.246	6.783	2.882	6.958
1	5	-0.096	-1.132	-0.360	-2.146	-0.732	-2.929	-1.123	-3.391	-1.441	-3.479
1	7	0.000	0.000	0.000	0.000	0.000	0.000	0.000	0.000	0.000	0.000
1	8	-0.100	-0.329	-0.369	0.587	-0.719	-0.721	-1.037	-0.708	-1.221	-0.560
1	9	0.500	0.165	0.185	0.294	0.360	0.362	0.518	0.354	0.610	0.280
1	12	0.174	-2.289	0.657	-4.345	1.337	-5.947	2.055	-6.911	2.641	-7.125
1	13	-0.086	1.145	-0.329	2.173	-0.669	2.793	-1.027	3.455	-1.321	3.562
3	4	8.238	0.000	6.997	0.000	5.074	0.000	2.663	0.000	0.000	0.000
3	5	-4.119	0.000	-3.499	0.000	-2.537	0.000	-1.332	0.000	0.000	0.000
3	8	-34.406	-5.983	-33.165	-11.787	-31.086	-17.232	-28.167	-22.137	-24.433	-26.348
3	9	17.203	2.991	16.582	5.894	15.543	8.616	14.083	11.068	12.212	13.174
3	10	0.000	0.000	0.000	0.000	0.000	0.000	0.000	0.000	0.000	0.000
7	8	8.913	-0.820	7.657	-1.610	5.708	-2.339	3.255	-2.973	0.528	-3.475
7	9	-4.457	0.410	-3.829	0.805	-2.854	1.170	-1.627	1.487	-0.264	1.737
7	10	0.000	0.000	0.000	0.000	0.000	0.000	0.000	0.000	0.000	0.000
7	12	8.593	0.203	8.981	0.389	9.461	0.547	9.850	0.668	9.996	0.755
7	13	-4.297	-0.101	-4.490	-0.195	-4.731	-0.273	-4.925	-0.334	-4.998	-0.387
8	9	-4.747	-0.020	-4.938	-0.032	-5.177	-0.031	-5.370	-0.019	-5.444	0.000
8	12	0.012	0.720	0.044	1.376	0.089	1.904	0.138	2.248	0.179	2.366
8	13	-4.013	0.099	-3.405	0.177	-2.464	0.216	-1.287	0.203	0.010	0.132
9	10	9.493	0.000	9.877	0.000	10.353	0.000	10.740	0.000	10.888	0.000
9	14	8.025	-0.198	6.809	-0.355	4.928	-0.433	2.574	-0.406	-0.020	-0.263

Elements of $C_{xy}(kk',\underline{q})$ for Spinel

in the 1.1.1 direction

k	k'	$q/q_{max}=.1$		$q/q_{max}=.2$		$q/q_{max}=.3$		$q/q_{max}=.4$		$q/q_{max}=.5$	
		real	imag	real	imag	real	imag	real	imag	real	imag
1	1	4.133	0.000	3.989	0.000	3.812	0.000	3.669	0.000	3.615	0.00
1	2	4.266	−1.549	4.472	−2.923	4.732	−3.982	4.939	−4.656	4.947	−4.948
1	3	7.532	−0.337	7.435	−0.758	7.265	−1.315	7.019	−2.008	6.714	−2.781
1	4	0.827	0.558	0.856	1.126	0.883	1.564	0.880	1.860	0.823	1.987
1	6	7.333	1.502	6.661	2.930	5.587	4.218	4.184	5.310	2.550	6.157
1	7	−13.991	4.524	−12.734	8.716	−10.700	12.274	−7.986	14.935	−4.741	16.511
1	8	22.693	1.919	22.397	3.831	21.924	5.727	21.295	7.596	20.529	9.425
1	10	−14.288	−0.761	−13.924	−1.648	−13.370	−7.742	−12.700	−6.052	−12.001	−5.510
1	11	7.144	0.447	6.981	0.972	6.706	1.625	6.327	2.404	5.874	3.252
1	12	1.162	−0.459	1.106	−0.889	1.002	−1.258	0.843	−1.534	0.626	−1.690
1	14	6.961	−1.350	6.266	−2.634	5.159	−3.794	3.720	−4.781	2.057	−5.549
3	4	3.983	0.000	3.385	0.000	2.457	0.000	1.291	0.000	0.000	0.000
3	6	−9.778	0.000	−8.337	0.000	−6.075	0.000	−3.201	0.000	0.000	0.000
3	7	3.131	−1.697	3.553	−3.200	3.868	−4.351	4.140	−5.060	4.228	−5.312
3	8	1.282	0.126	1.173	0.254	1.013	0.387	0.829	0.531	0.642	0.692
3	10	3.925	−0.025	3.520	0.062	2.900	0.337	2.147	0.819	1.362	1.468
7	8	3.986	−0.062	3.399	−0.142	2.489	−2.252	1.348	−0.040	0.088	−0.581
7	10	−10.754	1.132	−9.286	2.219	−6.974	3.209	−4.024	4.051	−0.712	4.687
7	11	4.185	−0.241	3.634	−0.499	2.753	−0.784	1.612	−1.092	0.323	−1.403
7	12	18.413	0.298	18.366	0.586	18.304	0.861	18.246	1.122	18.211	1.376
8	9	19.617	−0.000	19.569	0.000	19.509	0.000	19.457	0.000	19.438	0.000
8	10	4.222	−0.055	4.309	−0.090	4.418	−0.090	4.506	−0.055	4.540	0.000
8	12	3.821	0.008	3.277	0.030	2.407	0.075	1.285	0.146	0.018	0.237
8	13	−9.567	0.289	−8.148	0.520	−5.923	0.644	−3.101	0.627	0.035	0.459
8	14	3.990	0.463	3.413	0.89	2.516	1.254	1.385	1.525	0.127	1.683
10	14	4.173	0.246	3.586	0.478	2.649	0.686	1.438	0.860	0.075	0.990

BIBLIOGRAPHY.

Arndt,U.W., and Willis,B.T.M., (1966) "Single Crystal Diffractometer" [Cambridge University Press].

Bacon,G.E., (1952) Acta.Cryst., 5, 684

Bacon,G.E., (1962) "Neutron Diffraction" [Oxford: Clarendon Press].

Barth,T.F.W, and Posnjak,E., (1932) Z.Krist., 82, 325

Bickford,L.R., (1953) Rev.Mod.Phys. 25, 75.

Born,M., (1940) Proc.Camb.Phil.Soc., 36, 160.

Born,M., and Huang,K., (1954) "Dynamical Theory of Crystal Lattices" [Oxford University Press]

Born,M., and von Kármán, Th., (1912) Phys.Z. 13, 297.

Born,M., and von Kármán, Th., (1913) Phys.Z. 14, 65.

Bowlder,H., Martin,R.S., and Reinsch,J.H., (1968) Num.Maths.,11, 293.

Brabers,V.A.M., (1969) Phys.Stat. Soldi., 33, 563.

Bragg,W.H., (1915) Phil.Mag., 30, 305.

Brockhouse,B.N., (1958) Bull.Amer.Phys.Soc., 3, 233.

Brockhouse,B.N., and Iyengar,P.K., (1957) Phys.Rev., 111, 747.

Buras,B., and Giebultowicz,T., (1972) Acta.Cryst., A28, 151.

Carlisle,C.J., (1973) Ph.D. Thesis: University of Birmingham.

Cervinka,L., (1965) Czech.J.Phys.B., 15, 747.

Cheary,R.W., (1971) Ph.D. Thesis: University of Aston in Birmingham.

Cochran,W., (1959a) Z.Krist., 112, 465.

Cochran,W., (1959b) Phys.Rev.Letters., 2, 495.

Cochran,W., (1959c) Proc.Roy.Soc., A253, 260.

Cochran,W., (1960) Adv.Phys., 9, 387.

Cole,H., Chambers,F.W., and Dunn,H.M., (1962) Acta.Cryst., 15, 138.

Cooper,M.J.,Rouse,K.D., and Willis,B.T.M., (1968) Acta.Cryst. A24, 484.

Coppens,P., (1968) Proceedings of International Summer School on Thermal Neutron Scattering.
[In, "Thermal Neutron Scattering", Ed. B.T.M.Willis Oxford Univ Press (1970)]

Coppens,P., and Hamilton,W.C., (1970) Acta. Cryst., A26, 71.

Cowley,R.A., (1962) Acta.Cryst. 15, 687.

Cromer,T., (1965) Acta.Cryst., 18, 17.

Cromer,T., and Waber,J.T., (1965) Acta.Cryst. 18, 104.

Cruickshank,D.W.J., (1949) Acta.Cryst. 2, 65.

Cruickshank,D.W.J., (1956) Acta.Cryst. 19, 486.

Darwin,C.G., (1914) Phil.Mag., 27, 315, 675.

Dawson,B., (1967) Proc.Roy.Soc., 298A, 255.

Dawson,B., and Willis,B.T.M., (1967) Proc.Roy.Soc. A298, 307.

De Angelis,B.A., (1969) Ph.D. Thesis: The Pennsylvania State University.

Dick,B.G., and Overhauser,A.W., (1958) Phys.Rev., 112, 90.

Dolling,G., (1963) in "Inelastic scattering of neutrons in solids
             and liquids" Vol.II, p.37, I.A.E.A. Vienna.

Dolling,G., Cowley,R.A., and Woods,A.D.B., (1965) Can.J.Phys, 43, 1397.

Doraiswami,M.S., (1947) Proc.Indian Acad. Sc., A25, 413.

Dunitz,J.D., and Orgel,L.E., (1957) J.Phys.Chem.Solids. 3, 20.

Egelstaff,P.A., (1965) "Thermal Neutron Scattering"
             [Academic Press: New York; London].

Evans,B.J., Hafner,S.S., and Waber,H.P., (1971) J.Chem.Phys.,55, 5282.

Ewald,P.P., (1921) Ann.Phys. Lpz[4], 64, 253.

Fairweather,A., Roberts,F.F., and Welch,A.J.E., (1952) Rep.Prog.
             Phys., 15, 142.

Finch,G.I., Sinha,A.P.B., and Sinha,K.P., (1958) Proc.Roy.Soc., A242, 28.

Fischer,P., (1967) Z.Krist., 110, 197.

Goodenough,J.B., (1963) "Magnetism and the Chemical Bond",
             [London and New York: Interscience, p202].

Gorter,E.W., (1954) Philips.Res.Rep., 9, 295.

Gibbons,D.F., (1957) J.Appl.Phys., 28, 810.

Grimes,N.W., (1971) J.Phys.C, 4, L342.

Grimes,N.W., (1972a) Phil.Mag., 26, 1217.

Grimes,N.W., (1972b) Spectrochim. Acta., 28A, 2217.

Grimes,N.W., (1973a) J.Phys.C., 6, L78.

Grimes,N.W., (1973b) Phys.Stat.Solidi.(b), 58, K129.

Grimes,N.W., (1974a) Proc.Roy.Soc., A338, 223.

Grimes,N.W., (1974b) Proc.Roy.Soc., A338, 223.

Grimes,N.W., (1975) Phys in Technology, 6, 22.

Grimes,N.W., and Collett,A.J., (1971a) Phys.Stat.Solidi.(b), 43, 591.

Grimes,N.W., and Collett,A.J., (1971b) Nature. Lond., 230, 158.

Grimes,N.W., and Hilleard,R.J., (1970) J.Phys.C. 3, 866.

Hafner,S., (1961) Z.Krist., 115, 331.

Hamilton,W.C., (1958) Phys.Rev., 110, 1050.

Hamilton,W.C., (1964) "Statistics in Physical Science"
            [New York: The Ronald Press].

Hamilton,W.C., (1965) Acta.Cryst., 18, 502.

Hwang,L., Heuer,A.H., and Mitchell,T.E., (1973) Phil.Mag. 28, 241.

Heller,W.R., and Nowick,A.S., (1965) Adv.Phys., 14, 101.

Henning,J.C.M., and van den Boom,H., (1973) Phys.Rev.8B, 2255.

Heuer,A.H., and Mitchell,T.E., (1975) J.Phys.C., 8, L541.

Horton,G.K., and Leech,J.W., (1963) Proc.Phys.Soc., 82, 816.

Hudson,A., and Whitfield,H.J., (1967) Molec.Phys., 12, 165.

Iizunmi,M., and Shirane,G., (1975) S.S.Commun. 17, 433.

International Tables: [The International Tables for X-ray Crystallography]
            4 volumes (Brimingham: Kynoch Press).

James,R.W., (1948) "The Optical Principles of the Diffraction of
            X-rays" [London: G.Bell].

Johnson,F.A., (1965) Prog.Semi-Conductors, 9, 180.

Johnson,F.A., and Loudon,R, (1964) Proc.Roy.Soc., A281, 274.

Keating,D.T., Nunes,A., Batterman,B.W., and Hastings,J., (1971),
            Phys.Rev. B4, 2472.

Kellermann,E.W., (1940) Phil.Trans., A238, 513.

King,E.G., (1955) J.Phys.Chem., 59, 218.

Kino,Y., and Lüthi,B., (1971) S.S.Commun., 9, 805.

Kino,Y., Lüthi,B., and Mullen, (1972) J.Phys.Soc.Japan., 33, 687.

Kittel,C., (1971) "Introduction to Solid State Physics"
            [John Wiley and Sons].

Koops,C.G., (1951) Phys.Rev., 83, 121.

Larson,A.C., (1967) Acta.Cryst., A31, 273.

Lehmann,M., and Wilson,S., (1975) I.L.L. Internal publication
           No.74111T 2nd ed.

Lewis,M.F., (1966) J.Am.Acoust.Soc., 40, 728.

Lipson,H., and Cochran,W., (1966) "The Determination of Crystal Structures"
           [G.Bell: London]

Lotgering,F.K., (1962) J.Phys.Chem.Solids, 23, 1153.

Lou,F.H., and Ballentyne,D.W.G., (1968) J.Phys.C. 1, 608.

Lyddane,R.H.,Sachs,R.G., and Teller,E., (1941) Phys.Rev., 59, 673.

Manasevit,H.M., and Forbes,D.H., (1966) J.Appl.Phys. 37, 734.

Maradudin,A.A., and Flinn,P.A., (1963) Phys.Rev. 129, 2529.

Marumo,F., Isobe,M., Saito,Y, Yagi,T., and Akimoto,S., (1974)
           Acta.Cryst., B30, 1904.

McClure,D.S., (1957) J.Phys.Chem.Solids, 3, 311.

Meister,H., (1967) Nukleonik, 10, 97.

Millar,A., (1959) J.Appl.Phys., 30, 24S.

Moon,R.M., and Shull,C.G., (1964) Acta.Cryst., 17, 805.

Moran,T.J., and Lüthi,B., (1969) Phys.Rev., 187, 710.

Nelmes,R.J., (1975) Acta.Cryst., A31, 273.

Nishikawa,S., (1915) Proc.Tokyo.Math.Phys.Soc., 8, 199.

O'Horo,M.P., Frisillo,A.L., and White,W.B.,(1973) J.Phys.Chem.Solids, 34,23.

Peters,J., and Standley,K.J., (1958) Proc.Phys.Soc., 71, 131.

Polder,D., (1950) Proc.IEE, 97 pt(II), 246.

Pope,N.K., (1963) "Lattice dynamics" proceedings of an International
           Conference, Denmark: Pergamon Press, p147.

Peters,G., and Wilkinson,J.H., (1970) Num.Math., 16, 181.

Pryor,A.W., (1966) Acta.Cryst., 20, 138.

Pryor,A.W., and Willis,B.T.M., (1975) "Thermal vibrations in
           Crystallography" [Cambridge University Press].

Raccah,P.M., Bouchard,R.J., and Wold,A., (1966) J.Appl.Phys.,37, 1436.

Renninger,M., (1937) Z.Phys., 106, 141.

Rooksby,N.P., and Willis,B.T.M., (1953) Acta.Cryst., 6, 563.

Ross,D.K., and Carlisle,C.J., (1975) J.Appl.Cryst., 8, 292.

Rouse,K.D., Thomas,M., and Willis,B.T.M., (1976) J.Phys.C., 9.

Sabine,T.M., (1965) Acta.Cryst., 16, 834, L231.

Samuelsen,E.J., (1974) J.Phys.C., 7, L115.

Samuelsen,E.J., and Steinsvoll,O., (1974) Phys.Stat.Solidi (b) 61, 615.

Samuelsen,E.J., and Steinsvoll,O., (1975) J.Phys.C., 8, L427.

Sawaguchi,F., (1953) J.Phys.Soc. Japan., 8, 615.

Schmunk,R.E., Brugger,R.M., and Randolph,P.D., (1962) Phys.Rev. 128, 562.

Shirane,G., (1974) Rev.Mod. Phys., 46, 437.

Stahl-Brada,R., and Low,W., Phys.Rev., 116, 561.

Smit,J.,(1971) "Magnetic Properties of Materials" [McGraw-Hill].

Striefler,M., and Barsh,G.R., (1972) J.Phys.Chem.Sols., 33, 2229.

Stirling,W., (1972) J.Phys.C., 5, 2711.

Szigeti,B., (1949) Trans.Far.Soc., 45, 155.

Szigeti,B., (1950) Proc.Roy.Soc., A258, 377.

Tanaka,M., Tokoro,T., and Aiyama,Y., (1966) J.Phys.Soc.Japan, 29, 171.

Tarte,P., and Preudhomme,J., (1963) Acta.Cryst., 16, 227.

Tarte,P., and Preudhomme,J., (1971) Spectrochim.Acta., 27A, 1817.

Tokonami,M., (1965), Acta. Cryst., 19, 486.

van.Hove,L., (1953) Phys.Rev., 89, 1189.

van Uitert,L.G., (1956) Proc.IEE, 44, 1294.

van den Berg,K.G., Lodder,J.C., and Mensinga,T.C., (1976)
                    Thin.Sol.Films., 34, 243.

Verwey,E.J.W., and Heilmann (1947) J.Chem.Phys., 15, 174.

Verwey,E.J.W., Haagman,P.W., and Romiejn,F.C., (1947) J.Chem.Phys.,15, 181.

Verwey,E.J.W., de Boer,F., and van Santen,J.H., (1948)
                    J.Chem.Phys., 16, 1091.

Vieland,L.J., (1975) Acta. Cryst., A31, 753.

Wang,C.C., and Zanzucchi,P.J., (1971) J.Electrochim.Soc., 118, 586.

Waldron,R.D., (1955) Phys.Rev., 99, 1727.

Watanabe,H., and Brockhouse,B.N., (1962) Phys. Letters, 1, 189.

White,W.B., and De Angelis,B.A., (1967) Spectrochim.Acta., 23A, 985.

Willis,B.T.M., (1969) Acta.Cryst., A25, 484.

Woods,W.A., Cochran,W., and Brockhouse,B.N., (1960)
                Phys.Rev. 119,980.

Wooster,W.A., (1949) "Crystal Physics" [Cambridge University Press]

Wycoff,R.W.G., (1951) "Crystal Structures" [Interscience: New York]

Zacharisen,W.H., (1967) Acta. Cryst., 23, 558.

ACKNOWLEDGEMENTS.